Interaction Notes
Note 228
May 1975

Broadband Responses of Deliberate Aircraft Antennas, Part I

Tom K. Liu, K. S. H. Lee and Lennart Marin

The Dikewood Corporation, Westwood Research Branch
Los Angeles, Calif. 90024

Abstract

Sixteen specific deliberate aircraft antennas are analyzed in this report. The parameters of the Thévenin equivalent circuit for each antenna, namely, the effective height and the input impedance, are evaluated and presented in graphical form. The principles of operation of each antenna are also discussed.

PREFACE

This report contains the analysis of sixteen deliberate aircraft antennas, which was carried out between October 1973 and September 1974. Each chapter has been previously published in the AFWL DAA Memo Series.

Chapter 4 has been contributed by Thomas H. Shumpert* and Chapter 11 by James F. Prewitt, both of the Applied Research Group, The Dikewood Corporation, Albuquerque, New Mexico.

During the course of the work, many helpful suggestions and encouragements have been provided by the following AFWL personnel: Dr. Carl E. Baum, Dr. J. Phillip Castillo, Capt. Dennis R. Rossbach and Capt. W. Douglas Wilson. The authors are indebted to them.

*Now with Auburn University, Auburn, Ala.

CONTENTS

INTRODUCTION

In this report, we are concerned with the coupling of EMP energy into an aircraft via some specific antennas. With the possible exceptions of some HF and VLF/LF antennas, the deliberate antennas are physically small compared to the aircraft. The antennas are mounted on the aircraft in one of the following ways (Fig. 1): externally mounted, flush mounted, mounted inside a radome, or being part of the aircraft itself such as the vertical stabilizer.

In analyzing the EMP response of an antenna, we are concerned with the available induced current and voltage across a pair of accessible terminals of the antenna. This amounts to calculating the parameters of the Thévenin equivalent circuit (Fig. 2a) that completely describes the properties of the antenna at the terminals A,B. Sometimes, it is preferable to use the dual representation of the Norton equivalent circuit (Fig. 2b). In Fig. 2, V_{oc} is the open-circuit voltage, Z_{in} is the input impedance, I_{sc} is the short-circuit current, and Y_{in} is the input admittance, all being referred to the terminals A,B. It has to be emphasized that the structure of a typical aircraft antenna, especially the matching network, is usually very complicated and each antenna modeling therefore requires individual attention.

Another important consideration that is foreign to the usual antenna analysis is that one needs to perform the analysis over the broad frequency range within which the nuclear EMP has a significant amount of energy. This range is generally not within the in-bands of the antennas and special care has to be exercised in order to correctly apply the available formulas for this broad frequency range. Often, the desirable formulas are not available (in particular, those for the induced voltage or current), and it is necessary to derive appropriate expressions from first principles. Indeed, a few boundary-value problems have been solved to obtain appropriate formulas (SSN 193, IN 171, IN 175, IN 179, IN 182) in the course of analyzing specific antennas. Usually, over the frequency range within which EMP is important, the antennas are electrically small and quasi-static analyses yield sufficiently accurate results.

The first step in the analysis is to represent the components of an antenna by an equivalent circuit consisting of lumped circuit elements, transmission lines, equivalent sources, etc. The reduction of this equivalent circuit to the

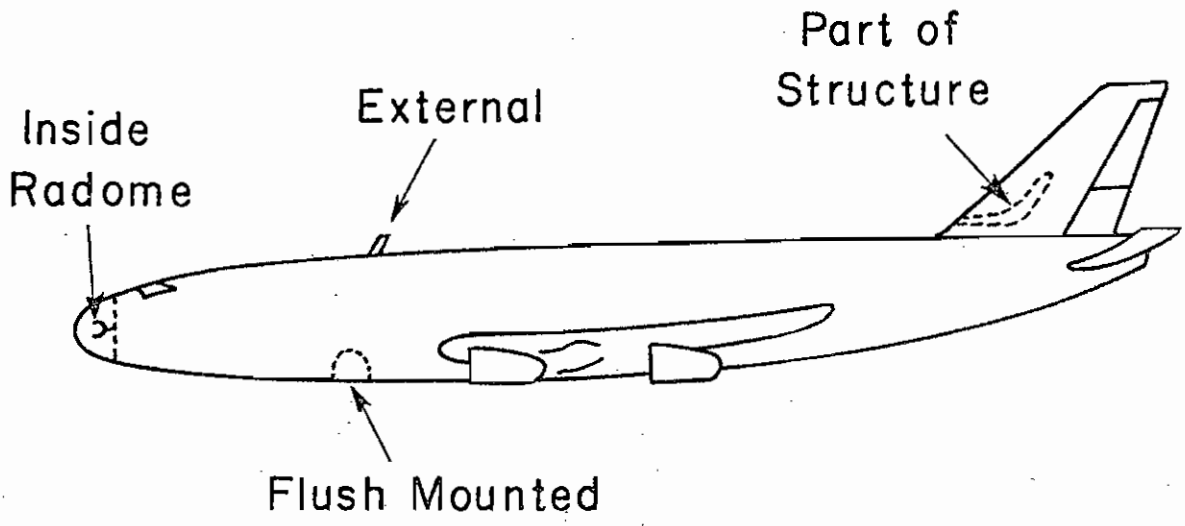

Fig. 1 Antennas mounted on an aircraft.

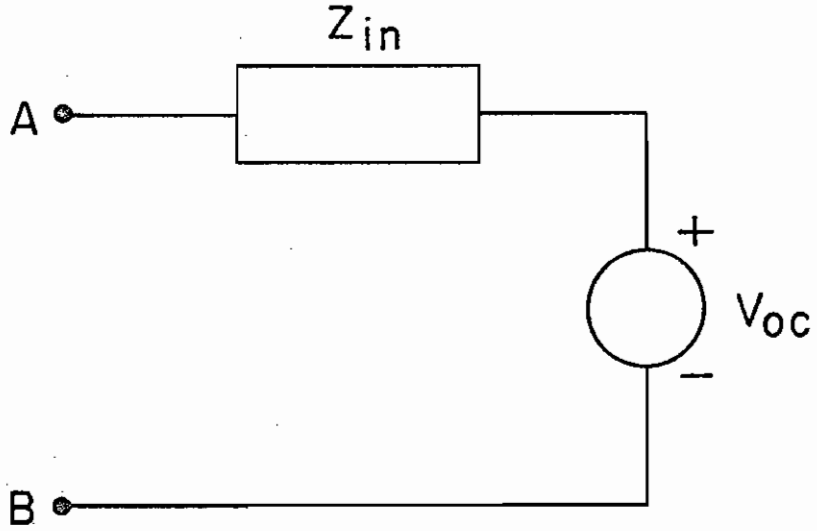

(a) Thévenin equivalent circuit

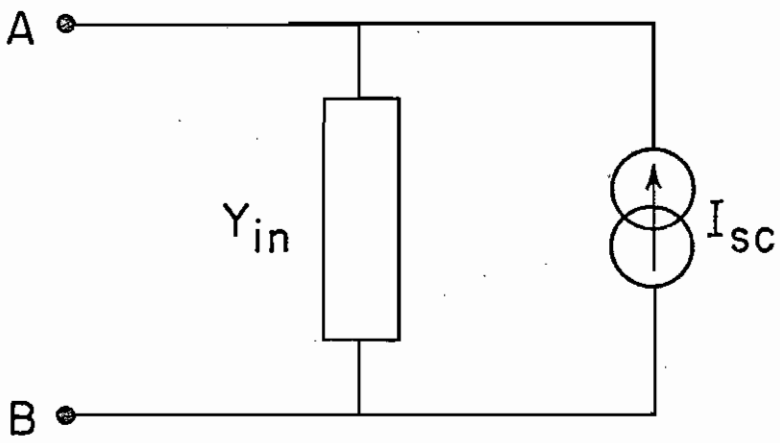

(b) Norton equivalent circuit

Fig. 2 Equivalent circuits of an antenna at the accessible terminals A,B. The parameters are related by : $Z_{in}Y_{in} = 1$, $V_{oc} = I_{sc}Z_{in}$.

Thévenin equivalent circuit is then accomplished by applying circuit analysis techniques. Elements of the equivalent circuit can be divided into two types: external elements and internal elements. External (or radiation) elements account for the transmitting (and/or receiving) characteristics of the antenna, and they are usually represented by a series combination of an induced (open-circuit) voltage source V_{ind} and an antenna impedance Z_a, or a parallel combination of an induced (short-circuit) current source I_{ind} and an antenna admittance Y_a. These quantities are shown in Fig. 3. Internal (or matching) elements account for the built-in matching networks that are necessary for the antenna to have a certain bandwidth and impedance level. The external quantities can usually be calculated by applying the simple existing antenna theory, or if necessary, by solving quasi-static boundary-value problems. The internal elements are usually passive elements, and often contain transmission lines.

The above division of the equivalent circuit elements can be illustrated by the following example. Consider the dipole antenna loaded by an inductance L as shown in Fig. 4a. At frequencies such that the wavelengths are much larger than the antenna length, the equivalent circuit is shown in Fig. 4b. Here, the division of internal and external elements is clearly illustrated.

With the exception of the HF and VLF/LF antennas, which will be described later it is useful to relate the induced voltage V_{ind} and the induced current I_{ind} to the *total local* electric field and the *total local* magnetic field. The choice of the excitation field is important. First, the total local field is the combination of the incident field and the scattered field from the aircraft in the absence of the antenna. Second, the polarization of the incident field is so chosen that the maximum voltage or current is induced on the antenna. Specifically, the total local electric field E_n normal to the surface is related to the local surface charge density σ by

$$E_n = \sigma/\varepsilon_o \tag{1}$$

and the total local tangential magnetic field $\underline{H}_t$ is related to the local surface current density $\underline{K}$ by

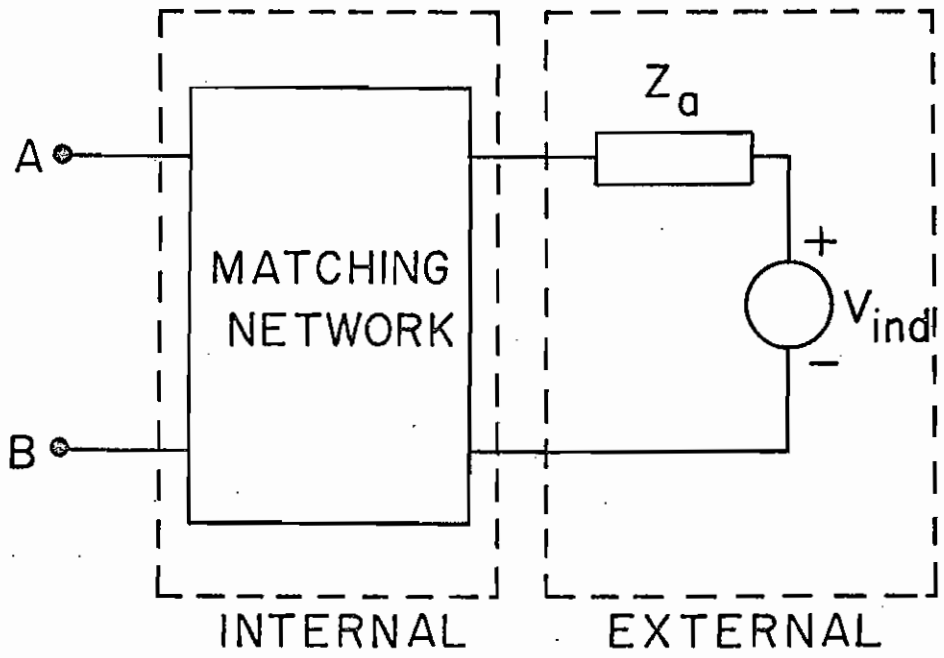

(a)

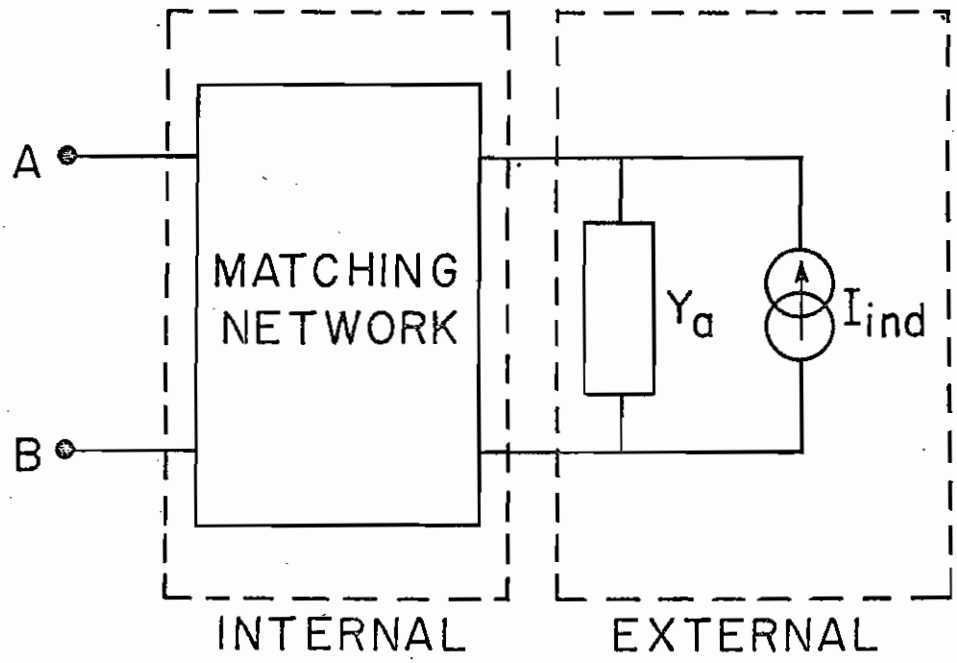

(b)

Fig. 3 External and internal quantities of an antenna.

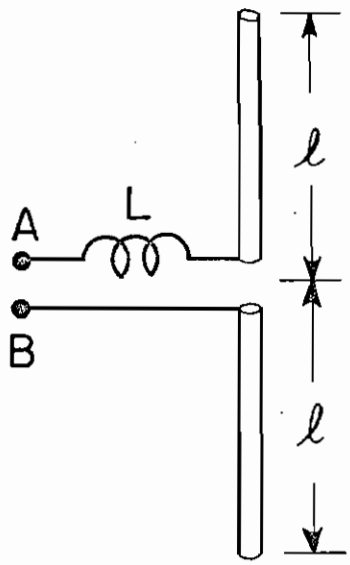

(a)

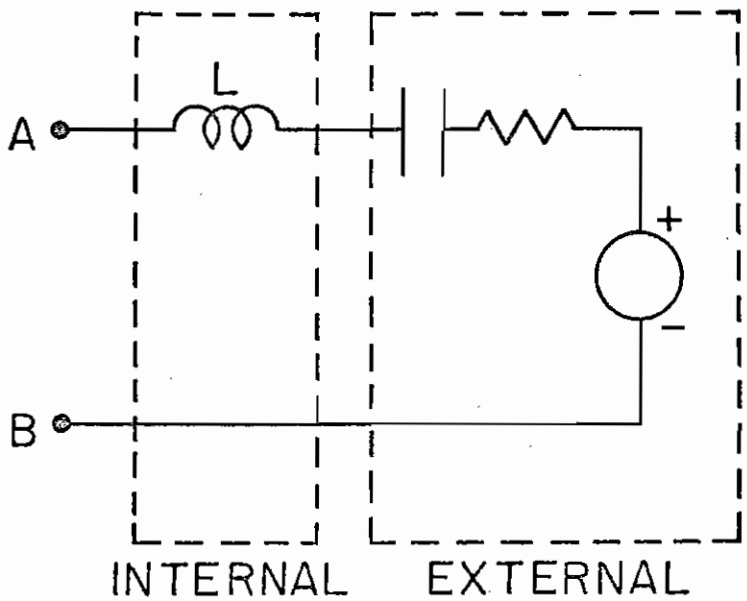

(b)

Fig. 4 (a) A dipole antenna with a series inductance and (b) the equivalent circuit for $\ell \ll \lambda$.

$$\underline{H}_t = \underline{K} \times \hat{n} \tag{2}$$

where $\hat{n}$ is the unit outward normal to the aircraft surface. The quantities σ and $\underline{K}$ can be obtained either by measurements or by external coupling calculations for a given incident excitation field.

For an electric-field excited antenna such as a monopole antenna, the external effective height h_e^e is defined such that

$$V_{ind}(\omega) = h_e^e(\omega)\ E_n(\omega) \tag{3}$$

and the external equivalent area A_{eq}^e is defined such that

$$I_{ind}(\omega) = j\omega\varepsilon_o\ A_{eq}^e(\omega)\ E_n(\omega) \tag{4}$$

Here, the superscript e denotes external quantities. For a magnetic-field excited antenna such as a loop antenna, we can similarly define the effective area (or effective aperture) A_e^e and the equivalent length ℓ_{eq}^e as follows:

$$V_{ind} = -\ j\omega\mu_o\ A_e^e(\omega)\ H_t(\omega) \tag{5}$$

and

$$I_{ind} = \ell_{eq}^e(\omega)\ H_t(\omega). \tag{6}$$

For a detailed discussion of h_e^e, A_{eq}^e, ℓ_{eq}^e, and A_e^e the reader is referred to SSN 38.

Once the equivalent circuit in Fig. 3 is obtained, the reduction to the Thévenin equivalent circuit of Fig. 2a can be accomplished using circuit analysis techniques. In this case, the open-circuit voltage V_{oc} of Fig. 2a depends on the *total local* electric field. The effective height h_e at the terminals A,B is defined such that

$$V_{oc}(\omega) = h_e(\omega)\ E_n(\omega) \tag{7}$$

Throughout this report, the effective height h_e and the input impedance will be calculated and presented in graphical form.

We now return to the cases of HF and VLF/LF antennas, which are not physically small compared with the aircraft. Due to the strong interaction between the incident field and the aircraft itself at the in-band frequencies of these antennas, it is preferable to relate the effective height of the antennas directly to the *incident field*. This amounts to solving both the antenna and the external coupling problems simultaneously. In these cases, the effective height h_e is given by

$$h_e(\omega) = V_{oc}(\omega)/E^{inc}(\omega) \tag{8}$$

where E^{inc} is the electric field of the *incident* EMP.

CHAPTER 1. AT-536/ARN MARKER BEACON ANTENNA ON AABNCP

I. General Description

The marker beacon antenna is flush mounted at the bottom of the fuselage at Station 1025. It is designed to receive the 75 MHz horizontally polarized (E) signals generated by the marker beacons located near the runways. A schematic diagram of the antenna is shown in Fig.1. The dimensions of the antenna (approximately 25.4 cm × 7.6 cm × 15.2 cm) are small compared with the operating wavelength, which is about 4 m.

II. Analysis

The antenna, as shown in Fig.1, is a loop inductively coupled by a much smaller loop to the coaxial feed line, which usually has a characteristic impedance of 50Ω. The antenna is series resonated by a capacitor, and the inductance coupling is adjusted to yield impedance matching to the feed line at the operating frequency.

This principle of operation suggests the equivalent circuit in Fig.2. The inductances L_1 and L_2 are associated with the small and the big loops, respectively, with a mutual inductance M between them. The capacitance C is the combined value of the tuning capacitance and the stray capacitances. R is the radiation resistance of the big loop. The voltage source, V_{ind}, is the voltage induced on the big loop and is given by

$$V_{ind} = -j\omega F B_t A_e \tag{1}$$

where B_t is the total magnetic field tangential to the aircraft skin in the absence of the antenna. The effective area A_e of a loop is about the same as the physical area of the loop. The factor F accounts for the reduction of the total magnetic flux into the antenna cavity. This factor is treated in detail in an Interaction Note (IN 179). For a cylindrical depression, F has been calculated in IN 10.

The circuit in Fig.2 is represented by a Thévenin equivalent circuit in Fig.3 at the transmission line terminals. Essentially, the feed line sees the antenna with input impedance Z_{in} and an open-circuit voltage V_{oc}. These quantities are given by

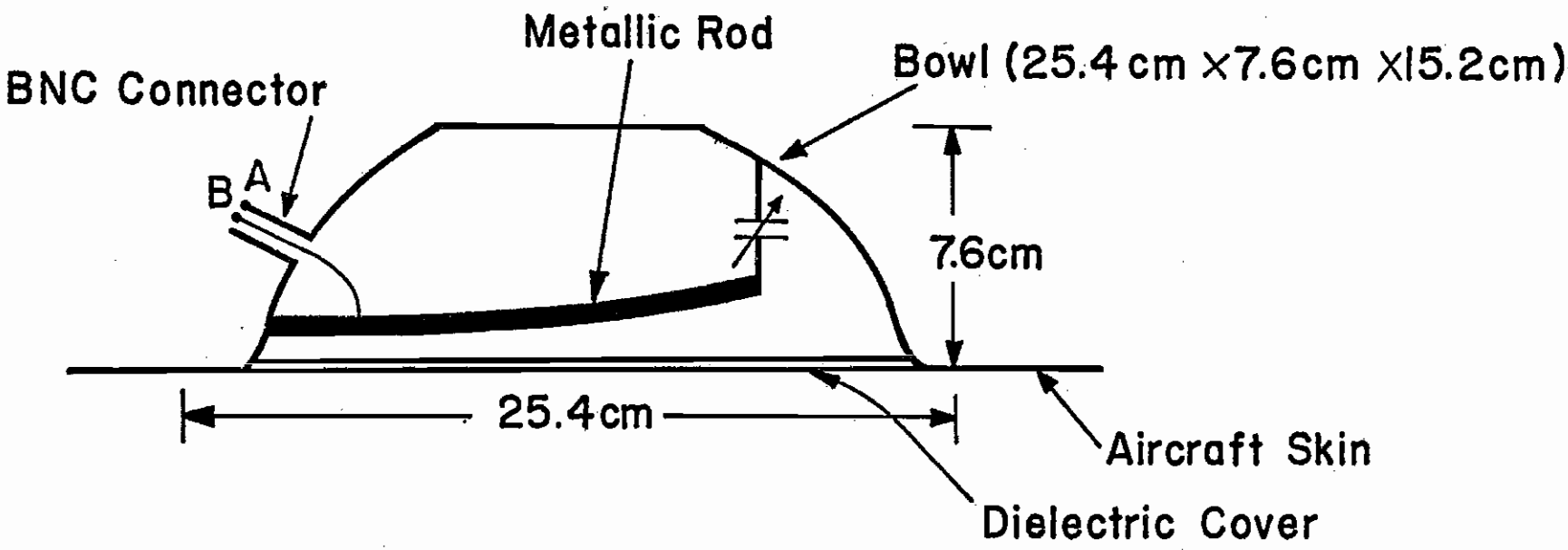

Fig.1 Schematic diagram of the marker beacon antenna.

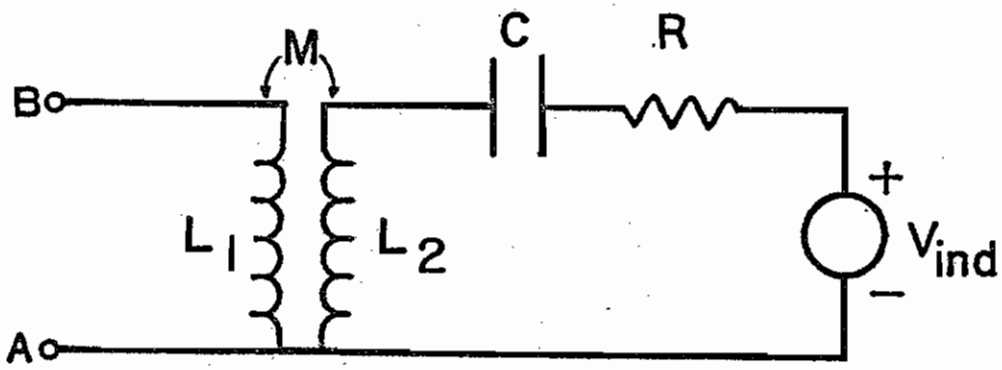

Fig.2 Lumped equivalent circuit of the marker beacon antenna.

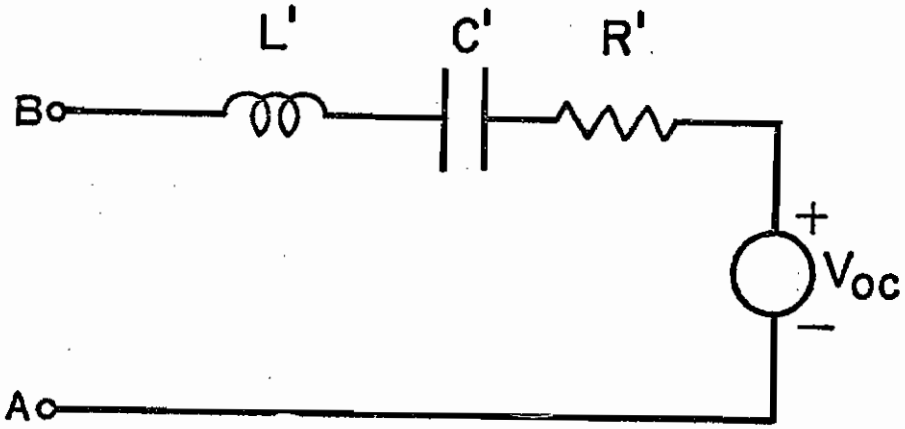

$$L' = L_2 \left[\omega M / \left(\frac{1}{j\omega C} + j\omega L_2 + R\right)\right]^2$$

$$C' = C \left[\omega M / \left(\frac{1}{j\omega C} + j\omega L_2 + R\right)\right]^2$$

$$R' = R \left[\omega M / \left(\frac{1}{j\omega C} + j\omega L_2 + R\right)\right]^2$$

$$V_{oc} = V_{ind} \left[j\omega M / \left(\frac{1}{j\omega C} + j\omega L_2 + R\right)\right]$$

Fig.3 Thévenin equivalent circuit of the marker beacon antenna.

$$Z_{in} = \omega^2 M^2 \left[\frac{1}{j\omega C} + j\omega L_2 + R\right]^{-1} \tag{2}$$

and

$$V_{oc} = N(\omega)\ V_{ind} \tag{3}$$

where

$$N(\omega) = j\omega M \left[\frac{1}{j\omega C} + j\omega L_2 + R\right]^{-1} \tag{4}$$

The above expressions are obtained by assuming that the inductance L_1 is negligible compared with L_2; this is the case when the small loop is considerably smaller than the big loop. The factor $N(\omega)$ may be regarded as the frequency-dependent transformer ratio.

For impedance-matching purposes, the antenna is designed so that at the operating frequency of $f_o = 75$ MHz, the input impedance of the antenna is resistive and equal to the characteristic impedance Z_o of the transmission line. This requires the series resonant condition at f_o:

$$1 - \omega_o^2 L_2 C = 0, \tag{5}$$

thus making Z_{in} in equation (2) purely resistive.

III. Numerical Results

In this section, the circuit parameters of the Thévenin equivalent circuit are estimated and $Z_{in}(\omega)$ and $N(\omega)$ are evaluated. It is observed that these two quantities are extremely narrow banded with vanishing out-of-band values. We present only the in-band values. Due to the lack of precise values of the dimensions of the antenna, reasonable guesses have been exercised.

The radiation resistance for a loop small compared with the wavelength λ is given by

$$R = 31200\ (A/\lambda^2)^2 \qquad \text{Ohms} \tag{6}$$

where A is the area of the loop. It is to be noted that R affects the values Z_{in} and $N(\omega)$ only at the operating frequency, and hence we use $\lambda = c/f_o$ where c is the speed of light. For out-of-band operations, the reactance dominates and the effect of R is negligible. The inductance L_2 is given by

$$L_2 = (2\pi)^{-1} \mu_o \, p \, \ell n \, (p/2\pi a) \tag{7}$$

where p is the perimeter of the loop and a is the radius of the wire. The estimation of the value of M is more complicated and may be detailed in a forthcoming Interaction Note. The capacitance C is obtained from (5).

From equations (5), (6) and (7) we find that $R \approx 25$ mΩ, $L_2 \approx 90$ nH, $M \approx 2.5$ nH, $C \approx 50$ pF. These values combine to yield a resonant frequency of 75.03 MHz with a resistive input impedance of 55.6Ω and transformer ratio of j47. The responses show very narrow band behavior and only a small frequency range is plotted in Fig.4 for Z_{in} and Fig.5 for $N(\omega)$.

Equations (1) and (3) show the dependence of V_{oc} on the product $F B_t A_e$. The magnetic field B_t depends on the induced current on the aircraft and should be measured just outside the antenna. Because of the extremely narrow band characteristics of the antenna, only this very small frequency range of B_t value is important. Very roughly, in the frequency domain, $V_{oc}(\omega)$ vanishes except at ω_o, where it is given by

$$V_{oc}(\omega_o) = 3 \times 10^8 \, B_t(\omega_o) \quad \text{volts} \tag{8}$$

Time domain response of the open-circuit voltage can be obtained by the Fourier transform.

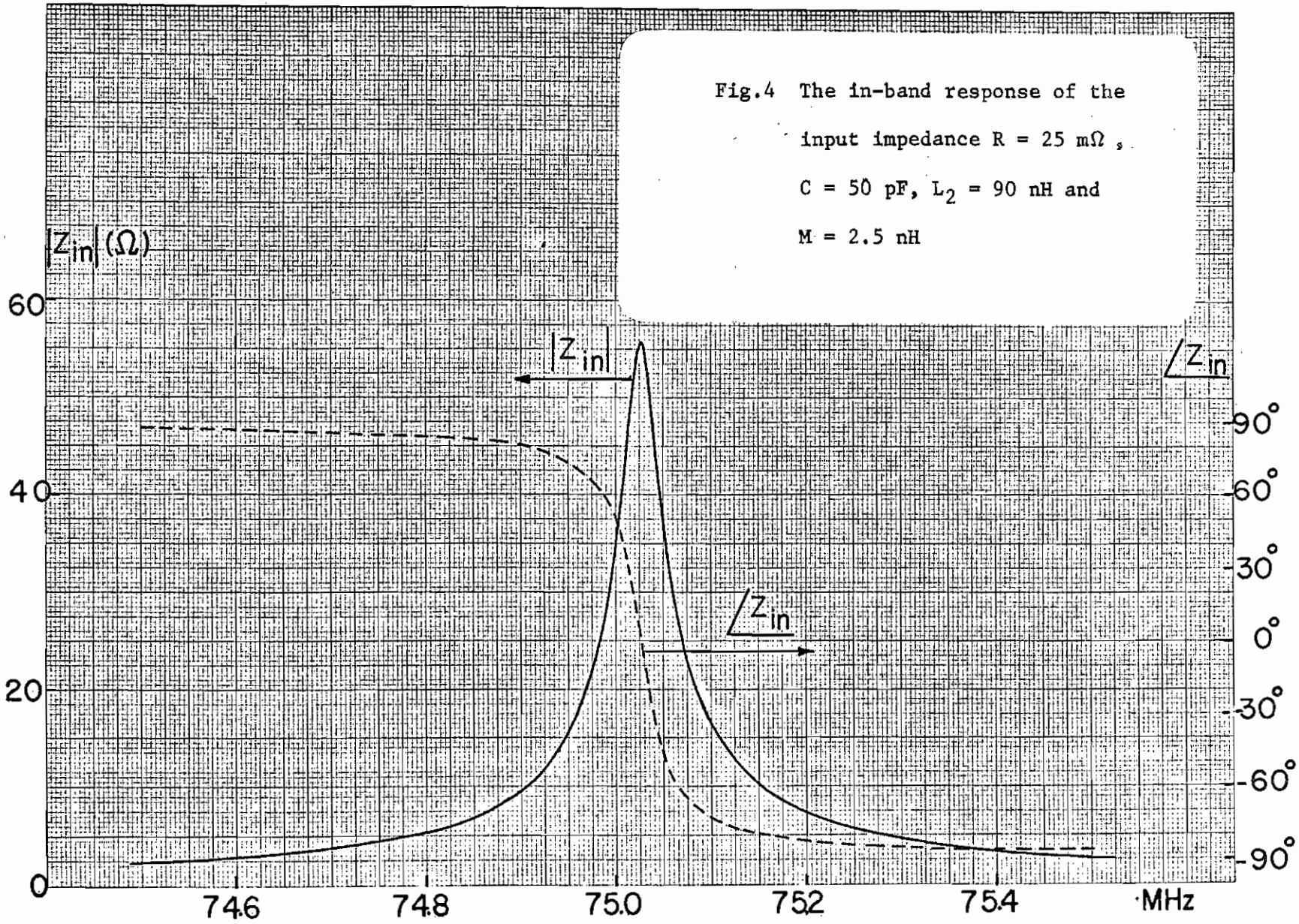

Fig.4 The in-band response of the input impedance R = 25 mΩ, C = 50 pF, L_2 = 90 nH and M = 2.5 nH

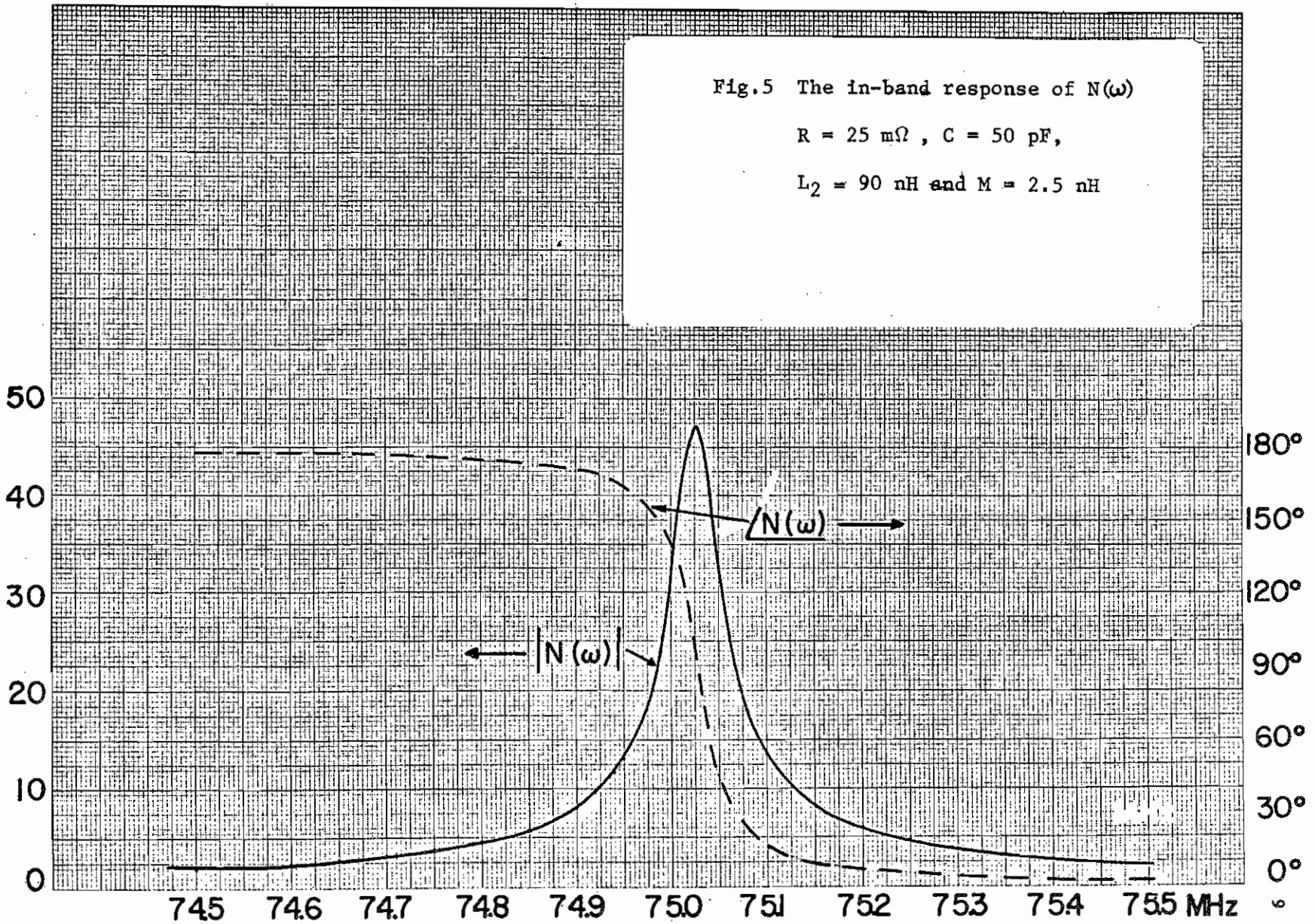

Fig.5 The in-band response of $N(\omega)$

$R = 25\ m\Omega$, $C = 50$ pF,

$L_2 = 90$ nH and $M = 2.5$ nH

CHAPTER 2. 137A-5 LF-MF ADF LOOP ANTENNA AND 65B06732 LF-MF ADF SENSE ANTENNA

I. General Description

The LF-MF automatic direction finder antennas are used to receive vertically polarized signals in the frequency range 0.19 - 1.75 MHz (wavelengths ≈ 170 meters to 1600 meters). There are two identical systems, each system consisting of one loop antenna and one sense antenna, which is a "rectangular annular" slot. In the ADF mode of operation, the omnidirectional receiving pattern of the sense antenna, whose radiation pattern is identical to that of a short monopole, is combined with the figure-eight receving pattern of the loop antenna to produce a resultant cardioid pattern, as shown in Fig.1. This principle of operation gives the null detection of the direction and sense of the received signal.

The loop antenna, as shown in Fig.2, is mechanically fixed with an electrically rotatable pattern. The antenna consists of two pairs of mutually perpendicular coils wound around four ferrite arms, with the parallel coils electrically connected in shunt. The coils are housed in an area measuring about 30.5cm × 42.5cm. The two pairs of coils are connected to the two orthogonal goniometer windings, and the incident field is reproduced within the shielded enclosure of the goniometer. This field is picked up by a small rotor coil which operates exactly like a loop. The cardioid pattern is obtained by properly combining the output of this rotor coil with the output of the sense antenna. It is to be noted that the cardioid radiation (or receiving) pattern will be modified due to the presence of the aircraft, especially at the upper operating frequency (1.75 MHz) which is close to the first resonance frequency of the aircraft. The two loop antennas are flush mounted on the bottom center line of the fuselage at stations 1005 and 1068.

Each sense antenna, as shown in Fig.3, is a "rectangular annular" slot antenna. The two sense antennas, which are flush mounted, are located at the bottom of the fuselage at body station 1490, and at right and left buttock line 89, respectively.

II. Analysis

II.1 ADF Loop Antenna

The Thévenin equivalent circuit of an electrically small receiving loop

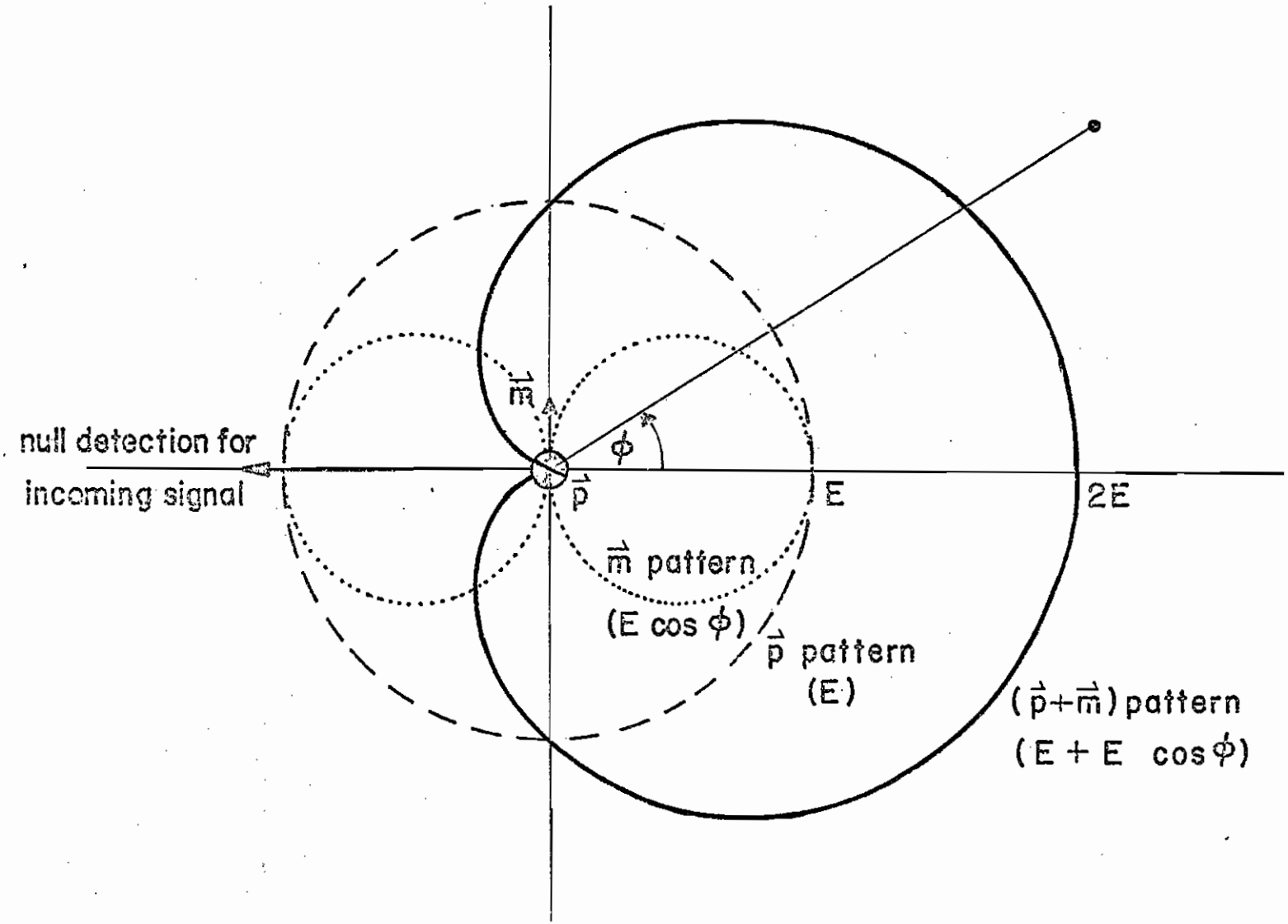

Fig.1. Principle of ADF: Resultant radiation pattern of a loop ($\vec{m}$) and a stub ($\vec{p}$) in a plane containing $\vec{m}$ and perpendicular to $\vec{p}$.

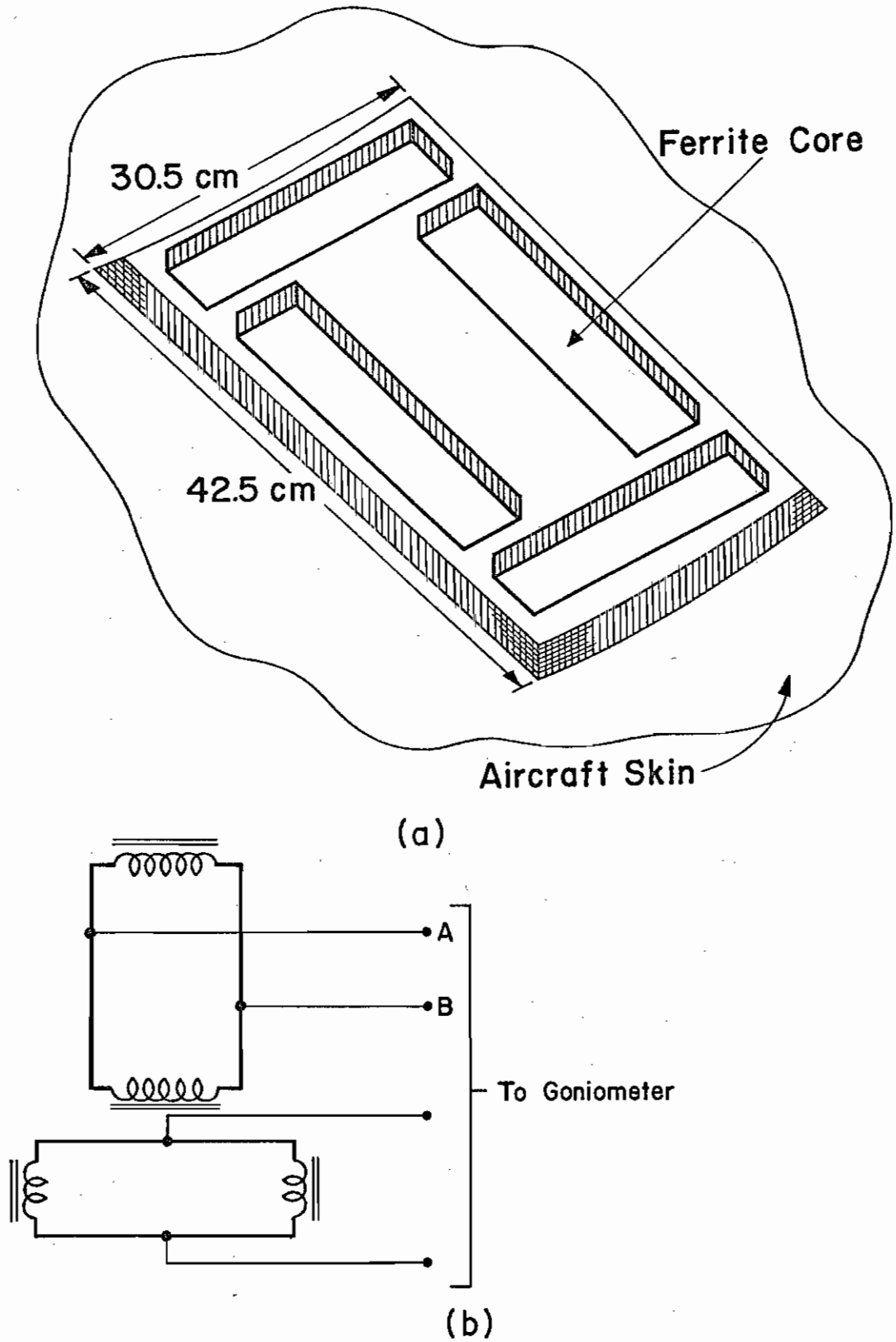

Fig.2 Schematic diagram of the LF-MF ADF loop antenna: (a) physical layout, (b) electrical connection.

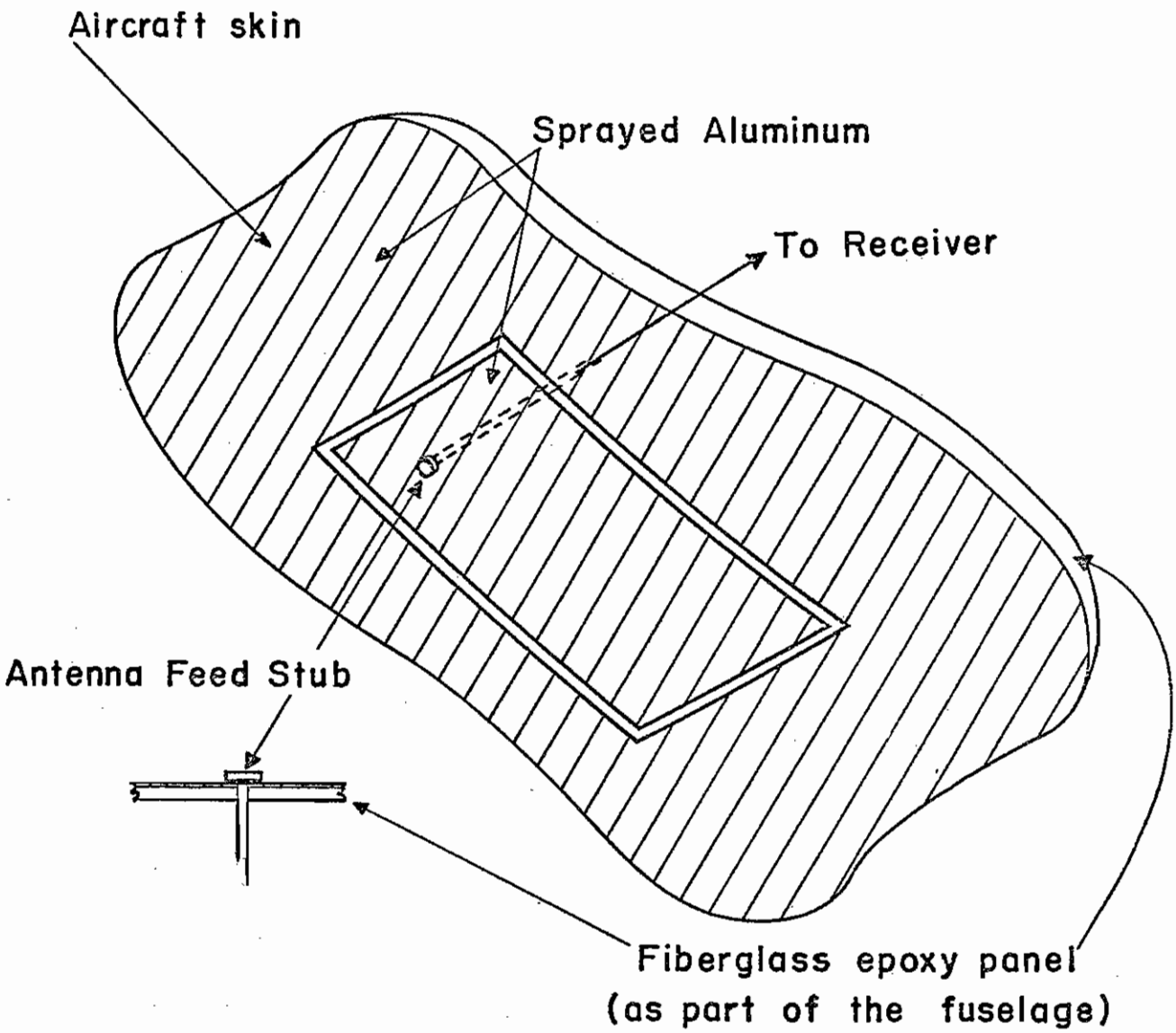

Fig.3 Schematic diagram of the LF-MF ADF sense antenna. The antenna is in the form of a "rectangular annular" slot.

antenna is shown in Fig.4. The parameters of a loop antenna with N-turns closely wound on a ferrite core with cross-sectional perimeter p, length ℓ and permeability μ are given by

$$L = \mu_e N^2 A/\ell \tag{1}$$

$$V_{ind} = -j\omega(\mu_e/\mu_o) B_t A_e \tag{2}$$

and

$$R = 31200(NA/\lambda^2)^2 \text{ ohms} \tag{3}$$

Here, μ_e is the effective permeability due to the presence of the ferrite core and is plotted in Fig.5, A_e is the effective area of the loop and is about N times the cross-section area A of the coil, and B_t is the total magnetic field normal to the loop.

We now apply the above results to the ADF loop antenna. Since there is no significant interaction between the two pairs of orthogonal coils, they can be treated independently. However, in the following analysis, we have to take into account the mutual inductance M between the coils in each pair of parallel coils. The equivalent circuit for each pair of shunt-connected parallel coils is shown in Fig.6(a), where the terminals A, B are the feed points of the antenna. Circuit analysis reveals that the two equivalent sources, V_{ind}, must have polarities as shown in the figure in order for V_{oc} to be non-zero. The resultant Thévenin equivalent circuit is shown in Fig.6(b). In general, M is considerably smaller that L.

In the equivalent circuit of Fig.6(b), the open-circuit voltage and the input impedance depend on the physical properties of the antenna structure and the total magnetic field tangent to the aircraft skin. It is recommended that these two parameters be determined from suitable measurements.

II.2 ADF Sense Antenna

The Thévenin equivalent circuit for an electrically small "rectangular annular" slot antenna is shown in Fig.7. Such a slot has a radiation pattern identical to that of a short monopole. The capacitance C and equivalent area A_{eq} of this slot antenna can be calculated from the results in SSN 98 and SSN 106:

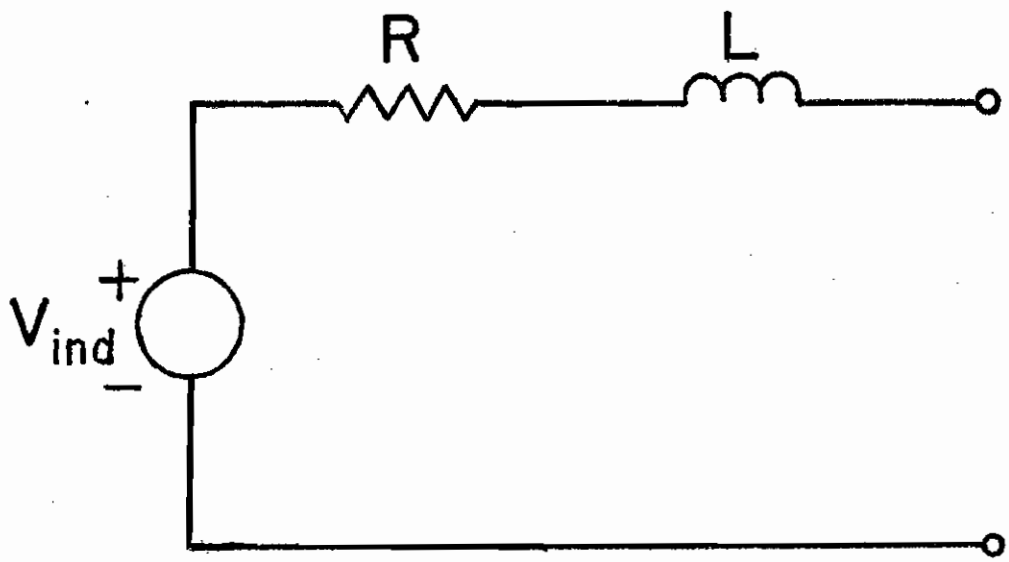

Fig.4. Equivalent circuit of an electrically small receiving loop antenna.

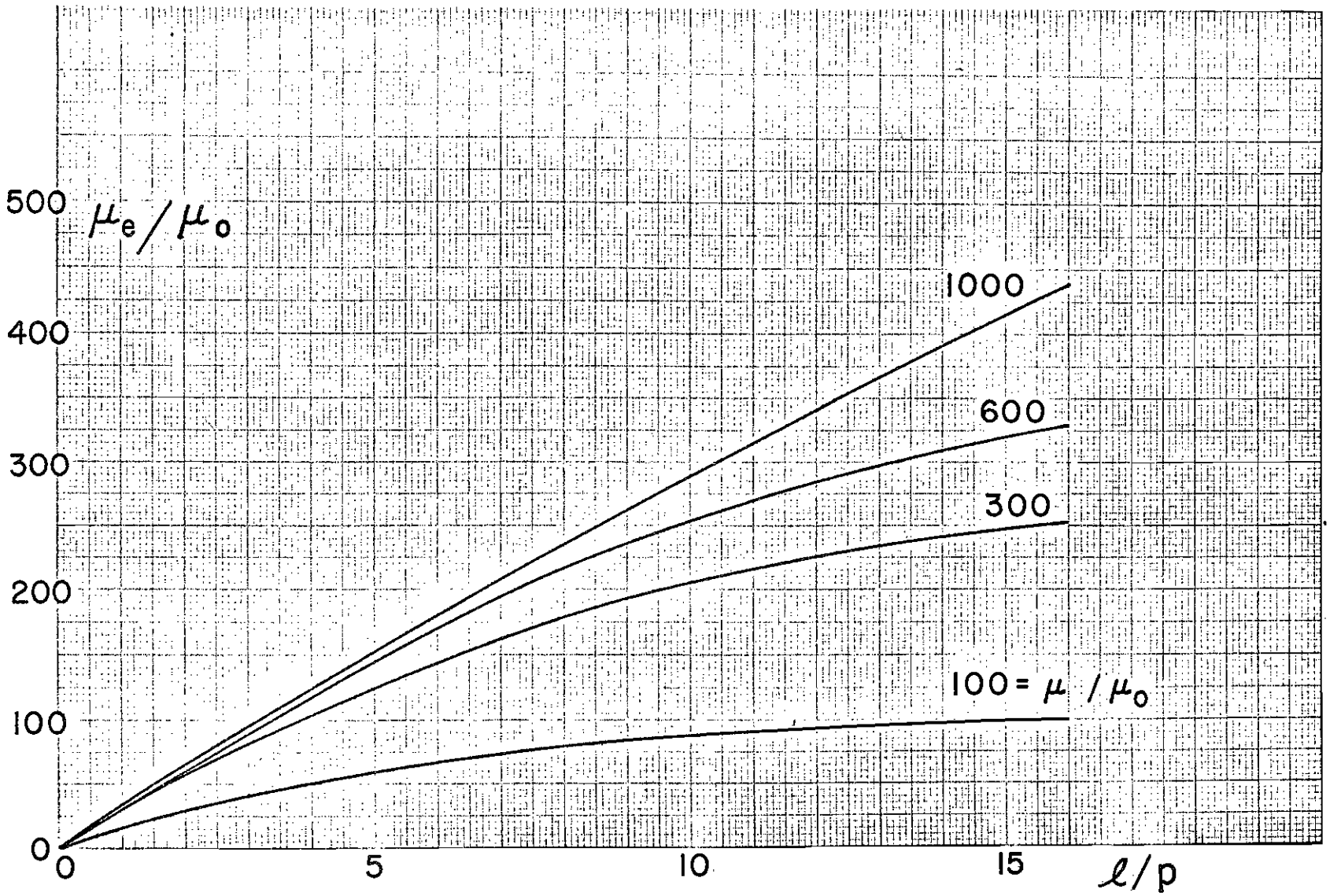

Fig.5 Effective permeability of a coil wound on a ferrite core with cross-sectional perimeter p, length ℓ and permeability μ.

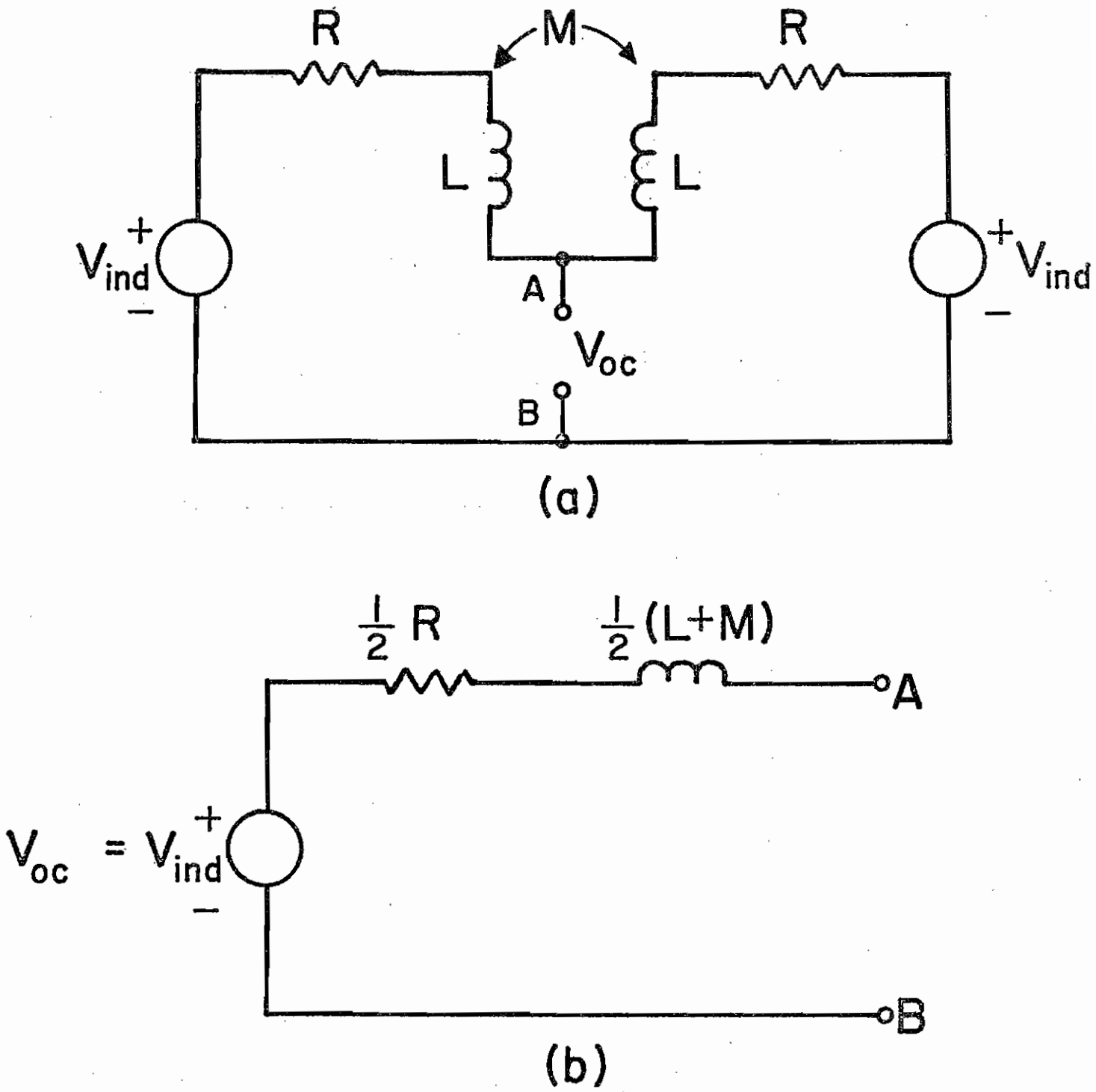

Fig.6. (a) Equivalent circuit of a pair of parallel coils connected in shunt. (b) Resultant Thévenin equivalent circuit of (a).

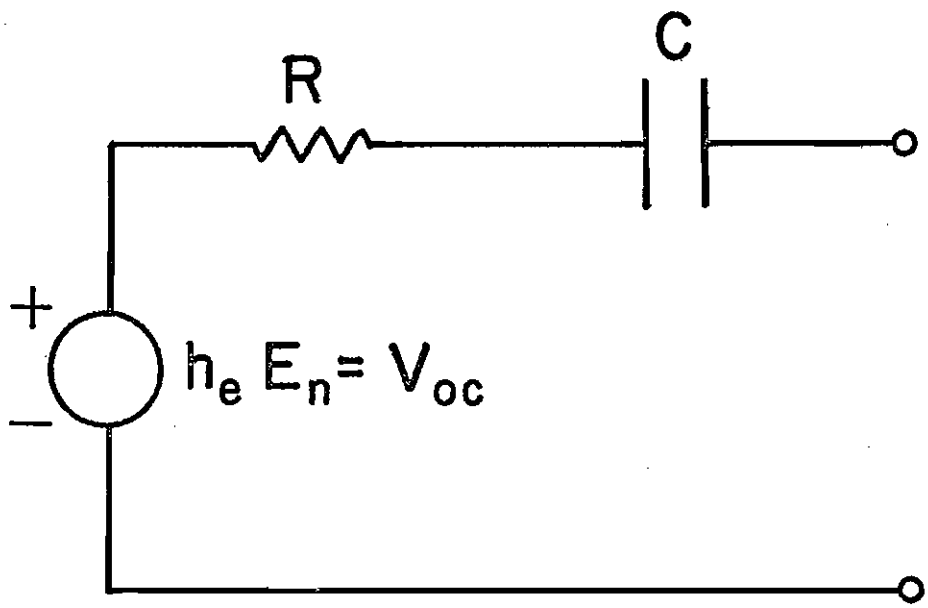

h_e = 6.9 cm

$R = 1580\ (h_e/\lambda)^2$ Ohms

C = 119 pF

Fig.7 Thévenin equivalent circuit of an electrically small "rectangular annular" slot antenna.

$$C = 119 \text{ pF}$$

$$A_{eq} \approx 0.93 \text{ m}^2 \tag{4}$$

from which one gets for the effective (equivalent) height

$$h_e = \frac{\varepsilon A_{eq}}{C} = 6.9 \text{ cm}$$

The radiation resistance is the same as that of a short monopole and given by

$$R = 1580(h_e/\lambda)^2 \text{ ohms} \tag{5}$$

The open circuit voltage is given by

$$V_{oc} = h_e E_n \tag{6}$$

where E_n is the total electric field normal to the aircraft skin when the slot is short-circuited.

Even though the information on the matching networks for these two antennas is not available, there must be some circuit elements at the driving points to provide impedance matching in the operating frequency range. For out-of-band operation, the impedances looking into the antennas through the matching networks would be high, and the short-circuit current across the observation terminals would be small. For EMP responses, it suffices to consider only the in-band frequency range (0.19 - 1.75 MHz), within which EMP energy is quite significant.

CHAPTER 3. AT-1076A/A UHF BLADE ANTENNA ON AABNCP

I. General Description

The UHF blade antennas are used for transmission and reception of vertically polarized signals in the frequency range 225 - 400 MHz (wavelengths ≈ 0.75 - 1.33 m). There are fourteen such antennas, externally mounted at various locations on the top center line and the bottom center line of the fuselage. The one undergoing the AABNCP low level testing is located at the bottom center line of the fuselage at station 690. The antenna, as shown schematically in Fig.1, has a height of 22.9 cm, a width of 8.7 cm and a maximum thickness of 1.9 cm. It operates as a capacitively top-loaded sleeve monopole, with a shunt stub forming a d.c. path from the upper part of the antenna to the aircraft skin. The stub thus provides protection to the transmitter and the receiver against large low-frequency excitations such as those due to EMP or lightning.

II. Analysis

The antenna is re-sketched in Fig.2(a) to show the salient features of the electrical connections. In the frequency range of interest, the potential is constant on each half of the antenna, i.e. points marked by D are at one potential and points marked by A are at another potential. An equivalent circuit of the antenna is shown in Fig.2(b). The three transmission lines with characteristic impedances Z_{01}, Z_{02}, Z_{03} are used as the transformer sections, as detailed in Fig.1. They provide impedance transformation for matching purposes. Another impedance matching arrangement is the small capacitance between points G and D. Within the frequency range of interest, this capacitance appears as a capacitive load between points F and D. The load is represented by the capacitance $C_e(\omega)$, the value of which can be evaluated by using transmission-line theory. The shunt stub, short-circuited at both ends, appears inductive across D and H and across A and H within the frequency range of interest. The resultant effect of this stub can therefore be represented by an inductance $L(\omega)$. It is obvious that the stub provides protection to the transmitter and receiver against large low frequency signals.

The capacitance C_p accounts for the effect contributed by the two metallic plates, separated by a dielectric spacer. Again, this capacitive

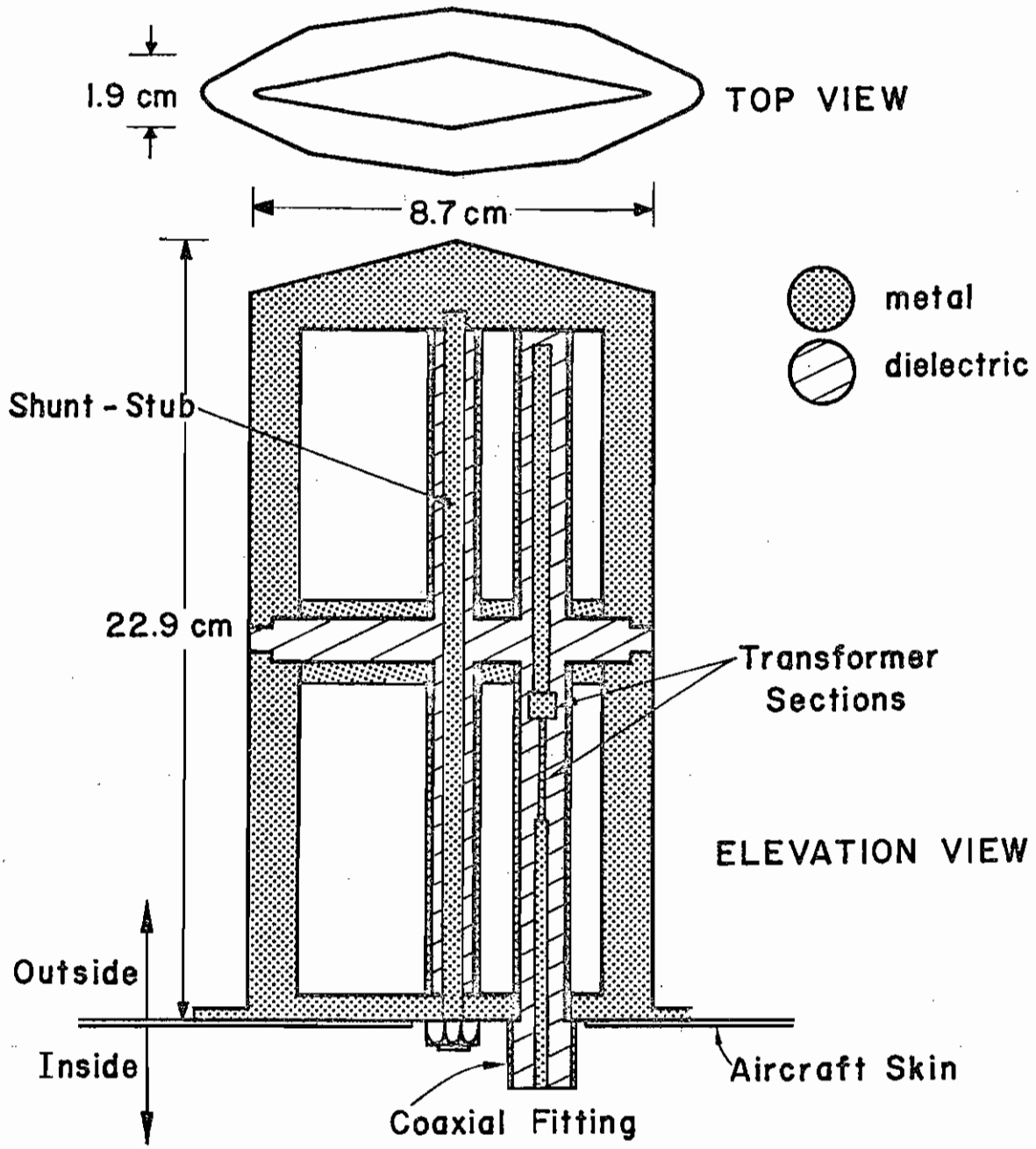

Fig.1 Schematic diagram of the UHF blade antenna.

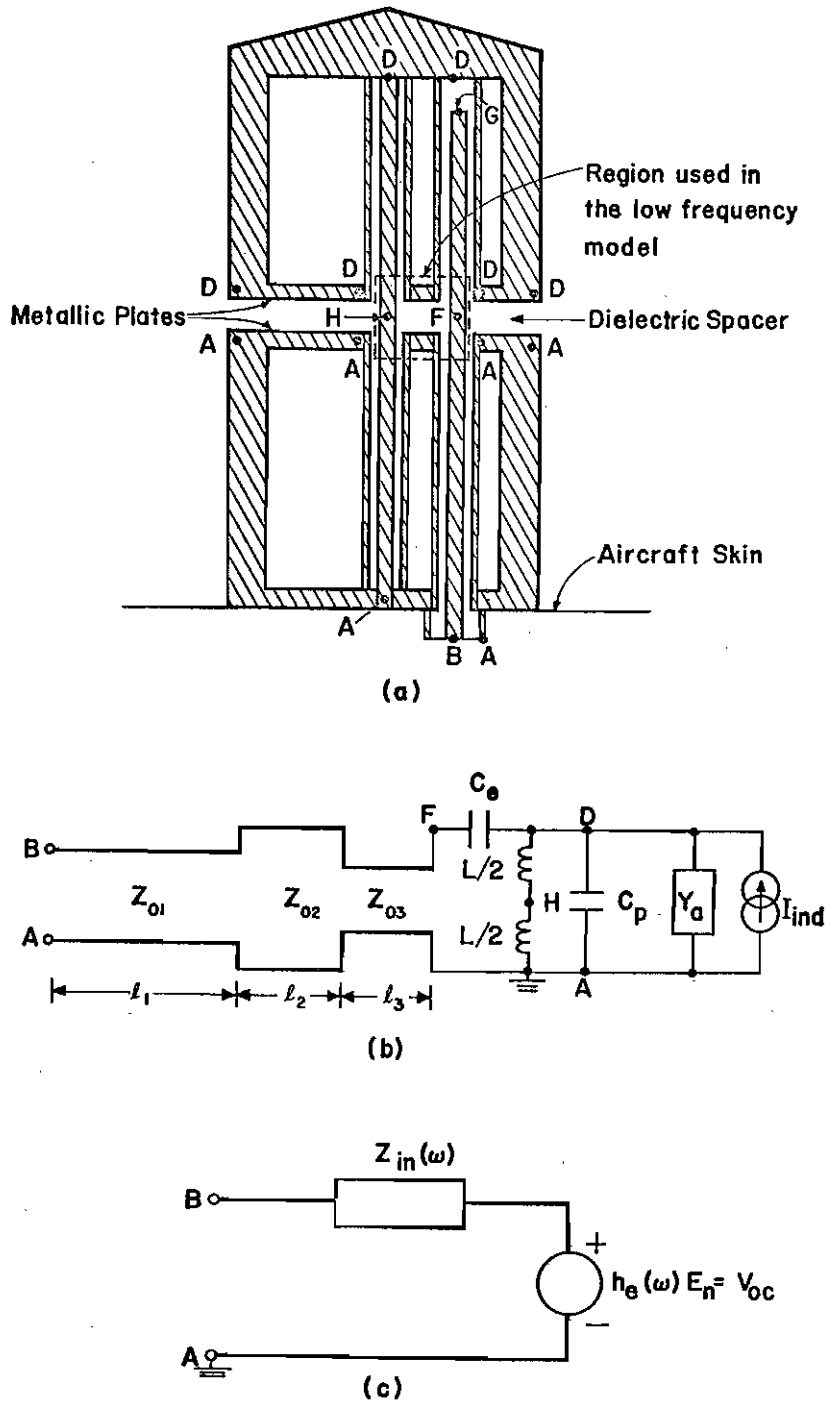

Fig.2 (a) The sketch of the blade antenna, showing electrical connections.
(b) The equivalent circuit and
(c) The Thevenin equivalent circuit at the terminals AB.

value can be adjusted for matching purposes. The radiating properties of the antenna is represented in the equivalent circuit by the external antenna admittance $Y_a(\omega)$, whose value can be obtained from the theory of the sleeve monopole. I_{ind} is the induced short-circuit current on the blade at the gap, and is given by

$$I_{ind} = j\omega E_n \, 3\varepsilon_o \pi ab[1-(b/a)^2][1-(c/a)^2]^{\frac{1}{2}}$$

$$\cdot[4(b/a)\{F(\phi\backslash\alpha) - E(\phi\backslash\alpha)]^{-1} \qquad (1)$$

where

$$\phi = \sin^{-1}[1-(c/a)^2]^{\frac{1}{2}}$$

$$\alpha = \sin^{-1}\left[\left(1-(b/a)^2\right)/\left(1-(c/a)^2\right)\right]^{\frac{1}{2}}$$

and E_n is the total electric field at the location (but in the absence) of the antenna, and is normal to the fuselage. In this case, a = 22.9 cm, b = 4.3 cm and c = 1.0 cm. Numerically,

$$I_{ind} = 6.67 \times 10^{-13} \, j\omega E_n \text{ amperes} \qquad (2)$$

The detailed derivation of I_{ind} has been presented in SSN 193.

The Thévenin equivalent circuit, as shown in Fig.2(c), is readily obtained by circuit analysis. The open-circuit voltage is expressed in terms of a complex equivalent height $h_e(\omega)$, which is defined by

$$V_{oc} = h_e(\omega) \, E_n \qquad (3)$$

Both the input impedance $Z_{in}(\omega)$ and the equivalent height $h_e(\omega)$ depend on the external antenna admittance $Y_a(\omega)$.

Low-frequency circuit model

At low frequencies, some otherwise negligibly small induced signals may become more significant. In Fig.3(a), we present a modified equivalent circuit to take into account these low-frequency contributions. One such contribution comes from the small region enclosed by the dashed lines in Fig.2(a). This region forms a small loop with a small inductance L_1 in series with the capacitive load C_e and the inductance L which represents the effect of the shunt stub. The voltage V_i induced in this loop is given by Faraday's law of induction and is related to the time derivative of the magnetic field normal to this loop.

Also, there will be some small but nonzero induced charges on the center conductor of the driving element of the antenna. These charges produce a current I_i, as shown in Fig.3(a), between the center conductor and the rest of the antenna, i.e., between F and D in Fig.2(a).

At low frequencies, the three transmission-lines (Fig.2(b)) can be represented by lumped elements as shown in the following way. Since the impedance Z_L looking into the right at FA is mainly capacitive and its magnitude is large, the input impedance of the driving transmission-line with length ℓ_3 is

$$Z_3 = Z_{03} \frac{Z_L + j\, Z_{03} \tan \beta\ell_3}{Z_{03} + j\, Z_L \tan \beta\ell_3}$$

$$\simeq \frac{1}{1/Z_L + j\omega C_3' \ell_3} \qquad (4)$$

where Z_{03} and β are the characteristic impedance and propagation constant of the transmission-line, respectively, and

$$C_3' = 1/c\, Z_{03}$$

is the distributed capacitance per unit length. Hence the influence of the transmission-line can be represented by a shunt capacitance C_{t3}. Since the resultant impedance of Z_L and this shunt capacitance still has a large magnitude, the other cascading transmission-lines can also be similarly represented by

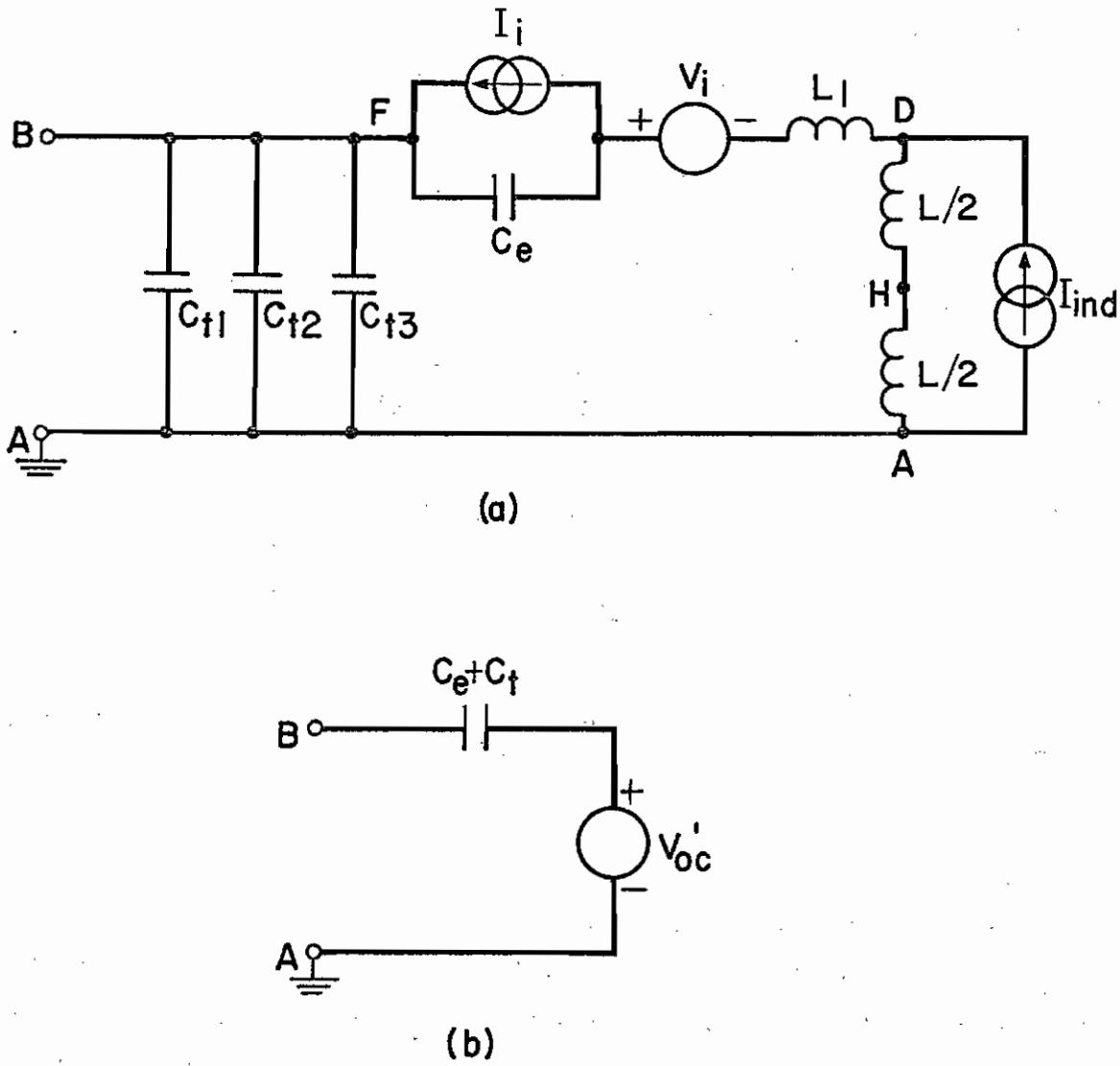

Fig.3 Low Frequency model of the blade antenna

(a) the equivalent circuit and

(b) the Thévenin equivalent circuit at the terminals AB.

lumped capacitances C_{t2} and C_{t1}.

The two remaining equivalent circuit elements in Fig.2(b), namely, the capacitance C_p and the admittance Y_a, have very small effect at low frequencies and can be neglected.

The low frequency Thévenin equivalent circuit is shown in Fig.3(b) where

$$Z'_{in} = 1/j\omega(C_e + C_t) \tag{5}$$

$$V'_{oc} = (1 + C_e/C_t)(j\omega L\, I_{ind} + V_i + I_i/j\omega C_e) \tag{6}$$

and

$$C_t = C_{t1} + C_{t2} + C_{t3}$$

In the above expressions, it is assumed that

$$1/j\omega C_e >> j\omega(L + L_1) \tag{7}$$

The low-frequency values of C_e and L are derived from transmission-line theory similar to that of (4).

III. Numerical Results

The model presented in Fig.3 is applicable only at very low frequencies. However, the valid approximation of (7) indicates that the addition of low frequency components in Fig.3 does not affect the input impedance appreciably compared to the model in Fig.2(b). Further, since the quantities V_i and I_i are associated with a very small area and a very small surface, respectively, their contribution would not be very significant, and the open circuit voltage given by Fig.2(c) is adequately accurate even at low frequencies. The numerical evaluation of $Z_{in}(\omega)$ and $h_e(\omega)$ is based on the model of Fig.2.

The admittance $Y_a(\omega)$ of the sleeve monopole is presented in Fig.4. Other circuit quantities are evaluated using the methods outline in section II.

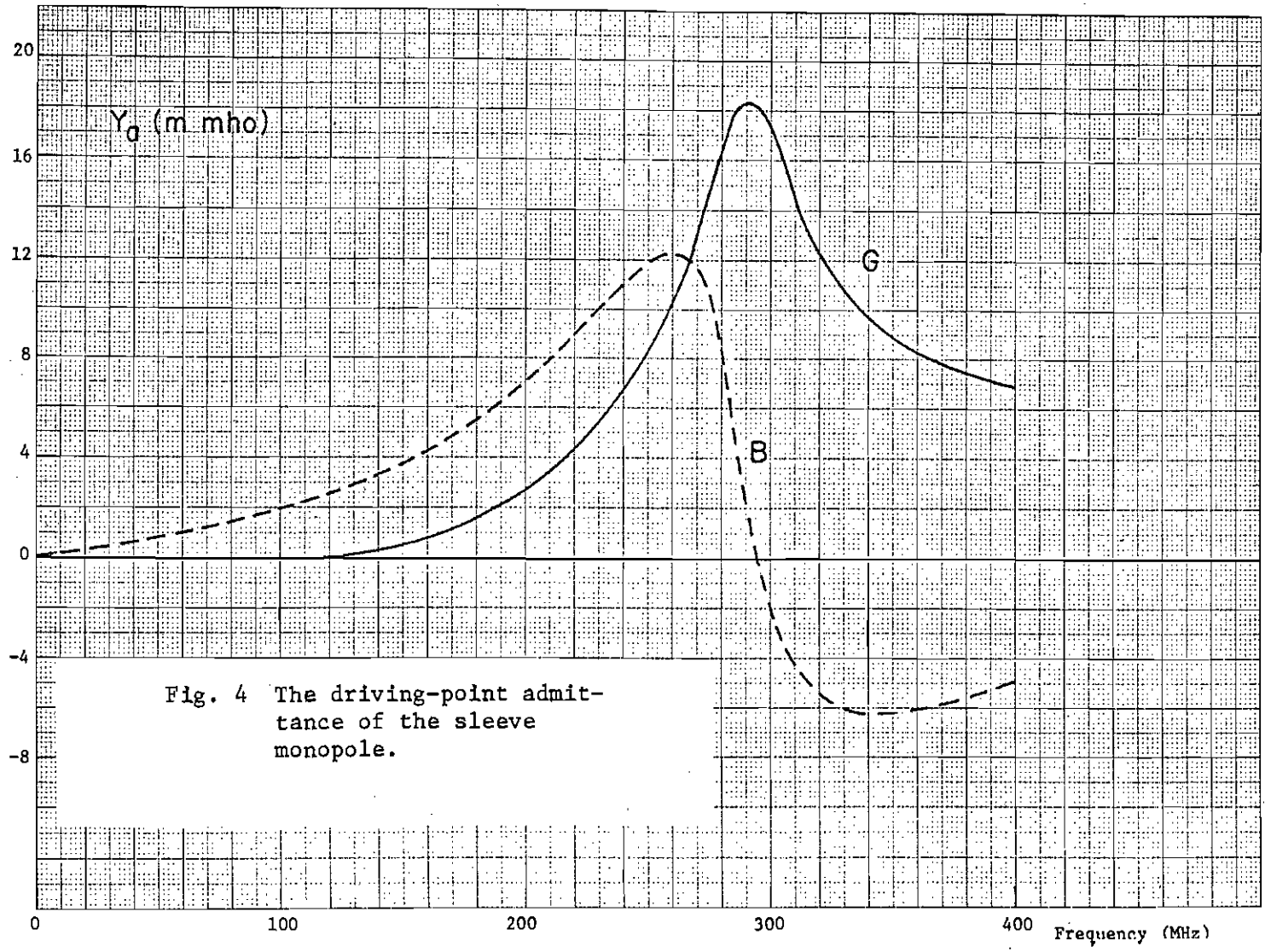

Fig. 4 The driving-point admittance of the sleeve monopole.

The input impedance is presented in Fig.5. We notice the reasonably well-matched impedance level at the in-band frequecy range and the striking mismatch at the out-of-band range. The complex equivalent height is presented in Fig.6.

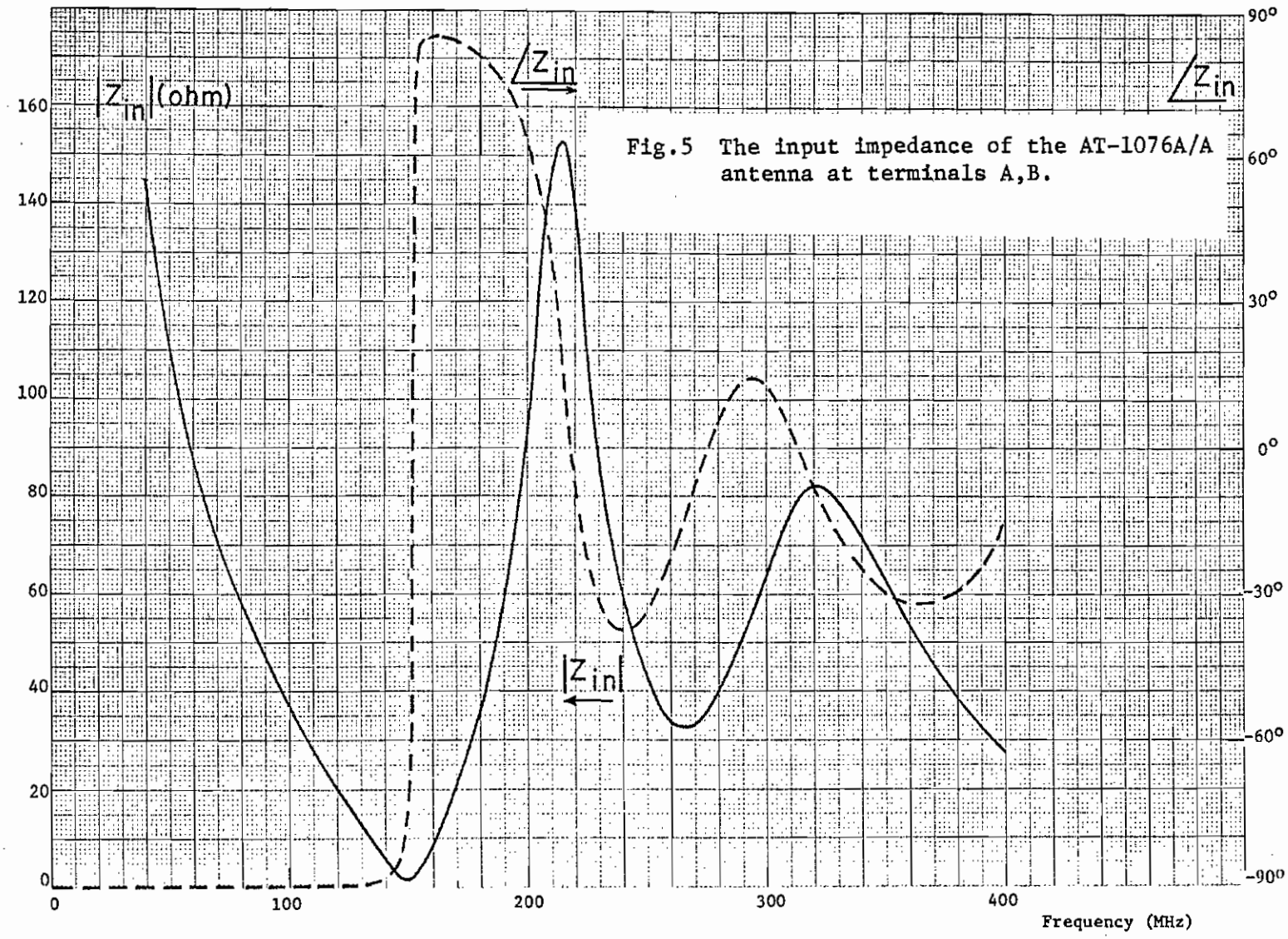

Fig.5 The input impedance of the AT-1076A/A antenna at terminals A,B.

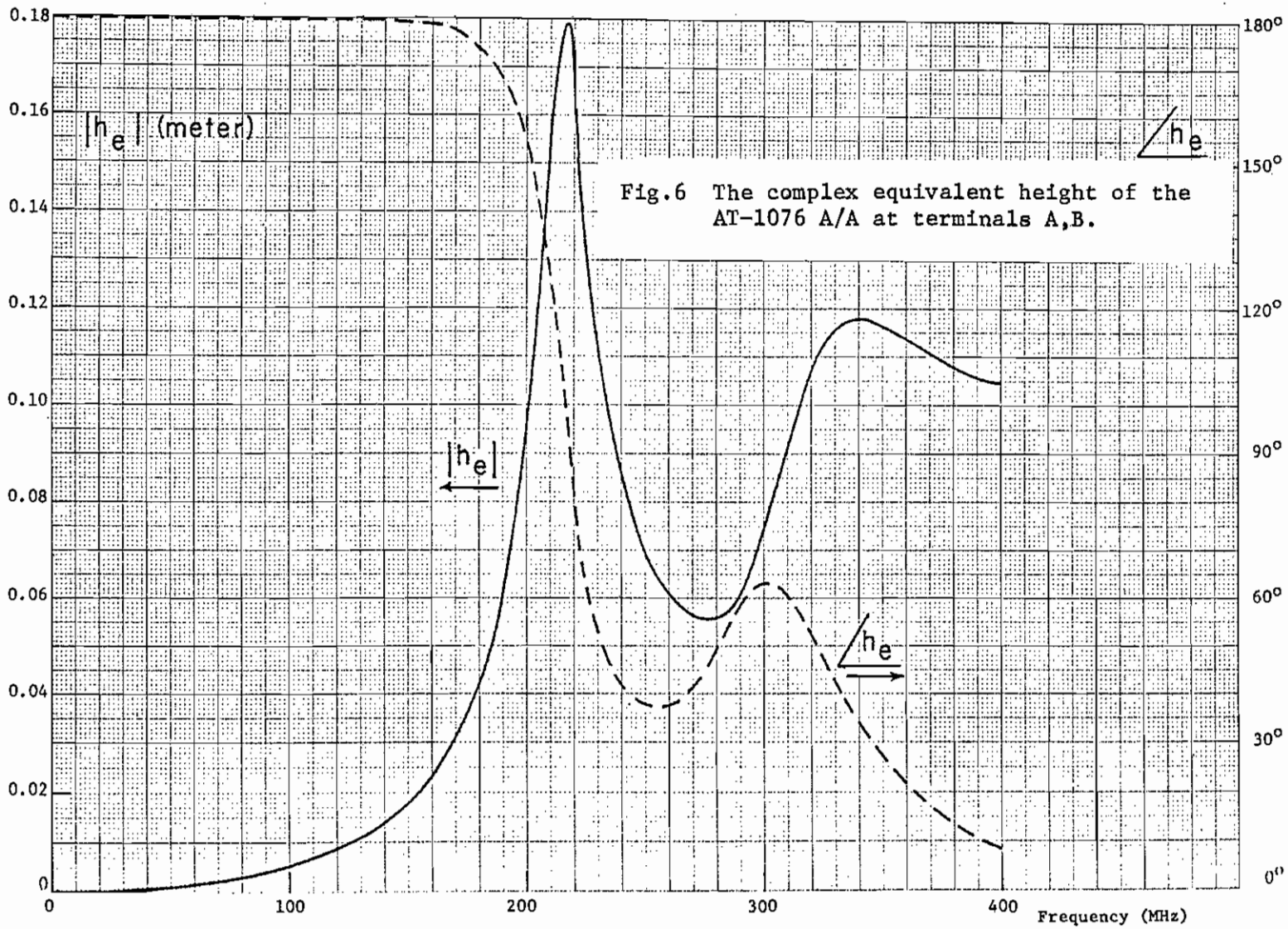

Fig.6 The complex equivalent height of the AT-1076 A/A at terminals A,B.

CHAPTER 4. HF WIRE ANTENNA ON THE AABNCP

I. General Description

The HF wire antenna is used for long range communication. It operates in the 2-30 MHz region (wavelengths, 10-150 meters). The antenna is of total length, 28.3 meters, and consists of a WS 25 U single conductor cable with polyethelene dielectric cover. The driving point is located at station 1328 on the top of the fuselage, and the termination is electrically connected to the vertical stabilizer at station 245. The antenna as it appears on the AABNCP is shown in Figure 1.

II. Analysis

For frequencies below the first major resonance of the loop formed by the HF wire, the fuselage, and the vertical stabilizer, coupling to the HF wire antenna may be approximated using the analysis of an electrically small loop. Hence the analysis presented in this chapter isvalid for frequencies below about 1.5 MHz. For frequencies near or above 1.5 MHz, the HF wire antenna cannot be considered as an electrically small loop. The problem of determining the coupling to this antenna for these higher frequencies is a complex boundary value problem. This boundary value problem requires consideration of the interaction of the HF wire with the total aircraft structure. The analysis of this antenna above 1.5 MHz is presently being investigated and may appear as a future Interaction Note.

The triangular loop formed by the HF wire antenna, the fuselage, and the vertical stabilizer is shown in Figure 2 along with the appropriate dimensions. The radius of this effective loop is assumed to be the radius of the HF wire antenna itself. The restriction imposed for small loop analyses may be used to determine the approximate upper limit of the frequencies which may be considered. This restriction requires that the largest dimension of the loop measured from its terminals (points A-B in Figure 2) must be less than or equal to approximately one-seventh of the

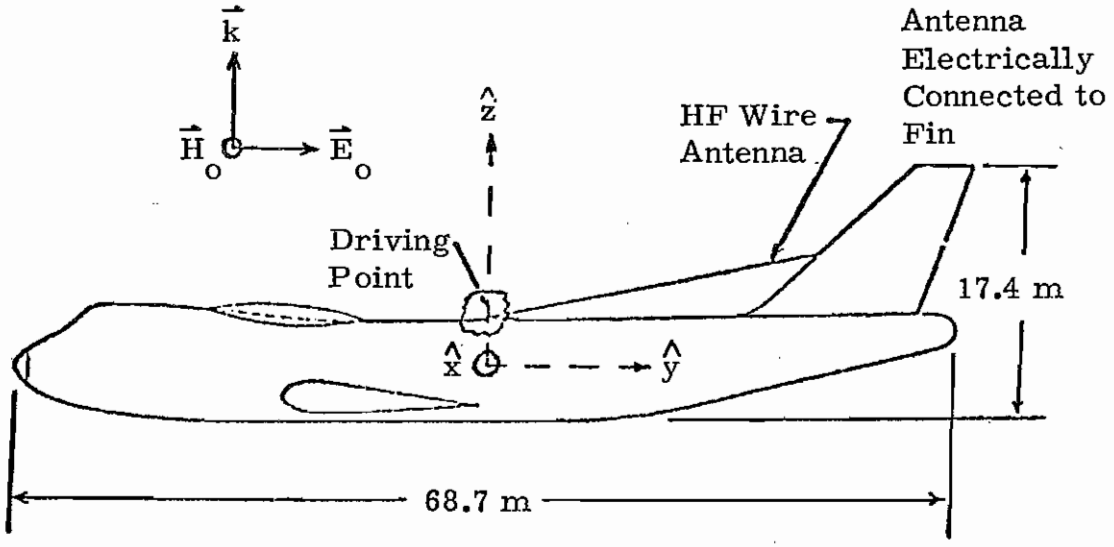

SCHEMATIC DIAGRAM

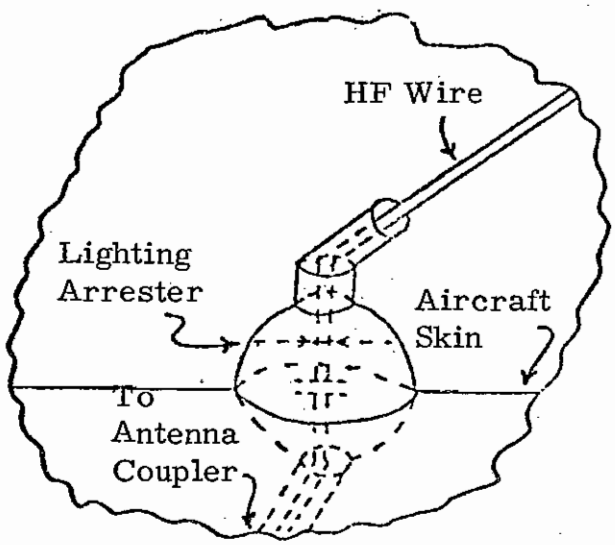

DRIVING POINT CONFIGURATION

FIGURE 1

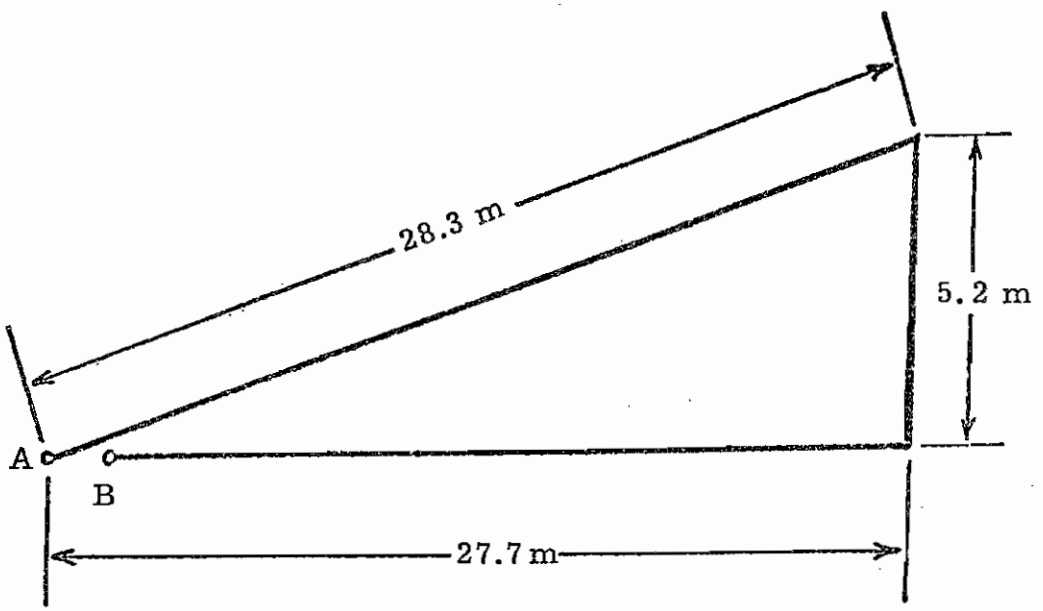

EFFECTIVE LOOP

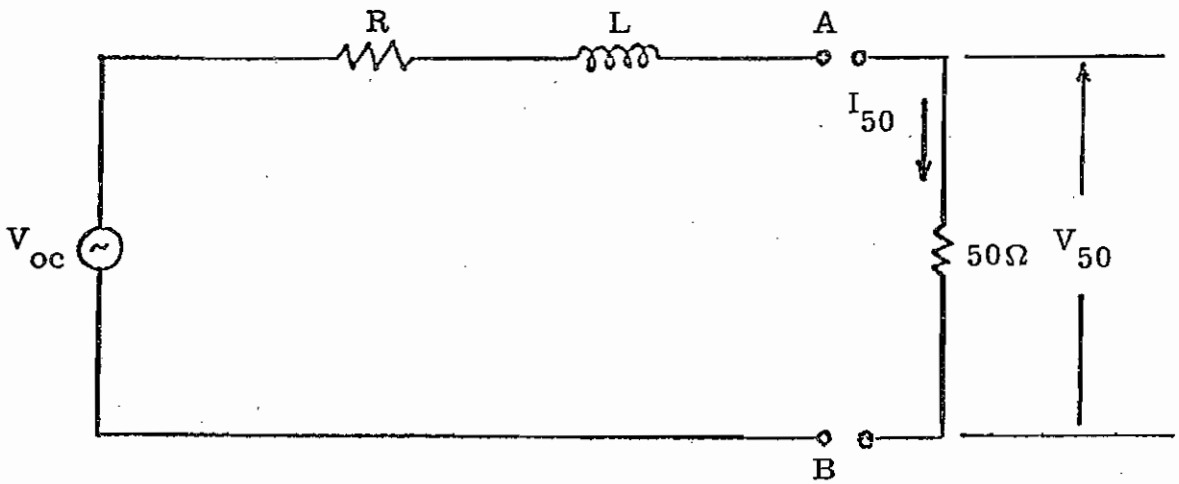

EQUIVALENT CIRCUIT

FIGURE 2

smallest wavelength to be considered in the analysis. For the loop containing the HF wire antenna, the largest dimension, d_{max}, is approximately 28 meters. Hence,

$$\frac{d_{max}}{\lambda_{min}} \leq \frac{1}{7} \tag{1}$$

or

$$f_{max} \leq \frac{c}{7d_{max}}, \tag{2}$$

and

$$f_{max} \leq 1.5 \text{ MHz} \tag{3}$$

Therefore, since this analysis uses the small loop approximations, it will not be valid above about 1.5 MHz.

According to the standard expressions for electrically small loops, the radiation resistance is given as

$$R \simeq 320\pi \left(\frac{A}{\lambda^2}\right)^2 \Omega \text{ (ohms)} \tag{4}$$

where A is the effective area of the loop in meters^2 and λ is the wavelength in meters. For this loop, the effective area is

$$A \simeq \frac{1}{2}(28\text{m})(5\text{m}) = 70 \text{ m}^2 \tag{5}$$

Then R may be written as a function of frequency,

$$R(f) \simeq \frac{320\pi^4}{c^4} A^2 f^4 \ \Omega \text{ for } f \leq 1.5 \text{ MHz}, \tag{6}$$

or

$$R(f_{MHz}) \simeq 20 f_{MHz}^4 \times 10^{-3} \ \Omega \text{ for } f_{MHz} \leq 1.5 \tag{7}$$

The inductance of a small loop is related to the loop size (perimeter) and the radius of the wire forming the loop. This inductance may be written as

$$L \simeq \mu_o \frac{p}{2\pi} \ell n \frac{p}{2\pi a} \tag{8}$$

where p is the loop perimeter in meters, a is the radius of the loop wire in meters, μ_o is the free space permeability in farads/meter, and L is the inductance in henrys. For the loop under consideration,

$$L \simeq (4\pi \times 10^{-7}) \frac{61.2}{2\pi} \ell n \frac{61.2}{2\pi(0.002)} \text{ henrys}, \tag{9}$$

or

$$L \simeq 104 \ \mu\text{henrys for } f \leq 1.5 \text{ MHz}. \tag{10}$$

The input impedance, Z_{in}, looking into terminals A-B in Figure 2 is

$$Z_{in} = R + j\omega L . \tag{11}$$

For this loop

$$Z_{in}(f_{MHz}) = 20 \times 10^{-3} f_{MHz}^{4} + j 653 f_{MHz} \Omega \text{ for } f_{MHz} \leq 1.5 . \tag{12}$$

The equivalent circuit to determine the coupling into the loop is shown in Figure 2. The circuit elements are evaluated according to the equations given above. The open-circuit voltage is determined from the effective loop area and the local fields near the loop. These local fields must be calculated using an aircraft model or must be measured in the test environment. The open-circuit voltage is given as

$$V_{oc} \simeq -j\omega B_T A_{eff} , \tag{13}$$

where A_{eff} is the effective area of the loop in meters^2 and B_T is the component of the total magnetic flux density normal to the loop. (NOTE: B_T must be known from previous theoretical or experimental determinations of the local fields on or near the airframe in the immediate vicinity of the antenna itself.)

The open-circuit voltage, V_{oc}, actually represents a pair of voltage sources in series. The magnetic field normal to the loop is enhanced by the presence of the large cylindrical current-carrying fuselage. This field enhancement comes from two distinct considerations. First, incident electric field components along either the fuselage, wings, or vertical stabilizer induce currents on the fuselage. These currents on the fuselage produce circumferential magnetic fields around the fuselage and consequently through the loop under consideration. The voltage induced in the loop, $V_{ind}^{(1)}$, by this means is given by

$$V_{ind}^{(1)}(\omega) = j\omega\mu_o \iint_{\substack{\text{loop}\\\text{area}}} H_\phi^{(1)}(\omega)\, dA\,, \tag{14}$$

where

$$H_\phi^{(1)}(\omega) = \frac{I_{max}(\omega)}{2\pi r}\,, \tag{15}$$

and r is the cylindrical coordinate measured outward normal from the axis of the cylindrical fuselage. $I_{max}(\omega)$ is the magnitude of the current induced on the fuselage (assumed to be a uniform current distribution) as a function of frequency. The second consideration in the enhancement of the magnetic field normal to the loop is the actual distortion of the incident magnetic field due to the presence of the fuselage. The voltage induced in the loop, $V_{ind}^{(2)}$, by this means is given by

$$V_{ind}^{(2)}(\omega) = j\omega\mu_o \iint_{\substack{\text{loop}\\\text{area}}} H_\phi^{(2)}(\omega)\, dA \tag{16}$$

where $H_\phi^{(2)}(\omega)$ can be approximated as the solution to the magnetostatic problem of the perfectly conducting infinite cylinder immersed in and perpendicular to a uniform magnetic field.

The expression for $H_\phi^{(2)}(\omega)$ may be written as

$$H_\phi^{(2)}(\omega) = \left(1 + \frac{a^2}{r^2}\right) H_o(\omega)\cos\phi \tag{17}$$

where $H_o(\omega)$ is the magnitude of the uniform magnetic field surrounding the conducting cylinder.

III. Numerical Results

In order to simplify the discussion of the actual coupling to the loop, suppose a cartesian coordinate system is superimposed on the aircraft in flight as indicated in Figure 1. To determine the sign of the voltage, $V_{ind}^{(1)}$, the convention shall be adopted that currents induced along the fuselage in the positive y-direction generate a positive potential drop from terminal A to terminal B. Similarly, $V_{ind}^{(2)}$ shall be positive from A to B when the incident magnetic field, $\vec{H}_o$, is in the positive x-direction. Consequently the incident fields as oriented in Figure 3 induce additive voltages across terminals A-B.

The model considered here is useful only at those frequencies below the resonance of the loop where the loop may be considered electrically small. The input impedance as defined by equation (12) is plotted as a function of frequency in Figure 3.

As indicated in the previous section, the open-circuit voltage source, V_{oc}, may be approximated as a pair of voltage sources in series. The magnitudes of the two sources are determined by evaluating the integrals given in equations (14) and (16). These two voltage sources are defined as follows:

$$V_{ind}^{(1)}(\omega) \simeq j(16)\left(\frac{\omega\mu_o}{2\pi}\right) I_{max}(\omega) , \tag{18}$$

or

$$V_{ind}^{(1)}(f_{MHz}) \simeq j\,20\, f_{MHz} I_{max}(f_{MHz}) ; \tag{19}$$

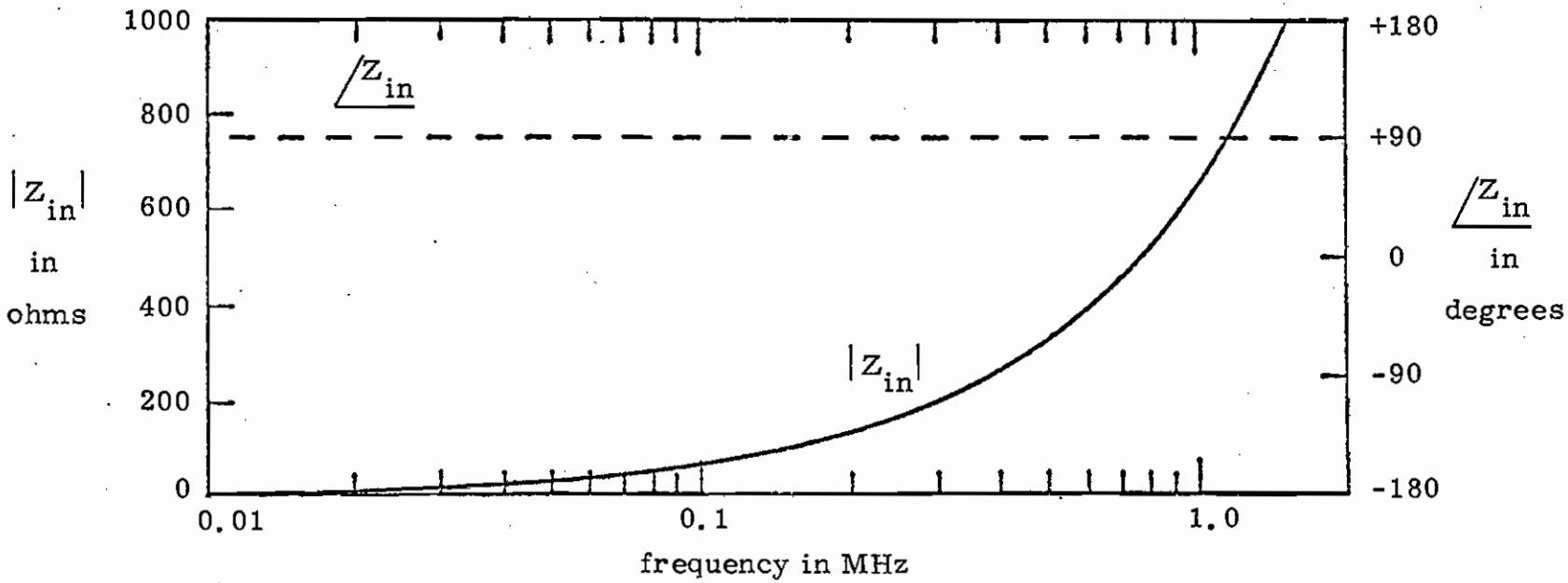

INPUT IMPEDANCE

FIGURE 3

and

$$V_{ind}^{(2)}(\omega) \simeq j(107)\left(\frac{\omega\mu_o}{\eta_o}\right) E_o(\omega) , \tag{20}$$

or

$$V_{ind}^{(2)}(f_{MHz}) \simeq j2.24 f_{MHz} E_o(f_{MHz}) \tag{21}$$

From equations (18) and (20) it is possible to define two parameters useful in representing the coupling to the loop. The inductive magnetic coupling coefficient, $\mathcal{L}$, is defined as

$$V_{ind}^{(1)}(\omega) \simeq j\omega\mathcal{L} I_{max}(\omega) \tag{22}$$

Hence, using equation (18),

$$\mathcal{L} \simeq 3.2\ \mu\text{henrys} \tag{23}$$

The effective area of the loop is defined as

$$V_{ind}^{(2)}(\omega) = j\omega\mu_o H_o A_{eff} \tag{24}$$

From equation (20),

$$A_{eff} \simeq 107\ m^2 . \tag{25}$$

Finally, it is desired to determine the voltage across a 50Ω resistive load attached across the antenna terminals A-B. Figure 4 presents the magnitude of the ratio of the 50Ω load voltage, V_{50}, to the open circuit voltage, V_{oc}.

IV. Conclusions

For frequencies below about 1.5 MHz the HF wire antenna has been modeled as an electrically small loop antenna. An equivalent circuit representation and appropriate lumped element values have been determined and presented. As expected, the radiation resistance increases rapidly with frequency. However, it is negligible when compared to the high inductive reactance of the loop over the frequency range of interest. It is demonstrated that at relatively low frequencies, $f \leq 10$ KHz, almost all of the voltage induced in the loop appears across the 50Ω load resistance. As frequency increases, the voltage across the 50Ω load decreases and represents less than 10% of the voltage induced in the large loop for frequencies near 1 MHz.

For frequencies near or above 2 MHz, the HF wire antenna cannot be considered as electrically small. The problem of coupling to this antenna in-band and above-band is a complex boundary value problem. This boundary value problem is currently being investigated and may appear as a future Interaction Note.

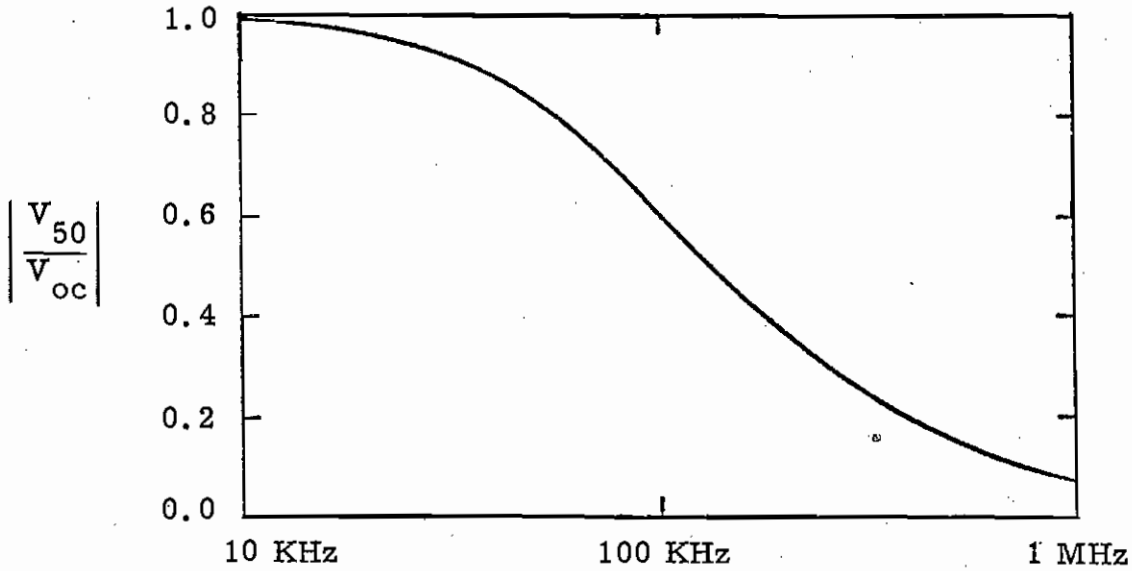

VOLTAGE ACROSS 50 Ω LOAD

FIGURE 4

CHAPTER 5. B559 & B561 GLIDE SLOPE TRACK ANTENNA ON AABNCP

I. General Description

The two glide slope track antennas are installed on the front edges of the aft nose wheel doors of the aircraft. They are used for the reception of horizontally polarized signals in the frequency range 329-335 MHz (wavelength ≃ 0.90 - 0.91 m) after the landing gear is lowered on the approach. The track antenna, as shown schematically in Fig.1, is in the form of a planar slot with maximum dimensions 20.3 cm × 3.8 cm. The antenna is sandwiched between two dielectric boards, each with a thickness of 0.3 cm and a relative dielectric constant 3.5.

II. Analysis

The relationship between the input impedance Z^s_{in} of a slot antenna and the input impedance Z^d_{in} of the complementary dipole antenna is well-known, and is given by

$$Z^s_{in}\, Z^d_{in} = \frac{1}{4} Z_o^2 \tag{1}$$

where Z_o is the intrinsic impedance. We will derive the input impedance Z^s_{in} of the track antenna by first finding that of the more familiar dipole antennas, i.e., Z^d_{in}.

The track antenna is re-sketched in Fig.2(a), with its complementary antenna shown in Fig.2(b). The complementary antenna is a planar folded dipole antenna, loaded at both ends by two metal strips. The analysis can be carried out by decomposing the voltage and current into a symmetric mode, as shown in Fig.3(b), and an antisymmetric mode, as shown in Fig.3(c).

The symmetric mode is easily identified as the main contributor to the radiation. For this mode the currents on both branches are identical; so one can replace this structure by its equivalent dipole antenna (Fig.3(d)), loaded at both ends, and with an effective wire radius given by

$$a_{eff} = \frac{1}{2}(wd)^{\frac{1}{2}} \tag{2}$$

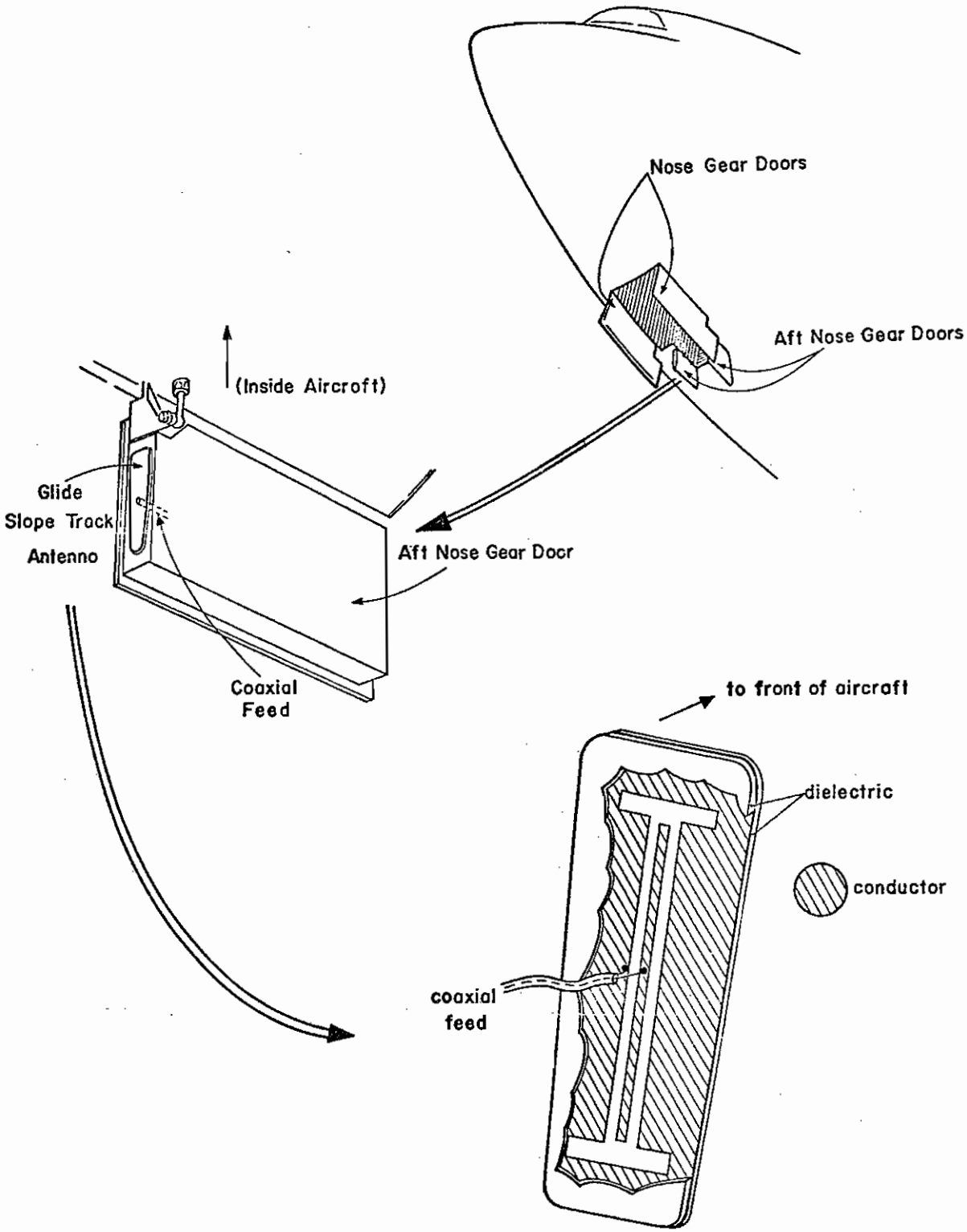

Fig.1 Location and schematic diagram of the track antenna.

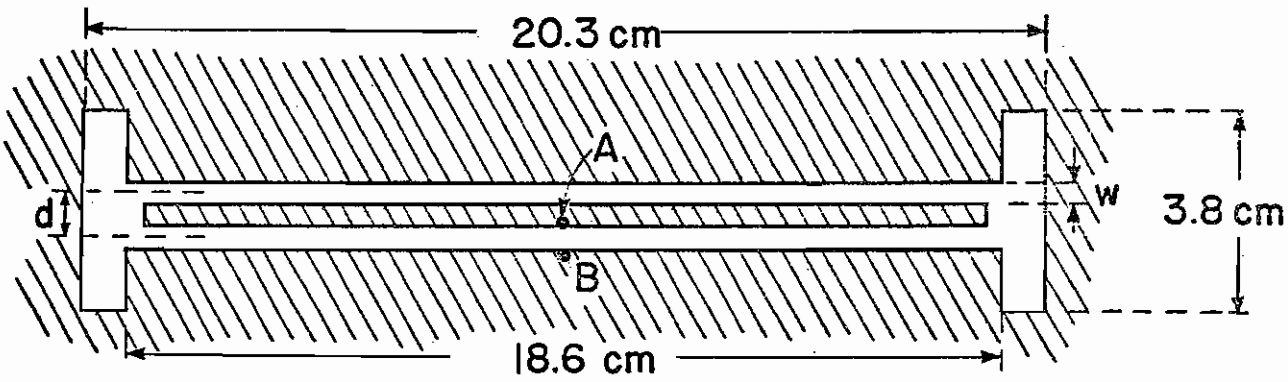

(a)

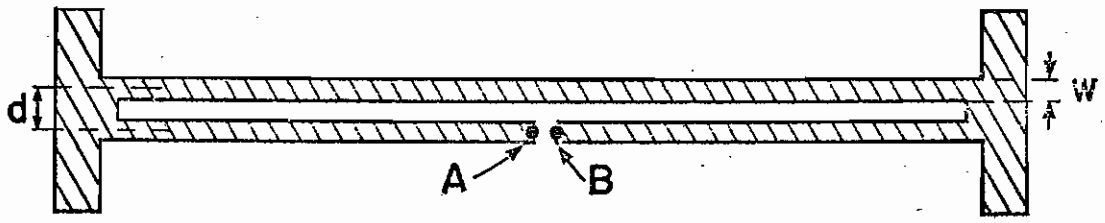

(b)

Fig.2. (a) The glide slope track antenna and
(b) its complementary folded dipole antenna.

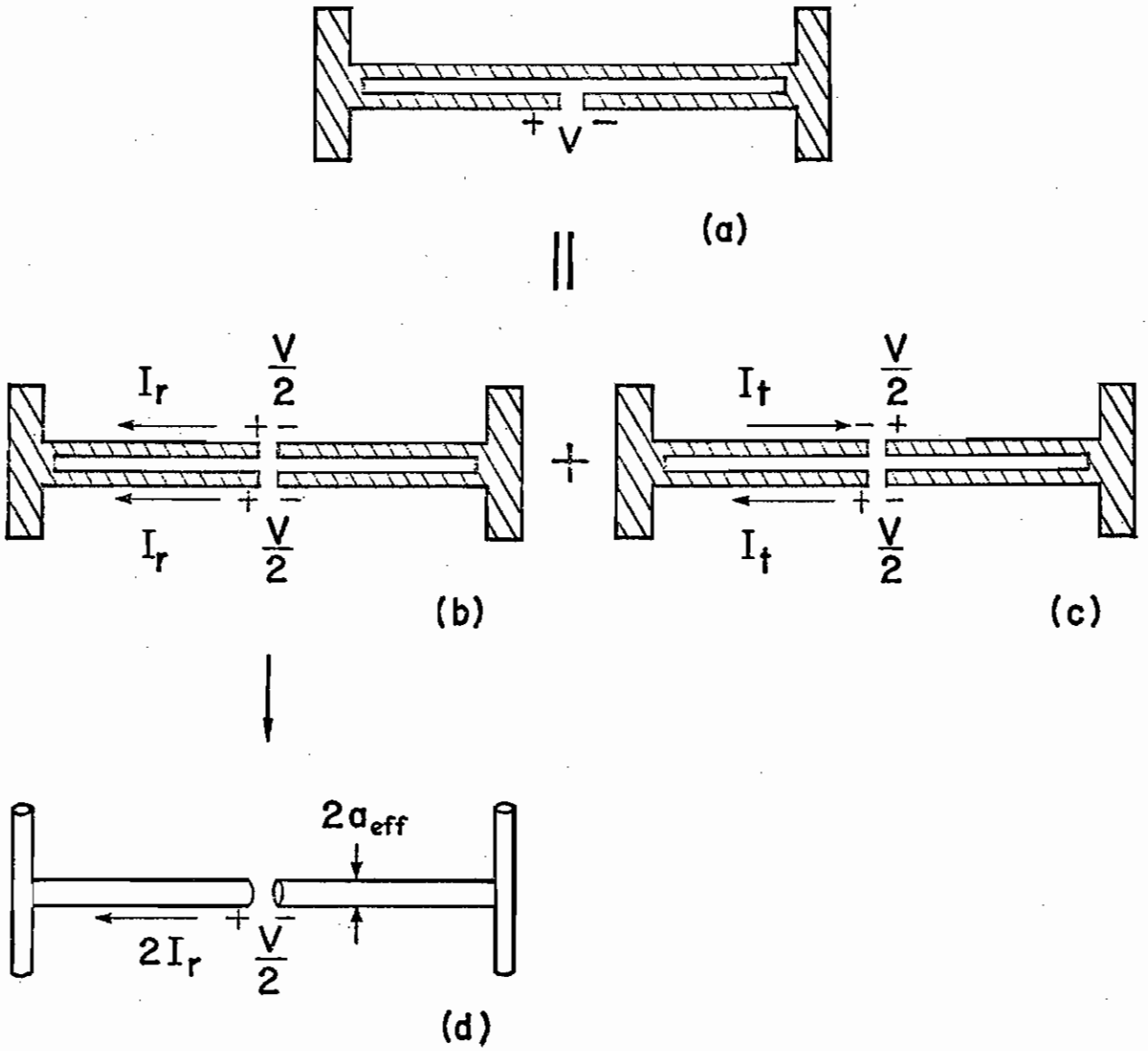

Fig.3. The complementary folded dipole antenna, shown in (a), can be decomposed into (b) a symmetric mode and (c) an anti-symmetric mode. The symmetric mode can also be represented by an equivalent dipole antenna in (d).

where, as shown in Fig.2(b), w is the width of the strip and d is the distance between the two strips. The input impedance Z_r for the symmetrical or radiation mode can thus be evaluated from dipole antenna theory, and is given by

$$Z_r = (V/2)/(2I_r) \tag{3}$$

The antisymmetric mode is basically a transmission-line mode and contributes little to the radiation. The impedance Z_t looking into either short-circuited transmission-line at the voltage source points is given by

$$Z_t = V/2I_t \tag{4}$$

and from transmission-line theory

$$Z_t = j\, Z_c \tan \beta \ell \tag{5}$$

where Z_c and β are the characteristic impedance and the propagation constant, respectively, of the transmission line. Specifically,

$$Z_c = Z_o \frac{K(m)}{K(m_1)} \tag{6}$$

where

$$m = \left(\frac{2d-w}{2d+w}\right)^2$$

$$m_1 = 1 - m$$

and $K(m)$ is the complete elliptic integral of the first kind. Equation (6) has been obtained by conformal mapping and its detailed derivations have been reported in an Interaction Note (IN 182).

The input impedance of the complementary folded dipole antenna is

$$Z_{in}^{d} = V/(I_r + I_t)$$

$$= \left(\frac{1}{4Z_r} + \frac{1}{2Z_t}\right)^{-1} \tag{7}$$

In the frequency range of interest, i.e., from d.c. to 400 MHz, the equivalent dipole antenna and the transmission-lines are considerably less than a quarter wavelength; hence Z_t is a purely inductive quantity, and Z_r has a negative imaginary part. The equivalent circuit of the complementary folded dipole is presented in Fig.4(a), with the sources to be described later.

The input impedance of the track antenna is given by (1) and (7)

$$Z_{in}^{s} = \frac{1}{4} Z_o^2 \left(\frac{1}{4Z_r} + \frac{1}{2Z_t}\right) \tag{8}$$

Now, the first term in (8) contains a positive imaginary part and represents an inductive quantity, whereas the second term is purely capacitive. The equivalent circuit can be viewed from Fig.3(b) together with the induced sources which are now detailed.

We will first examine the induced sources on the complementary folded dipole. As shown in Fig.4(a), the folded dipole has two induced voltage sources. The one denoted by V_{ind}^{d} is twice that of the induced voltage in the equivalent dipole antenna (Fig.3(d)), i.e.,

$$V_{ind}^{d} = 2\, h_e^{d}\, E_t \tag{9}$$

where h_e^{d} is the effective height of the equivalent dipole antenna and E_t the total incident electric field parallel to the dipole antenna as shown in Fig.4(a). This result is readily obtained by decomposing the antenna currents and voltages into symmetric and anti-symmetric modes as we did in the derivation of the impedance. The other source V_i^{d} is attributed to the voltage induced in the loop (Fig.3(d)) formed by the two sections of the short-circuited transmission-lines, and

$$V_i^{d} = -j\omega B_n\, A \tag{10}$$

where B_n is the total incident magnetic field normal to the loop with area A. Except at low frequencies, the open circuit voltage across A' B' is mainly

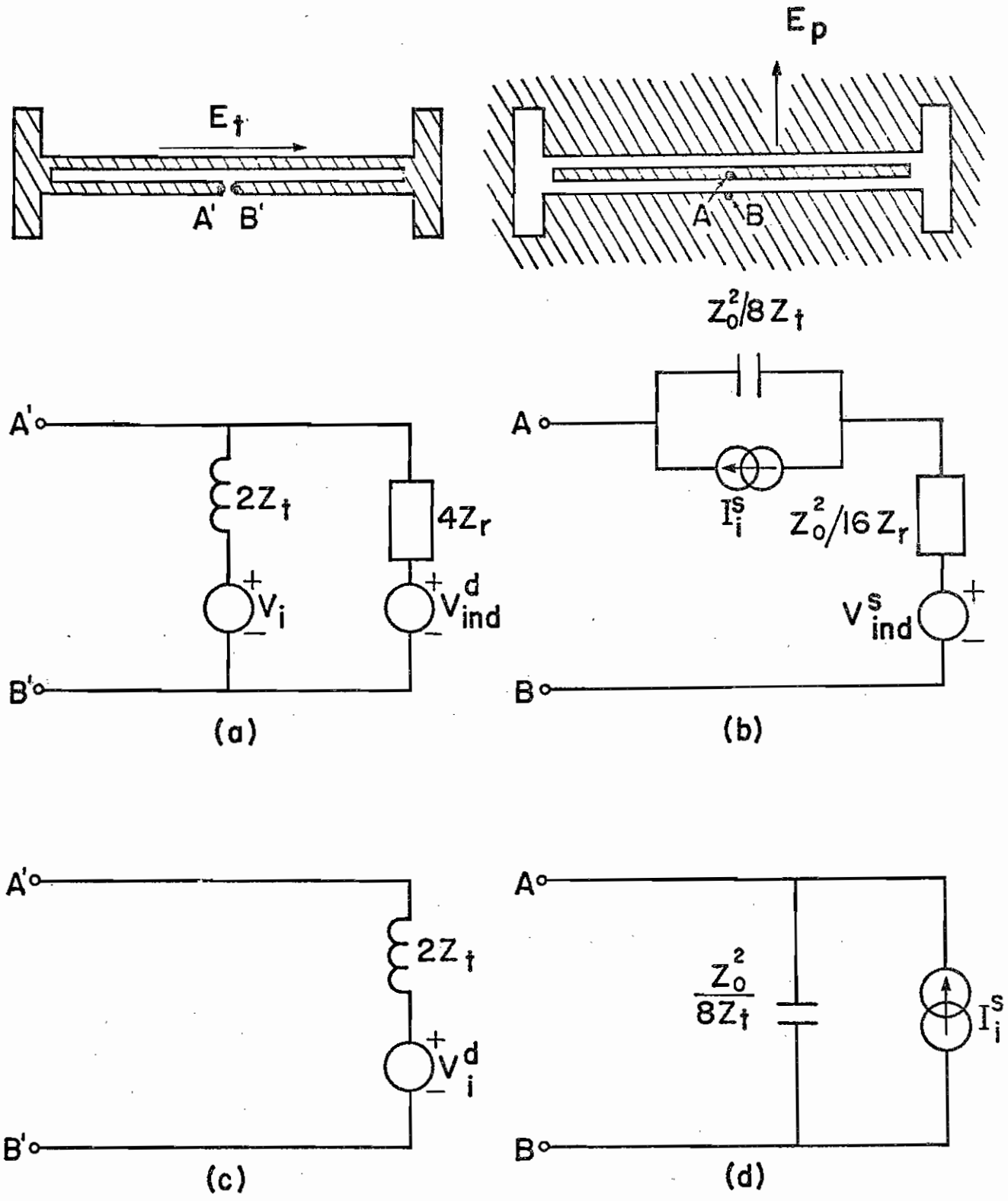

Fig.4. Equivalent circuits for (a) the complementary folded dipole antenna and (b) the track antenna. Also low-frequency equivalent circuits for (c) complementary folded dipole antenna, and (d) the track antenna.

contributed by V^d_{ind}.

The induced sources of the track antenna are shown in Fig.4(b). In this case, the counter part of V^d_i is I^s_i, given by

$$I^s_i = j\omega\varepsilon\, E_n\, A_{eq} \tag{11}$$

where E_n is the total electric field normal to the slot antenna when the slot is short-circuited and A_{eq} is the equivalent area of this configuration (see IN 89 and IN 92). The other source term V^s_{ind} is related to an effective height h^s_e for the track antenna by the following relationship

$$V^s_{ind} = h^s_e\, E_p \tag{12}$$

where V^s_{ind} is the counter part of V^d_{ind} of the complementary folded dipole antenna and E_p is the incident electric field in the plane of the antenna but perpendicular to the long-side of the track antenna, as shown in Fig.4(b). It is found that the effective height h^s_e is given by

$$h^s_e = h^d_e(Z_o/Z_r) \tag{13}$$

where Z_r has been previously defined. The derivation of (13) may be reported in a future Interaction Note and is briefly outlined here. From Maue's integral formulation of Maxwell's equations, it is observed that $\frac{1}{2} V^s_{ind}$ of the track antenna is the dual of I^d_{ind} of the complementary equivalent dipole antenna, where $I^d_{ind} = V^d_{ind}/Z_r$. Further duality between $\mu\underline{H}^{inc}$ in the track antenna problem and $-\varepsilon\underline{E}^{inc}$ in the complementary dipole antenna problem, together with (9) and (12) yields the result of (13).

At low frequencies one sees essentially a small loop in the complementary folded dipole antenna. This is equivalent to neglecting Z_r and V^d_{ind}, which have very small influence. This low-frequency equivalent circuit is presented in Fig.4(c). Similarly, at low frequencies, the essential contribution of the track antenna is due to the current source term I_i and the low-frequency equivalent circuit is presented in Fig.4(d).

III. Numerical Results

The input impedance Z_{in}^{s} of the track antenna is calculated from (8), where Z_t is given by (5) and (6) and Z_r is the impedance for the equivalent dipole antenna with end loads. In Fig.5, $Z_{in}^{s}(\omega)$ is plotted against frequency. It is evident that the track antenna is a relatively narrow band device. The open-circuit voltage $V_{oc}(\omega)$ at the terminals A B of the track antenna, from Fig.4(b), is approximately equal to V_{ind}^{s}, since I_i^s is in general a much smaller quantity (except at low frequencies), i.e.

$$V_{oc}(\omega) = V_{ind}^{s} = h_e^s E_p \tag{14}$$

The complex effective height $h_e^s(\omega)$ is presented in Fig.6.

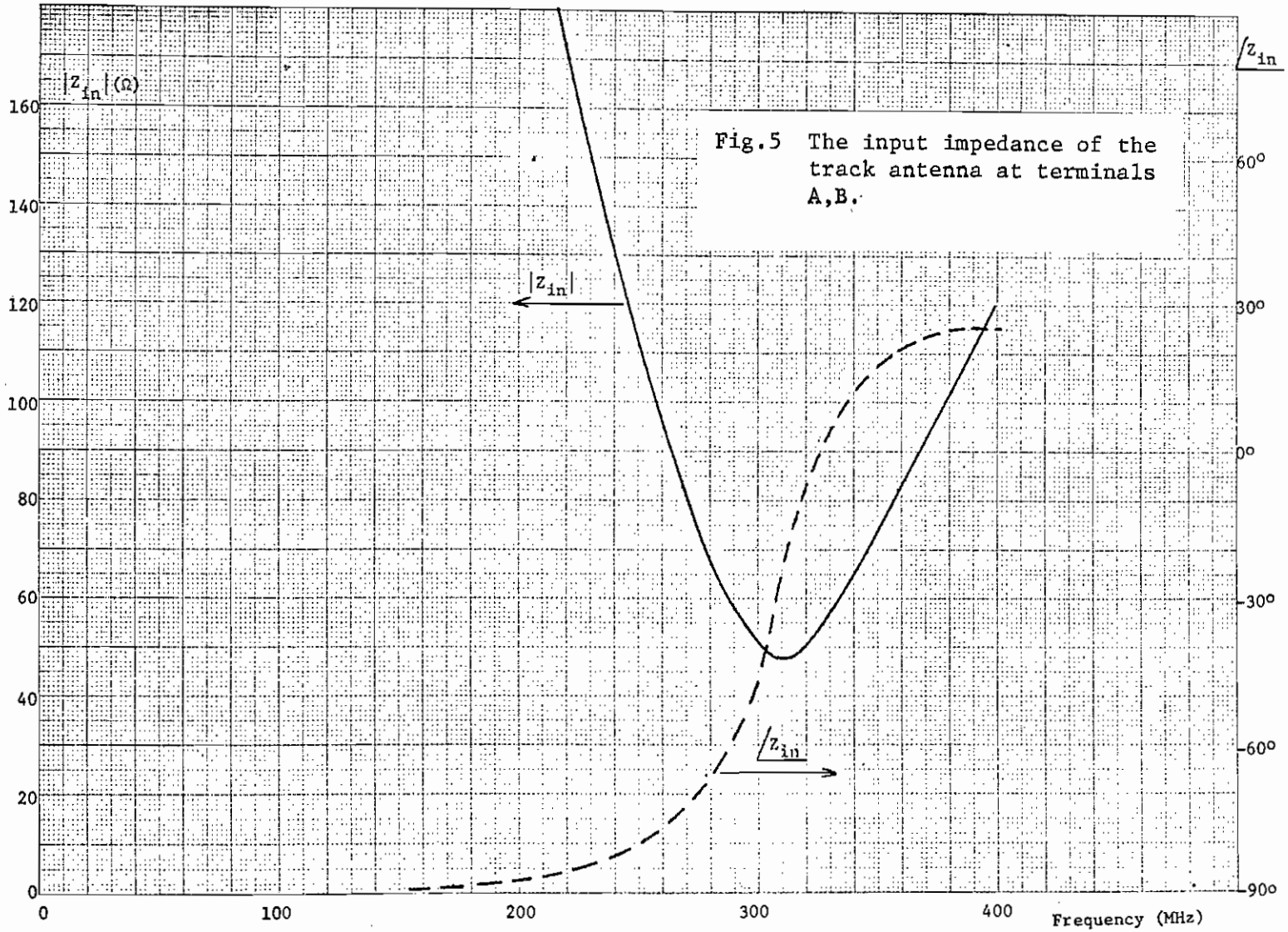

Fig.5 The input impedance of the track antenna at terminals A,B.

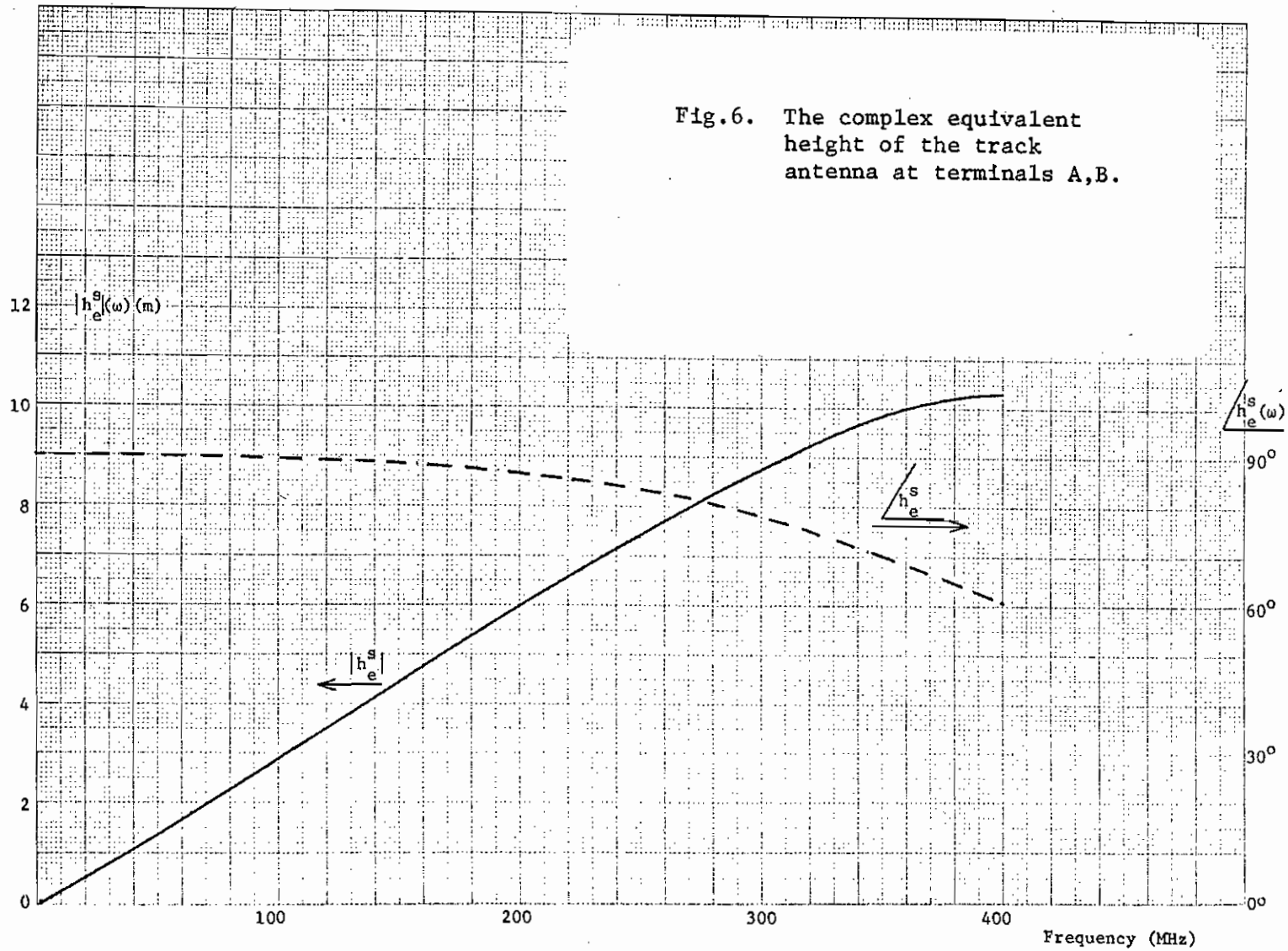

Fig.6. The complex equivalent height of the track antenna at terminals A,B.

CHAPTER 6. B558 GLIDE SLOPE CAPTURE ANTENNA ON AABNCP

I. General Description

There are two sets of glide slope capture antenna arrays on the AABNCP, each set consisting of two slot antennas. The arrays are flush mounted at the two aft nose gear doors. These antennas are used to receive the horizontally polarized signals in the frequency range 329 - 335 MHz (wavelengths $\approx$ 0.90 - 0.91 m) when the gear doors are closed. The capture antennas, as shown schematically in Fig.1, consist of a planar slot with dimensions 12.2 cm $\times$ 1.3 cm. The slot is capacitively coupled to a microstrip transmission-line via a tuning slug capacitor. The microstrip line itself also forms part of the impedance matching network, and is sandwiched between two dielectric boards each with a thickness of 0.3 cm and a relative dielectric constant of 3.5.

II. Analysis

A detailed drawing of the capture antenna is shown in Fig.2. The microstrip transmission-line, which feeds the slot via a tuning slug capacitor at F, has its strip conductor connected to the center conductor of a coaxial feed at E. The outer conductor of the coaxial line is in electrical contact with the aluminum ground plane. The antenna is equipped with two impedance matching mechanisms, one being the tunable capacitance at F between the slug and the strip conductor, and the other being the shunt stub section between D and H of the microstrip line. This shunt stub provides a reactive impedance compensation.

The input impedance Z_r of a simple slot antenna is related to the input impedance Z_d of the complementary strip antenna by

$$Z_r \, Z_d = \frac{1}{4} Z_o^2 \tag{1}$$

where Z_o is the intrinsic impedance. The effective height h_e^s of the slot antenna is related to the effective height h_e^d of the complementary strip antenna by

$$h_e^s = h_e^d \, (Z_o / 2Z_d) \tag{2}$$

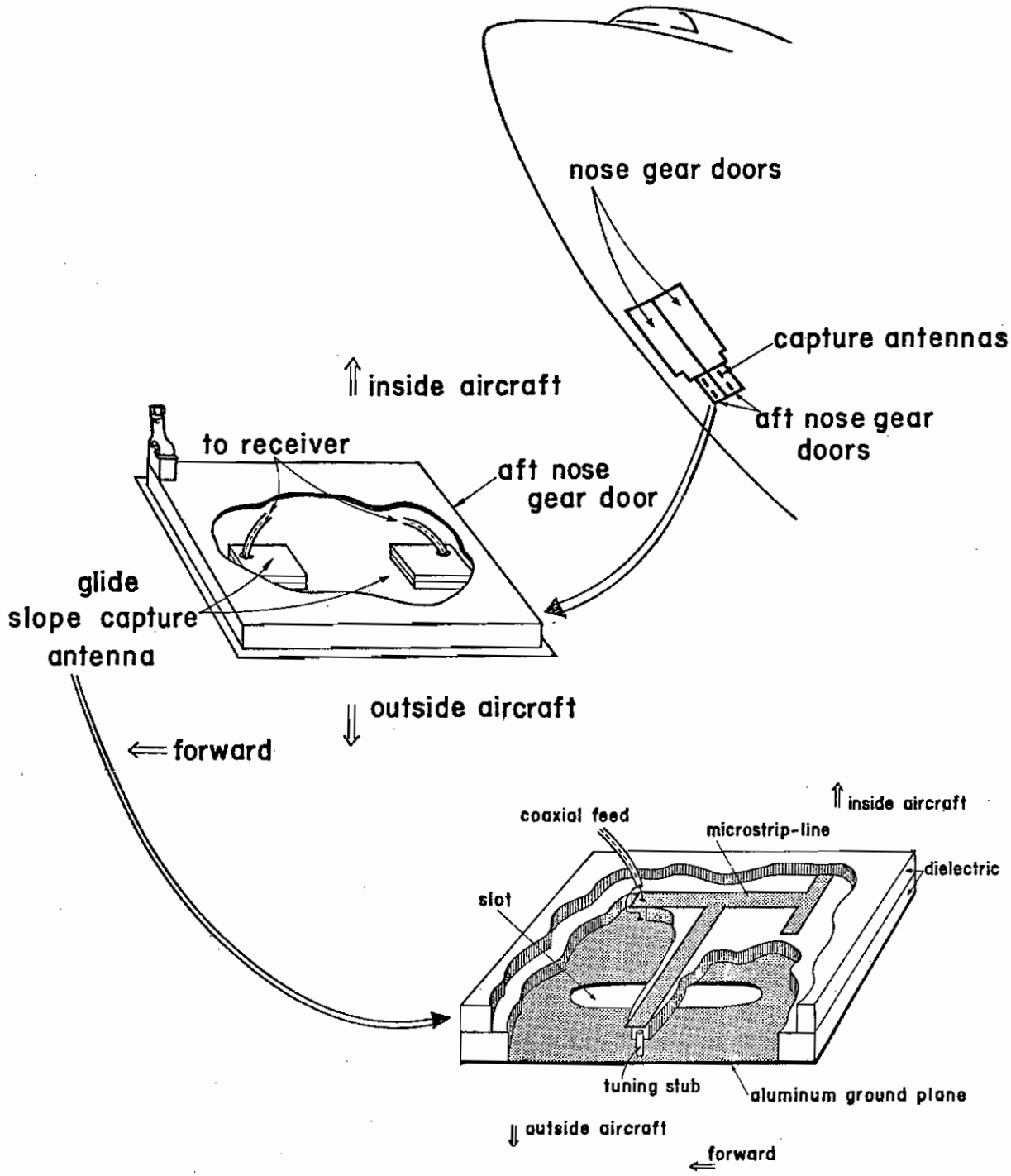

Fig.1(a). Location and schematic diagram of the capture antenna.

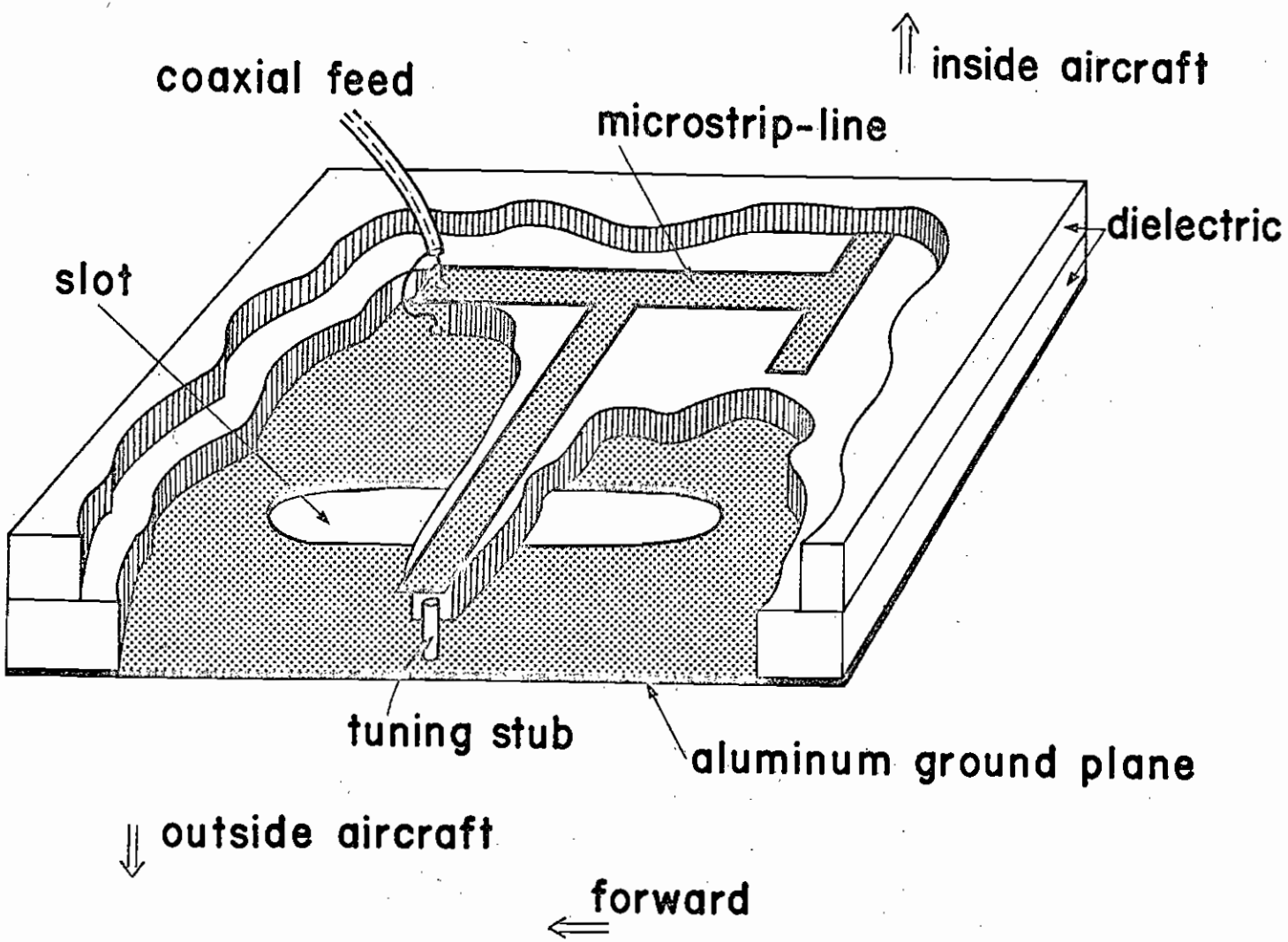

Fig.1(b). Englarged schematic diagram of the capture antenna.

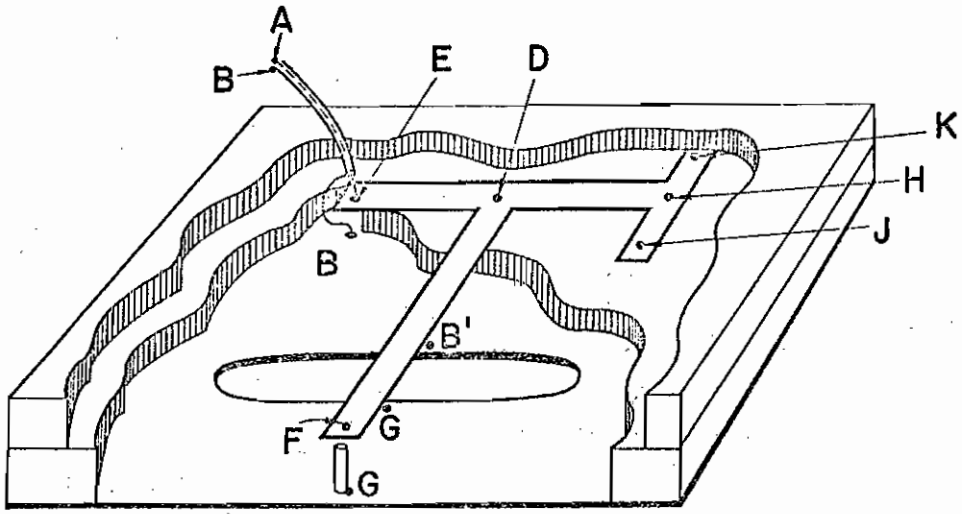

Schematic Diagram

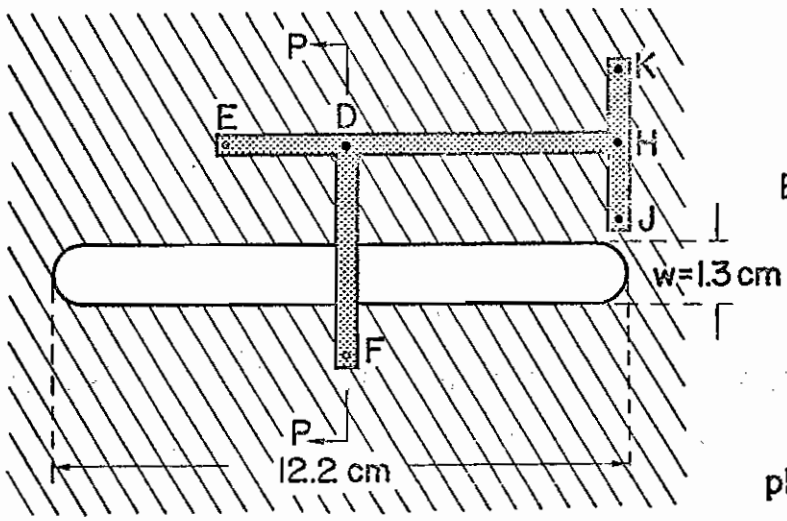

Plane View

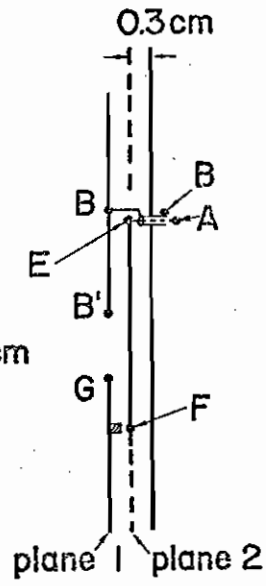

Side View PP
With Dielectric Removed

in plane 1

in plane 2

Fig.2(a). Detailed configuration of the capture antenna.

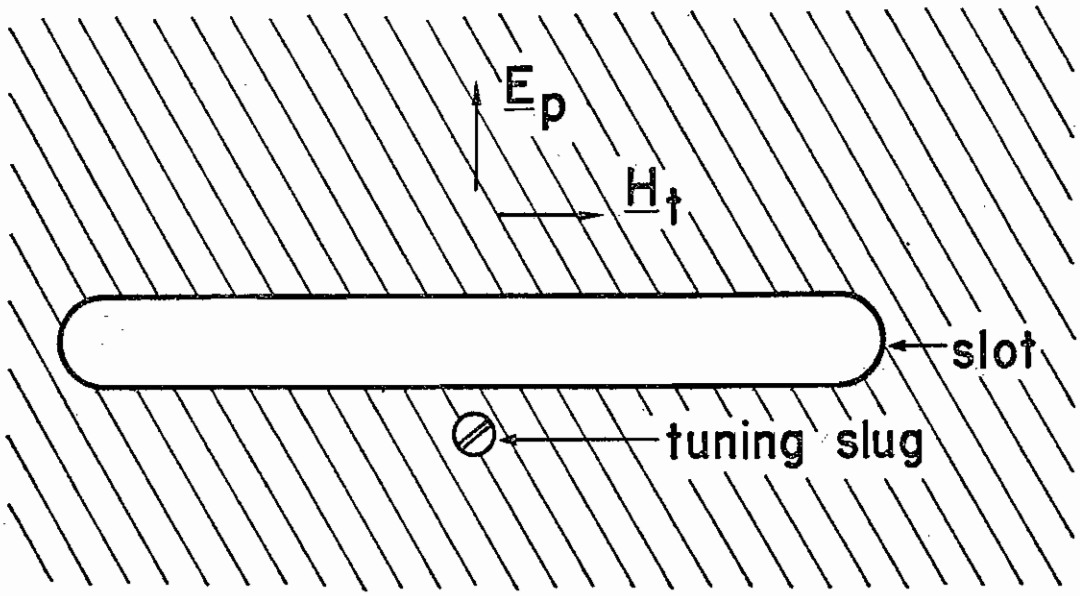

Plane View From Outside Aircraft

Fig.2(b). Plane view of the capture antenna from outside the aircraft.

Here, h_e^s is related to the induced voltage V_{ind} by

$$V_{ind} = h_e^s E_p \tag{3}$$

where E_p is the incident electric field in the plane of the antenna and perpendicular to the long side of the slot. The orientation of E_p is shown in Fig.2. All the above formulas were explained in Chapter 5*.

Alternatively, equations (2) and (3) can be derived in the following way. Introducing a vector equivalent length $\underline{\ell}_{eq}$ oriented in the direction of the long side of the slot, the short-circuit current I_{ind} induced in a thin wire placed across the center of the slot due to an incident magnetic field $\underline{H}^{inc}$ is

$$I_{ind} = 2\underline{\ell}_{eq} \cdot \underline{H}^{inc} \tag{4}$$

which can be deduced from the ideas of Babinet's principle. We can also express I_{ind} in terms of the skin current $\underline{K}$ in the absence of the slot, (i.e., when the slot is completely covered by metal),

$$I_{ind} = \underline{\ell}_{eq} \cdot (\underline{K} \times \hat{n}) = \underline{K} \cdot (\hat{n} \times \underline{\ell}_{eq})$$

where $\hat{n}$ is the unit vector normal to the screen (aircraft skin) surface. The induced voltage V_{ind} is then given by

$$V_{ind} = I_{ind} Z_r = (Z_o/2Z_d)\, \underline{\ell}_{eq} \cdot (Z_o \underline{H}^{inc}) \tag{5}$$

It turns out that $\underline{\ell}_{eq}$ is equal to the effective height $\underline{h}_e^d$ of the complementary strip antenna, as may be shown in a future Interaction Note. For the field excitation shown in Fig.(2),

*The two effective height expressions in this Chapter and Ch. 5 differ by a factor ½. It is to be noted that the expression in Ch. 5 is applicable to the case of a folded slot antenna.

$$V_{ind} = (Z_o/2Z_d)\ h_e^d(Z_o H_t)$$

where H_t is the incident magnetic field tangential to the antenna surface along the long side of the slot. This above equation is thus identical to (2) and (3), since the ratio of E to H for an incident plane wave is Z_o.

The equivalent circuit of the capture antenna is shown in Fig.3(a). The points marked by the letters A, B, D.... etc., can be identified with the physical locations in Fig.2. The capacitance C between points F and G accounts for the effect of the tuning slug and compensates in part the reactive part of Z_r. The different sections of the microstrip line in the present configuration have nearly identical characteristic impedance Z_c. The value of Z_c can be obtained from the results tabulated in SSN 90. The impedance Z_H represents the impedance at H of the two identical open-circuit stubs HJ and HK (Fig.2). This impedance is given by

$$Z_H = -\frac{1}{2}\, j\, Z_c \cot \beta \ell_4 \tag{6}$$

where β is the propagation constant of the microstrip line, and ℓ_4 is the length of each stub. When one end of a transmission line of length ℓ is excited by a generator whose source impedance is Z_ℓ and open-circuit voltage is V_ℓ, the input impedance Z_s and the open-circuit voltage V_s at the other end of the transmission line are given by

$$Z_s = Z_c \frac{Z_\ell + j\, Z_c \tan \beta\ell}{Z_c + j\, Z_\ell \tan \beta\ell} \tag{7}$$

and

$$V_s = V_\ell Z_c [Z_c \cos \beta\ell + j\, Z_\ell \sin \beta\ell]^{-1} \tag{8}$$

Equations (7) and (8) together with other circuit analysis techniques enable us to obtain the Thévenin equivalent circuit of Fig.3(b). We define a new complex effective height h_{eff} such that at the terminals AB, the open-circuit voltage

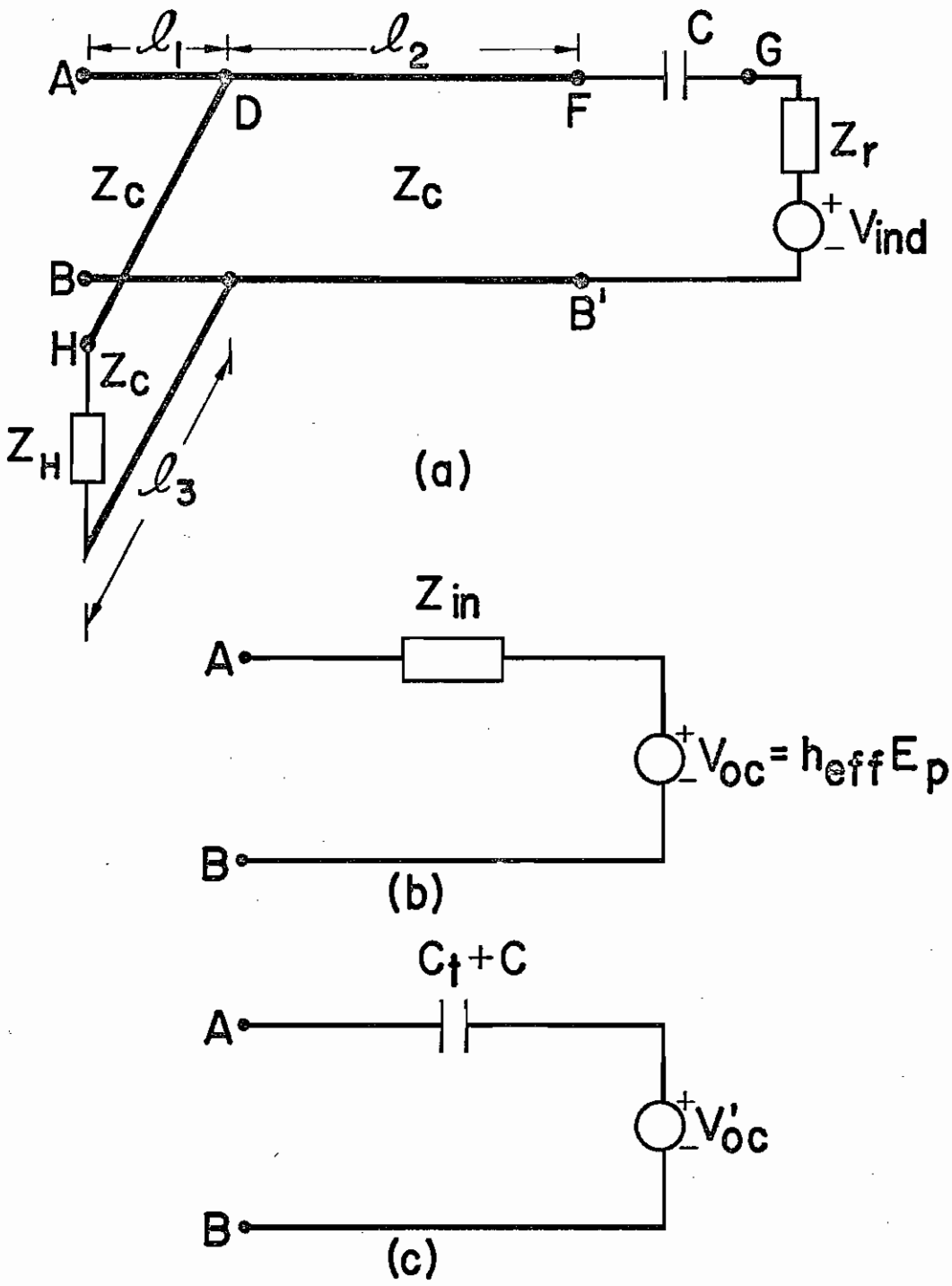

Fig.3. (a) Equivalent circuit of the capture antenna.
(b) The Thévenin equivalent circuit.
(c) Low frequency equivalent circuit.

V_{oc} is given by

$$V_{oc} = h_{eff} E_p \tag{9}$$

At low frequencies, as outlined in Chapter 3, each of the transmission lines can be represented by a shunt capacitance equal to the total capacitance of the line (product of the distributed capacitance per unit length and the length). We represent the total effect of all these lines by the capacitance C_t, which is given by

$$C_t = (Z_c c)^{-1} (\ell_1 + \ell_2 + \ell_3 + 2\ell_4) \tag{10}$$

where the lengths ℓ_1, ℓ_2, ℓ_3 and ℓ_4 are shown in Fig.3(a). At these frequencies, Z_r can be neglected and we have the low-frequency equivalent circuit as shown in Fig.3(c), where the input impedance and the open-circuit voltage are given by

$$Z'_{in} = 1/j\omega(C+C_t) \tag{11}$$

and

$$V'_{oc} = V_{ind} C/(C+C_t) \tag{12}$$

III. Numerical Results

The input impedance $Z_{in}(\omega)$ at the terminals A,B of the capture antenna is calculated and plotted against frequency in Fig.4. In Fig.5, we present the complex effective height h_{eff}. It is observed that the antenna is a narrow band device.

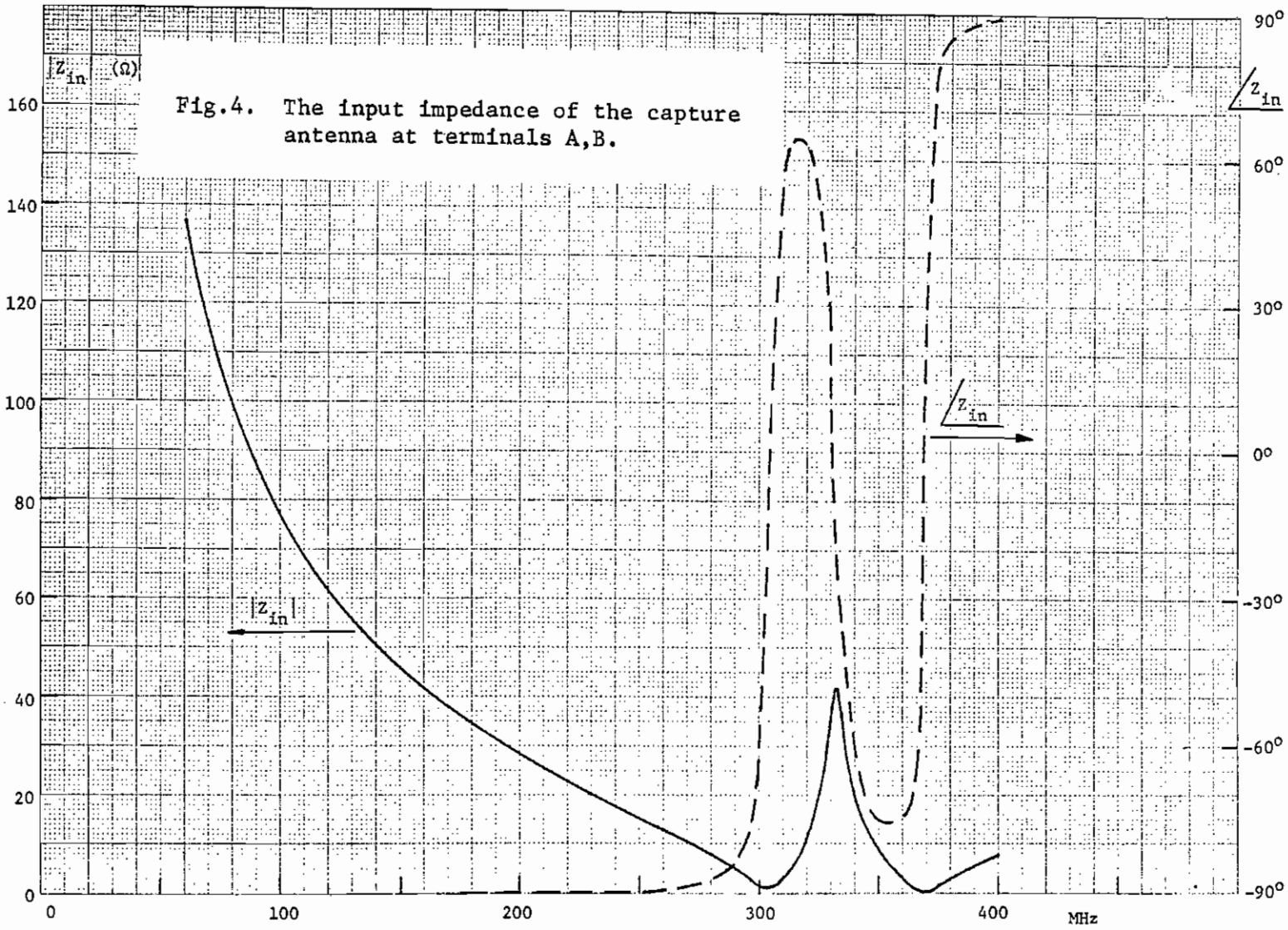

Fig.4. The input impedance of the capture antenna at terminals A,B.

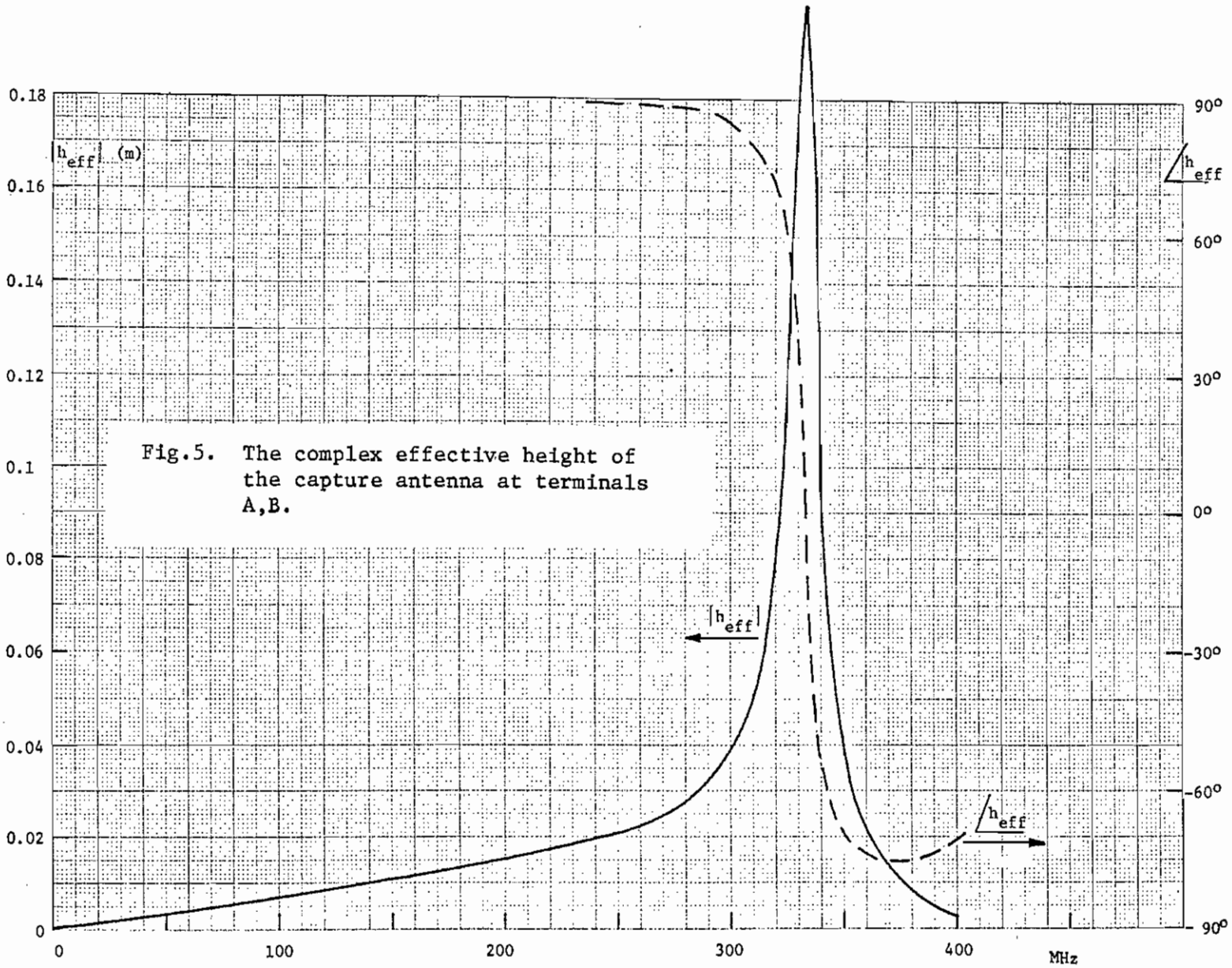

Fig.5. The complex effective height of the capture antenna at terminals A,B.

CHAPTER 7. DMPN3 LOW RANGE RADIO ALTIMETER ANTENNA ON AABNCP

I. General Description

The low range radio altimeter (LRRA) system provides information on the absolute altitude (height above terrain) during approach and landing phases of the flight operation. The antennas used for this purpose are the same for both the AABNCP and the B-1. Each aircraft carries two LRRA systems, and each system uses two identical horn antennas: one for transmitting the signal and the other for receiving the reflected signal from the ground. The antennas operate in the frequency range 4.2 - 4.4 GHz (wavelengths ≈ 6.8 - 7.1 cm). On the AABNCP, the four antennas are flush-mounted at the bottom of the fuselage around station 913 and station 933; on the B-1, they are flush-mounted at the bottom of the fuselage around Y_F 440. The antenna is a dielectric foam filled pyramidal horn and fed by a probe (see Fig.2). Externally, the antenna has a height of 7.4 cm and maximum cross-sectional diagonal of 13.2 cm. In Fig.1, the locations of the antennas on the two aircrafts and the external appearance of one horn are shown. In Fig.2, we present the internal view of the antenna having the dielectric foam removed.

II. Analysis

The wavelengths corresponding to the important part of the EMP spectrum are very large compared to the physical dimensions of the LRRA antenna. In calculating the effect of EMP on the horn antenna, it is therefore sufficient to carry out a quasi-static analysis. We will first consider the open-circuit voltage and then the input impedance. From theview point of mathematical tractability,the LRRA antenna can be described as a quasi-pyramidal horn with an infinite flange (Fig.3). The electrostatic potential distribution of Fig.3 can be found by the method of separation of variables in the spherical coordinates. Inside the horn, the potential V is given by

$$V(r,\theta,\phi) = \sum_{p=-\infty}^{\infty} \sum_{q=1}^{\infty} A_{pq}\left[r^{\nu_q} - r_i^{2\nu_q+1}\, r^{-\nu_q-1}\right]$$

$$\cdot\left[P_{\nu_q}^{\mu_p}(\cos\theta) - \left\{P_{\nu_q}^{\mu_p}(\cos\theta_1)/Q_{\nu_q}^{\mu_p}(\cos\theta_1)\right\} Q_{\nu_q}^{\mu_p}(\cos\theta)\right]\sin(\mu_p\phi) \qquad (1)$$

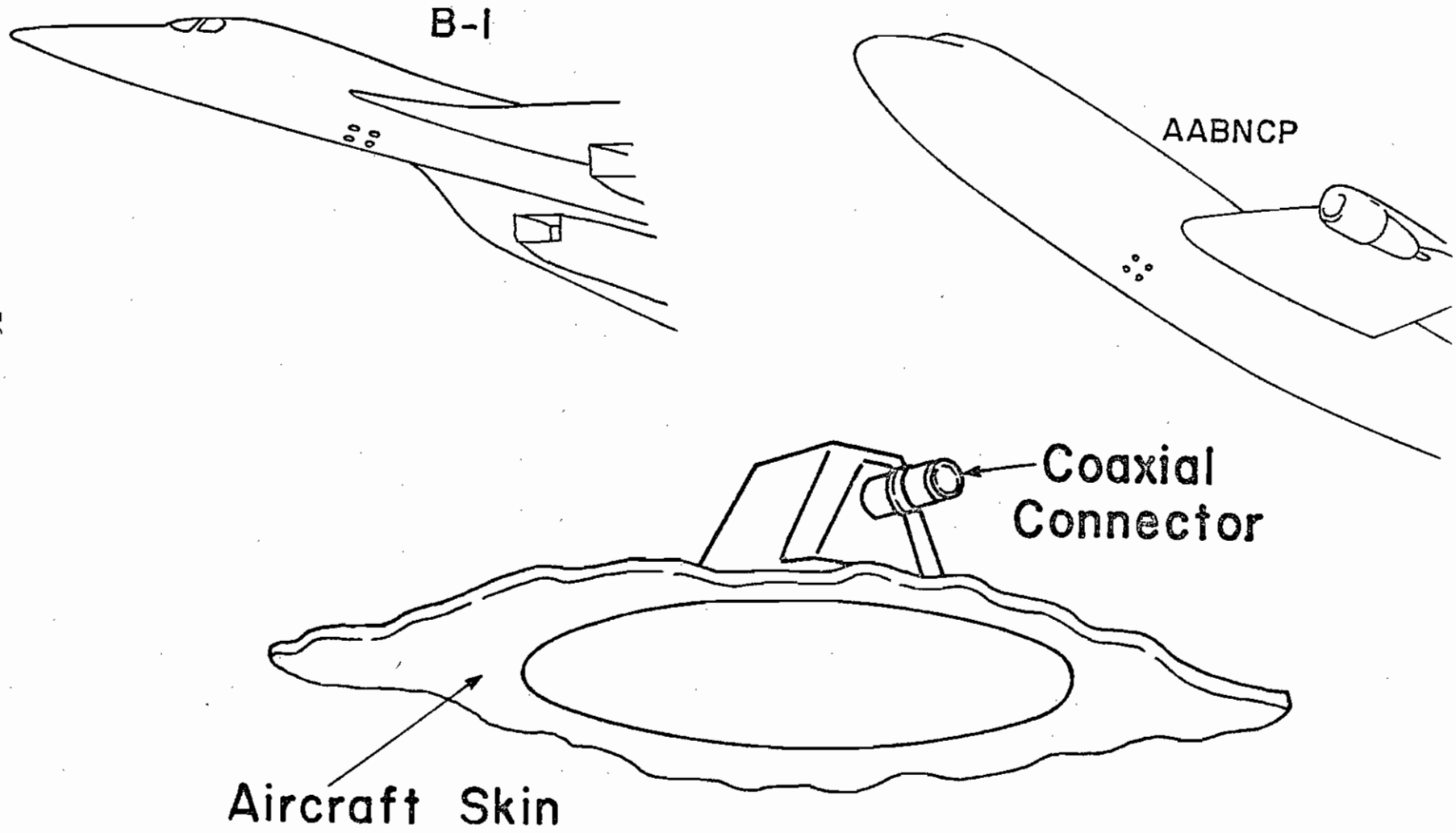

Fig.1. Location and external view of the LRRA Antenna.

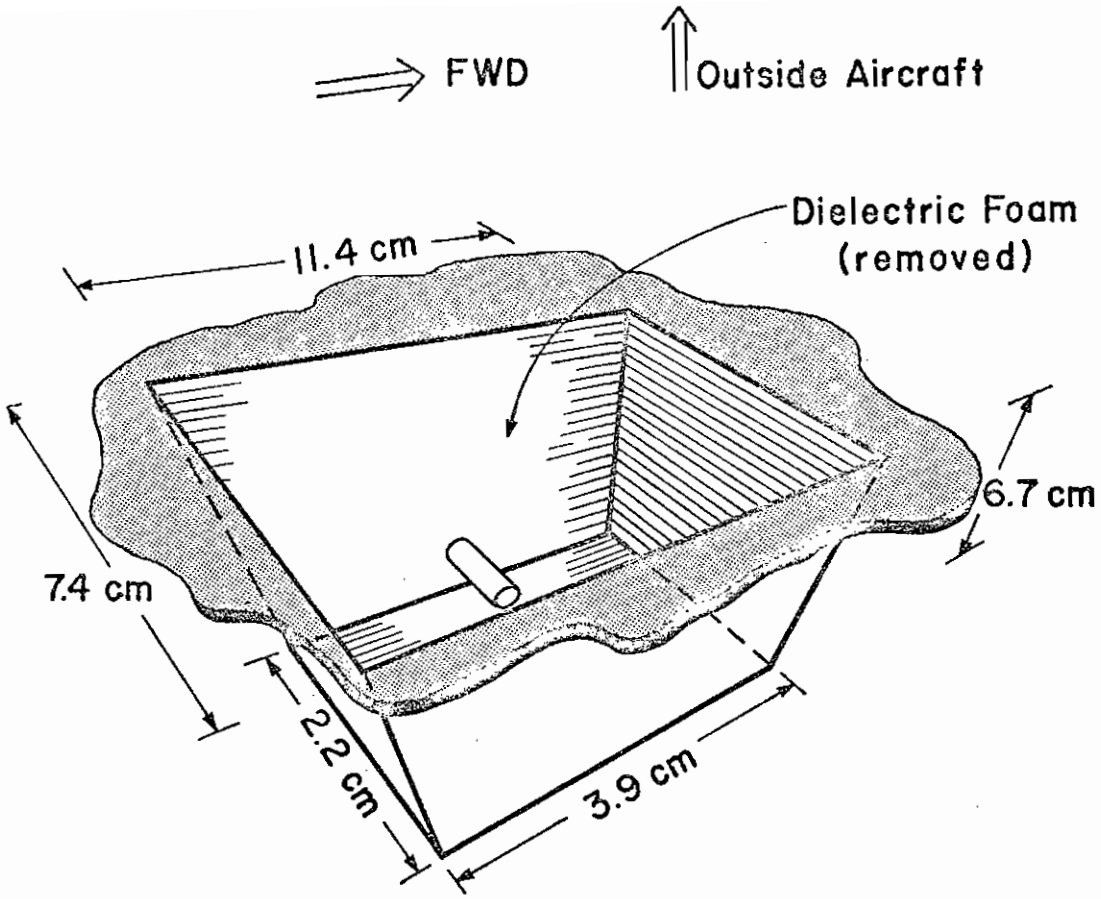

(a) Three-dimensional view.

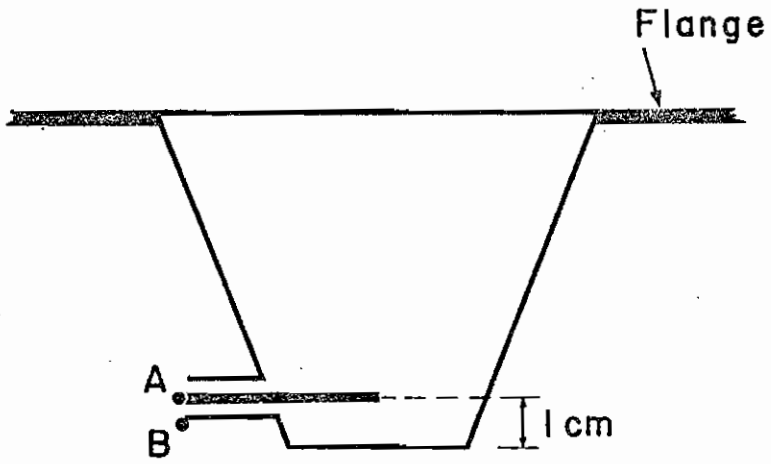

(b) Cross-sectional view through the probe.

Fig.2. Internal view of the LRRA Antenna.

where

$$\mu_p = p\pi/\phi_o, \quad p = 1,2,3.... \tag{2}$$

and the values ν_q ($q = 1,2,3....$) depend on θ_1 and μ_p, and are the roots of the following transcendental equation

$$P_{\nu_q}^{\mu_p}(\cos\theta_1)\, Q_{\nu_q}^{\mu_p}(-\cos\theta_1) - P_{\nu_q}^{\mu_p}(-\cos\theta_1)\, Q_{\nu_q}^{\mu_p}(\cos\theta_1) = 0 \tag{3}$$

In the above equations, r_i, θ_1 and ϕ_o are the horn parameters as defined in Fig.3, $P_\nu^\mu(\cos\theta)$ and $Q_\nu^\mu(\cos\theta)$ are the associated Legendre functions of degree ν and order μ, of the first and the second kind, respectively. The coefficients A_{pq} are determined from the field distribution in the aperture. Solution of (3) and the evaluation of A_{pq} are very time-consuming processes. For the present study, another simpler but reliable approach is adopted.

By studying the potential distribution inside the rectangular well depicted in Fig.4, upper and lower bounds of the voltage picked up by the probe in the horn can be obtained and, thus, the EMP induced voltage in the LRRA antenna can be estimated with a reasonable accuracy. In this chapter, we assume that the normal electric field E_p in the aperture of the horn to be the same as the electric field perpendicular to the fuselage, this field being due to the induced charge density on the aircraft. This assumption of the field distribution in the aperture over-estimates the result by a factor of approximately 1.5 (see IN 10). The potential in the rectangular well is found to be

$$V(x,y,z) = -(16\, E_p/\pi^3) \sum_{m\ \text{odd}} \sum_{n\ \text{odd}} \left\{ mn\left[(m/a)^2 + (n/b)^2\right]^{1/2} \cosh k_{mn}h \right\}^{-1}$$

$$\sin(m\pi z/a)\, \sin(n\pi y/b)\, \sinh(k_{mn}x) \tag{4}$$

where

$$k_{mn} = \pi\left[(m/a)^2 + (n/b)^2\right]^{1/2} \tag{5}$$

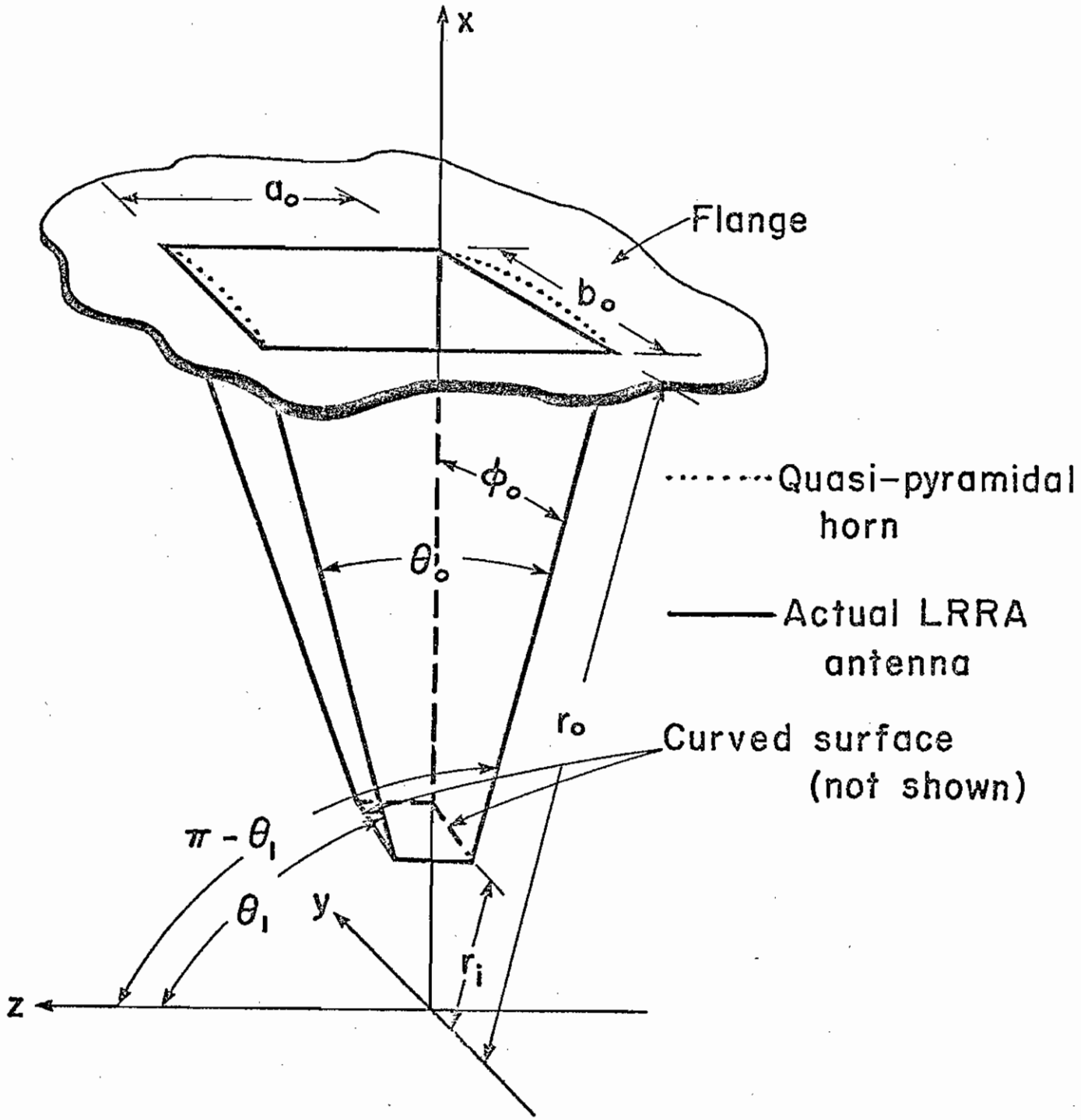

Fig.3. The LRRA Antenna and its geometrical approximation: the quasi-pyramidal horn.

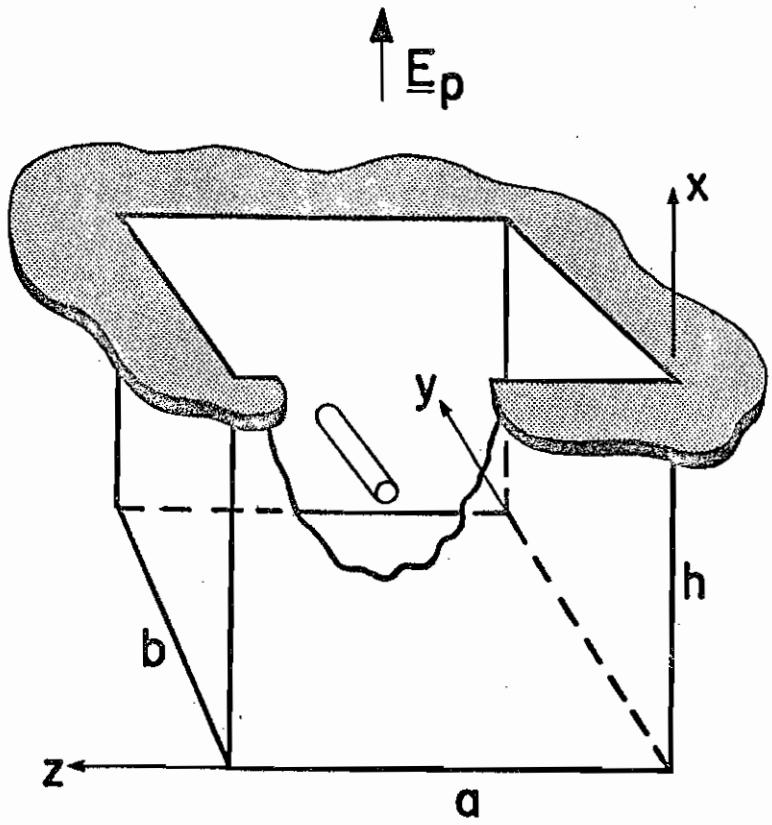

(a) Three-dimensional view.

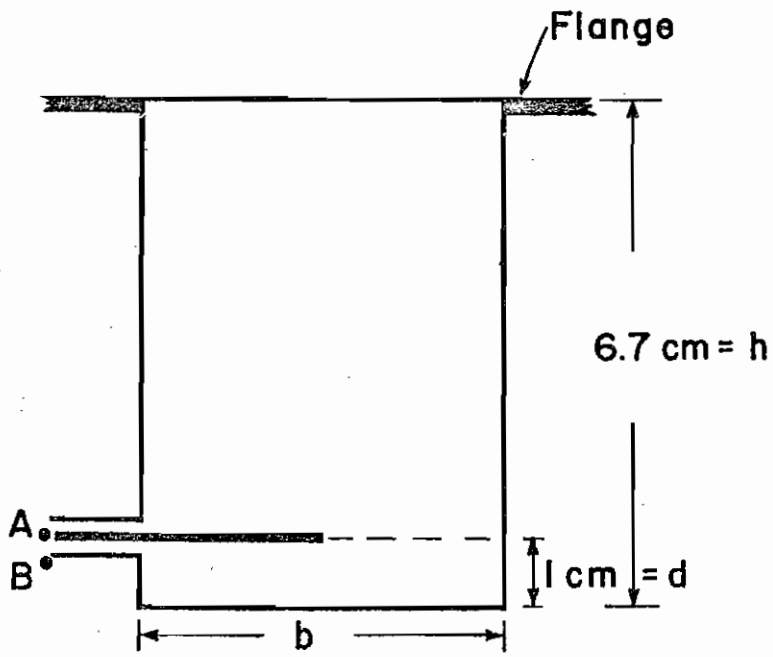

(b) Cross-sectional view through the probe.

Fig.4. Schematic diagram of the rectangular well.

It has to be pointed out that in the above expressions, the dielectric constant of the dielectric foam is taken to be that of free space. From (4) and (5), the open-circuit V_{oc} at the terminals AB (Fig.4b) can be obtained. Defining the effective height h_e of the antenna in Fig.4 as follows:

$$h_e = V_{oc}/E_p \tag{6}$$

we obtain, from (4) and (6) that

$$h_e = (16/\pi^3) \sum_{m \text{ odd}} \sum_{n \text{ odd}} \{ mn[(m/a)^2 + (n/b)^2]^{\frac{1}{2}} \}^{-1}$$

$$\cdot \sinh(k_{mn}d)/\cosh(k_{mn}h) \tag{7}$$

where $x = d$ is the vertical distance between the probe and the bottom wall of the well.

In Fig.5, we present the graph of h_e versus a/h with fixed values of d and h, and with b/a as a parameter. The point F in the graph corresponds to a rectangular well whose cross-sectional dimensions are those of the LRRA horn aperture, and this value of h_e is larger than the effective height of the LRRA horn antenna. The point G corresponds to a rectangular well with the cross-sectional dimensions of the small end of the LRRA horn, and this value of h_e is less than the effective height of the LRRA horn antenna. Thus, the effective height of the LRRA antenna varies between 10^{-6} m and 10^{-3} m. A reasonable estimate of this value is 2×10^{-4} m.

We now consider the input impedance of the LRRA antenna. Due to lack of information, the matching network will be left out in the following analysis. Since the wavelengths of interest are very large compared to the dimensions of the horn the input impedance is similar to that of a small dipole antenna in free space except for some factors (f_R and f_C) which account for the fact that the antenna is inside the horn. Hence, at low frequencies, the input impedance can be represented by a resistance R in series with a capacitance C, as shown in Fig.6.

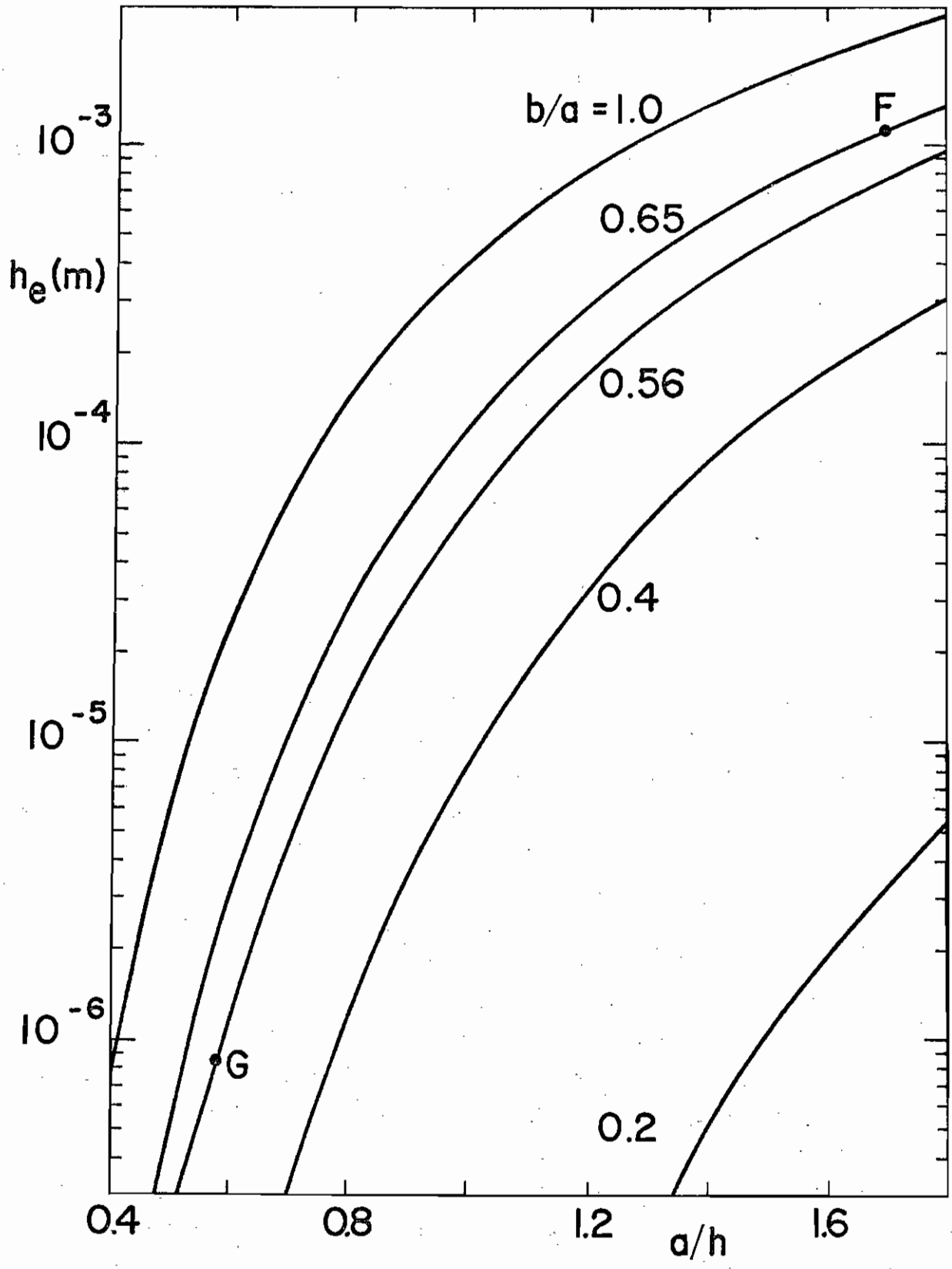

Fig.5. The effective height versus a/h with b/a as a parameter. Points F and G constitute upper and lower bounds.

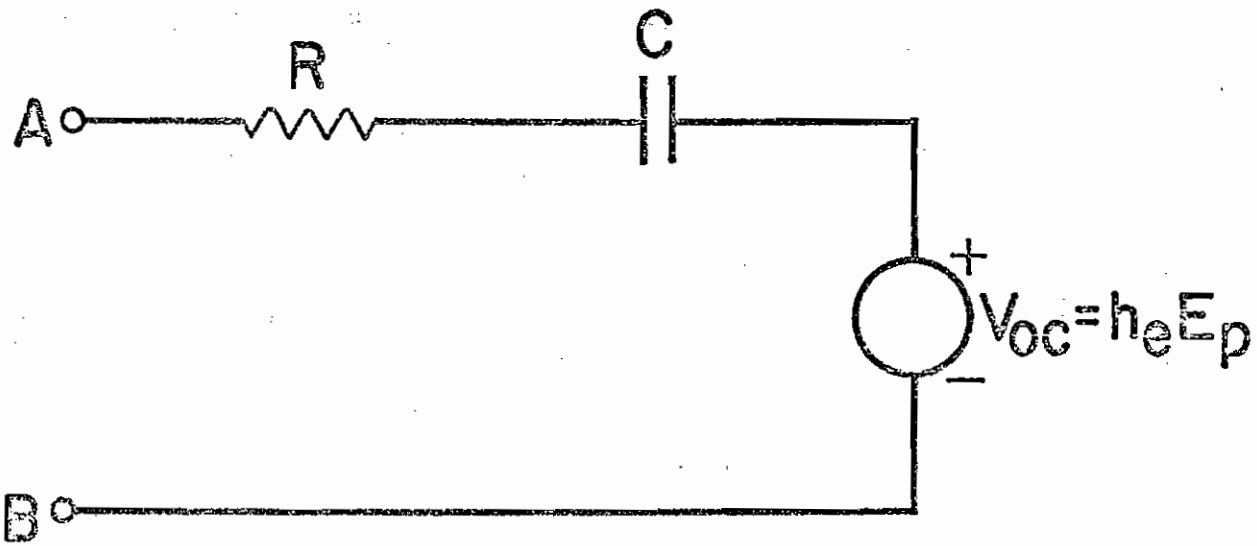

Fig.6. Thevenin equivalent circuit of the LRRA Antenna at terminals A,B.

The resistance R is given by

$$R = f_R R_o \tag{9}$$

where R_o is the radiation resistance in free space of a dipole antenna of length 2ℓ and it is given by

$$R_o \simeq \frac{2}{3} \pi Z_o (\ell/\lambda)^2 \tag{10}$$

where $Z_o = 377\ \Omega$ is the intrinsic impedance of free space. The factor f_R is roughly given by

$$f_R = (a_o b_o / 4\pi r_o^2)\ e^{-2k_{11}(h-d)} \tag{11}$$

where a_o and b_o are the dimensions of the aperture, and r_o is the distance from the vertex of the pyramidal horn to the aperture (see Fig.3). The quantity k_{11} is given by (5) with $m = n = 1$.

For the present problem,

$$f_R \simeq 1.5 \times 10^{-4} \tag{12}$$

For frequencies up to 100 MHz, the radiation resistance R is less than 1 $\mu\Omega$.

The input capacitance C is given by

$$C = f_C C_o \tag{13}$$

where C_o is the capacitance of a dipole antenna in free space with length 2ℓ and radius r_a; it is given by

$$C_o = \pi \epsilon_o \ell \Big/ \ell n(2\ell/r_a) \tag{14}$$

The factor f_C can be evaluated approximately from image theory. Thus

$$f_C = 2\left[1 - \frac{\ell}{2\ell n\left(\frac{2\ell}{r_a}\right)}\left\{\frac{1}{2d} + \left(\frac{1}{a} - \frac{1}{\sqrt{a^2+d^2}}\right) + 2\left(\frac{1}{b} - \frac{1}{\sqrt{b^2+(2d)^2}}\right)\right\}\right]^{-1} \qquad (15)$$

As expected, (15) indicates that the walls of the horn cause an increase in the capacitance. For the present problem

$$f_C \simeq 2.5 \qquad (16)$$

and the capacitance is approximately 0.3 pF. Thus, the input impedance of the horn antenna is predominantly capacitive and it is about $-j$ 5000 Ω at 100 MHz.

CHAPTER 8. AS-1918/AR UHF/IFF-TACAN BLADE ANTENNA ON B-1

I. General Description

The blade antenna described in this chapter is used for transmission and reception of vertically polarized signals in two frequency ranges: a UHF range of 225-420 MHz (wavelengths ≈ 0.75 - 1.33m) and an L-band range of 900 - 1220 MHz (wavelengths ≈ 0.25 - 0.31m). The antenna, as shown schematically in Fig. 1, consists of two sections: the UHF section which is fed via a low-pass filter, and the L-band section which is fed via a high-pass filter. Each section is basically a capacitively top-loaded sleeve monopole; hence the principles of operation are similar to those of the blade antenna AT-1076A/A analyzed in Ch. 3. The filters are installed to minimize band interferences. The two probes in Fig. 1 monitor the radiated signals and they play no role in the operation of the antenna. The following analysis will therefore not include these probes.

The antenna has a height of 20.5cm, a width of 15.2cm at the base and 12.7cm at the top. The maximum thickness is 1.2cm. There are two such antennas on the B-1, mounted externally on the top of the fuselage at stations Y_F 390 and Y_F 720. The two UHF/IFF-TACAN blade antennas (AS-1919/AR) mounted externally on the bottom of the fuselage at Y_F 1030, LX_F 145 and RX_F 145, respectively, are very similar in operation to the one under study in this chapter.

- - - - - - - - - - - - - - -

The theory of operation, and hence the analysis of each section of this antenna is analogous to that of the AT-1076A/A antenna. However, there are some important differences that have to be carefully taken into account in the present analysis, they are: (i) the low-pass filter in the UHF section and the high-pass filter in the L-band section; the presence of the filters may affect the out-of-band operation to a significant extent, (ii) the four chokes in the upper half of the antenna; and (iii) the effects of the elements in one section on the performance of the other section, e.g., the effect of the UHF radiation gap on the L-band characteristics.

Another important consideration is the dc paths linking the three parts of the antenna. The dc paths formed by the shunt stubs provide protection to the transmitter and the receiver against large low-frequency excitations such as those due to EMP or lightning. As shown in Fig. 2, parts denoted by D and D' are connected by the stub passing through the point H. This stub forms the

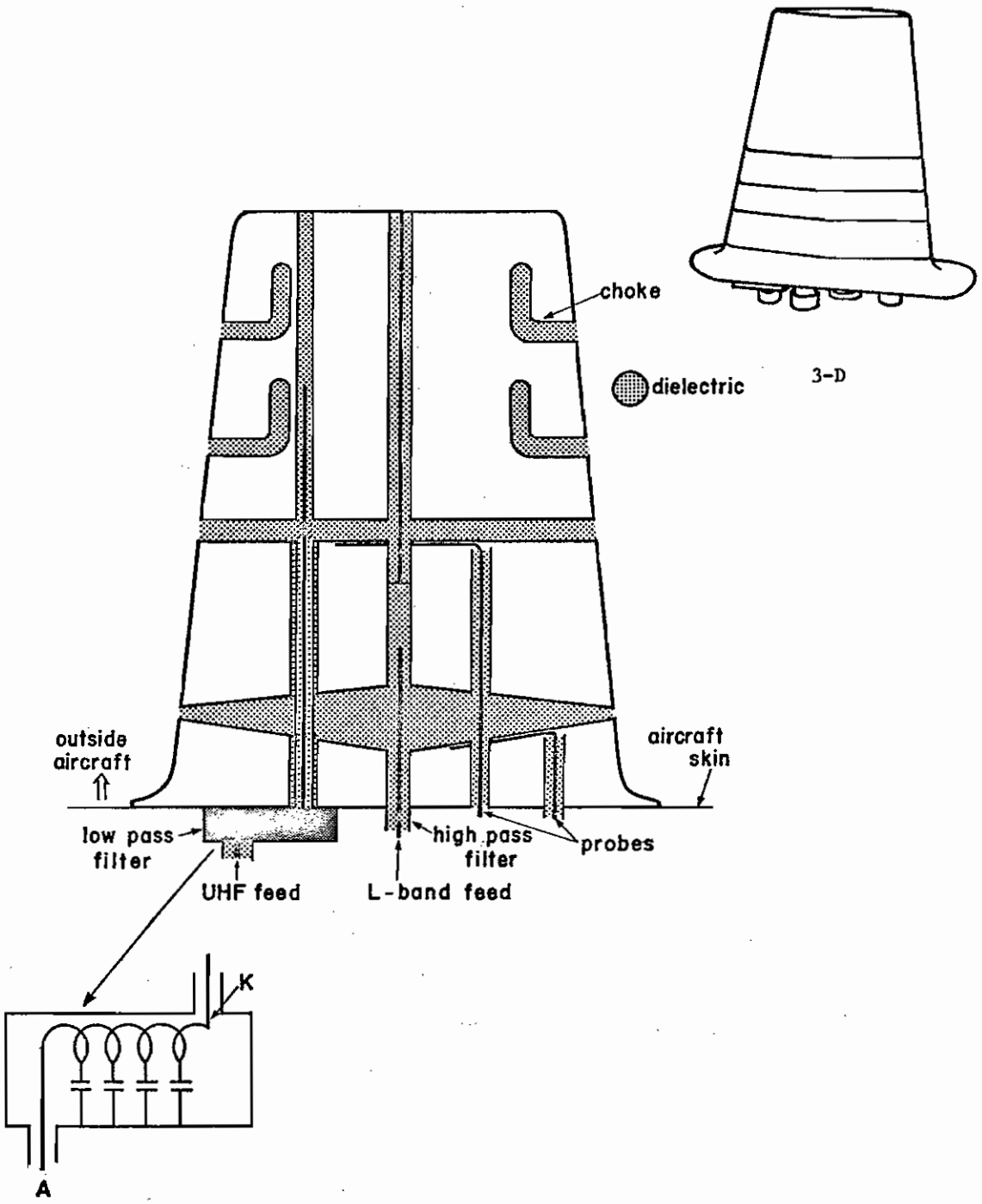

Fig.1 Schematic diagram of the blade antenna

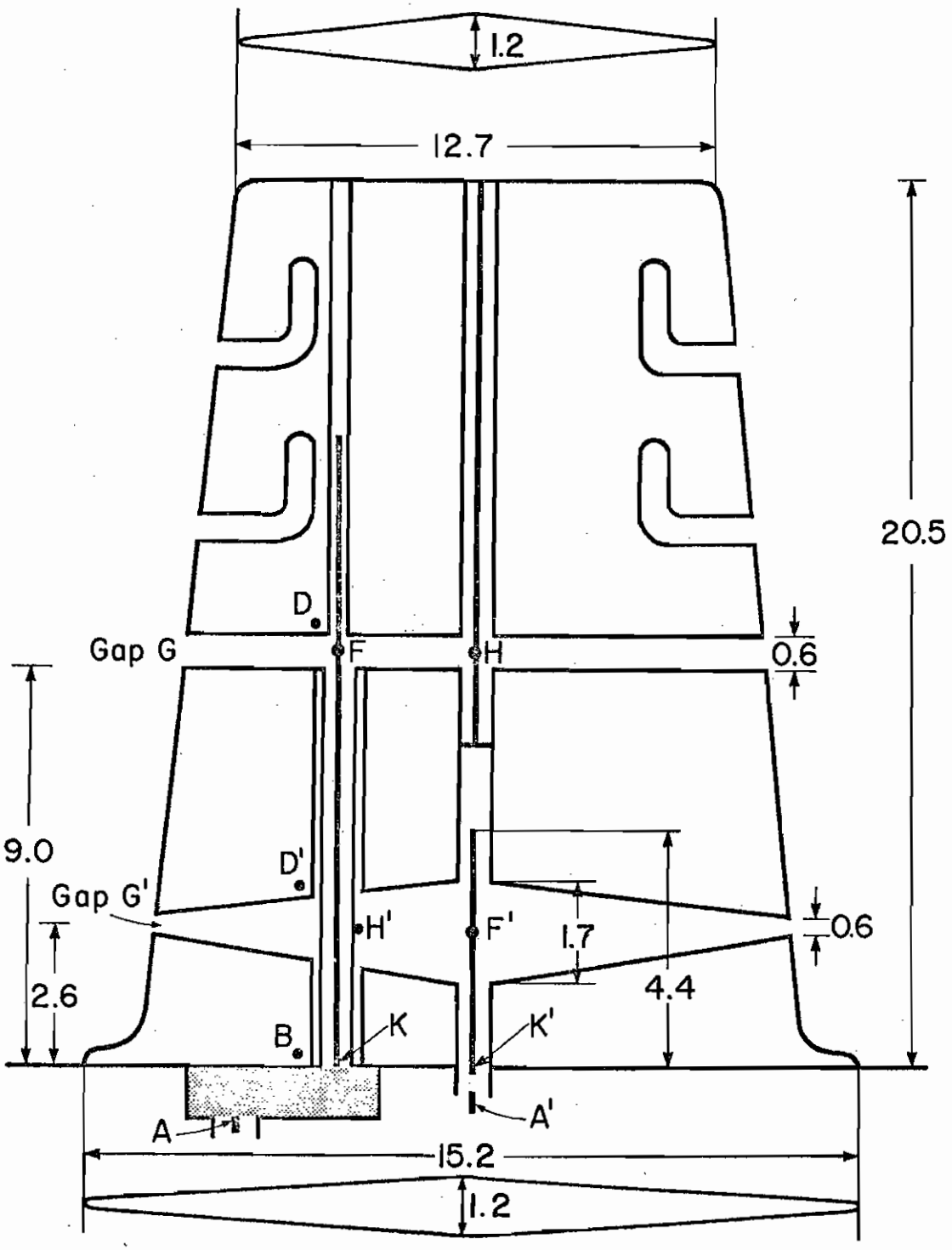

Fig.2. The sketch of the blade antenna, showing electrical connections.

center conductor of a coaxial line with the outer conductor broken at the gap G. This gives rise to a dc path between D and D' without destroying the radiation properties of the gap. Similarly, parts D' and B are connected by the tube passing through the point H'. This tube is the inner conductor of a coaxial line with the outer conductor broken at the gap G'. In addition, the tube also serves as the outer conductor of the driving transmission line for the UHF section.

II. Analysis of the UHF Section

The antenna is re-sketched in Fig. 3(a) showing the salient features of the UHF section. The frequency range within which most EMP energy is confined is well within the pass band of the low-pass filter. This filter can thus be left out in the analysis without any noticeable error. The equivalent circuit of the UHF section is shown in Fig. 3(b).

The radiation properties of the UHF section is represented by the external admittance $Y_a(\omega)$, whose value can be obtained from the theory of an asymmetrically driven monopole. When it is used as a receiving antenna, the induced short-circuit current I_{ind} on the blade across the gap G is given by (see SSN 193)

$$I_{ind} = j\omega\varepsilon_o E_n \pi a^2 [1 - (x/a)^2][1 - (b/a)^2][1 - (c/a)^2]^{\frac{1}{2}} [F(\varphi\backslash\alpha) - E(\varphi\backslash\alpha)]^{-1} \quad (1)$$

where

$$\varphi = \sin^{-1}[1 - (c/a)^2]^{\frac{1}{2}},$$

$$\alpha = \sin^{-1}[\{1 - (b/a)^2\}\{1 - (c/a)^2\}]^{\frac{1}{2}}$$

$F(\varphi\backslash\alpha)$ and $E(\varphi\backslash\alpha)$ are incomplete elliptic integrals of the first and the second kind, respectively. The quantities a, b and c are the total height, the half width at the base and the half thickness at the base, respectively. Furthermore, x denotes the height of the gap above the base of the antenna. The quantity E_n is the total electric field near the location of the antenna and is normal to the fuselage. Substituting the appropriate dimensions of the UHF blade in (1), one gets

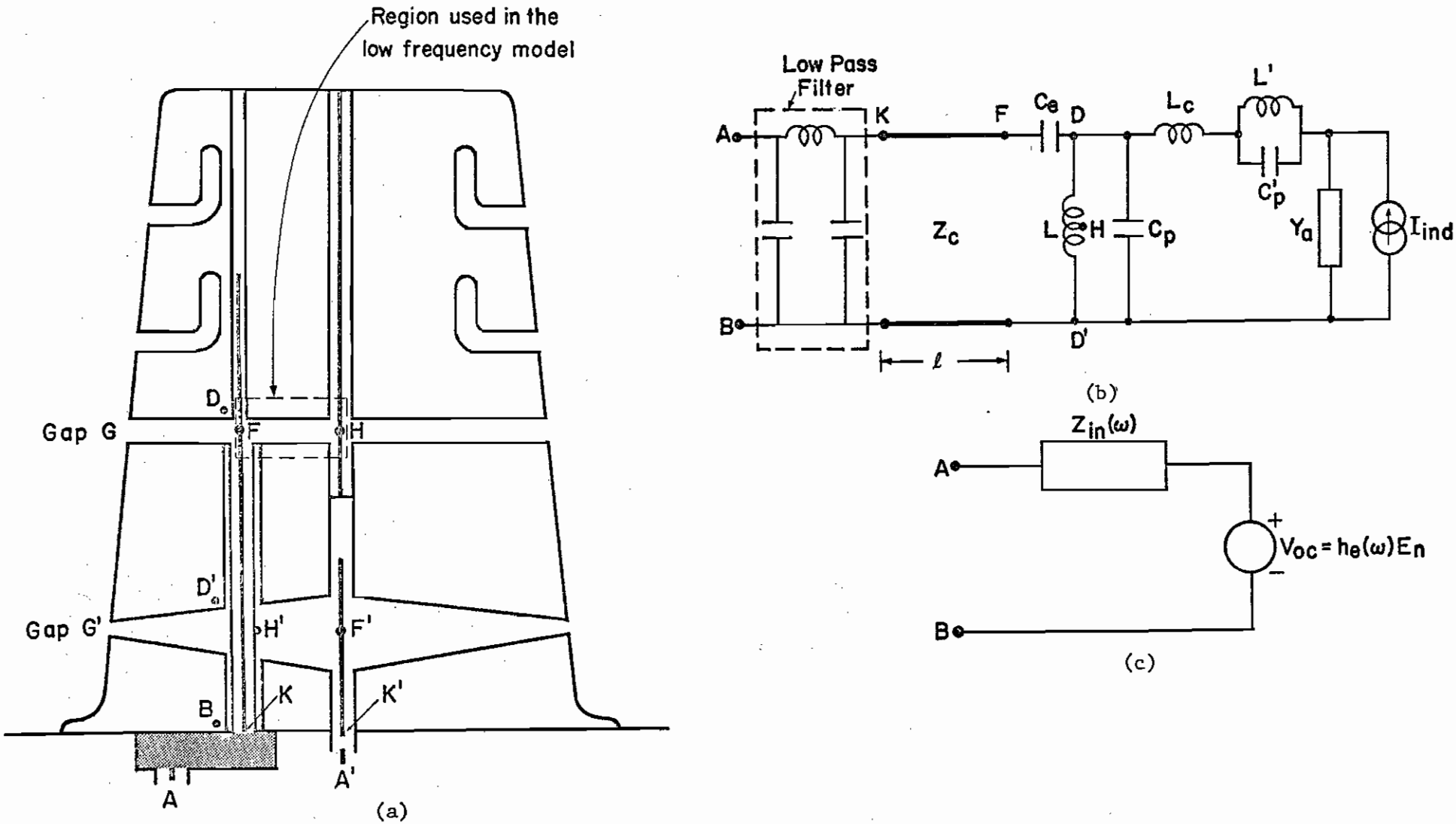

Fig.3. (a) the blade antenna; (b) the equivalent circuit; (c) the Thévenin equivalent circuit at terminals A,B.
The above is for the UHF section.

$$I_{ind} = 6.97\times10^{-2}\ j\omega\varepsilon_o E_n$$

$$= 6.17\times10^{-13}\ j\omega E_n \qquad \text{Amperes.}$$

The other elements in Fig. 3(b) are now identified with the aid of Fig. 3(a). The quantity C_p represents the capacitance between the two metallic plates at the gap G. The shunt stub from D to D' through the point H is actually a transmission line short-circuited at both ends, and therefore the influence of the stub appears as an inductive load and is represented by the inductance L. From the point F to the point D, there is a short section of an open-circuited transmission line for impedance matching purpose. This transmission line appears as a capacitive load and is represented by the capacitance C_e. The UHF section is fed by a transmission line with characteristic impedance Z_c and length ℓ.

The inductance L_c accounts for the chokes in the upper half of the antenna. The purpose of these chokes is to reduce the coupling between the UHF section and the L-band section at the L-band frequencies. The inductance L' and the capacitance C_p' are due to the presence of the gap G'. These quantities represent the effect of the gap G' (for the L-band section) on the UHF section.

The equivalent circuit in Fig. 3(b) can be reduced to the Thévenin equivalent circuit in Fig. 3(c) using circuit analysis techniques. The open-circuit voltage V_{oc} is expressed in terms of a complex effective height $h_e(\omega)$, which is defined by

$$V_{oc} = h_e(\omega)E_n. \qquad (2)$$

Low-frequency circuit model

At low frequencies, some otherwise negligibly small induced signals may become more significant. A low-frequency equivalent circuit is shown in Fig. 4(a) which takes into account these low-frequency contributions. One such contribution comes from the small region enclosed by the dashed lines in Fig. 3(a). This region forms a small loop with a small inductance L_1 in series with the

capacitive load C_e and the inductance L which represents the effect of the shunt stub. The induced voltage V_i in this loop is given by Faraday's law of induction and is related to the time derivative of the magnetic field normal to this loop. Another low-frequency contribution is due to some small but non-zero induced charges on the center conductor of the open-circuit transmission line. These charges produce a current I_i, as shown in Fig. 4(a), between the center conductor and the rest of the antenna, i.e., between F and D in Fig. 3(a).

As pointed out in Chapter 3, at low frequencies, the influence of the transmission line in Fig. 3(b) can be represented by a capacitance C_t, which is equal to the product of the distributed capacitance per unit length and the length of the transmission line. As observed in Fig. 4(a), other elements, such as C_p, Y_a, C_p', L_c and L' are neglected since they have very little effect at low frequencies.

The low frequency Thévenin equivalent circuit is shown in Fig. 4(b), where the open circuit voltage is

$$V_{o,\ell f} = (1 + C_e/C_t)(j\omega L I_{ind} + V_i + I_i/j\omega C_e) \tag{3}$$

and the input impedance becomes

$$Z_{i,\ell f} = 1/j\omega(C_e + C_t) \tag{4}$$

In the above expressions, it is assumed that

$$1/j\omega C_e >> j\omega(L + L_1)$$

Numerical results

Based on the above circuit model (Fig. 3(b)) the values of input impedance and effective height are plotted versus frequency in Fig. 5 and Fig. 6, respectively. As expected, we observe the capacitive behavior of the antenna at low frequencies and the fairly well matched behavior at the in-band frequencies (225 - 420 MHz).

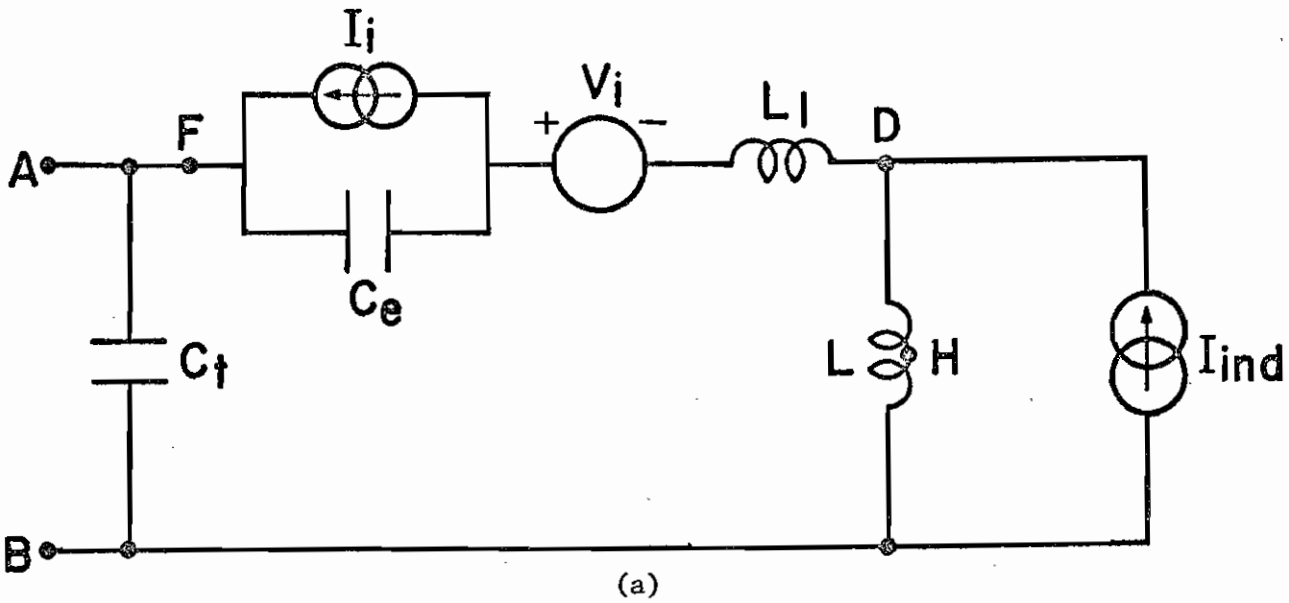

(a)

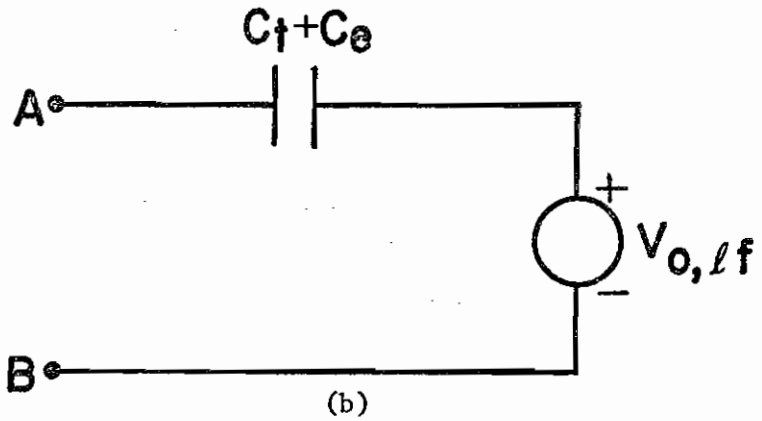

(b)

Fig.4. Low frequency model of the UHF section
(a) the equivalent circuit
(b) the Thévenin equivalent circuit at terminals A,B.

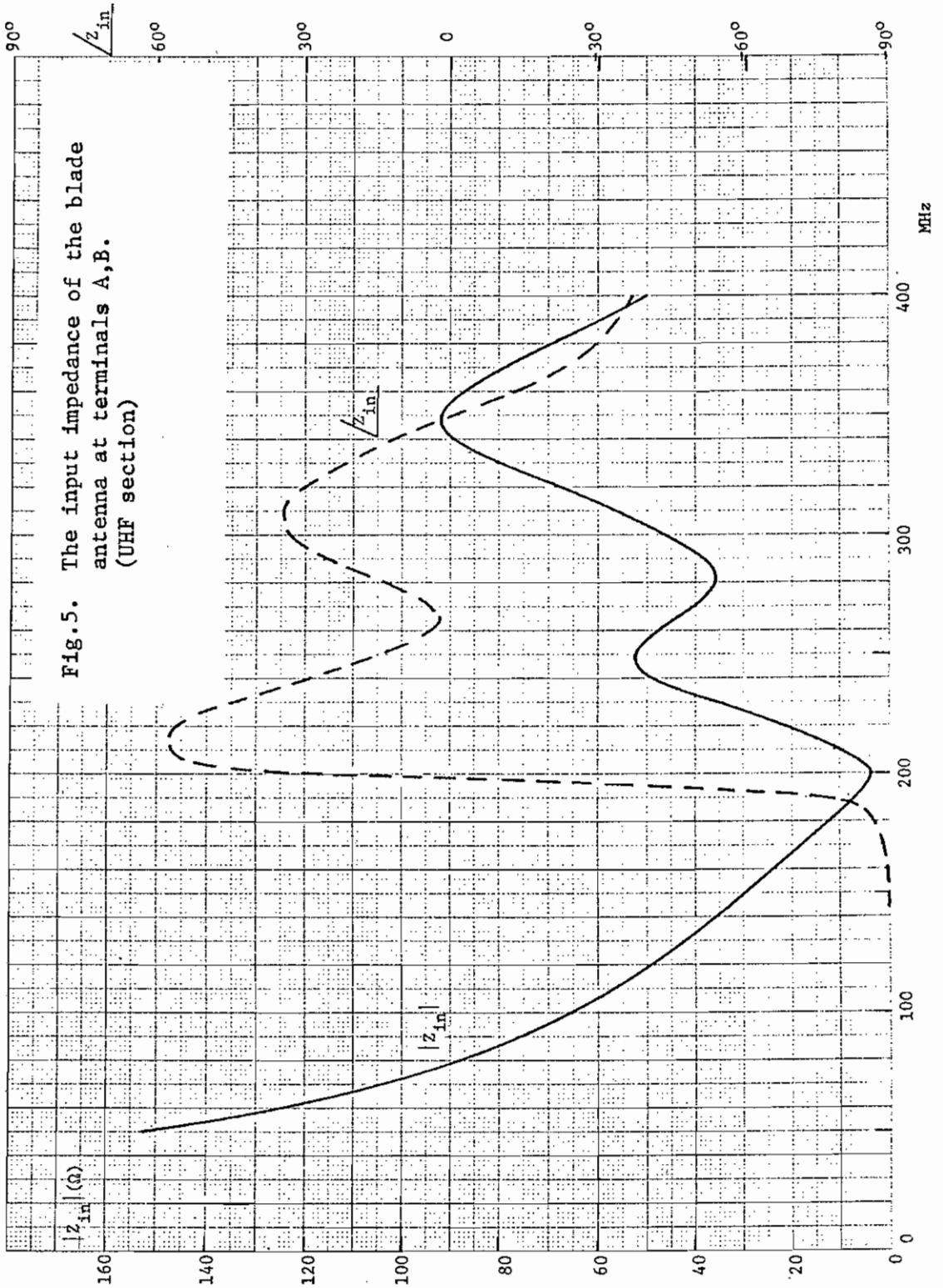
Fig.5. The input impedance of the blade antenna at terminals A,B. (UHF section)
$|z_{in}|$ (Ω)
$\angle z_{in}$
$|z_{in}|$
$\angle z_{in}$
MHz
0
20
40
60
80
100
120
140
160
100
200
300
400
90°
60°
30°
0
-30°
-60°
-90°

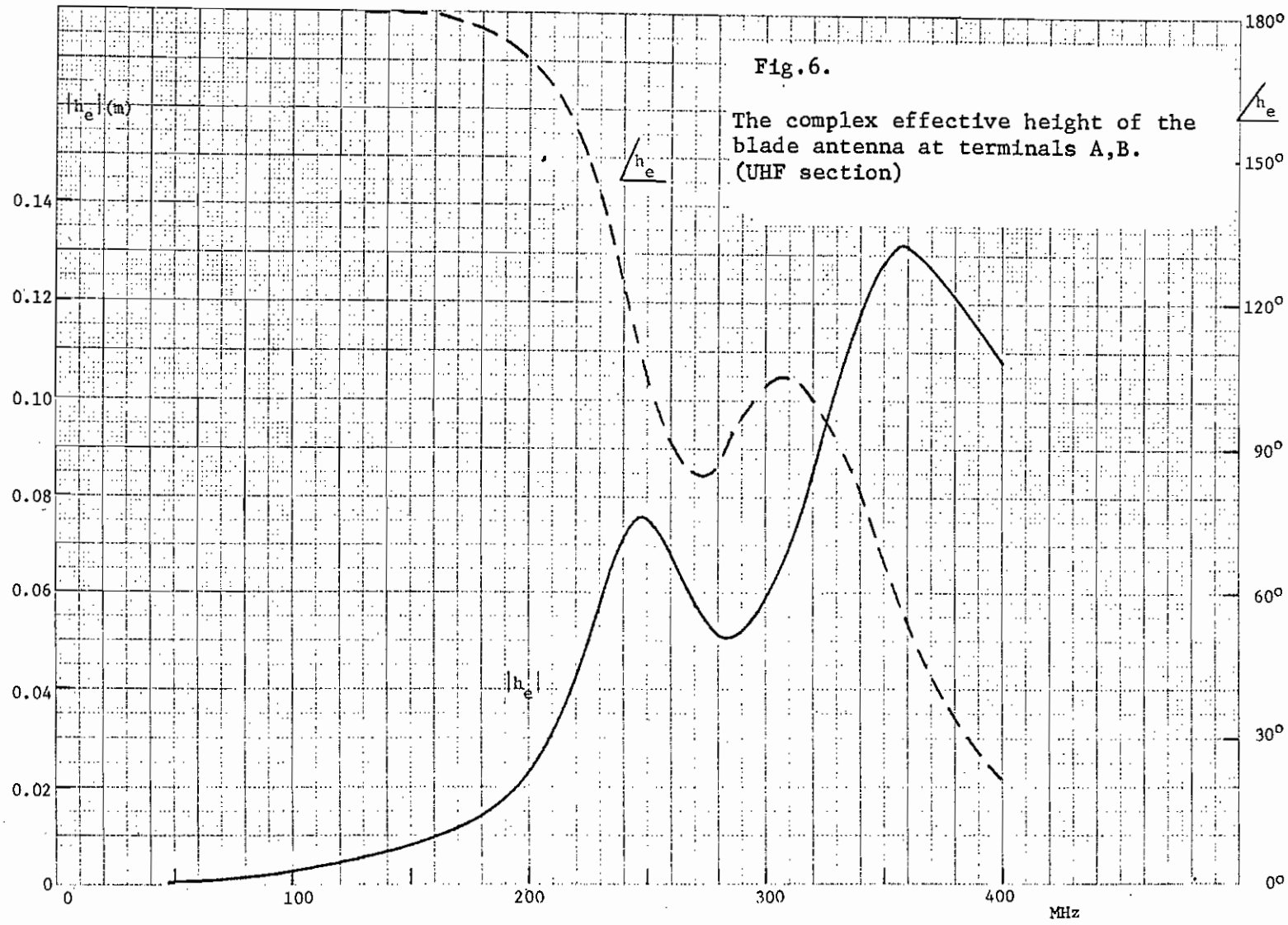

Fig.6.

The complex effective height of the blade antenna at terminals A,B. (UHF section)

III. Analysis of the L-Band Section

In principle, the L-band section works very similarly to the UHF section. However, the high-pass filter has to be taken into account at the frequency range of interest. This filter is actually a capacitor in series with the driving transmission line at the input terminals. We represent it by C_f' in the equivalent circuit in Fig.7(b). The rest of the circuit resembles that of Fig.3(b), with the prime to indicate the L-band quantities, e.g. Y_a' is the L-band external admittance corresponding to Y_a of the UHF section. The parallel circuit of L and C_p represents the effect of the UHF gap G on the L-band section. It has to be pointed out that this equivalent curcuit, while it is correct for the EMP frequencies, is not valid for the in-band operation. The in-band model will be detailed later.

In Fig.7(b), the induced current I_{ind}' is again given by (1) with a being the full height of the antenna and x the height of the gap G' above the base. We obtain

$$I_{ind}' = 9.15\times10^{-2}\ j\omega\epsilon_o E_n$$

$$= 8.10\times10^{-13}\ j\omega E_n \quad \text{Amperes.}$$

The Thévenin equivalent circuit is shown in Fig.7(c), where the open circuit voltage V_{oc}' is related to the complex effective height $h_e'(\omega)$ by

$$V_{oc}' = h_e'(\omega)E_n \tag{5}$$

In-band circuit model

For the in-band operation around 1 GHz, the chokes block current flow between the upper half and the lower half of the antenna. Thus, the effective radiator, as shown in Fig.8(a), contains only the lower (B) and the middle (D') parts of the blade antenna. The equivalent circuit is shown in Fig.8(b), where we remove the choke L_c and the influence from the UHF gap G, namely L and C_p. The effect of the filter C_f' can be neglected in this frequency range because the operation is within its pass band. The external admittance

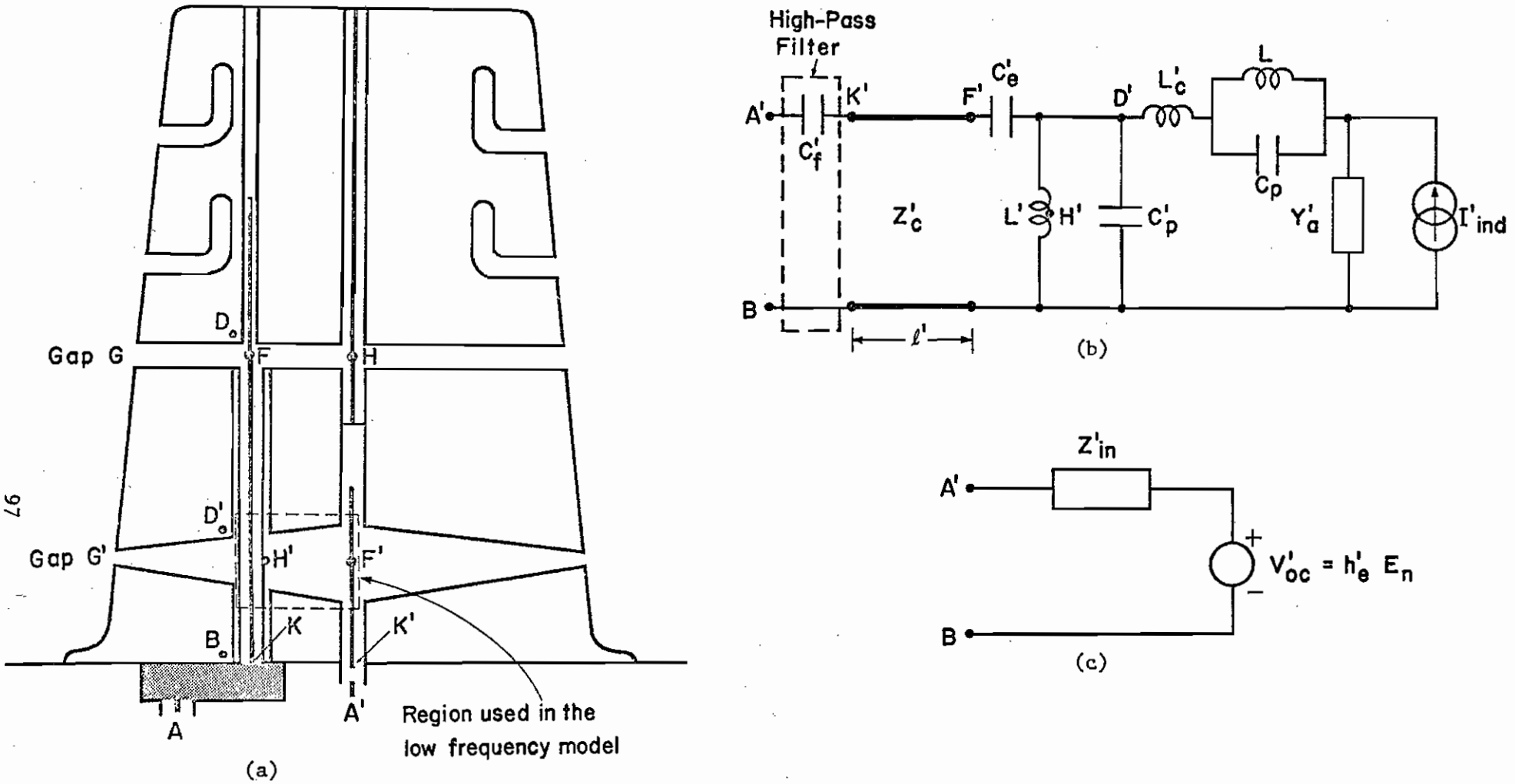

Fig.7. The out-of-band model of the L-band section.

(a) the antenna
(b) the equivalent circuit
(c) the Thévenin equivalent circuit at terminals A',B

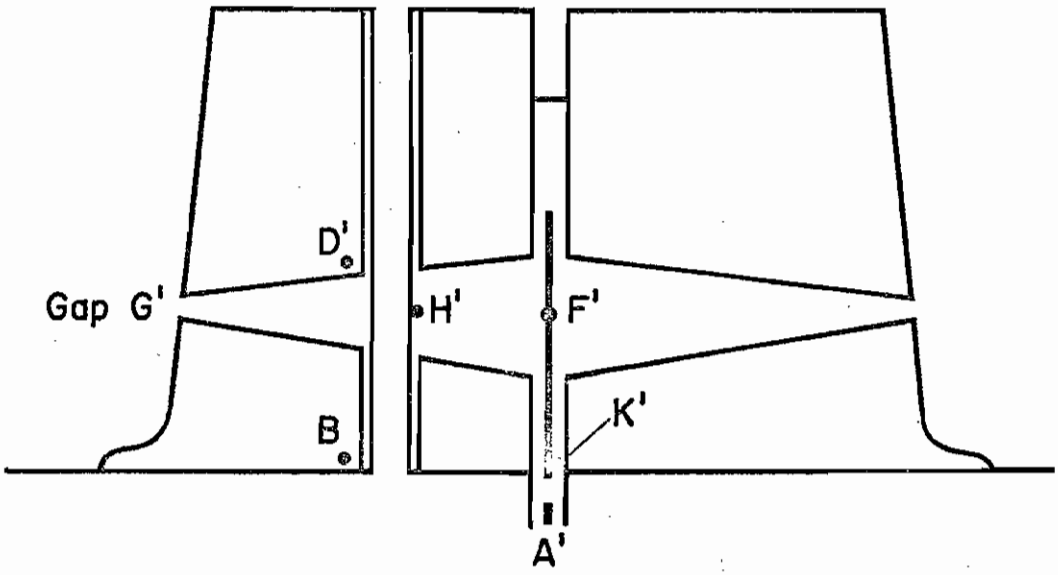

(a)

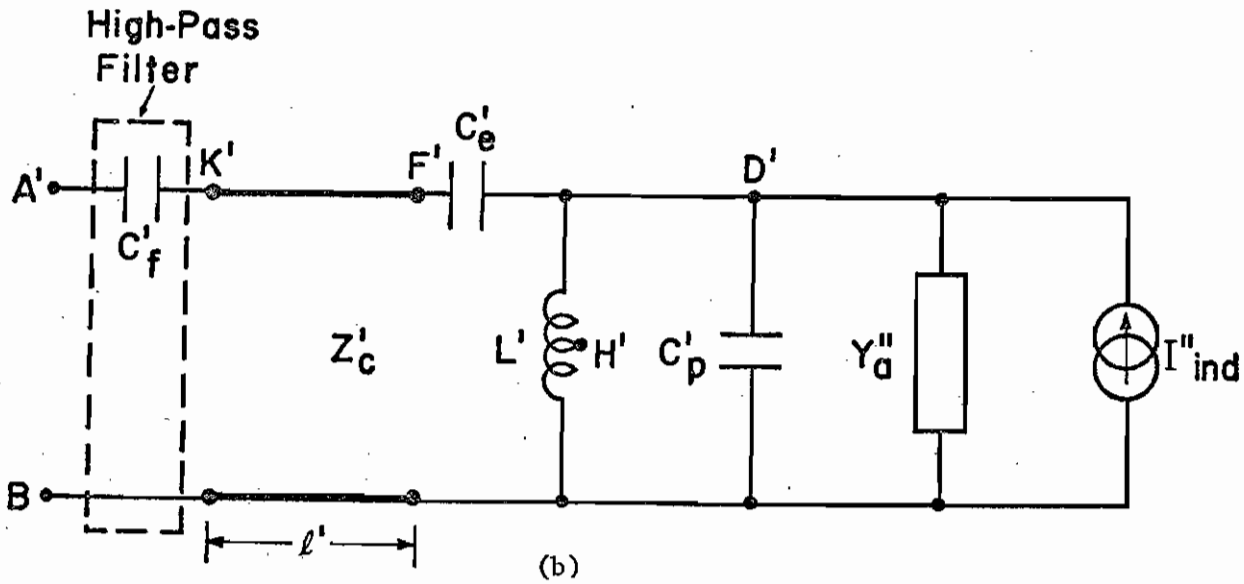

(b)

Fig.8. The in-band model of the L-band section

(a) the L-band section

(b) the equivalent circuit

Y''_a and the induced current I''_{ind} can now be calculated for the antenna in Fig.8(a), and

$$I''_{ind} = 3.15\times10^{-2}\ j\omega\epsilon_o E_n$$

$$= 2.79\times10^{-13}\ j\omega E_n.$$

Since the EMP contains very little energy in the L-band, we will not make any detailed numerical calculations for this frequency range.

Low-frequency circuit model

The low-frequency equivalent circuit resembles that of Fig.4 with the addition of the capacitance C'_f. This is shown in Fig.9.

Numerical result

Based on the circuit model of Fig.7(b), the input impedance and the complex effective height are numerically calculated and plotted versus frequency in Fig.10 and Fig.11, respectively. It is noticed that for frequencies below 400 MHz, the input impedance is primarily due to the filter C'_f, as expected.

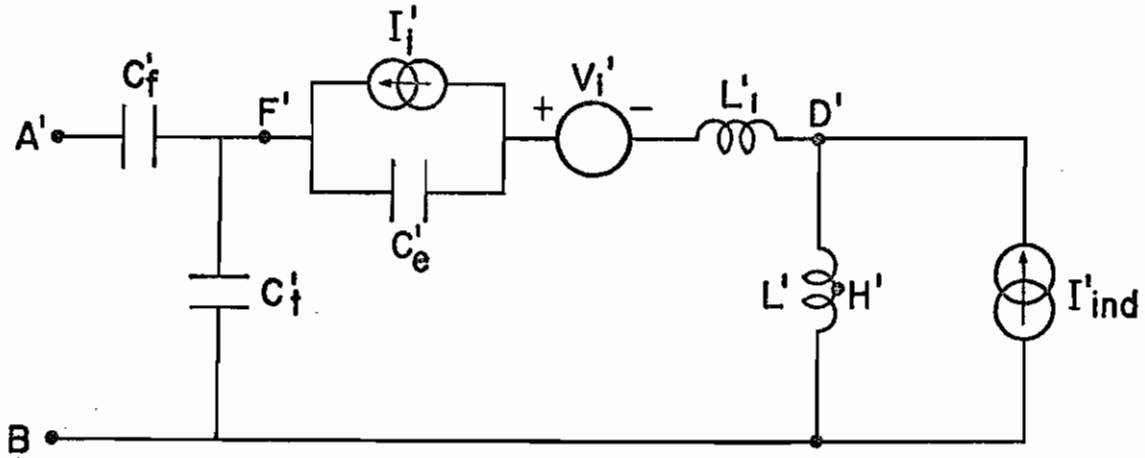

(a)

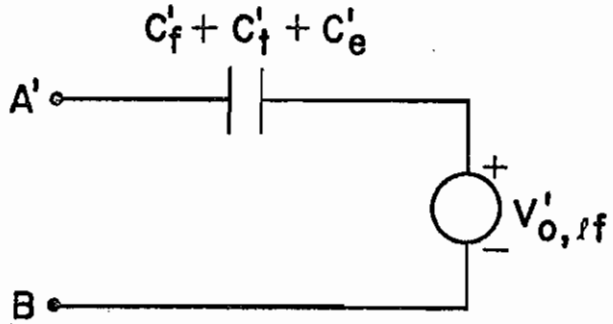

(b)

Fig.9. Low frequency model of the L-band section

(a) the equivalent circuit

(b) the Thévenin equivalent circuit at terminals A',B

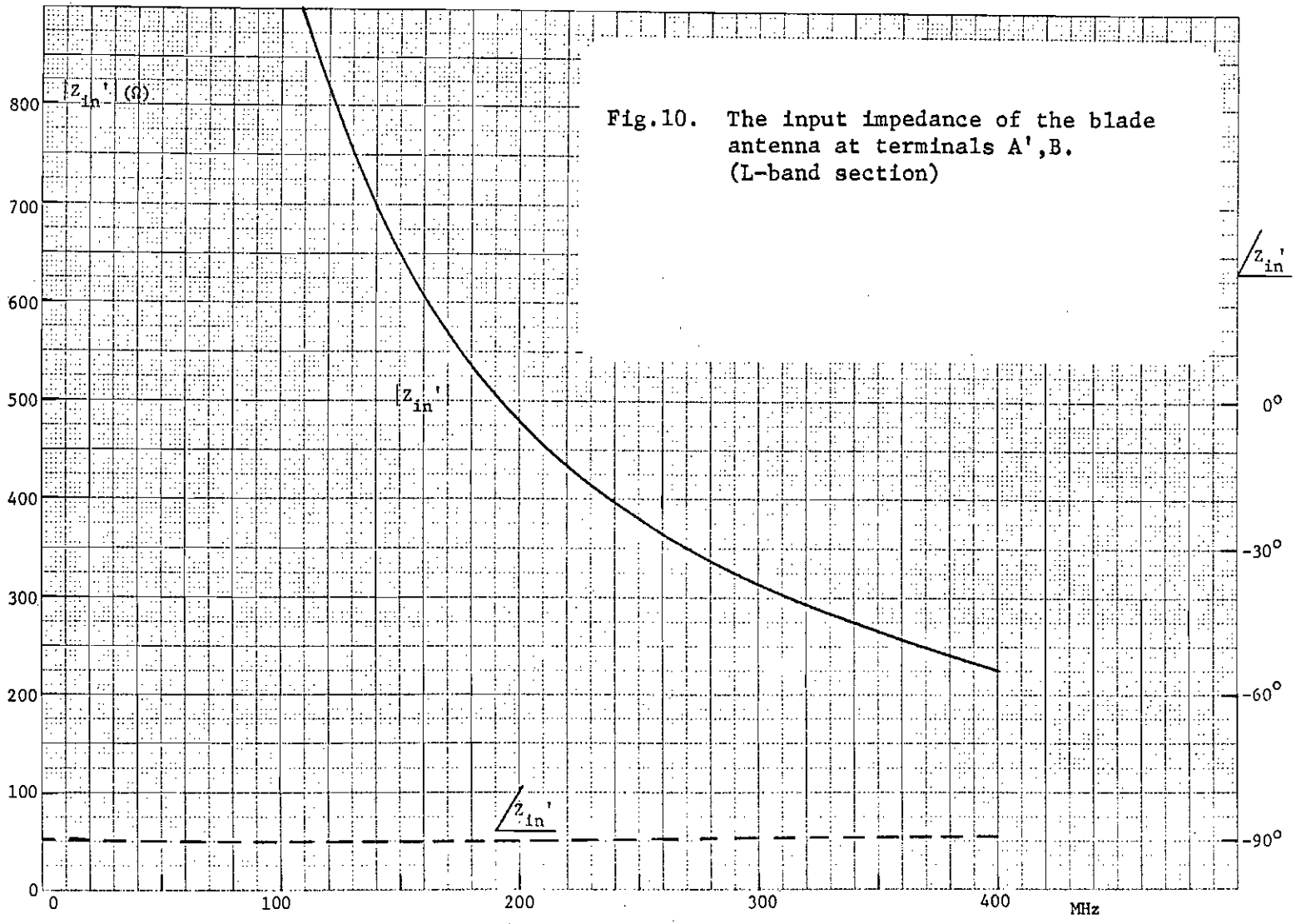

Fig.10. The input impedance of the blade antenna at terminals A',B. (L-band section)

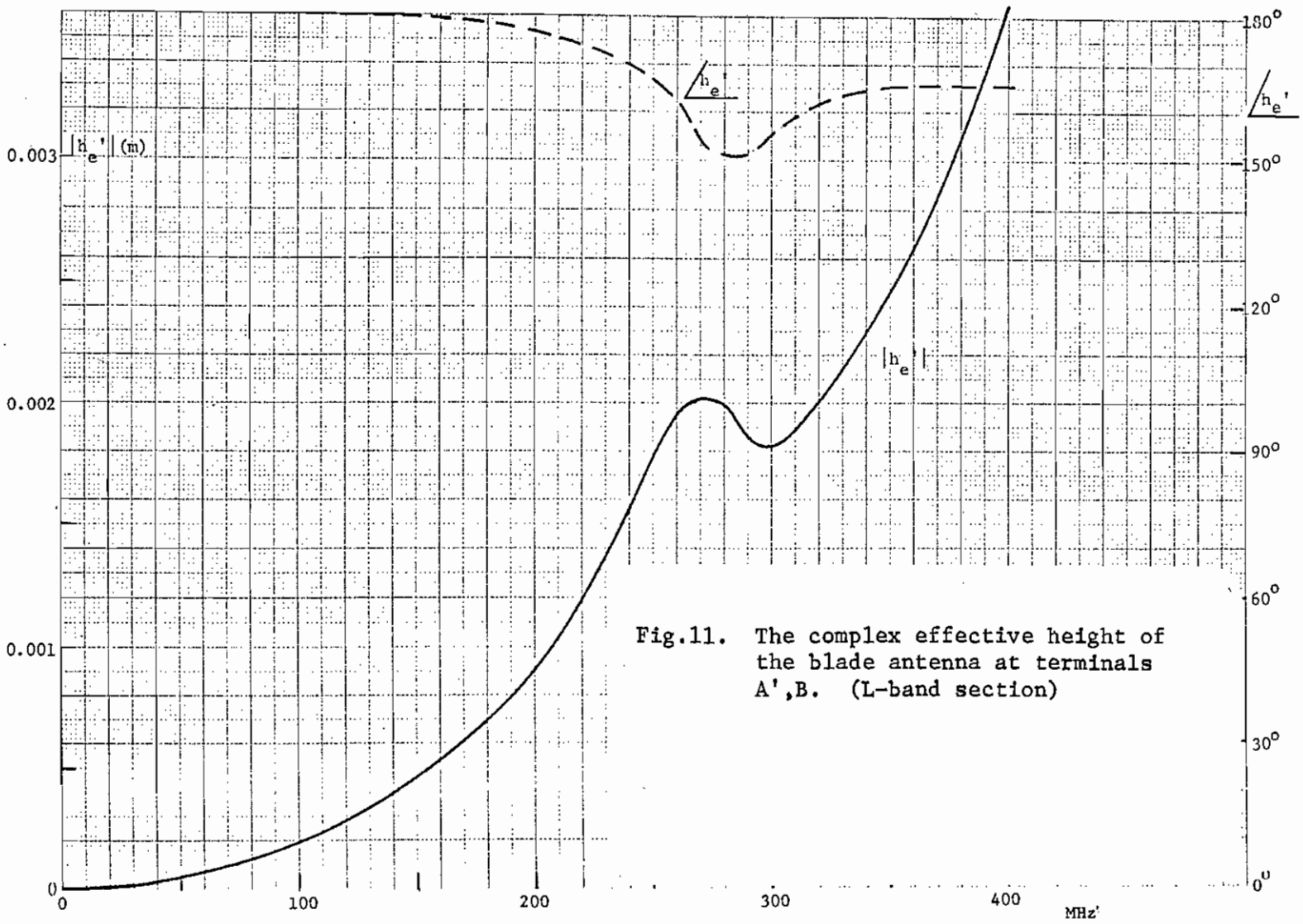

Fig.11. The complex effective height of the blade antenna at terminals A',B. (L-band section)

CHAPTER 9. RADAR ALTIMETER ANTENNA ON B-1

I. General Description

The radar altimeter system provides information on the absolute altitude (height above terrain) during approach and landing phases of the flight operation. There are two such systems on the B-1, and each system uses two identical horn antennas (Transco part no. 01-34-04550): one for transmitting the signal and the other for receiving the reflected signal from the ground. The antennas operate in the frequency range 4.25 - 4.35 GHz (wavelengths ≈ 6.9 - 7.1 cm), and they are flush-mounted at the bottom of the fuselage at about Y_F 440. In Fig. 1, the approximate location of the antennas and the external appearance of one antenna are shown. The antenna is in the form of a pyramidal horn, with a height of 4.4 cm and an aperture of 7.6 cm × 10.2 cm. The feeding element is a slotted coaxial line (Fig. 2).

II. Analysis

The wavelengths corresponding to the important portion of the EMP spectrum are very large compared to the physical dimensions of the altimeter antenna. Hence, in calculating the effect of EMP on this antenna, it is sufficient only to carry out a quasi-static analysis. We will first consider the open-circuit voltage and then the input impedance.

The voltage pick-up mechanism is illustrated in Fig. 2(b). The voltage across AB is approximately the same as that across DB. The potential at D, i.e., the center conductor, is approximately equal to that at D' and, hence, D", since the short coaxial line on the right hand side is short-circuited by the wall of the antenna. The outer conductor of the coaxial line and the walls of the horn antenna form a loop. A voltage is induced across D"B (hence AB) due to the magnetic flux linkage through the loop. Hence, a magnetostatic problem should be solved in order to calculate the open-circuit voltage across AB.

From the viewpoint of mathematical tractability, the horn antenna can be described as a quasi-pyramidal horn with an infinite flange as shown in Fig. 3. The scalar magnetic potential φ^* can be obtained by the method of separation of variables in the spherical coordinates. The magnetic field $\underline{H}$ is related to φ^* by

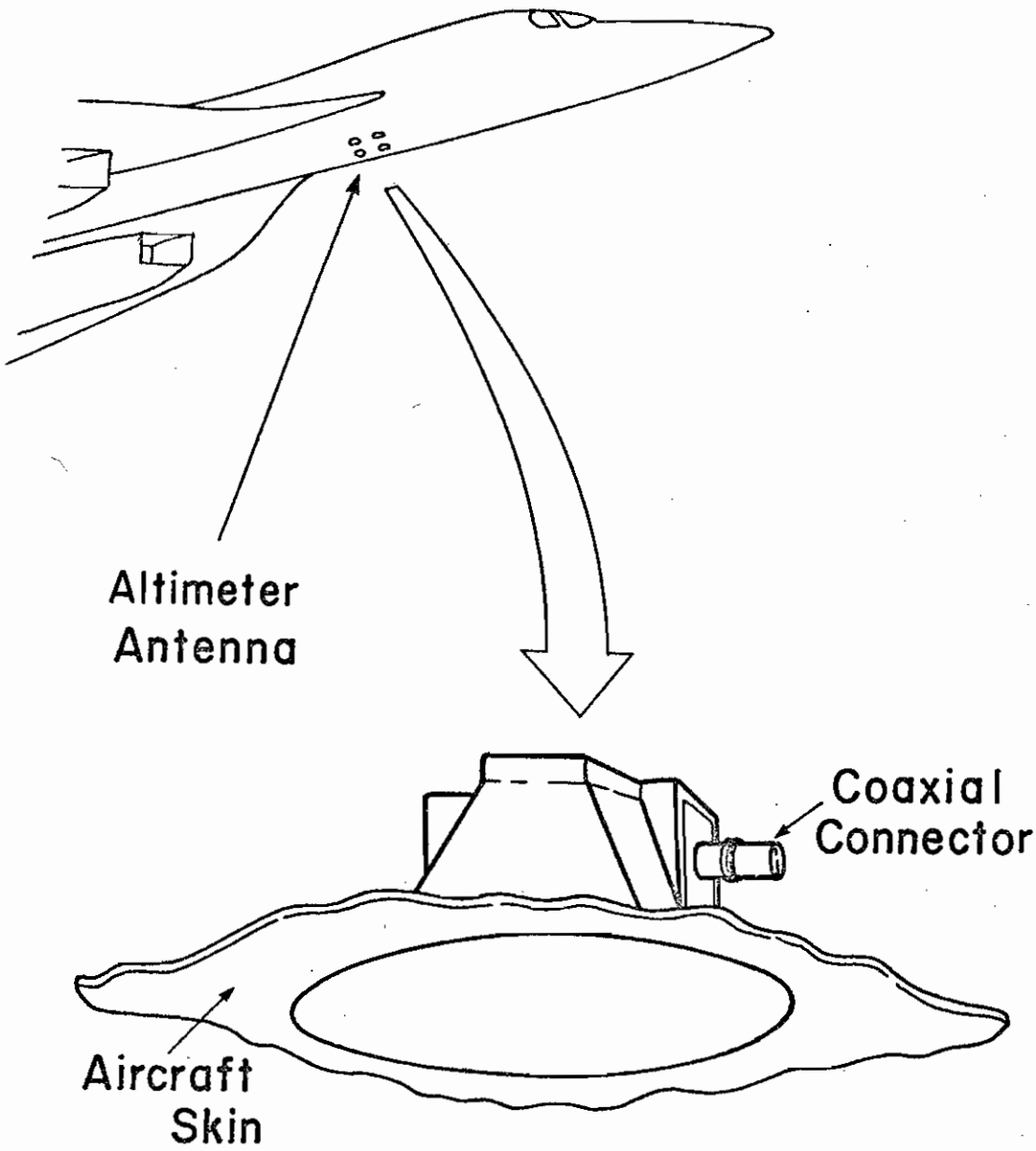

Fig.1. Location and external view of the Altimeter Antenna.

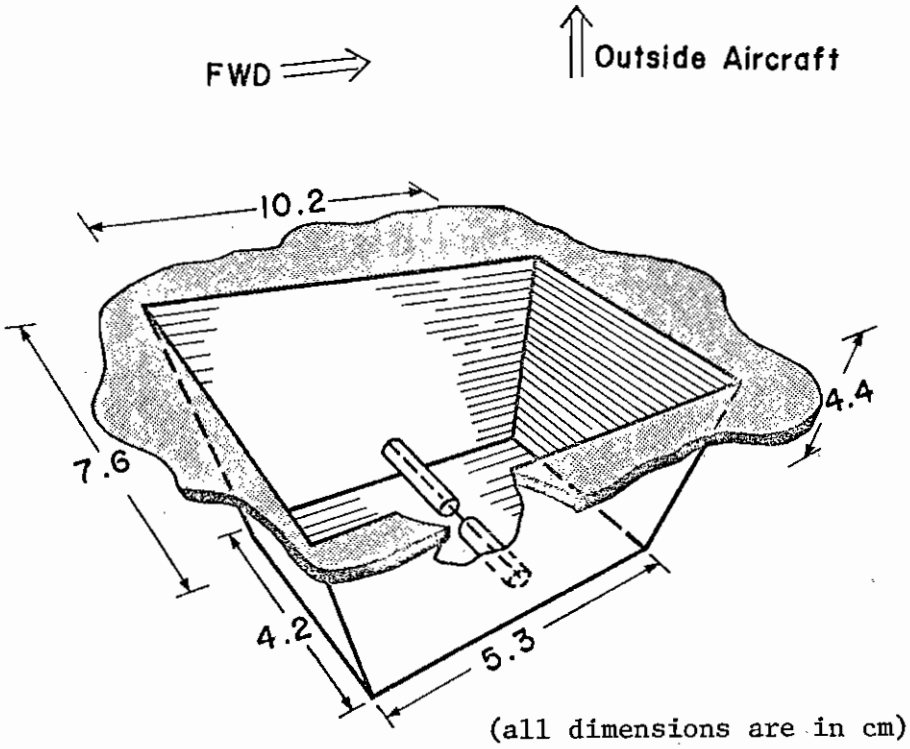

(a) Three-dimensional view.

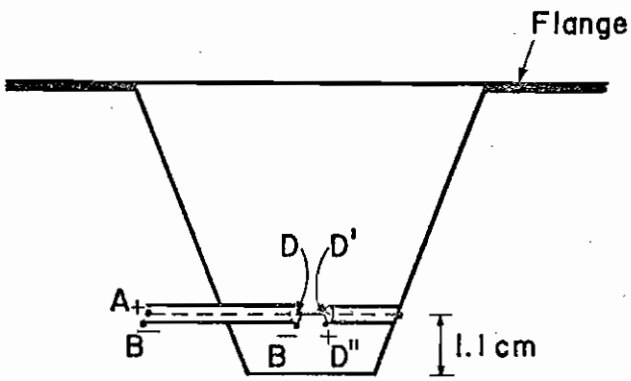

(b) Cross-sectional view through the feeding element.

Fig.2. Internal view of the Altimeter Antenna.

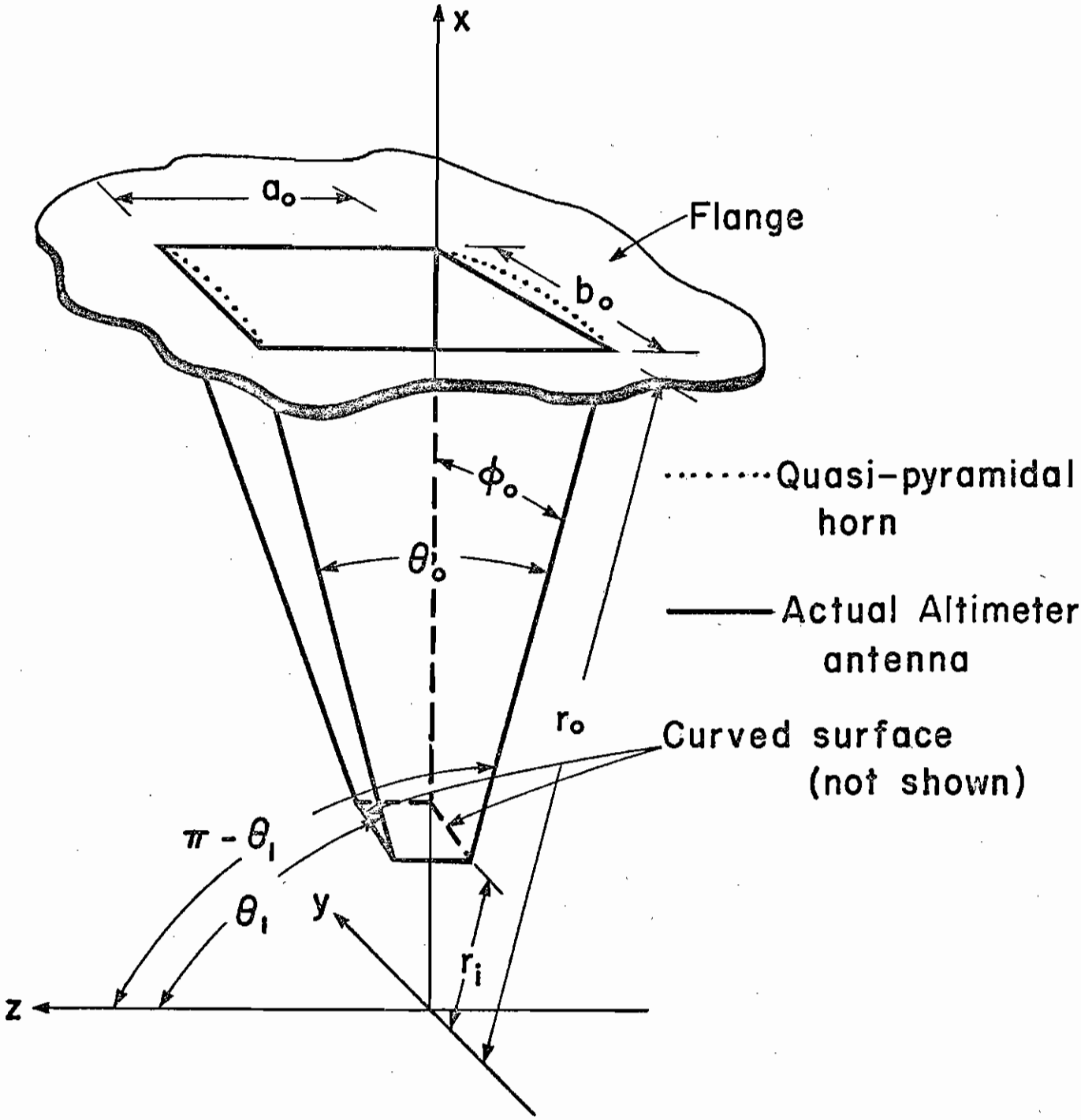

Fig.3. The Altimeter Antenna and its geometrical approximation: the quasi-pyramidal horn.

$$\underline{H} = -\nabla\varphi^* . \tag{1}$$

Inside the horn, the magnetic potential φ_i^* is given by

$$\varphi_i^*(r,\theta,\phi) = \sum_{p=-\infty}^{\infty} \sum_{q=1}^{\infty} A_{pq}\left[r^{\nu_q} + \nu_q/(\nu_q+1)r_i^{2\nu_q+1} r^{-\nu_q-1}\right]$$
$$\cdot\left[P_{\nu_q}^{\mu_p}(\cos\theta) - \left\{\frac{d}{d\theta} P_{\nu_q}^{\mu_p}(\cos\theta_1)/\frac{d}{d\theta} Q_{\nu_q}^{\mu_p}(\cos\theta_1)\right\} Q_{\nu_q}^{\mu_p}(\cos\theta)\right]\cos(\mu_p\phi) \tag{2}$$

where

$$\mu_p = p\pi/\phi_o, \qquad p = 0,\pm1,\pm2,....$$

and the values ν_q $(q = 1,2,3,....)$ depend on θ_1 and μ_p, and are the roots of the following transcendental equation:

$$\frac{d}{d\theta} P_{\nu_q}^{\mu_p}(\cos\theta_1) \frac{d}{d\theta} Q_{\nu_q}^{\mu_p}(-\cos\theta_1) - \frac{d}{d\theta} P_{\nu_q}^{\mu_p}(-\cos\theta_1) \frac{d}{d\theta} Q_{\nu_q}^{\mu_p}(\cos\theta_1) = 0$$

Thus, the normal derivative of φ_i^* in (2) vanishes on the four walls of the horn. In the above equations, r_i, θ_1 and ϕ_o are the horn parameters as defined in Fig. 3, $P_\nu^\mu(\cos\theta)$ and $Q_\nu^\mu(\cos\theta)$ are the associate Legendre functions of degree ν and order μ, of the first and the second kind, respectively. The coefficients A_{pq} are determined from the field distribution in the aperture.

Using Green's second identity with a Green's function G such that $\partial G/\partial n$ vanishes on the flange of the horn (which has a normal $\hat{n}$), the exterior scalar magnetic potential φ_e^* is given by

$$\varphi_e^* = \varphi_o^* - \int_S G \frac{\partial\varphi_e^*}{\partial n'} dS' \tag{3}$$

where φ_o^* is the incident magnetic potential. The Green's function satisfies the differential equation

$$\nabla^2 G(\underline{r};\underline{r}') = -\delta(\underline{r} - \underline{r}') \tag{4}$$

with the condition

$$\frac{\partial}{\partial n} G(\underline{r};\underline{r}') = 0 \qquad \text{at the flange} \tag{5}$$

The coefficients A_{pq} is obtained by solving (3) together with the boundary conditions

$$\varphi_e^* = \varphi_i^* \qquad \text{at the aperture} \tag{6a}$$

and

$$\frac{\partial \varphi_e^*}{\partial n} = \frac{\partial \varphi_i^*}{\partial n} \qquad \text{at the aperture} \tag{6b}$$

As can be seen, the solution of (2)-(6) is an extremely tedious and time-consuming process and will not be carried out in this report but may be studied in a future Interaction Note if warranted.

By studying the potential distribution inside a rectangular well with an infinite flange as depicted in Fig. 4, upper and lower bounds of the voltage induced across the terminals A,B of the horn antenna can be obtained from which the EMP induced voltage in the altimeter antenna can be estimated with a reasonable accuracy. The magnetic potential φ_i^* inside the rectangular well is found to be

$$\varphi_i^*(x,y,z) = \sum_{m=-\infty}^{\infty} \sum_{n=-\infty}^{\infty} C_{mn} \cos(m\pi z/a)\cos(n\pi y/b)\cosh(k_{mn}x) \tag{7}$$

where

$$k_{mn} = \pi\left[(m/a)^2 + (n/b)^2\right]^{\frac{1}{2}} \tag{8}$$

For the rectangular coordinates shown in Fig. 4, the Green's function, satisfying (4) and (5), is given by

$$G = (1/4\pi)\left[\left\{(x - x')^2 + (y - y')^2 + (z - z')^2\right\}^{-\frac{1}{2}} + \left\{(x + x')^2 + (y - y')^2 + (z - z')\right\}^{-\frac{1}{2}}\right]$$

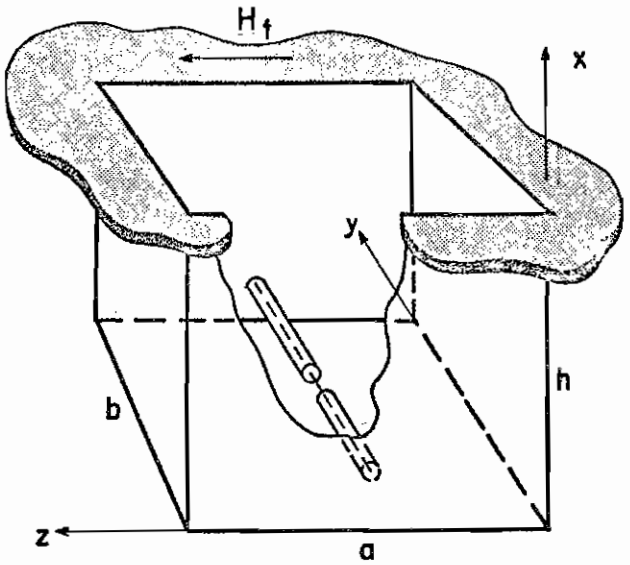

(a) Three-dimensional view.

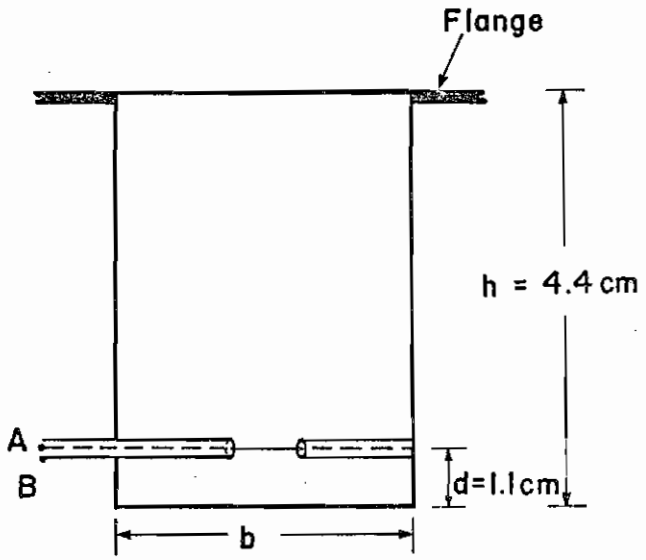

(b) Cross-sectional view through the feeding element.

Fig.4. Schematic diagram of the rectangular well.

For an incident magnetic field in the z-direction †

$$\underline{H}_o = H_t \hat{z},$$

we have

$$\varphi_o^* = H_t z.$$

By imposing conditions (6), the following integral equation is obtained for C_{mn}:

$$\sum_{m=-\infty}^{\infty} \sum_{n=-\infty}^{\infty} C_{mn} \cos(m\pi z/a)\cos(n\pi y/b)\cosh(k_{mn}h)$$

$$= H_t z - (1/2\pi) \sum_{m=-\infty}^{\infty} \sum_{n=-\infty}^{\infty} C_{mn} k_{mn} \sinh(k_{mn}h)$$

$$\cdot \int_o^a \int_o^b \left\{(y - y')^2 + (z - z')^2\right\}^{-\frac{1}{2}} \cos(m\pi z'/a)\cos(n\pi y'/b)dy'dz' \quad (9)$$

where, again

$$k_{mn} = \pi\left\{(m/a)^2 + (n/b)^2\right\}^{\frac{1}{2}} \quad (10)$$

The summation on the right hand side of (9) accounts for the coupling between the rectangular well and the half space above the flange. A complete solution of (9) requires considerable effort. However, if the coupling term is neglected, the result so obtained will be over-estimated by a factor of approximately 1.5 (see IN 10 for the case of a circular cylinder). This procedure amounts to assuming that the tangential magnetic field in the aperture is the same as the incident one. With this assumption, the z-component of the magnetic field inside the rectangular well becomes

---

†This assumed direction of $\underline{H}_o$ gives maximum induced voltage. For arbitrary direction the superposition principle applies.

$$H_z = 8H_t \sum_{m\ \text{odd}} \{m\pi \cosh(m\pi h/a)\}^{-1} \sin(m\pi z/a)\cosh(m\pi x/a) \qquad (11)$$

The open-circuit voltage V_{oc} at the terminals AB is given by

$$V_{oc} = -j\omega\mu_o H_t A_e \qquad (12)$$

where A_e is the effective area defined by

$$A_e = \int_o^a \int_o^d (H_z/H_t)\,dx\,dz$$

$$\simeq 16a^2 \sinh(\pi d/a) \Big/ \{\pi^3 \cosh(\pi h/a)\}.$$

The quantity a is the width of the well in the z-direction, and d is the height of the feed above the base. A plot of the effective area versus a/h is presented in Fig. 5. The point F in the graph corresponds to a rectangular well whose cross-sectional dimensions are those of the altimeter horn aperture, and this value of A_e is larger than the effective area of the altimeter antenna. The point G corresponds to a rectangular well with the cross-sectional dimensions equal to those of the small end of the altimeter antenna, and this value of A_e is smaller than the effective area of the altimeter antenna. Thus, the effective area of the altimeter antenna varies between 0.5 cm^2 and 1.25 cm^2. A reasonable estimate is

$$\text{effective area} \simeq 1.07\ cm^2$$

We now consider the input impedance of the altimeter antenna. Since the wavelengths of interest are very large compared to the dimensions of the horn, the input impedance is similar to that of a small loop antenna in free space except for a factor f_R which accounts for the fact that the loop radiates less efficiently due to its location inside the horn. At the frequency range of interest, the input impedance can be represented by a resistance R in series with an inductance L, as shown in Fig. 6.

The resistance R is given by

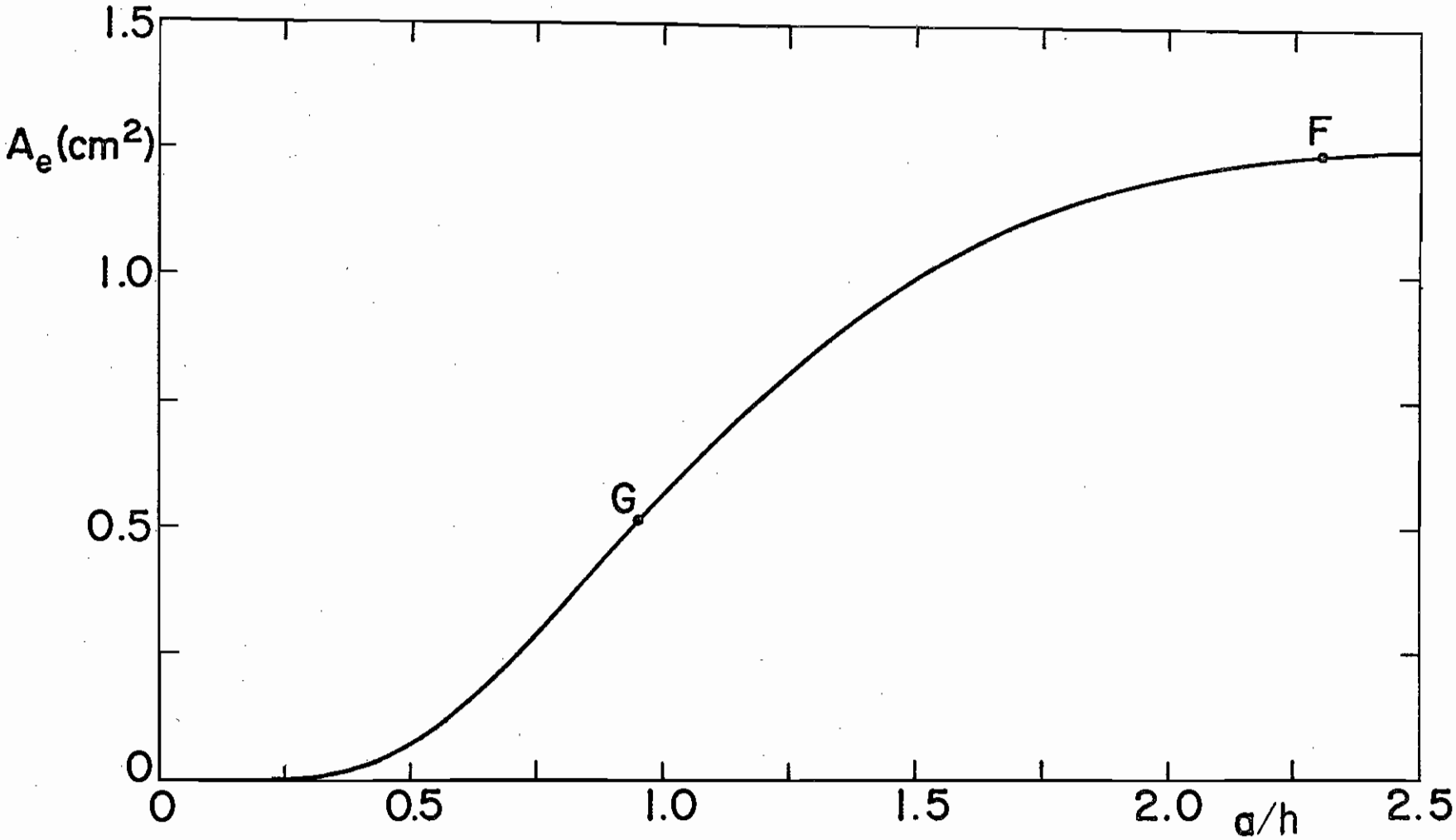

Fig.5. The equivalent area versus a/h. Points F and G constitute upper and lower bounds.

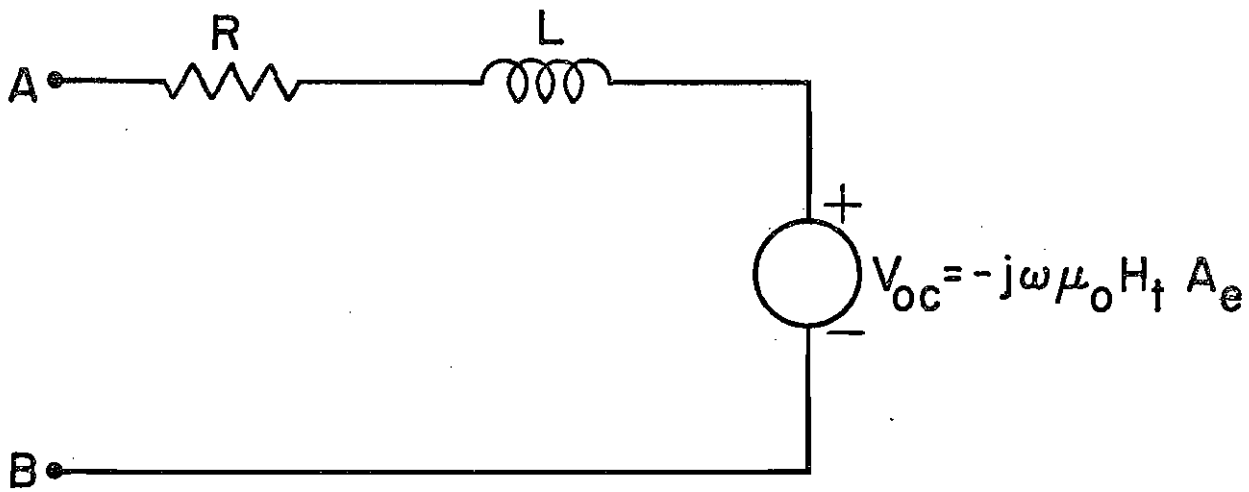

Fig.6. Thévenin equivalent circuit of the Altimeter Antenna at terminals A,B.

$$R = f_R R_o \tag{13}$$

where R_o is the radiation resistance in free space of a small loop with cross-sectional area A, and it is given by

$$R_o = 31200(Af^2/c^2)^2 \qquad \Omega$$

where f is the frequency and c is the speed of light in free space. The factor f_R is roughly given by

$$f_R = (a_o b_o/4\pi r_o^2) e^{-2\pi(h-d)/a}$$

where a_o and b_o are the dimensions of the aperture, and r_o is the distance from the vertex of the pyramidal horn to the aperture (see Fig. 3). For the present problem

$$f_R \approx 2.5\times10^{-2}.$$

The resistance R is very small and is given by

$$R \approx 1.7\times10^{-38} f^4 \qquad \Omega$$

where f is in Hz. At 100 MHz, the resistance is only about 1.7 $\mu\Omega$.

The inductance L is given by

$$L = (\mu_o p/2\pi)\ell n(p/2\pi r_a)$$

where p is the perimeter of the loop and r_a is the radius of the wire forming the loop. For this problem,

$$L = 25 \text{ nH}$$

Thus, the input impedance Z_{in} of the antenna is predominantly inductive, i.e.,

$$Z_{in} \simeq j\ 1.6\times10^{-7}\ f \qquad \Omega$$

where f is in Hz. At 100 MHz, the input impedance is about j 16 Ω.

CHAPTER 10. HF ANTENNA ON B-1

I. General Description

On the B-1, the excitation of the HF antenna is applied across a notch (i.e. open-ended slot), located on the vertical stabilizer. The slot is extended parallel to the leading edge of the vertical stabilizer for the purpose of providing impedance matching in the operating frequency range of 2 - 30 MHz (wavelengths ≃ 10 -150 m). The location and a schematic drawing of the notch antenna (sometimes called the shunt-fed antenna) are shown in Fig.1.

II. Analysis

Analysis of HF antennas on aircraft is a difficult tasks for the following reasons: First, the aircraft resonances are within the HF frequency range and so the complicated aircraft structure has to be taken into account in the analysis. Second, the HF antenna itself is usually not small compared with the main airframe. In this chapter, we analyze the HF notch antenna on the B-1 using the asymptotic theory for the current distribution on linear antennas. The result is valid up to the middle portion of the HF range (of about 16 MHz) where the fatness of the fuselage becomes appreciable. An accurate analysis for higher frequencies requires a much more complicated mathematical formulation and very elaborate numerical computation and is hence beyond the scope of this report.

It has to be emphasized, at this early stage, that in this chapter, the effective height and the input impedance are evaluated at the terminals A,B (Fig.1) of the notch antenna, thus *excluding* the HF coupler due to lack of information on the coupler. The HF coupler provides tuning to the notch antenna so that the combined unit has a reasonable impedance level at the in-band.

- - - - - - - - - - - - - -

The vertical stabilizer is very thin, and so the current flowing on the stabilizer is virtually the same as that on a plate. In Fig.2(a), we denote by I_2 the total current on the vertical stabilizer in the absence of the notch, and by I_1 the current that flows across the terminals of the notch. Considering the vertical stabilizer as a four-terminal network, simple circuit analysis reveals that the driving-point admittance Y_{in} at terminals A,B (Fig.2(b)) of the notch

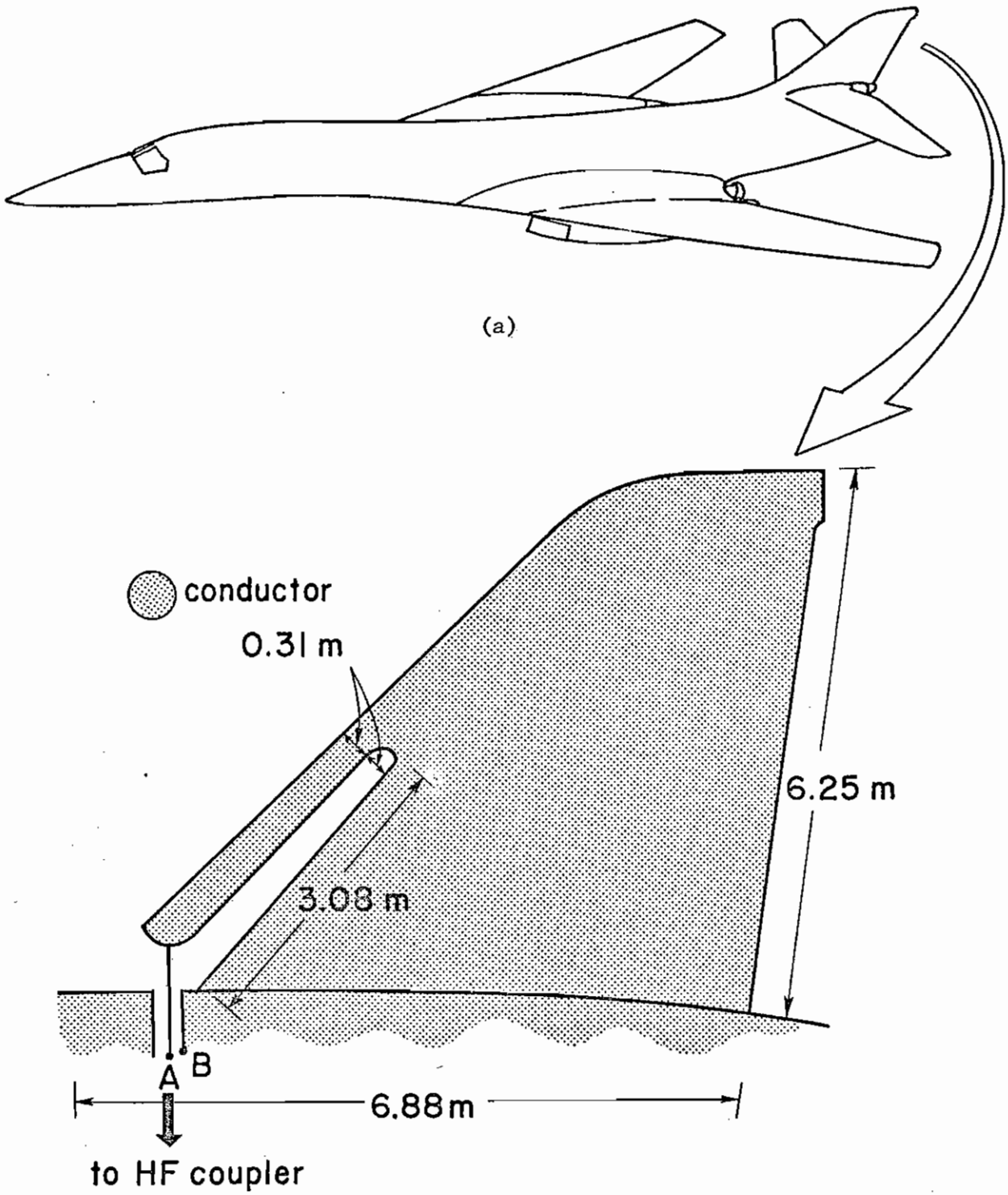

Fig.1. Location and schematic diagram of the HF notch antenna.

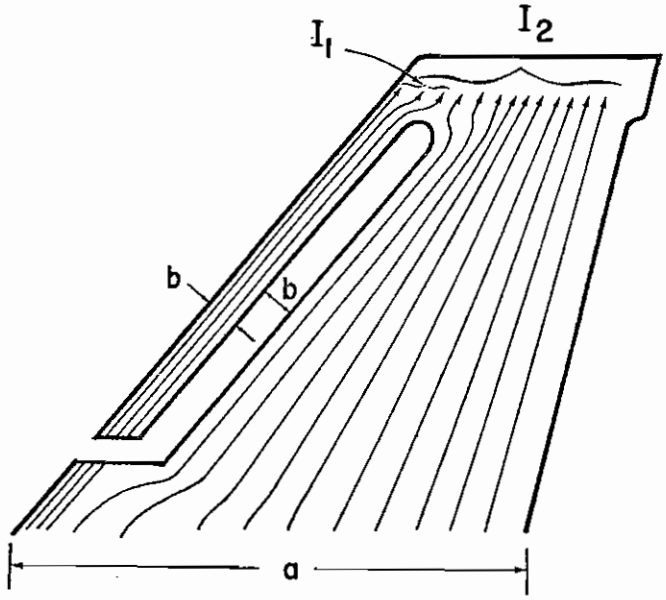

(a)

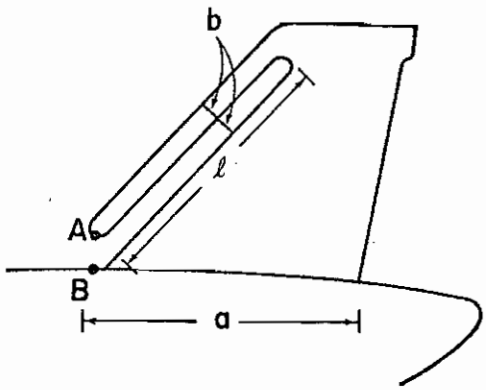

(b)

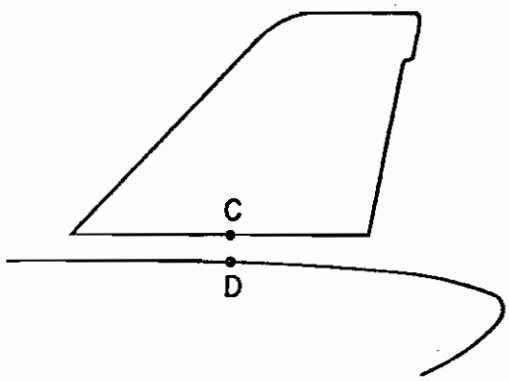

(c)

Fig.2. (a) Schematic current distribution on the notch antenna.
(b) The notch antenna showing the terminals A,B.
(c) The terminals C,D for calculating the antenna admittance Y_a.

antenna is related to the driving-point admittance Y_a of the antenna shown in Fig.2(c) by

$$Y_{in} = Y_t + (I_1/I_2)^2 Y_a \tag{1}$$

where Y_t is the admittance at A,B of the short-circuit transmission line formed by the extended slot parallel to the leading edge of the vertical stabilizer. The antenna in Fig.2(c) is formed by the vertical stabilizer without the notch, and it is driven across the gap which extends across the entire width of the stabilizer at the location of the open-ended slot. The equivalent circuit of the notch antenna is presented in Fig.3(a) where I_{ind} and Y_a are the induced current and antenna admittance of the antenna in Fig.2(c). The transmission line is due to the extended slot and has the characteristic impedance Z_c and length ℓ. The transformer accounts for the fact that only part of the induced current on the vertical stabilizer flows across the notch terminals, and we define the transformer ratio n as (c.f. (1))

$$n = I_1/I_2 \tag{2}$$

Also in Fig.3(a) V_ℓ is the voltage picked up by the loop formed by the slot and is important at low frequencies. It is given by

$$V_\ell \simeq -j\omega\mu_o A H_n$$

where A is the area formed by the slot and H_n the magnetic field perpendicular to this area. At low frequencies, the equivalent circuit is reduced to that of Fig.3(c), where L is the inductance due to the short-circuit transmission line.

The transmission line, as formed by the two conductors separated by the slot, can be considered as two unequal width coplanar strips. The characteristic impedance of this transmission line, as will be given in IN 182, is 189 ohm for the dimensions appropriate to the B-1 HF antenna.

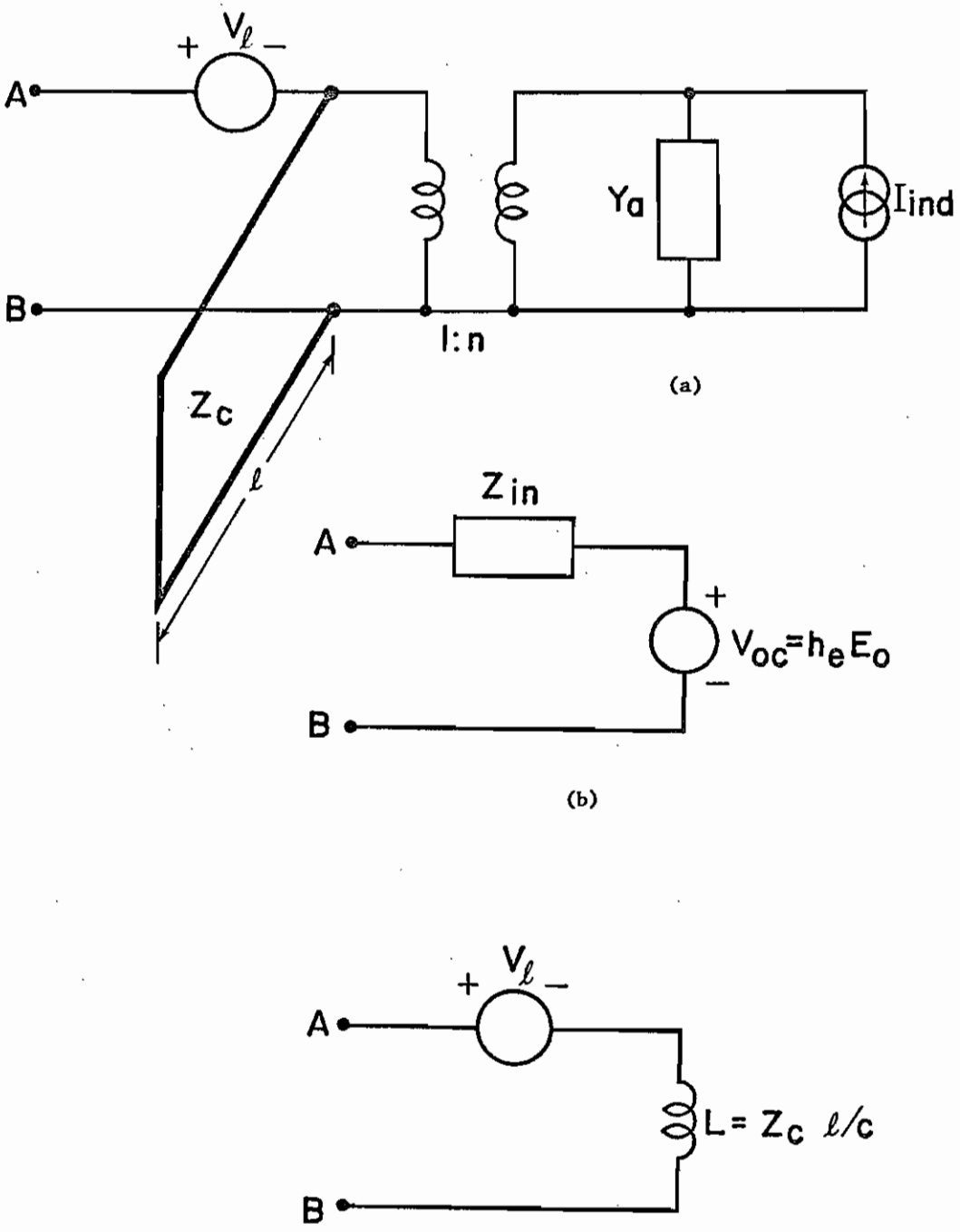

(c) The low frequency equivalent circuit.

Fig.3. (a) The equivalent circuit of the notch antenna.
(b) The Thevenin equivalent circuit.
(c) The low frequency equivalent circuit.

The transformer ratio n, as defined in (2), can be evaluated by first calculating the current distribution on the vertical stabilizer, and then using this current distribution to calculate the total current I_1 that passes across terminals A,B. The resulting formula is

$$n = I_1/I_2 = 1/2 - (1/\pi)\sin^{-1}(1-3b/2a) \tag{3}$$

where, as given in Fig.2, a is the width of the vertical stabilizer and b is both the width of the slot and the width of the conductor between the slot and the leading edge of the stabilizer. In Fig.4, n is plotted versus b/a. For the present case, n is about 0.12.

The antenna impedance Z_a, which is equal to the inverse of the antenna admittance Y_a, is evaluated by taking the whole airframe into account. This impedance is evaluated across terminals C,D of the simplified models of Fig.5 using the asymptotic theory of antenna current distribution. This theory is valid for all sweeps of the wings, including the aft wing position of Fig.5(a), and the forward wing position of Fig.5(b). Using this theory, the imaginary part of the antenna impedance at terminals C,D, i.e. the antenna reactance X_a, is given by

$$X_a = \frac{k}{Y_1}\cot k\ell_1 + \frac{k}{Y_2}\,\frac{1-\tan(k\ell_2)[\tan(k\ell_3) + (2Y_4/Y_2)\tan(k\ell_4)]}{\tan(k\ell_2) + \tan(k\ell_3) + (2Y_4/Y_2)\tan(k\ell_4)} \tag{4}$$

where $k(=\omega/c)$ is the wave number, ℓ_i and Y_i are the length and the shunt admittance per unit length of section i of the aircraft, respectively. As shown in Fig.5, section 1 is the vertical stabilizer, section 2 is the rear part of the fuselage, section 3 is the forward part of the fuselage, and section 4 denotes either wing. The quantity Y_i is given by

$$Y_i = \frac{j\omega 2\pi\epsilon_o}{0.116 - \ell n(ka_i)} \tag{5}$$

where a_i is the equivalent radius of section i. The real part of the antenna impedance at terminals C,D, i.e. the radiation resistance R_a, can be evaluated

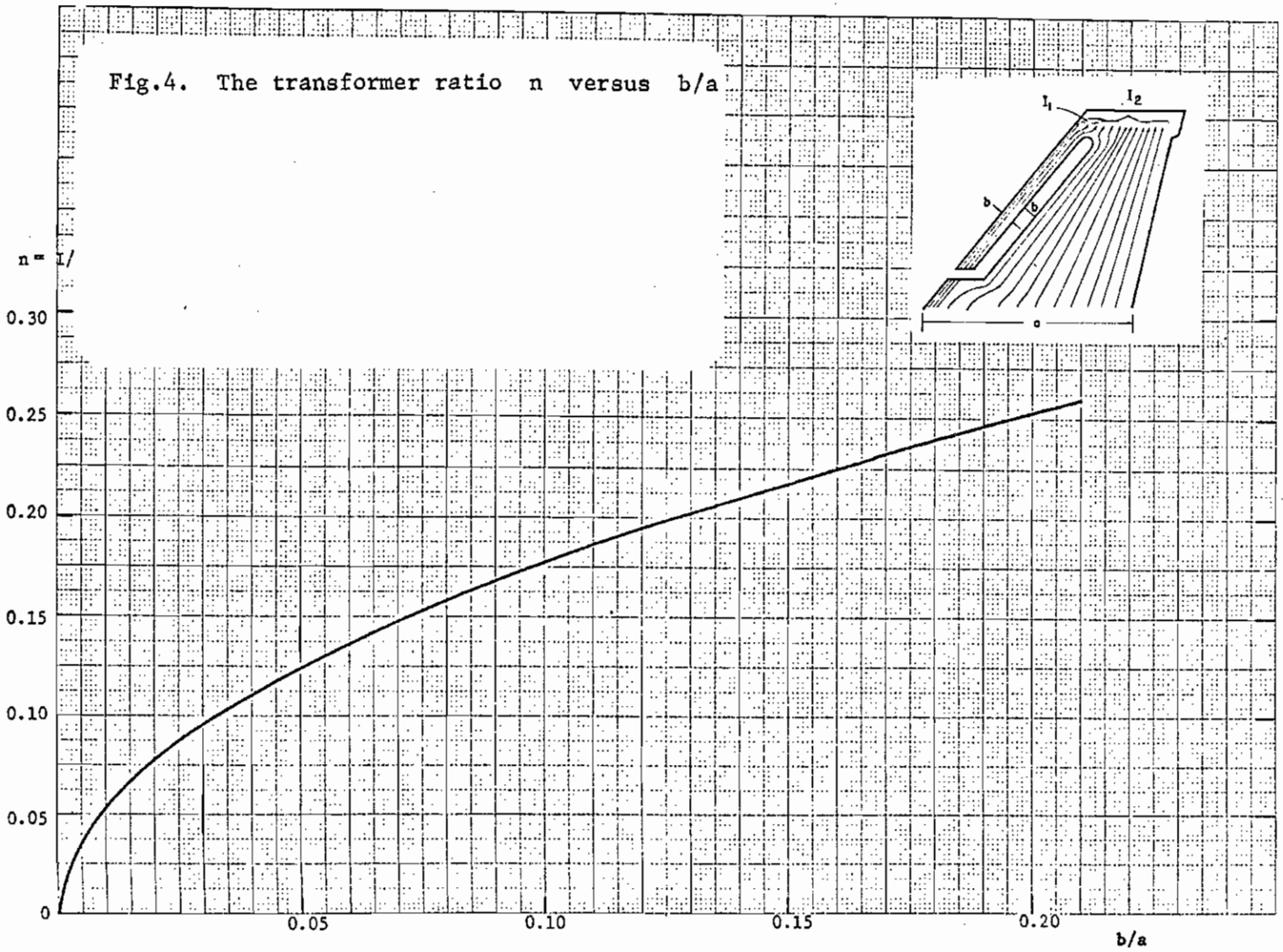

Fig.4. The transformer ratio n versus b/a

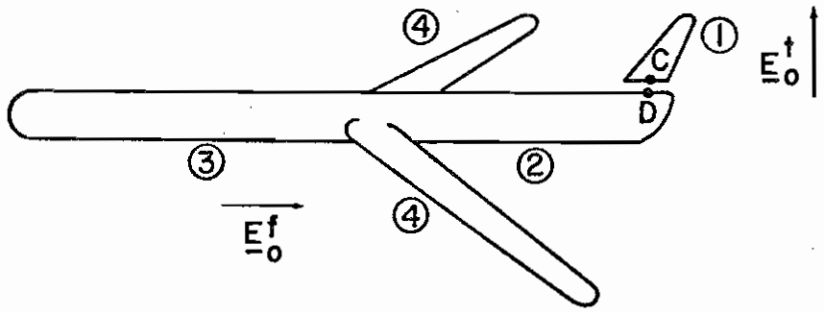

(a)

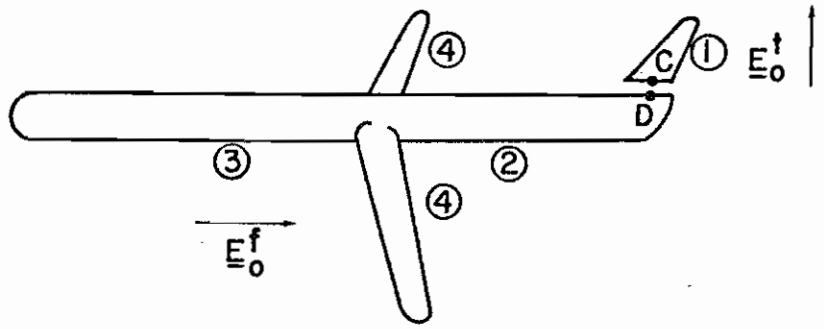

(b)

Fig.5. Models used for calculating currents on the aircraft

(a) the model corresponding to the aft wing position
(b) the model corresponding to the forward wing position.

in the following way: First, evaluate the current distribution on the aircraft by the asymptotic theory. Second, from the knowledge of the current distribution, evaluate the total radiated power by integrating the Poynting vector over all solid angles. The total radiated power enables us to obtain the radiation resistance. As can be observed in (4), at the resonances of the aircraft, the formula is not valid. In these frequency regions, we combine the asymptotic theory with a more elaborate antenna theory to get the results presented in Fig.6, where the antenna impedance remains finite. We observe that most resonances within the frequency range presented are associated with the fuselage and the wings. Other resonances due to more complicated mechanisms are also observed.

The input impedance at the terminals A,B is presented in Fig.7. It is observed that this impedance is mainly due to the transmission line. The reason is that the antenna admittance is reduced by a factor $n^2 = 0.014$ due to the transformer, and is small compared with the transmission line admittance. Again, we want to emphasize that the impedance curve in Fig.7 refers to the terminals A,B prior to the HF coupler, within which there are more impedance matching networks.

We now continue with the calculation of the effective height. To this end we consider the induced current I_{ind} across terminals C,D of the simplified models in Fig.5. The induced current depends on the polarization of the incident field. Two cases are of interest, namely, (i) the incident electric field being parallel to the vertical stabilizer, and (ii) the electric field being parallel to the fuselage. For these two cases, the asymptotic theory gives the following results:

(i) Incident electric field E_o^t parallel to vertical stabilizer

$$I_{ind}^t / E_o^t = \frac{j2\pi[1-\cos(k\ell_1)]\sin[k(\ell_2+\ell_3)]}{Z_o \ell n[(\ell_1+\ell_2+\ell_3)/a]\sin[k(\ell_1+\ell_2+\ell_3)]} \tag{6}$$

(ii) Incident electric field E_o^f parallel to fuselage

$$I_{ind}^f / E_o^f = \frac{j2\pi[1-\cos\{k(\ell_2+\ell_3)\}]\sin(k\ell_1)}{Z_o \ell n(\ell_1/a)\sin[k(\ell_1+\ell_2+\ell_3)]} \tag{7}$$

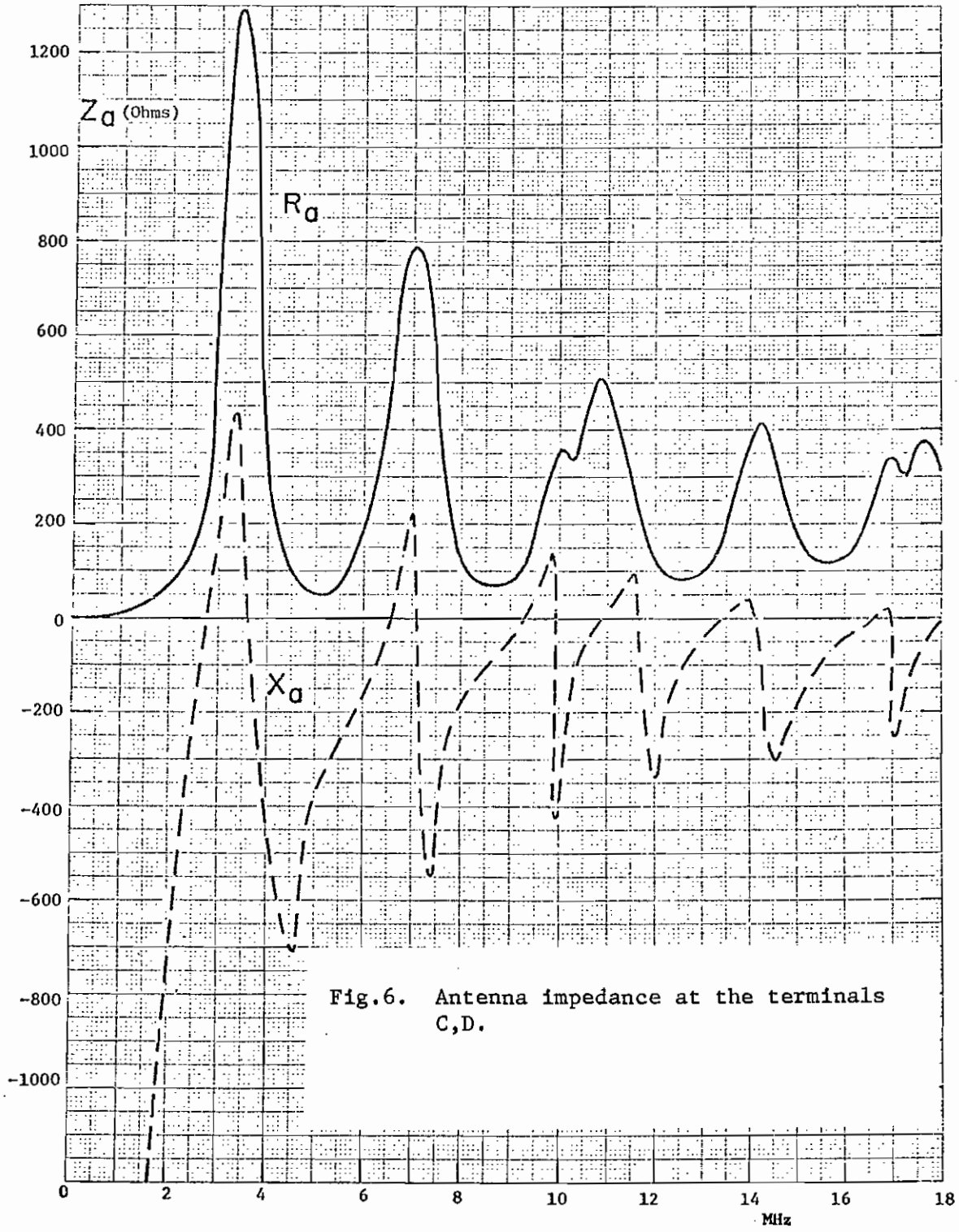

Fig.6. Antenna impedance at the terminals C,D.

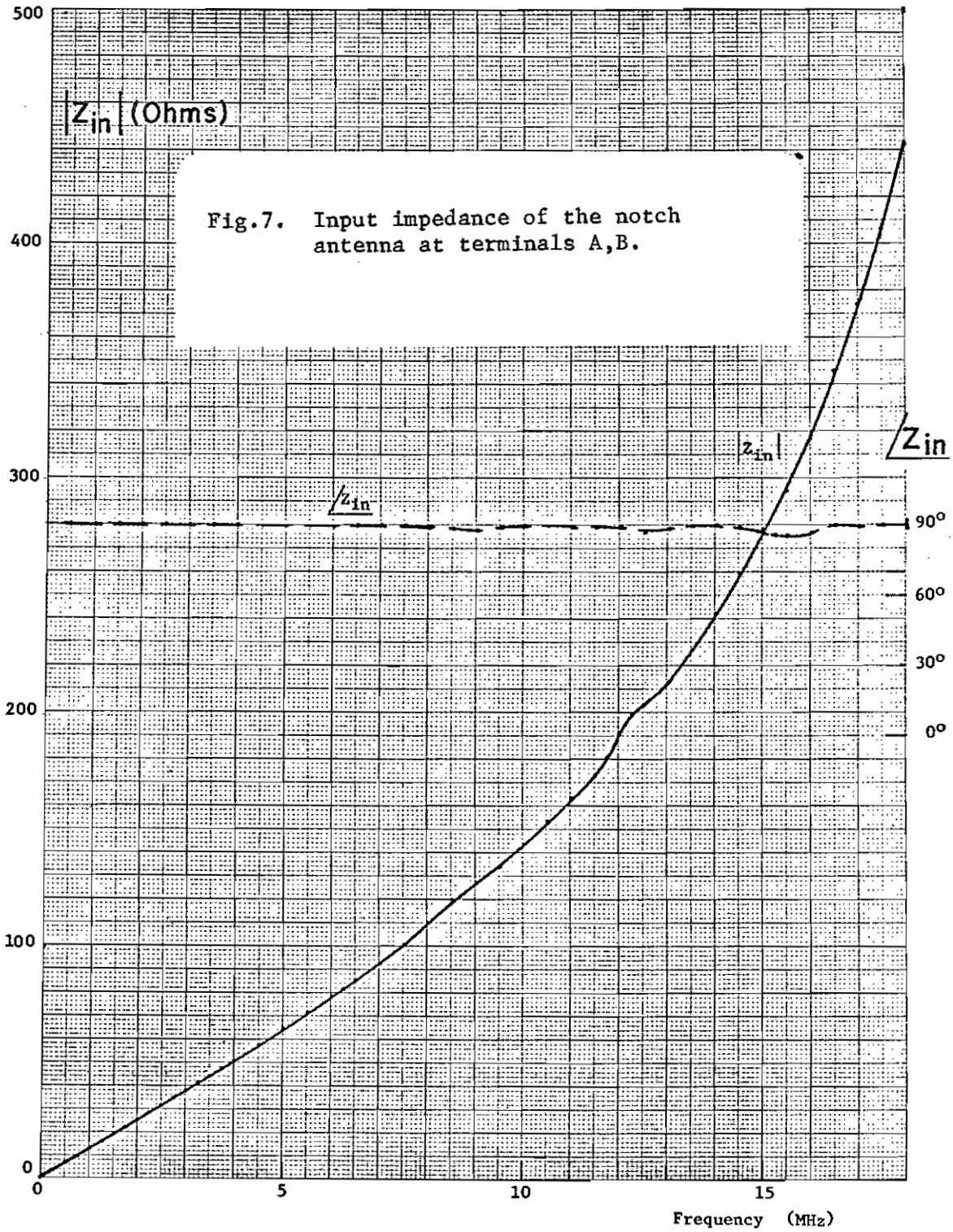

Fig.7. Input impedance of the notch antenna at terminals A,B.

where $Z_o \doteq 377\Omega$, ℓ_i is the length of section i of the airframe as defined in Fig.5, and a is the equivalent radius of the airframe. In (6) and (7), the contribution due to the wings has not been directly taken into account in the strict sense. However, for the B-1, the electrical path from a wing extremity to the vertical stabilizer is about the same as that from the nose to the vertical stabilizer, and hence the main resonances of the wings and the fuselage are in a sense accounted for. Equations (6) and (7) are just some of the results in Interaction Note 186 on the subject of the application of SEM and perturbation methods to EMP coupling with aircraft-like structures.

The open-circuit voltage can now be obtained by a simple analysis of the equivalent circuit shown in Fig.3(a). The current source I_{ind} is the short-circuit current induced across the terminals C,D, and is given by either (6) or (7) depending on the polarization of the incident field with respect to the aircraft. The open-circuit voltage V_{oc} thus also depends on the polarization of the incident field. Effective heights h_e^t and h_e^f can be defined to relate the open-circuit voltage to the *incident* electric field. For the case where the incident electric field, $E_o^t(\omega)$, is parallel to the vertical stabilizer, we define the effective height $h_e^t(\omega)$ so that the open-circuit voltage $V_{oc}^t(\omega)$ is given by

$$V_{oc}^t(\omega) = h_e^t(\omega)\ E_o^t(\omega). \tag{8}$$

Similarly, for the case where the incident electric field, $E_o^f(\omega)$, is parallel to the fuselage, the effective height $h_e^f(\omega)$ is defined so that the open-circuit voltage $V_{oc}^f(\omega)$ is given by

$$V_{oc}^f(\omega) = h_e^f(\omega)\ E_o^f(\omega). \tag{9}$$

We again observe that (6) and (7) are not valid at the resonances of the aircraft. As in the analysis of the antenna impedance discussed above, we combine (6) and (7) with a more elaborate antenna theory so that the induced current remains finite. The two effective heights at terminals A,B are presented in Fig.8 and Fig.9. Let us emphasize again that in (8) and (9), the *incident* electric fields are used in the definitions of the effective heights.

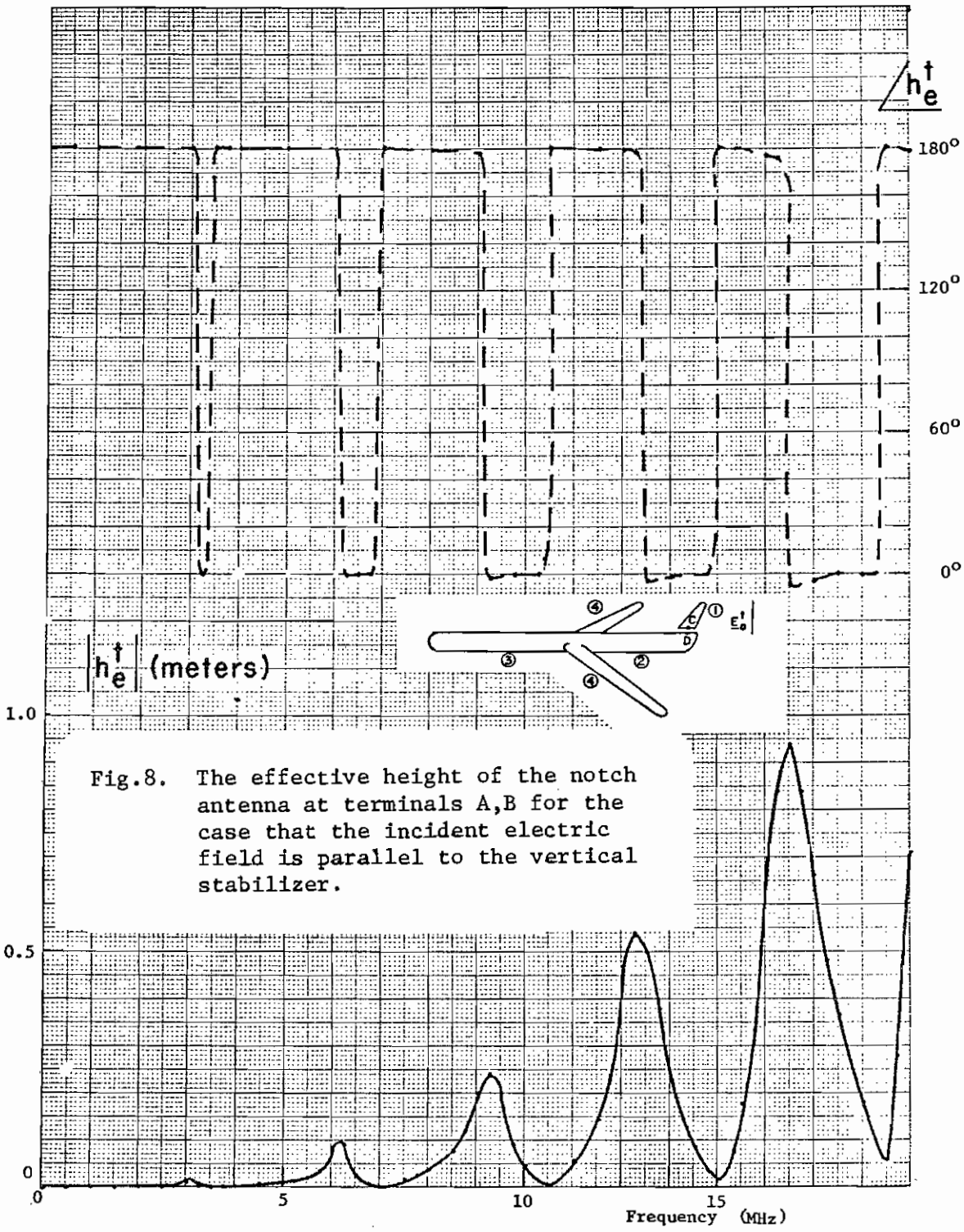

Fig.8. The effective height of the notch antenna at terminals A,B for the case that the incident electric field is parallel to the vertical stabilizer.

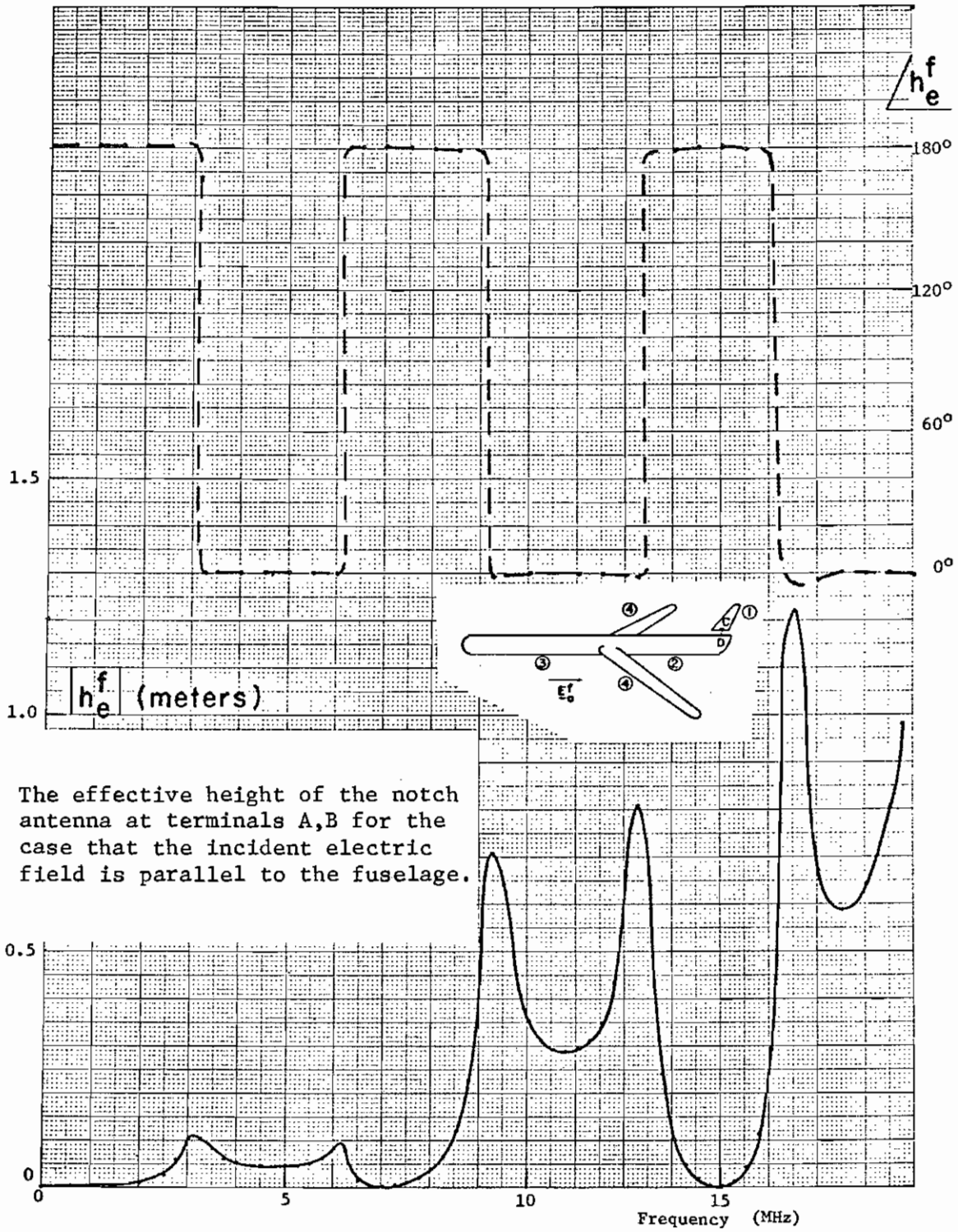

Fig.9. The effective height of the notch antenna at terminals A,B for the case that the incident electric field is parallel to the fuselage.

CHAPTER 11. AL 1216-1 GLIDESLOPE ANTENNA ON B-1

I. General Description

The B-1 glideslope antenna is located on the lower forward radar bulkhead at location Y_F - 160. It has an operational frequency range of 329-335 MHz. The antenna, approximately 7.6 cm wide and 11.4 cm high, is situated on a ground plane which is a 96.5 cm wide segment of a 71.8 cm radius circle. The antenna is tilted forward from the horizontal at an angle of 17°.

II. Analysis

The glideslope antenna, depicted in Figure 1, is a two-turn Moebius half-loop. For low frequencies the antenna, due to its location and orientation, is excited predominantly by the magnetic field produced by the H anti-symmetric current mode* induced on the aircraft wings by the EMP. This field will be distorted due to the presence of the fuselage. This distortion could be estimated by modeling the fuselage as a semi-infinite axially symmetric body as in SSN 102. In that analysis the shape of the body is sought which corresponds to the known field of a given magnetic source distribution and also resembles the body of interest. However, since the incident field assumed in SSN 102 is perpendicular to that considered here, and since an extension of that analysis to the present case is non-trivial, distortion is not considered in this analysis. The total magnetic field appearing at the glideslope antenna calculated here can be used as the incident field in such an analysis of the distortion.

There are several conducting obstacles located in the radome near the glideslope antenna such as radar dishes and electronic packages. In addition the bulkhead itself is directly behind the antenna ground plane. Little information is available concerning the electrical characteristics of the bulkhead and conducting obstacles such as their electrical contact with each other or with the glideslope ground plane.

---

*See IN 85 for definition of field conventions.

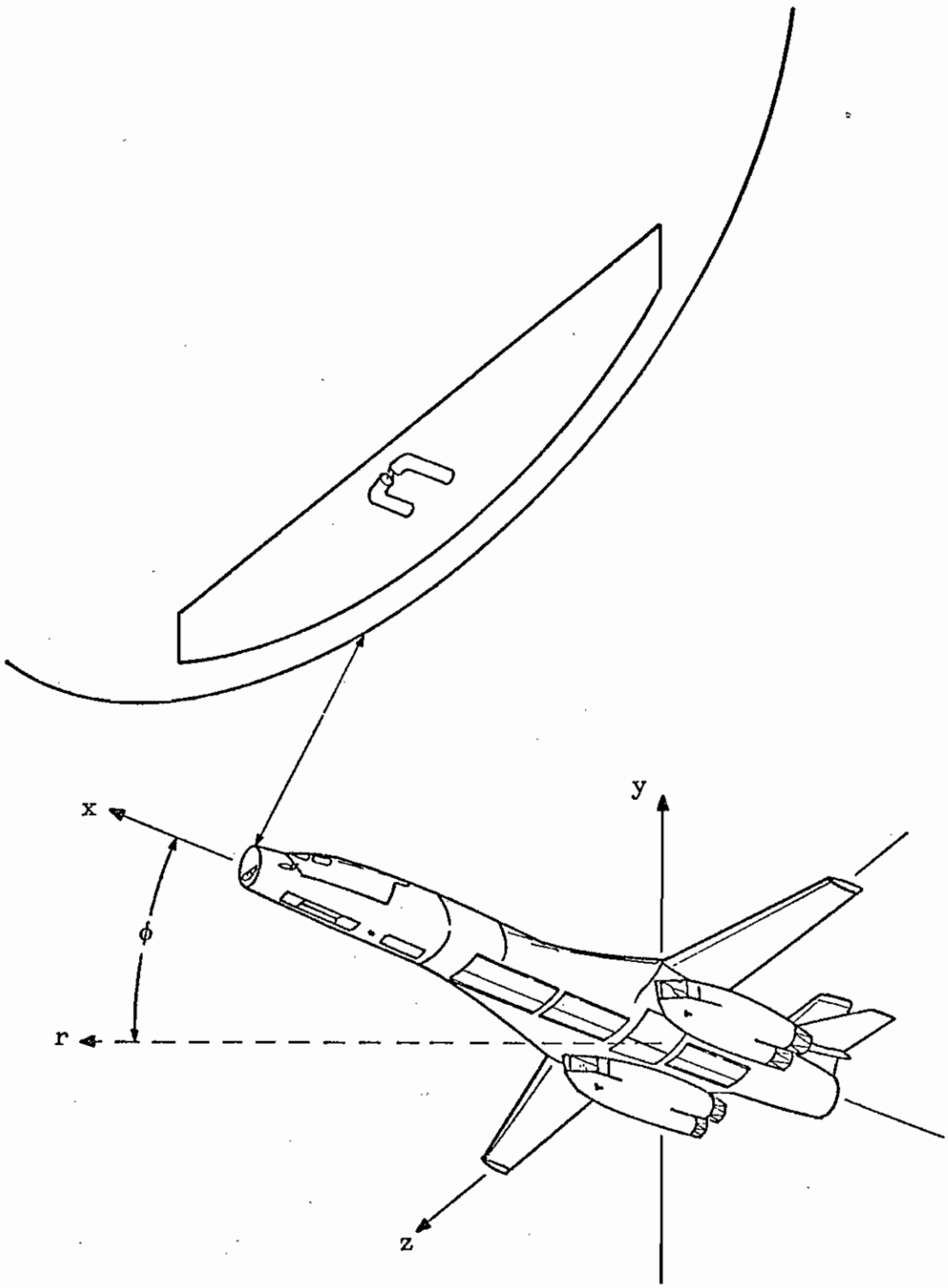

Fig. 1.--Configuration of the AL 1216-1 glideslope antenna and geometry used in analysis.

Often, however, a bulkhead is a sparse metallic structure which supports the radome and the instruments located there. For the purposes of this analysis it will be assumed that the glideslope antenna is mounted on an infinite ground plane with no other conducting obstacles present. It is realized that this is a gross approximation since we have already mentioned that several radar dishes are mounted near the antenna. However, until more detail concerning the electrical characteristics of these obstacles can be obtained, it is felt that they should be neglected. Although the bulkhead actually represents a finite ground plane to the glideslope antenna with respect to the incident EMP wavelength, no detailed analysis exists for the behavior of a two-turn Moebius half-loop oriented above a finite ground plane, and hence the loop is assumed to be mounted on an infinite plane.

This analysis uses a perpendicular crossed-wire model to predict the skin currents on the B-1 configuration. Hence these results apply for the B-1 in subsonic flight configuration only, i.e., the wings are not swept but are fully extended.

To first order the currents running along the B-1 fuselage possess rotational symmetry about the x-axis. Such currents produce only magnetic fields in the y-z plane, which do not couple with the glideslope antenna. However, H anti-symmetric current modes on the aircraft wings produce magnetic fields in the ϕ-direction which do couple with the glideslope antenna. Assuming an incident electromagnetic plane wave, the wing currents are obtained by utilizing the crossed-wire theory of IN 85 encoded in the computer program XWIR1. The largest currents on the wings are produced by a plane wave with an electric field polarization parallel to the wings. Given the aircraft wing currents the resulting magnetic field, $\tilde{B}_{\phi}(\omega)$, can be simply obtained. In order to obtain an analytical expression for $\tilde{B}_{\phi}(\omega)$, the wing currents obtained from XWIR1 are approximated by

$$\tilde{I}(z,\omega) = 1.26\, \tilde{I}_{o}(\omega) \sin [k(\ell - |z|)] .$$

Figure 2 gives the actual current distribution (solid line) and the approximated current distribution (dashed line) as a function of position near the structure resonance ($k\ell = 1.3$). Since the magnetic field produced by the wing current is proportional to its integral over the wing length, the normalization constant of the analytical fit to the current is chosen such that the total areas under the actual curve and analytical curve are approximately equal. $\tilde{I}_o(\omega)$, the wing root current, is shown as a function of frequency in Figure 3. Here ℓ is the wing half-length, and $k = \omega/c$ is the propagation constant. The magnetic field at the glideslope antenna due to the induced wing currents is then[1]

$$\tilde{B}_\phi(\ell, 0, \omega) = \frac{1.26\, j\mu_o \tilde{I}_o(\omega)}{2\pi\ell} \left(e^{-\sqrt{2}\, jk\ell} - e^{-jk\ell} \cos k\ell \right)$$

since the plane $z = 0$ passes through the glideslope. The magnitude of this field, normalized to the magnitude of the incident electric field, is given in Figure 4 as a function of frequency. The B-1 wing half-length is taken as $\ell = 20.9$m. The total magnetic field at the glideslope antenna is a sum of the incident magnetic field, $\tilde{B}_o(\omega)$, and that produced by the induced wing currents.

[1] King, R. W. P., The Theory of Linear Antennas, pg. 525.

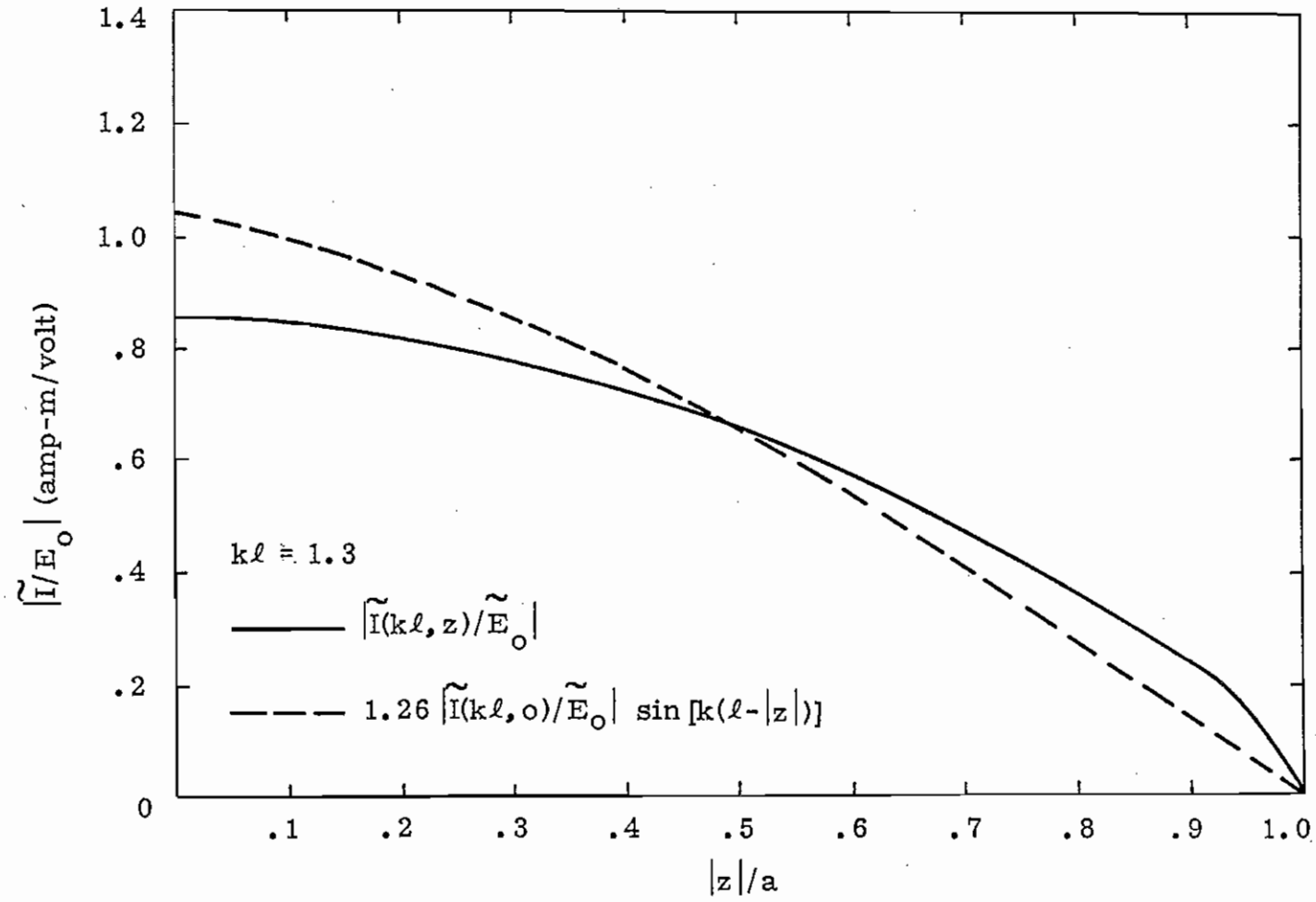

Fig. 2.--Actual and approximate current distributions as a function of position for $k\ell = 1.3$. The distributions are normalized to the magnitude of the incident electric field.

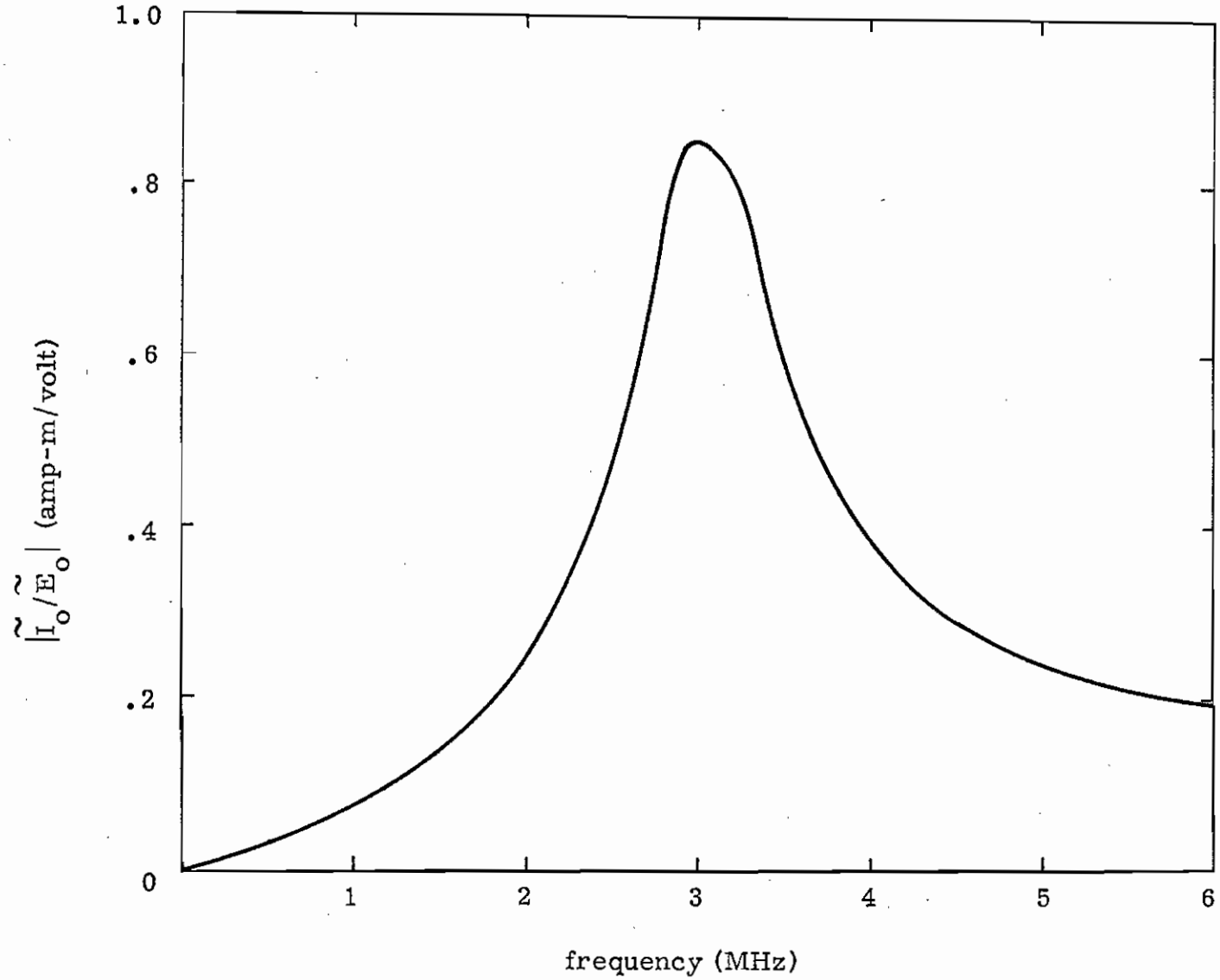

Fig. 3. -- Wing root current as a function of frequency, normalized to the magnitude of the incident electric field.

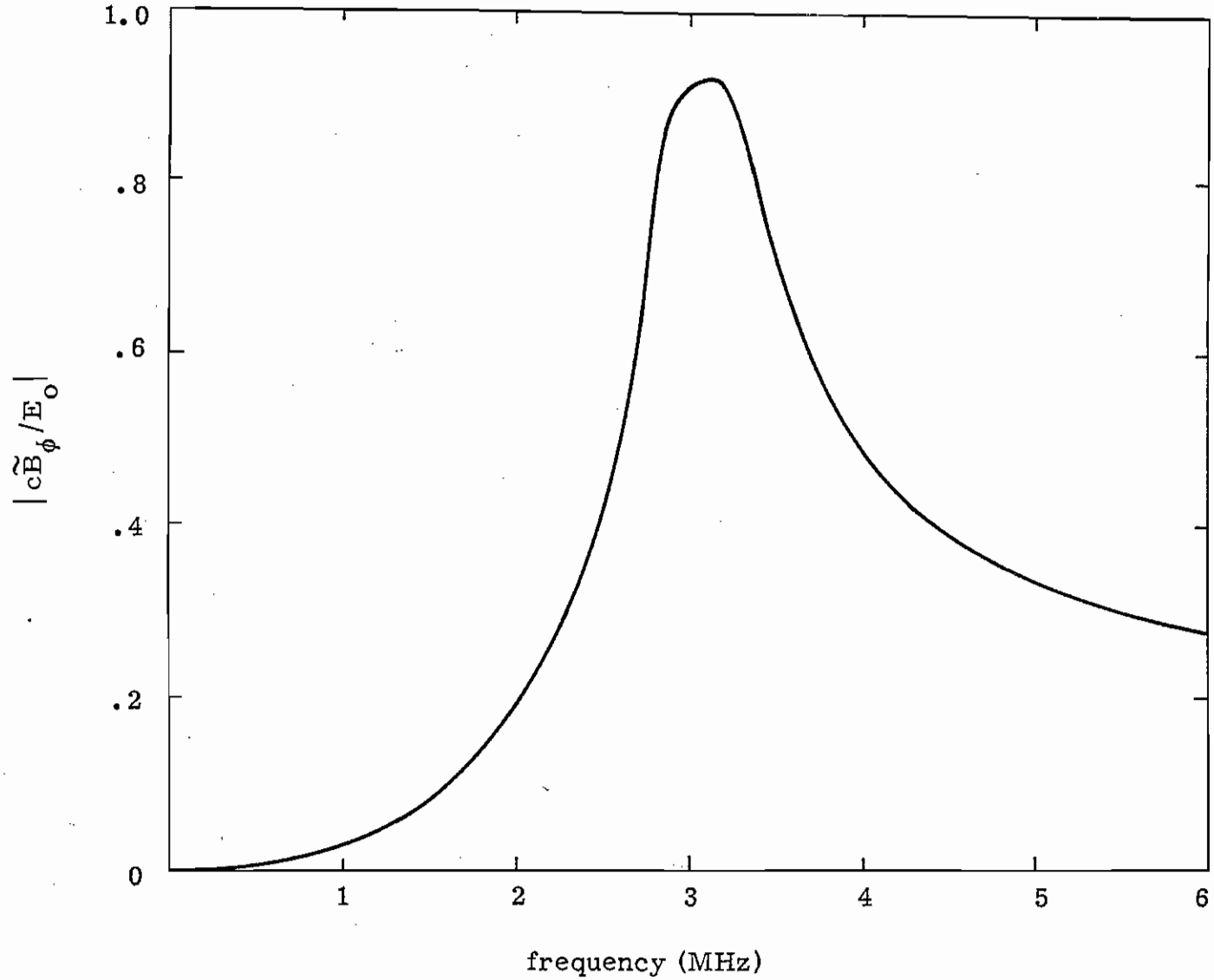

Fig. 4. -- Magnetic field at the glideslope antenna normalized to the magnitude of the incident electric field.

Thus we write the voltage induced across the gap in the glide-slope antenna as

$$V_{gap}(t) = V_{B_\phi}(t) + V_{B_o}(t)$$

$$V_{gap}(t) = -\frac{\partial}{\partial t}\left[B_\phi(\ell, 0, t) + B_o(t)\right] A_{eff.}$$

or

$$\tilde{V}_{gap}(\omega) = -j\omega\left[\tilde{B}_\phi(\ell, 0, \omega) + \tilde{B}_o(\omega)\right] A_{eff.}$$

As a worst case, we take the incident field at the antenna to have the same phase as $\tilde{B}_\phi(\ell, 0, \omega)$ for all frequencies. Then substituting the expression for $\tilde{B}_\phi(\ell, 0, \omega)$,

$$\left|\tilde{V}_{gap}(\omega)\right| = -\left[\frac{1.26\mu_o\left|\tilde{I}_o(\omega)\right|}{2\pi\ell}\left|e^{-\sqrt{2}jk\ell} - e^{-jk\ell}\cos k\ell\right| + \left|\tilde{B}_o(\omega)\right|\right]\omega A_{eff.}$$

For low frequencies we approximate each arm of the antenna by the circuit in Figure 5a). The resulting potential at the base of each arm from the center conductor to ground is V_{arm} (Point A to Point B in Figure 5b)). By the nature of the Moebius loop[2], the open-circuit voltage appearing across the antenna inputs, V_{oc}, is twice that across the arm. Applying Thevenin's theorem to the circuit of Figure 5a), we obtain the circuit of 5b) and the relations

$$\tilde{V}_{oc}(\omega) = \tilde{2}V_{arm}(\omega) = \frac{2V_{gap}(\omega)}{1-\omega^2 LC}$$

$$Z_{in} = \frac{Z_{arm}}{2} = \frac{j\omega L}{2(1-\omega^2 LC)}$$

---

[2] Baum, C. E., AFWL Sensor and Simulation Note 7, "Characteristic of the Moebius Strip Loop."

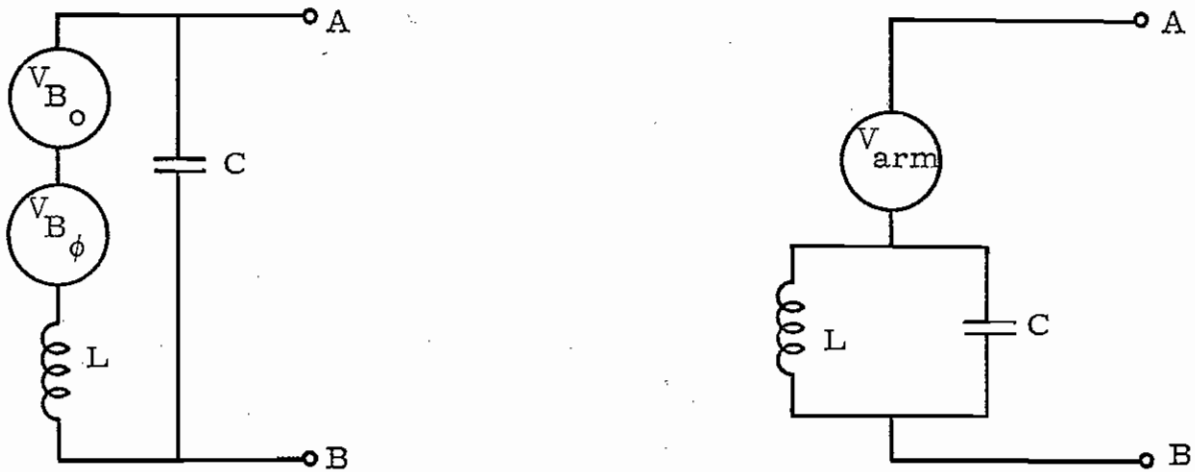

Fig. 5. -- a) Low frequency circuit approximation of each glideslope arm

b) Thevenin equivalent circuit for the circuit of a)

III. Numerical Results

In order to estimate C, we assume the coaxial cable constituting the antenna arms to have an impedance $Z_o = 50\Omega$. The capacitance per unit length is then

$$C' = \frac{1}{cZ_o} = 66.7 \times 10^{-12} \text{ farad/m.}$$

Each arm has a length

$$\ell' = 9.79 \text{ cm}$$

so that the capacitance of one arm is

$$C = 6.53 \times 10^{-12} \text{ farad}$$

In order to estimate L, we calculate the inductance of a circular loop with the same area as the glideslope loop:

$$A = \left[\frac{\pi(3.81)^2}{2} + (7.62)^2\right] \text{ cm}^2$$

$$= .00809 \text{ m}^2$$

The radius of the circular loop is then

$$a = \sqrt{\frac{2}{\pi} A}$$

$$= .0718 \text{ m.}$$

The radius of the coaxial cable shield is

$$b = .00795 \text{ m.}$$

so that the inductance of one arm of the loop is approximately

$$L = \frac{\mu_o a}{4}\left[\ell n \frac{8a}{b} - 2\right]$$

$$= 5.14 \times 10^{-8} \text{ henry.}$$

Thus

$$LC = 3.36 \times 10^{-19} \text{ sec}^2/\text{rad}^2.$$

At $f = 3$ MHz, $\omega = 1.88 \times 10^7$ rad/sec and

$$\omega^2 LC = 1.19 \times 10^{-4}$$

so that for frequencies of interest we can assume

$$V_{arm} \equiv V_{gap}.$$

Thus the magnitude of the voltage drop across the antenna terminals normalized to the incident electric field, i.e., the effective height, becomes

$$h_e = \left| \frac{\tilde{V}_{oc}(\omega)}{\tilde{E}_o(\omega)} \right| = \left[\frac{1.26\mu_o}{\pi \ell} \left| \frac{\tilde{I}_o(\omega)}{\tilde{E}_o(\omega)} \right| \left| e^{-\sqrt{2}jk\ell} - e^{-jk\ell} \cos k\ell \right| + \left| \frac{\tilde{B}_o(\omega)}{\tilde{E}_o(\omega)} \right| \right] \omega A_{eff.}$$

This is plotted as a function of frequency in Figure 6. Here $A_{eff.}$ is the effective loop area perpendicular to the magnetic field.

$$A_{eff.} = A \cos 17^o$$
$$= .00774 \text{ m}^2.$$

In order to obtain the voltage response of the antenna to an arbitrary incident electromagnetic field, $|\tilde{V}_{oc}(\omega)/E_o(\omega)|$ is multiplied by the frequency domain function $|\tilde{E}_o(\omega)|$. The magnitude and phase of the input impedance are given in Figure 7 as functions of frequency. The present analysis is valid up to approximately 15 MHz.

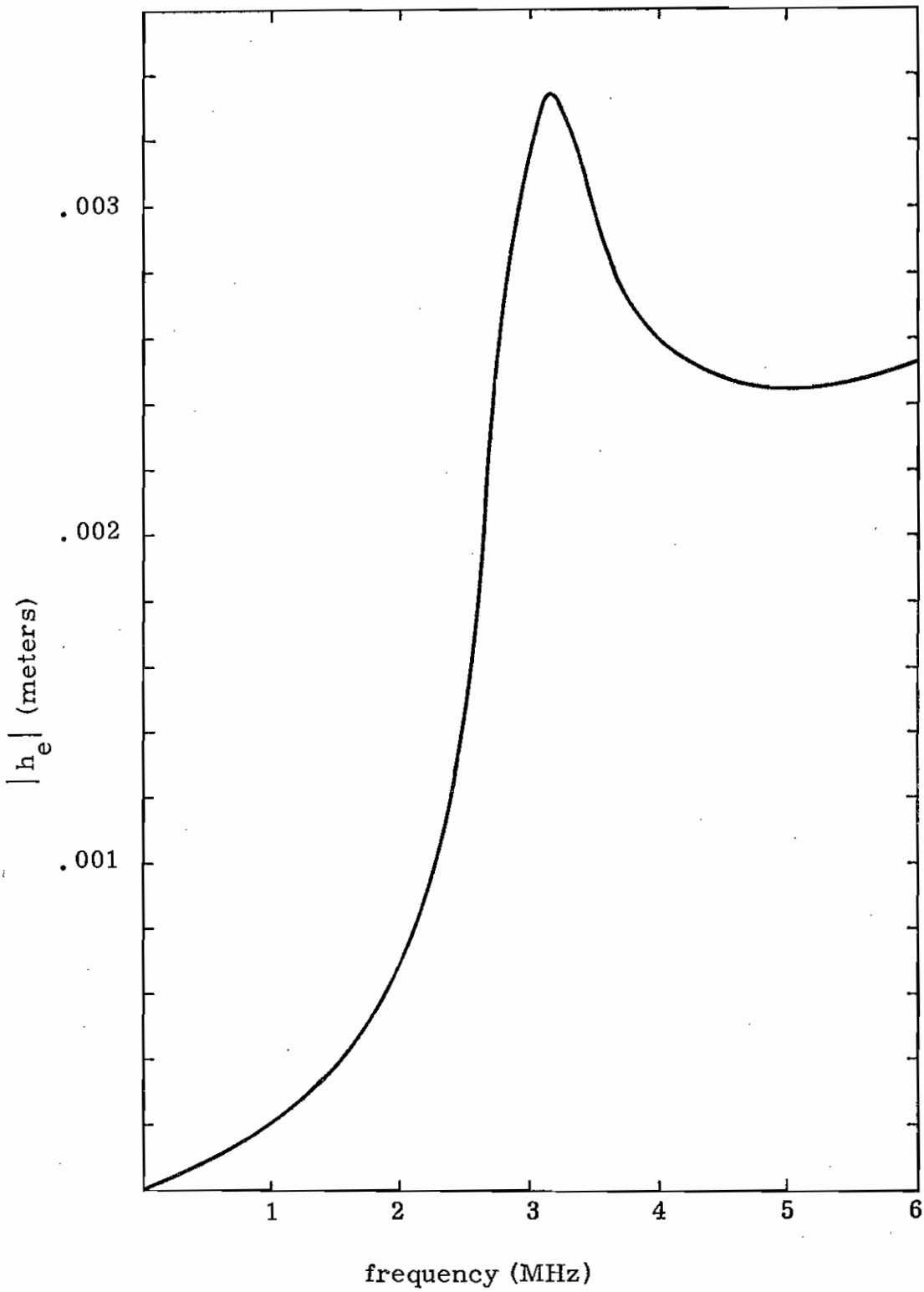

Fig. 6.--Effective height of the glideslope antenna relating the open-circuit voltage at the antenna terminals to the incident electric field.

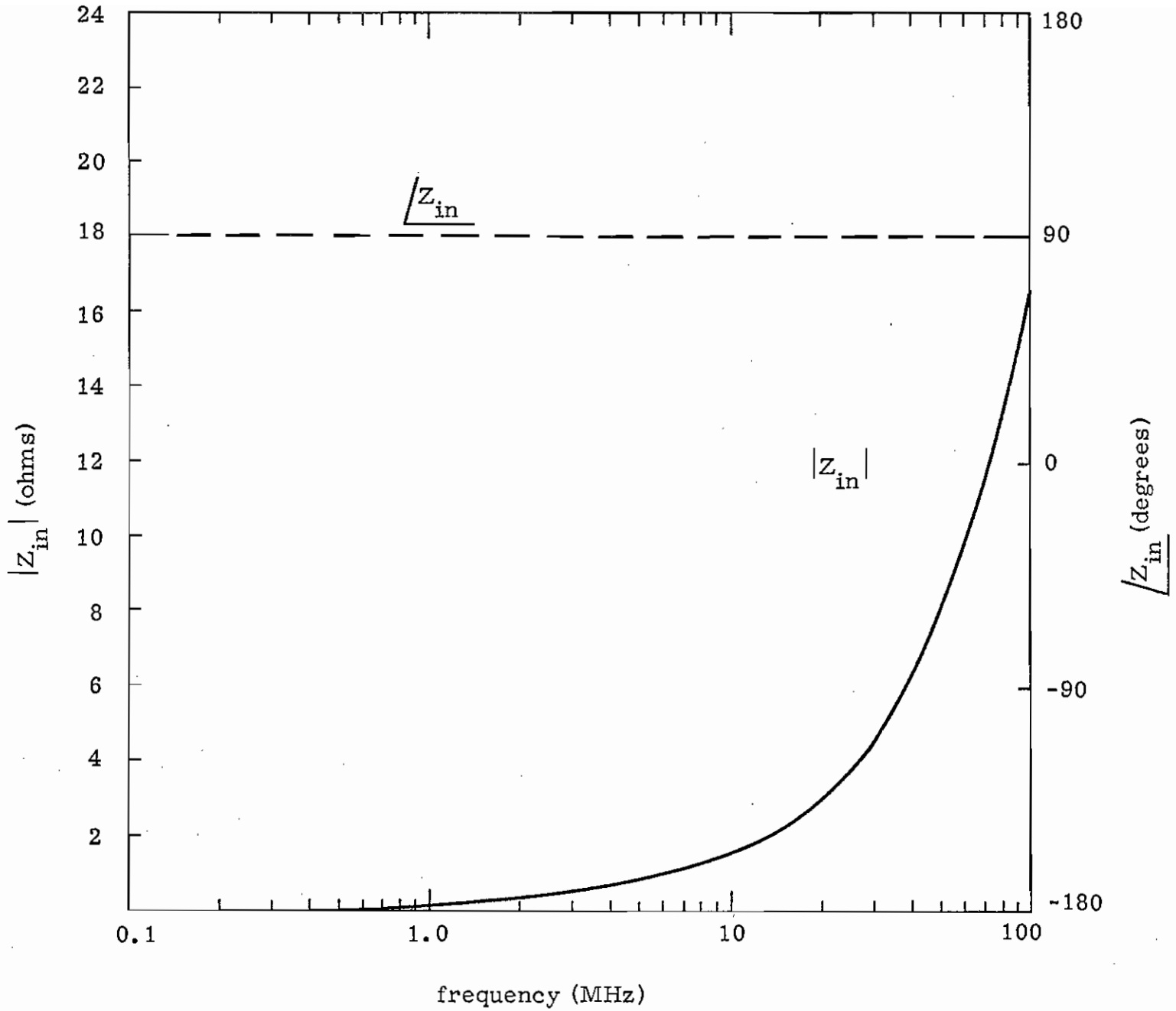

Fig. 7.--Input impedance of the glideslope antenna.

CHAPTER 12. AL 1211-1 X-BAND RENDEZVOUS ANTENNA ON B-1

I. General Description

The antenna of the tanker rendezvous beacon of the B-1 is flush-mounted near the top of the vertical stabilizer at Y_{VS} 284, Z_{VS} 196. The two radiating rectangular apertures of the antenna are located on each side of the vertical stabilizer and they are connected and fed by a WR 112 waveguide. A schematic picture of the antenna system is given in Fig.1. The waveguide, as shown in Fig.2, has cross-sectional dimensions of 2.85 cm × 1.26 cm and a length of 12.88 cm. The excitation element of the waveguide is a probe protruding to roughly the center of the waveguide. The operating frequency of the antenna is at 9.375 GHz (wavelength ≃ 3.2 cm).

II. Analysis

The wavelengths corresponding to the important part of the EMP spectrum are very large compared to the physical dimensions of the rendezvous antenna. Therefore, in calculating the effect of EMP on this antenna it is sufficient to carry out a quasi-static analysis. In the course of studying this antenna we found that it is necessary to carry out both a quasi-electrostatic analysis and a quasi-magnetostatic analysis to find the response of the antenna.

We will first calculate the open-circuit voltage and then the input impedance. At low frequencies, the input impedance of a probe is a series combination of a radiation resistence R and a capacitance C. The equivalent circuit of the antenna at terminals A,B is shown in Fig.3.

II.1 Effective height

We first consider the problem of the induced open-circuit voltage. Referring to Fig.2, the potential and the electric field inside the waveguide can be obtained by solving a Laplace equation using the method of separation of variables. Specifically, inside the waveguide

$$\nabla^2\phi = 0 \tag{1}$$

where ϕ is the potential and ϕ vanishes on the walls of the waveguide. The coefficients in the series solution of ϕ are obtained by matching $-\partial\phi/\partial z$ with the total local electric field E_p normal to the aircraft skin at the apertures

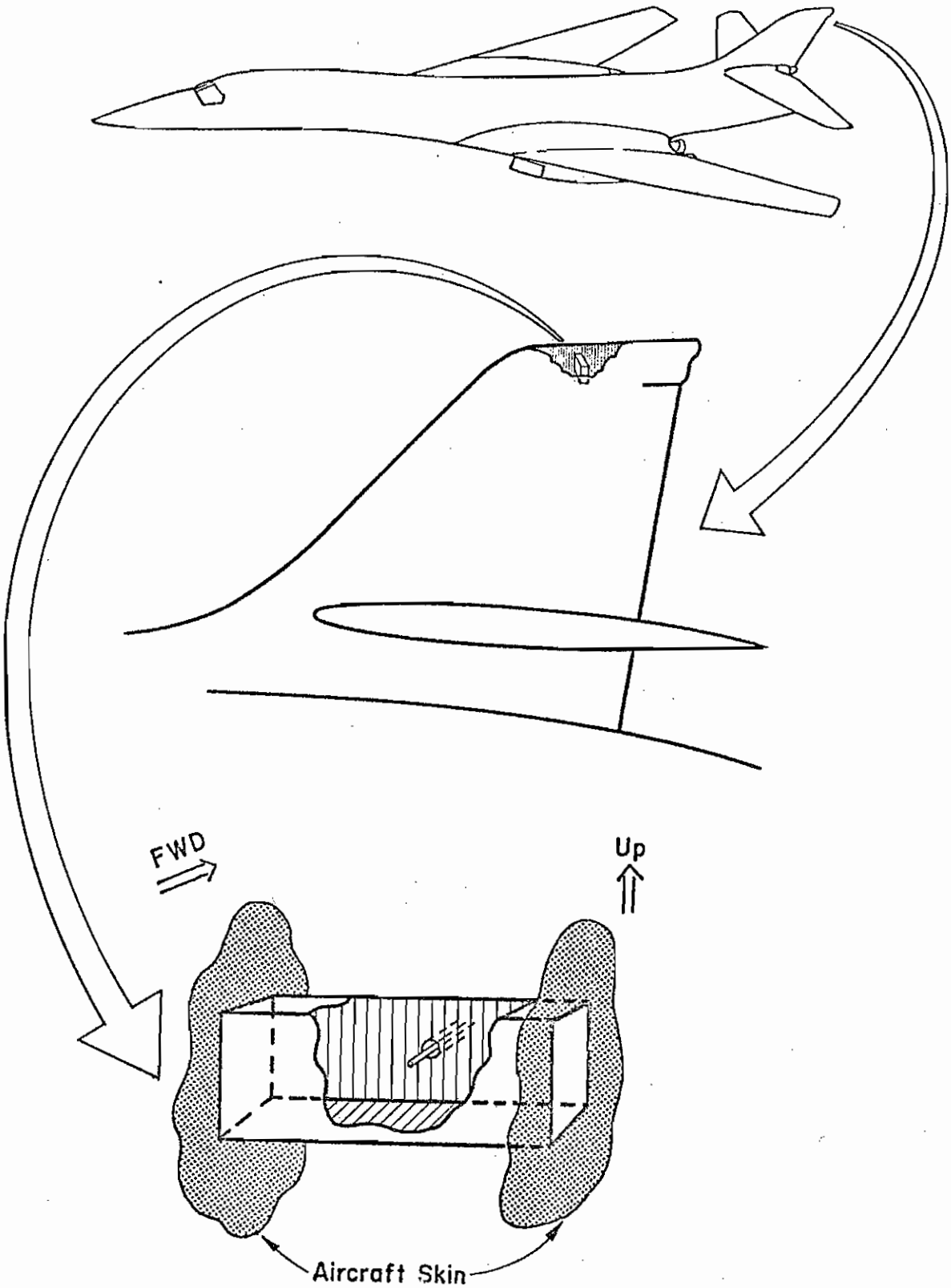

Fig.1. Location and schematic diagram of the X-band rendezvous antenna.

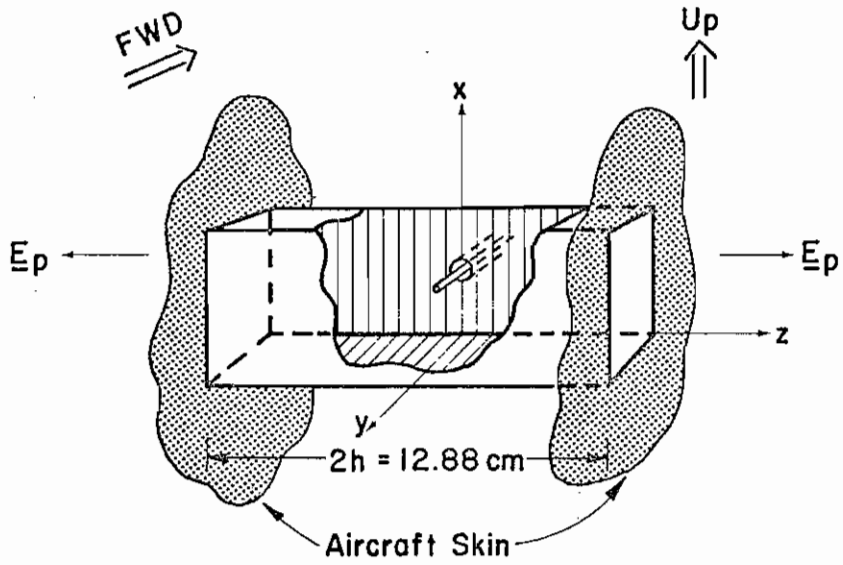

(a)

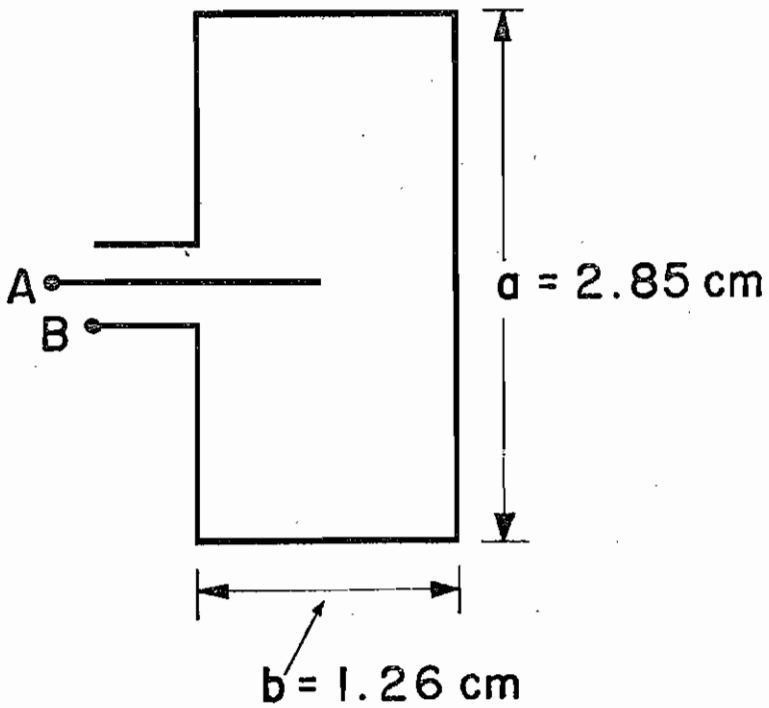

(b)

Fig.2. The rendezvous antenna
(a) 3-dimensional view
(b) cross-sectional view through the probe.

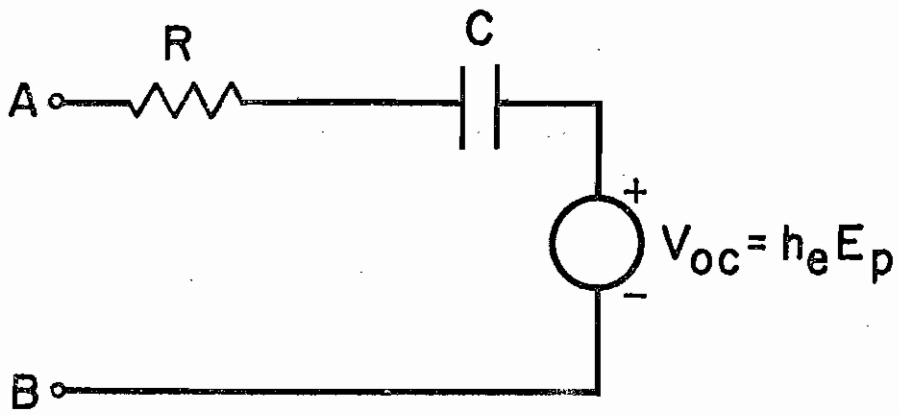

Fig.3. The Thévenin equivalent circuit of the rendezvous antenna at the terminals A,B.

of the antenna. This electric field, E_p, is proportional to the surface charge density σ on the aircraft skin near the apertures, i.e.

$$E_p = \sigma/\varepsilon_o.$$

In this analysis, we assume E_p to be uniform across the apertures. The calculated induced voltage due to this assumption will exceed the actual induced voltage by a factor of approximately 1.5 (see IN 10). The solution of (1) with the appropriate boundary conditions can alternatively be obtained by taking the low-frequency approximation of the evanescent TM modes resulting from a conventional waveguide analysis. Therefore, let V_{oc}^{TM} denote the open-circuit voltage due to this quasi-electrostatic analysis and we find

$$V_{oc}^{TM} = \frac{1}{2}\phi_{tip}$$

$$= \frac{-8E_p}{\pi^3} \sum_{m\ \text{odd}} \sum_{n\ \text{odd}} \left[\frac{\sin(n\pi/2)\ \sin(n\pi/2)}{mn[(m/a)^2+(n/b)^2]^{\frac{1}{2}}\ \sinh\{\pi h[(m/a)^2+(n/b)^2]^{\frac{1}{2}}\}} \right] \quad (2)$$

where ϕ_{tip} is the solution of (1) evaluated at the tip of the probe, and the dimensions a,b and h are shown in Fig.2.

Since the length $2h$ of the waveguide is considerably longer than the cross-sectional dimensions, it is important to account for the attenuation of the modes in determining the strengths of the field surrounding the voltage probe. From the rectangular waveguide theory, it is expected that the TE_{10} mode is least attenuated among all evanscent modes. In fact, for the geometry under study, the evanescent TE_{10} mode contributes most significantly to the induced voltage of the antenna at frequencies above 100 KHz. The evaluation of the TE_{10} mode involves the solution of a quasi-magnetostatic problem.

For the quasi-magnetostatic problem, the following equation is solved within the waveguide

$$\nabla^2\phi^* = 0 \quad (3)$$

where ϕ^* is the scalar magnetic potential and is related to the magnetic field $\underline{H}$ by

$$\underline{H} = -\nabla\phi^* \tag{4}$$

In solving (3), the appropriate boundary condition to be used is that the normal derivative of ϕ^* vanishes at the walls of the waveguide. The coefficients in the series solution of ϕ^* are obtained by matching $-\partial\phi^*/\partial x$ with the total local magnetic field H_t tangential to the aircraft skin at the apertures of the antenna. This tangential magnetic field H_t is equal to the aircraft skin currents in magnitude. From the continuity equation for the skin currents and skin charges one has the following relation:

$$H_t = E_p/Z_o \tag{5}$$

where $Z_o = 377\Omega$ is the intrinsic impedance of free space. It is important to note that again, the assumption of uniform field H_t across the apertures in (5) yields a result that is over-estimated by a factor of at most 1.5. The electric field E_y tangential to the voltage probe can be obtained from the following equation, keeping in mind that $E_z = 0$ for the TE modes:

$$\nabla\times\underline{E} = -j\omega\mu\underline{H} \tag{6}$$

The induced open-circuit voltage due to this electric field will be denoted by V_{oc}^{TE} and can be obtained from a knowledge of E_y as

$$V_{oc}^{TE} = \frac{1}{2}\int_0^{a/2} E_y\, dy$$

$$= \frac{j\omega abE_p}{c\pi^2} \sum_{m\ odd}\left[\frac{\sin(m\pi/2)}{m^2 \sinh(m\pi h/a)}\right] \tag{7}$$

where c is the speed of light. The total resulting open-circuit voltage is the sum of V_{oc}^{TM} and V_{oc}^{TE}, i.e.,

$$V_{oc} = V_{oc}^{TM} + V_{oc}^{TE}$$

We define an effective height $h_e(\omega)$ at the terminals A,B (Fig.2) such that

$$V_{oc}(\omega) = -h_e(\omega)\ E_p(\omega) \tag{8}$$

Hence,

$$h_e(\omega) = \frac{8}{\pi^3} \sum_{m\ \text{odd}} \sum_{n\ \text{odd}} \left[\frac{\sin(m\pi/2)\ \sin(n\pi/2)}{mn[(m/a)^2+(n/b)^2]^{\frac{1}{2}}\ \sinh\{\pi h[(m/a)^2+(n/b)^2]^{\frac{1}{2}}\}} \right]$$

$$-\frac{j\omega ab}{c\pi^2} \sum_{m\ \text{odd}} \left[\frac{\sin(m\pi/2)}{m^2\ \sinh(m\pi h/a)} \right] \tag{9}$$

The effective height $h_e(\omega)$ is plotted in Fig.4 on a log-log scale and again in Fig.5 on a linear scale. For frequencies below 50 KHz, the effective height is due mainly to the dominant TM mode and it is constant in frequency; above 120 MHz, it is due mainly to the dominant TE mode and is a linear function of frequency. A comparison of (2) and (7) with the corresponding results from the waveguide theory shows that the formulas are good up to at least 500 MHz.

II.2 Input impedance

We now consider the input impedance of the rendezvous antennas. Since the wavelengths of interest are very large compared to the whole antenna, the input impedance is similar to that of a small dipole antenna in free space except for some factors, f_R and f_C, which account for the fact that the probe is inside the waveguide. At low frequencies, the input impedance is represented by a resistance R in series with a capacitance C, as shown in Fig.3.

The resistance R is given by

$$R = f_R\ R_o \tag{10}$$

where R_o is the radiation resistance of a dipole antenna of length 2ℓ and is given by

$$R_o = \frac{2\pi Z_o}{3} \left(\frac{\ell}{\lambda}\right)^2 \tag{11}$$

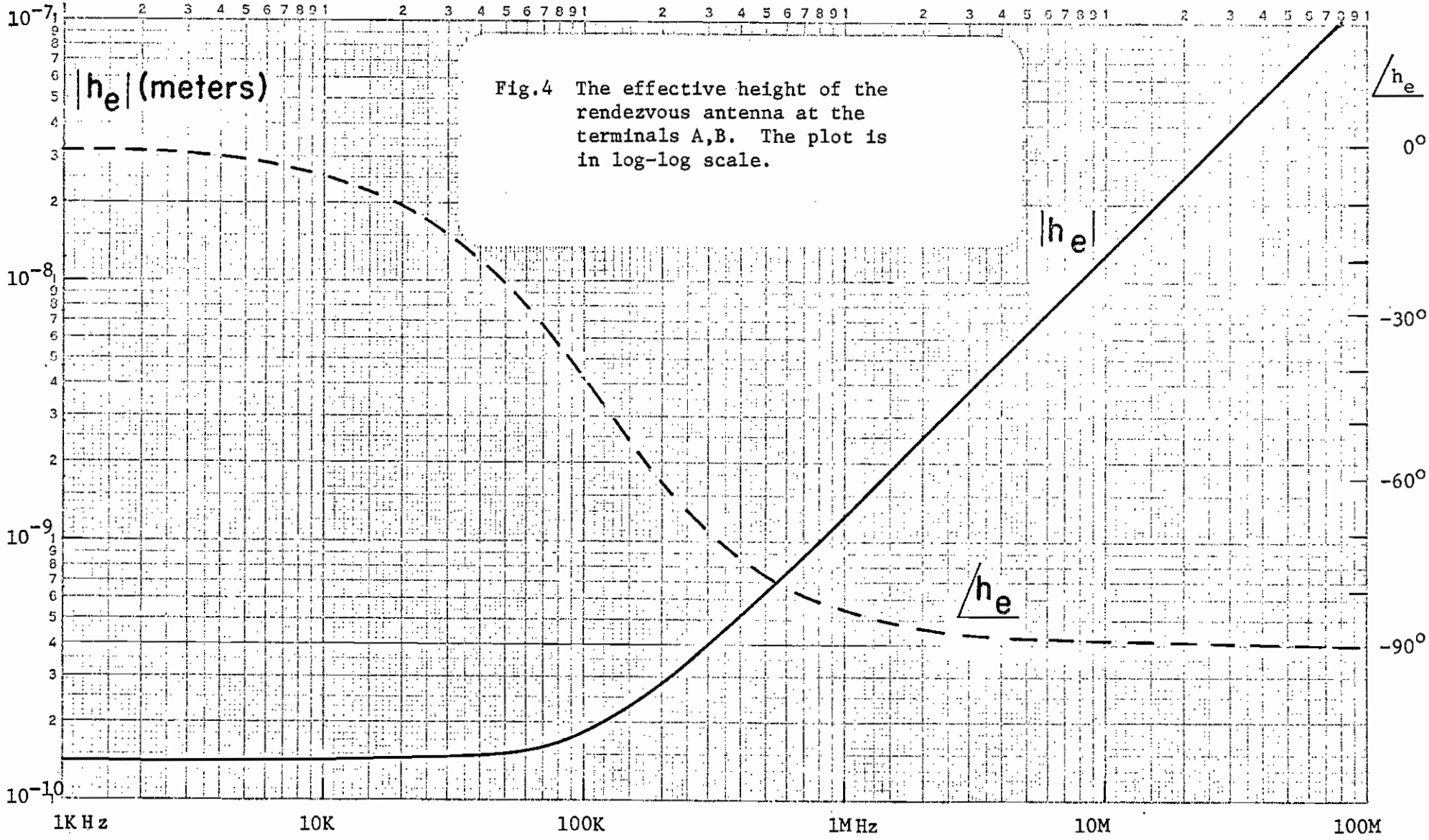

Fig.4 The effective height of the rendezvous antenna at the terminals A,B. The plot is in log-log scale.

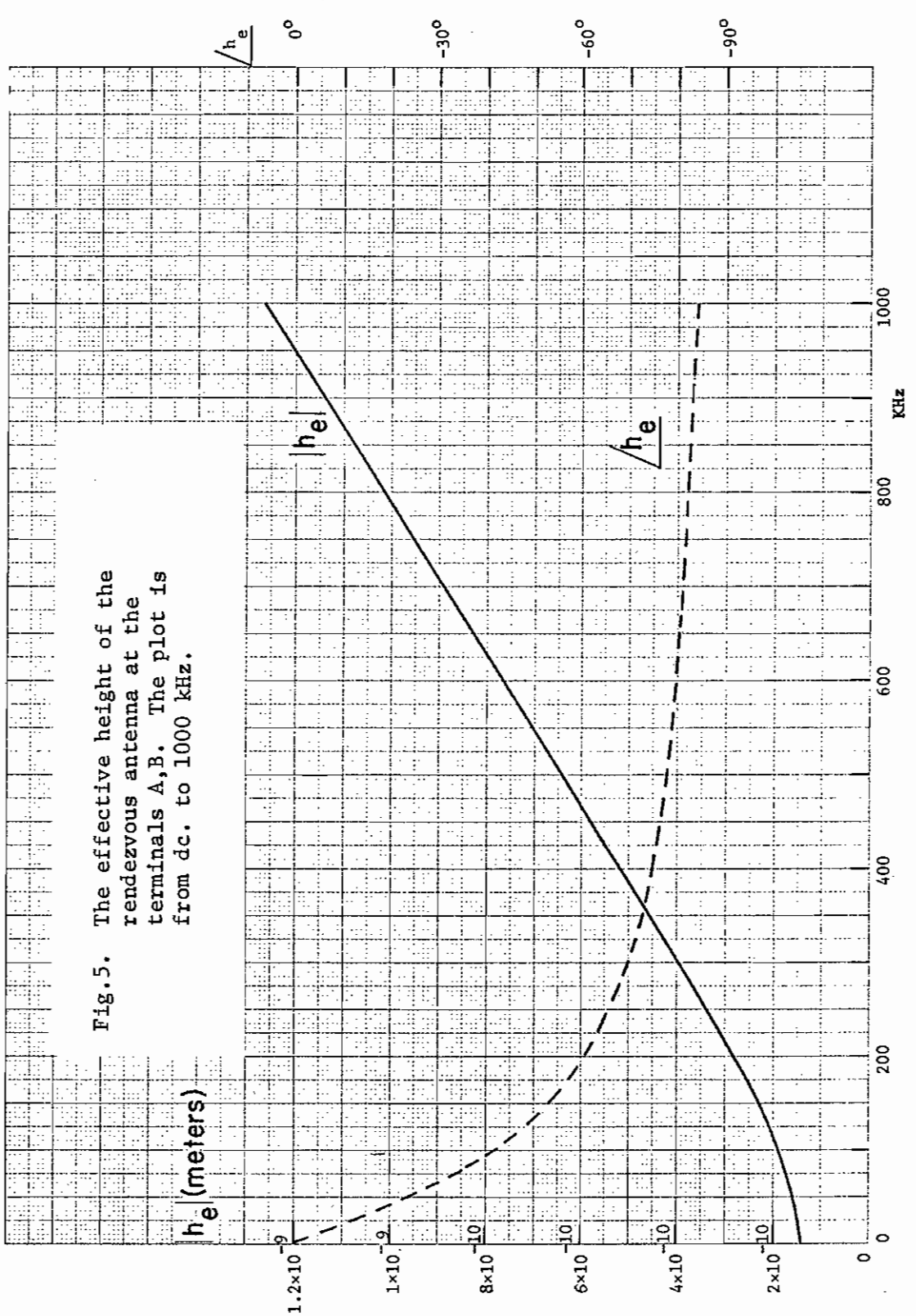

Fig.5. The effective height of the rendezvous antenna at the terminals A,B. The plot is from dc. to 1000 kHz.

The factor f_R is proportional to $\exp(-2\pi h/a)$ and is of the order of 5×10^{-27}. Thus R is very small ($R \simeq 5\times10^{-11}\ \Omega$ at 100 MHz) and can be left out in the calculation of the input impedance.

The input capacitance C is given by

$$C = f_C\, C_o \tag{12}$$

where C_o is the input capacitance of a dipole antenna in free space with length 2ℓ and radius r_a; it is given by

$$C_o = \pi\varepsilon_o \ell \Big/ \ell n(2\ell/r_a) \tag{13}$$

The factor f_C can be evaluated approximately from image theory and it turns out that

$$f_C \simeq 2\left[1 - \frac{\ell}{2\ell n(2\ell/r_a)}\{1/b + 2/a\}\right]^{-1} \tag{14}$$

For the present problem

$$f_C \simeq 2.6$$

$$C \simeq 0.21\ \text{pF}.$$

The input impedance is now given approximately by

$$Z_{in} \simeq -j/\omega C$$

and Z_{in} is presented in Fig.6.

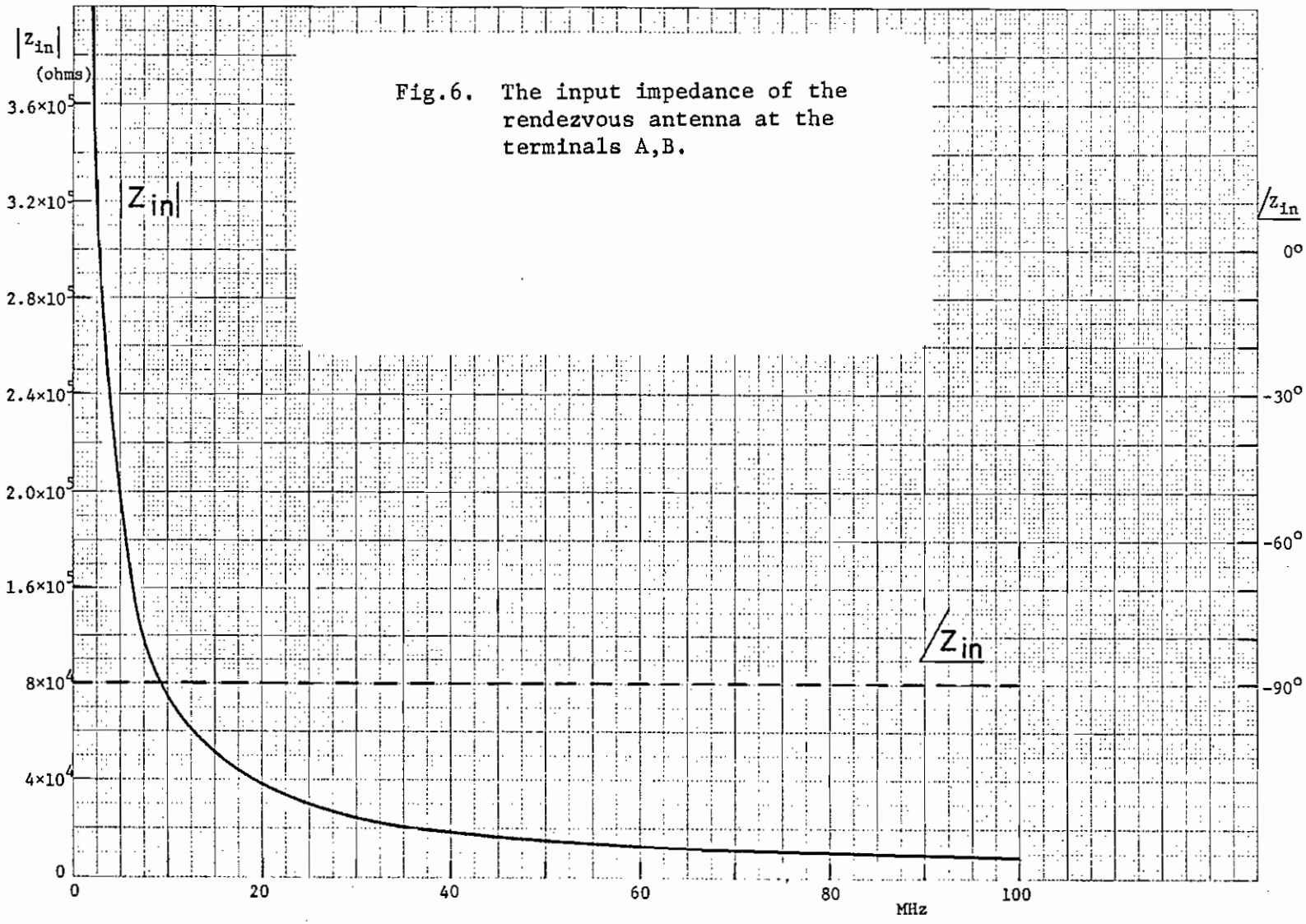

Fig.6. The input impedance of the rendezvous antenna at the terminals A,B.

CHAPTER 13. RESPONSE OF THE HF WIRE ANTENNA ON AABNCP IN THE RESONANCE REGION

In this chapter we calculate the response of the HF wire antenna on the AABNCP for frequencies up to 13 MHz. The calculations are based on the asymptotic theory of the current distribution on linear antennas. In the low-frequency limit (below 1.5 MHz) the results obtained here reduce to the quasi-static results already reported in Chapter 4.

I. General Description

The HF wire antenna is used for communication purposes and operates in the frequency range of 2-30 MHz (wavelengths ≈ 10-150 m). One end of the antenna is driven at station 1326 on the top center line of the fuselage and the other end of the wire is electrically connected to the vertical stabilizer at fin station 245. This arrangement is schematically shown in Fig.1. The wire itself is 28.3 m long and consists of a WS 25 U single conductor cable with polyethelene dielectric cover.

II. Analysis

When calculating the response of HF wire antennas on an aircraft, the whole airframe has to be taken into account, since the length of the wire is an appreciable fraction of the length of the fuselage. The asymptotic theory of current distribution on linear antennas enables us to directly calculate the parameters as well as the open-circuit voltage in the Thévenin equivalent circuit, as shown in Fig.2, of the HF wire antenna at terminals A,B (see Fig.1). For the AABNCP, the asymptotic theory is valid up to 13 MHz.

Before we proceed with the analysis, it is important to emphasize that the input impedance Z_{in} and the effective height h_e are evaluated at the terminals A,B of the HF wire antenna, thus *excluding* the lightning arrestor and the HF coupler due to lack of information on these two devices. The HF coupler provides tuning to the HF antenna, so that the combined unit has a reasonable impedance level at in-band frequencies.

II.1 Input Impedance

A simplified model of the AABNCP is depicted in Fig.3. By using the asymptotic theory for the antenna current distribution, the reactive part of the input impedance is found to be

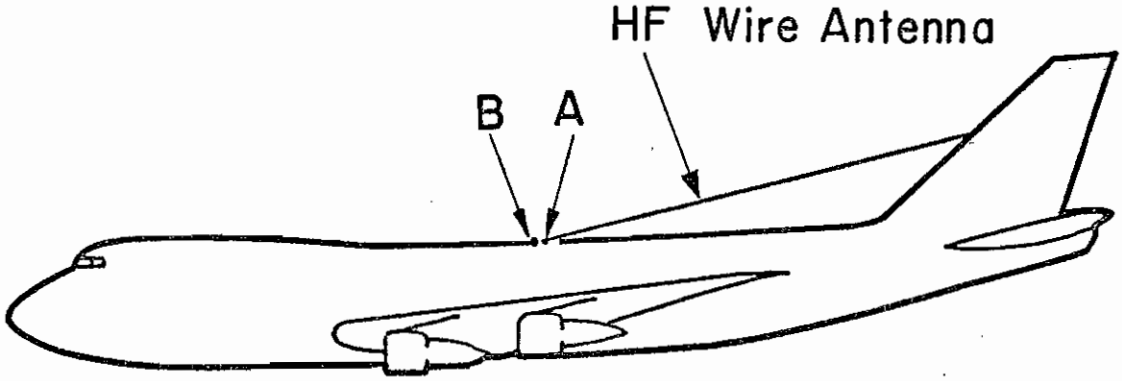

(a)

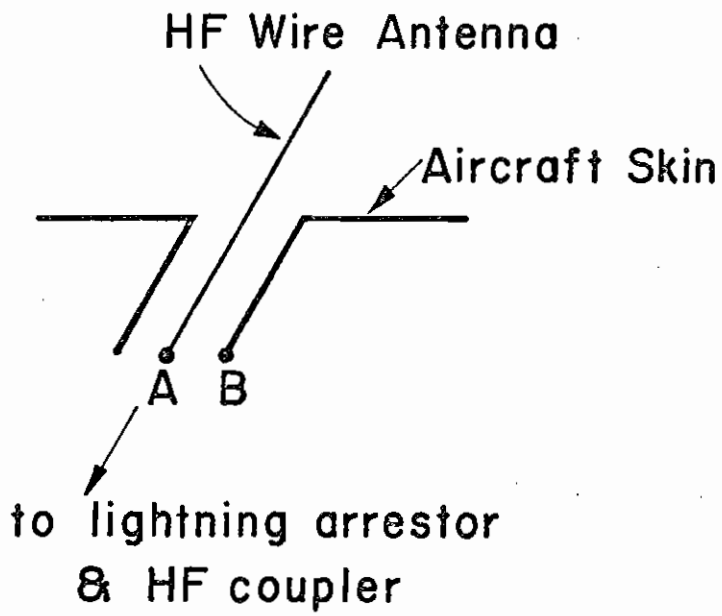

(b)

Fig.1. (a) Schematic diagram and
(b) The feed point of the HF wire antenna.

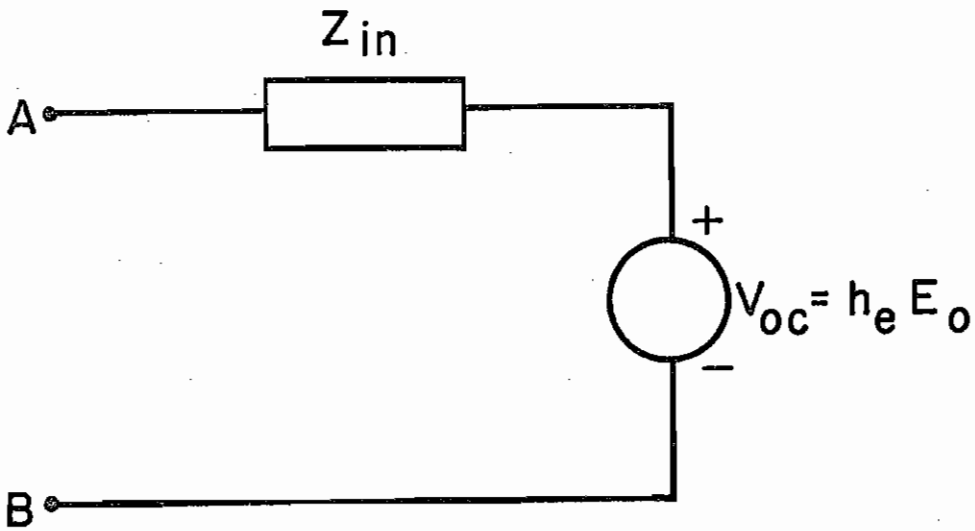

Fig.2. The Thévenin equivalent circuit of the HF wire antenna.

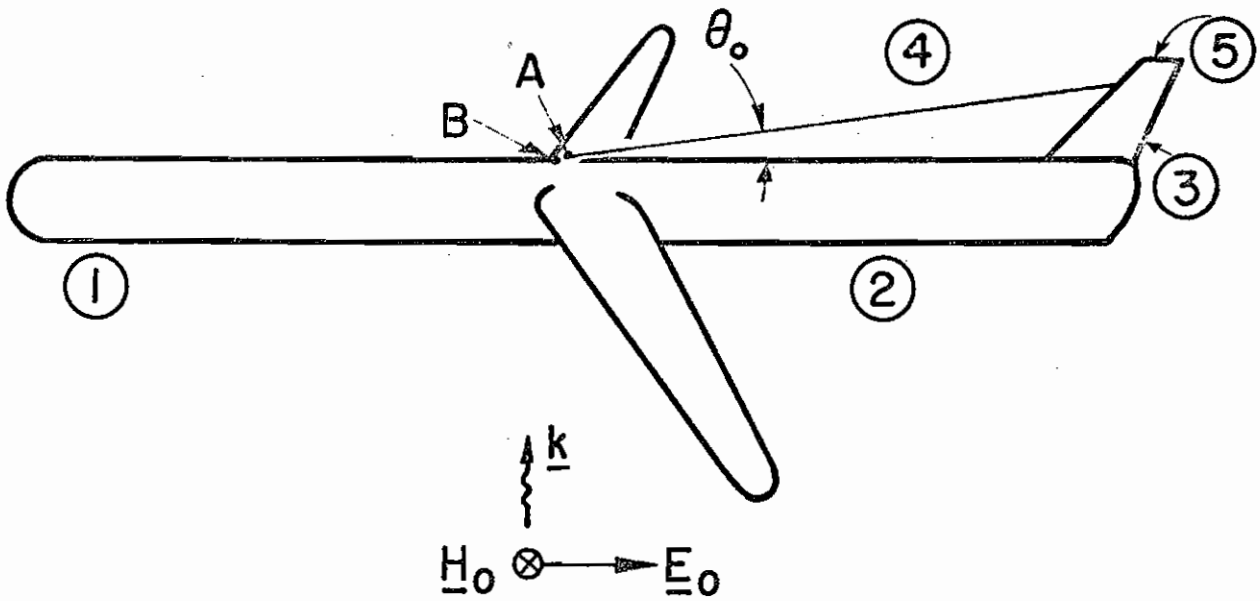

Length of section 1 = 34.4 m
" " " 2 = 27.6 m
" " " 3 = 6.2 m
" " " 4 = 28.3 m
" " " 5 = 3.2 m

Fig.3. Model of the aircraft used in the asymptotic theory.

$$\mathrm{Im}(Z_{in}) = (4\pi\Omega_f/Z_o)\Big\{(\Omega_w/\Omega_f)\sin(k\ell_4)\tan(k\ell_5) + \cos\, k(\ell_2+\ell_3) - \cos(k\ell_4)$$

$$+\alpha[\sin\, k(\ell_2+\ell_3) + (\Omega_w/\Omega_f)\sin(k\ell_4)]\Big\}\Big\{\tan(k\ell_1)\cos\, k(\ell_2+\ell_3)$$

$$+ \sin\, k(\ell_2+\ell_3) + \alpha[\tan(k\ell_1)\sin\, k(\ell_2+\ell_3) - \cos\, k(\ell_2+\ell_3)]\Big\}^{-1} \qquad (1)$$

where $k = \omega/c$ is the wave number, $Z_o = 377$ ohms is the intrinsic impedance of free space, ℓ_i is the length of section i of the aircraft. As shown in Fig.3, section 1 denotes the forward part of the fuselage, section 2 is the rear part of the fuselage, sections 3 and 5 are the vertical stabilizers below and above the anchor point of the wire, respectively, and section 4 denotes the wire. The quantity Ω_w is given by

$$\Omega_w = 2\, \ell n(\ell_4/a_4) \qquad (2)$$

where a_4 is the radius of the wire; and

$$\Omega_f = 2\, \ell n(\ell_{af}/a_{af}) \qquad (3)$$

where ℓ_{af} and a_{af} are the length and the average radius of the entire airframe, respectively. The quantity α in (1) is found to be

$$\alpha = -\Big\{(\Omega_4/\Omega_f)[\tan(k\ell_1)\cos\, k(\ell_2+\ell_3) + \sin\, k(\ell_2+\ell_3) + \tan(k\ell_5)\cos(k\ell_4)]$$

$$+ \sin(k\ell_4)\Big\}\Big\{(\Omega_4/\Omega_f)[\tan(k\ell_1)\sin\, k(\ell_2+\ell_3) - \cos\, k(\ell_2+\ell_3)$$

$$+ \cos(k\ell_4)]\Big\}^{-1}$$

By using the current distribution on the aircraft as predicted by the asymptotic theory, the integration of the Poynting vector over all solid angles yields the total radiated power. The total radiated power enables us to obtain

the radiation resistance, i.e., the real part of the input impedance. As can be easily seen, (1) is not valid at the resonances of the aircraft. At the resonance frequencies, we combine the asymptotic theory with a more elaborate antenna theory to get the result presented in Fig.4, where the input impedance remains finite. Again we emphasize that the input impedance presented in Fig.4 refers to the terminals A,B prior to the HF coupler.

It is of interest to point out that the low-frequency limit of (1) is of the form ωL, where L is the inductance of the loop formed by sections 2, 3 and 4. This result is identical to that reported in Chapter 4.

II.2 Effective height

In evaluating the effective height at A,B, only the case that the incident electric field $\underline{E}_o$ is parallel to the fuselage is considered (see Fig.3). This case corresponds to the worst case that a maximum current is induced on the aircraft. In this case, the short-circuit current I_{sc} induced at the driving-point of the HF wire antenna turns out to be

$$I_{sc} = (j4\pi E_o/Z_o k)\left\{[B_1 - B_2\tan(k\ell_1)][\cos k(\ell_2+\ell_3) + \alpha \sin k(\ell_2+\ell_3)] - \alpha B_5 + B_3 + (\Omega_w/\Omega_f) B_4[\tan(k\ell_5) + \alpha]\right\}\left\{(\Omega_w/\Omega_f)\sin(k\ell_4)\tan(k\ell_5) + \cos k(\ell_2+\ell_3) - \cos(k\ell_4) + \alpha[\sin k(\ell_2+\ell_3) + (\Omega_w/\Omega_f)\sin(k\ell_4)]\right\}^{-1} \quad (5)$$

where

$$B_1 = \Omega_f^{-1}[1 - \cos(k\ell_1)]$$

$$B_2 = \Omega_f^{-1} \sin(k\ell_1)$$

$$B_3 = \Omega_w^{-1}\left\{\cos(k\ell_3) - \cos k(\ell_2+\ell_3) - [\cos(k\ell_4) - \cos(k\ell_4 \cos\theta_o)]/\cos\theta_o - j[\sin(k\ell_4 \sin\theta_o) - \sin\theta_o \sin(k\ell_4)]/\cos\theta_o\right\}$$

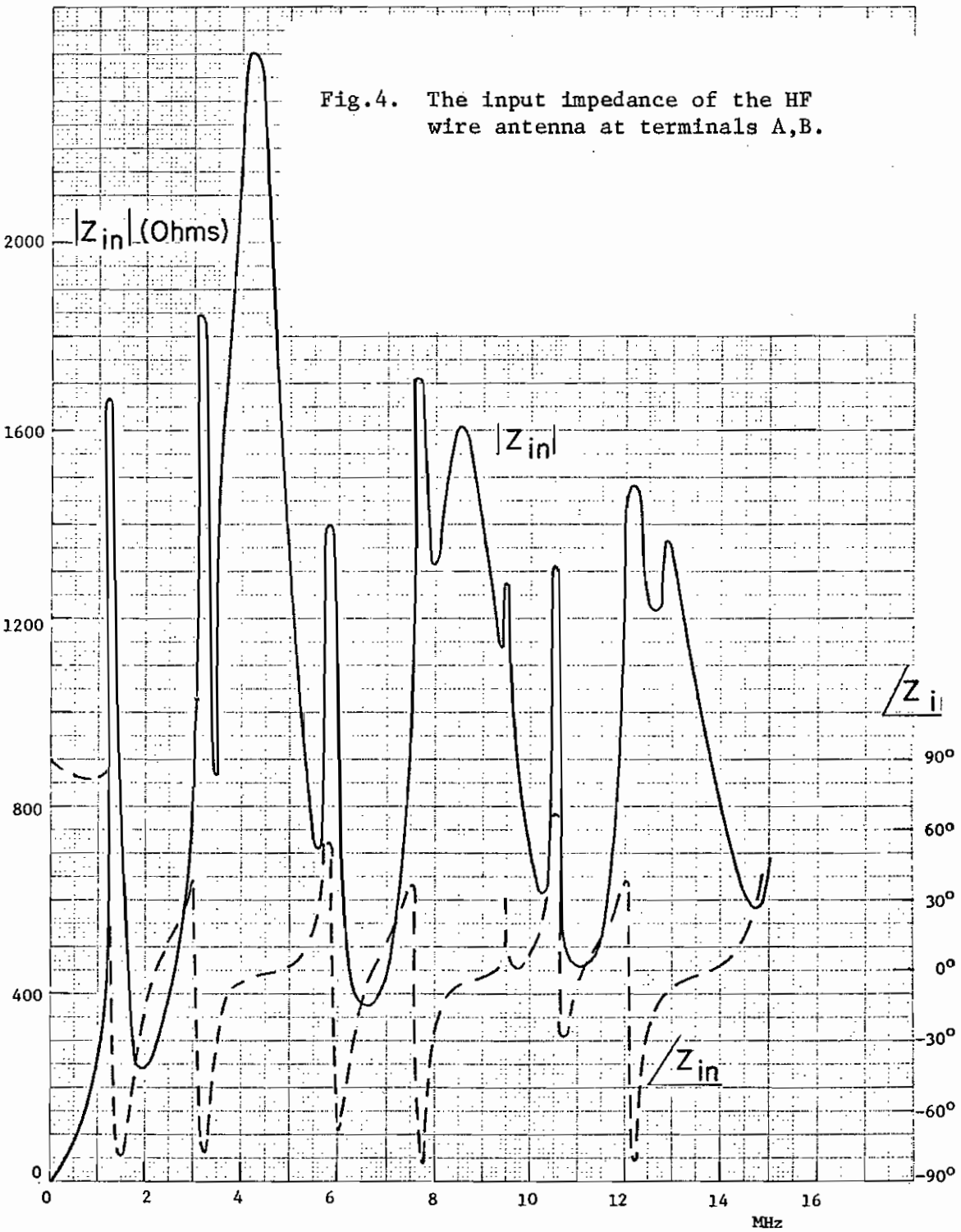

Fig.4. The input impedance of the HF wire antenna at terminals A,B.

$$B_4 = -(\Omega_w \cos\theta_o)^{-1}\left\{-\sin(k\ell_4) + \sin\theta_o \sin(k\ell_4 \sin\theta_o)\right.$$

$$\left. + j \sin\theta_o[\cos(k\ell_4 \sin\theta_o) - \cos(k\ell_4)]\right\}$$

and

$$B_5 = \Omega_f^{-1}[\sin k(\ell_2+\ell_3) - \sin(k\ell_3)]$$

The angle θ_o is the angle between the wire antenna and the fuselage, as shown in Fig.3.

The open-circuit voltage V_{oc} at terminals A,B is given by

$$V_{oc} = I_{sc} Z_{in} \tag{6}$$

and the effective height $h_e(\omega)$ at terminals A,B is defined by

$$V_{oc}(\omega) = h_e(\omega) E_o(\omega) \tag{7}$$

where E_o, as mentioned previously, is the *incident* electric field. The effective height can be calculated using (5), (6) and (7) together with the result of Fig.4. As in the analysis of the input impedance, a more elaborate antenna theory is applied at the resonance frequencies where (5) is not valid. The effective height at terminals A,B is presented in Fig.5. We emphasize once again that in the definition of h_e, the *incident* free-space electric field E_o is used.

Finally, we mention that the low-frequency limit of the open-circuit voltage as given in (7) is equal to that of the loop formed by sections 2, 3 and 4. This result is, of course, identical to that already reported in Chapter 4.

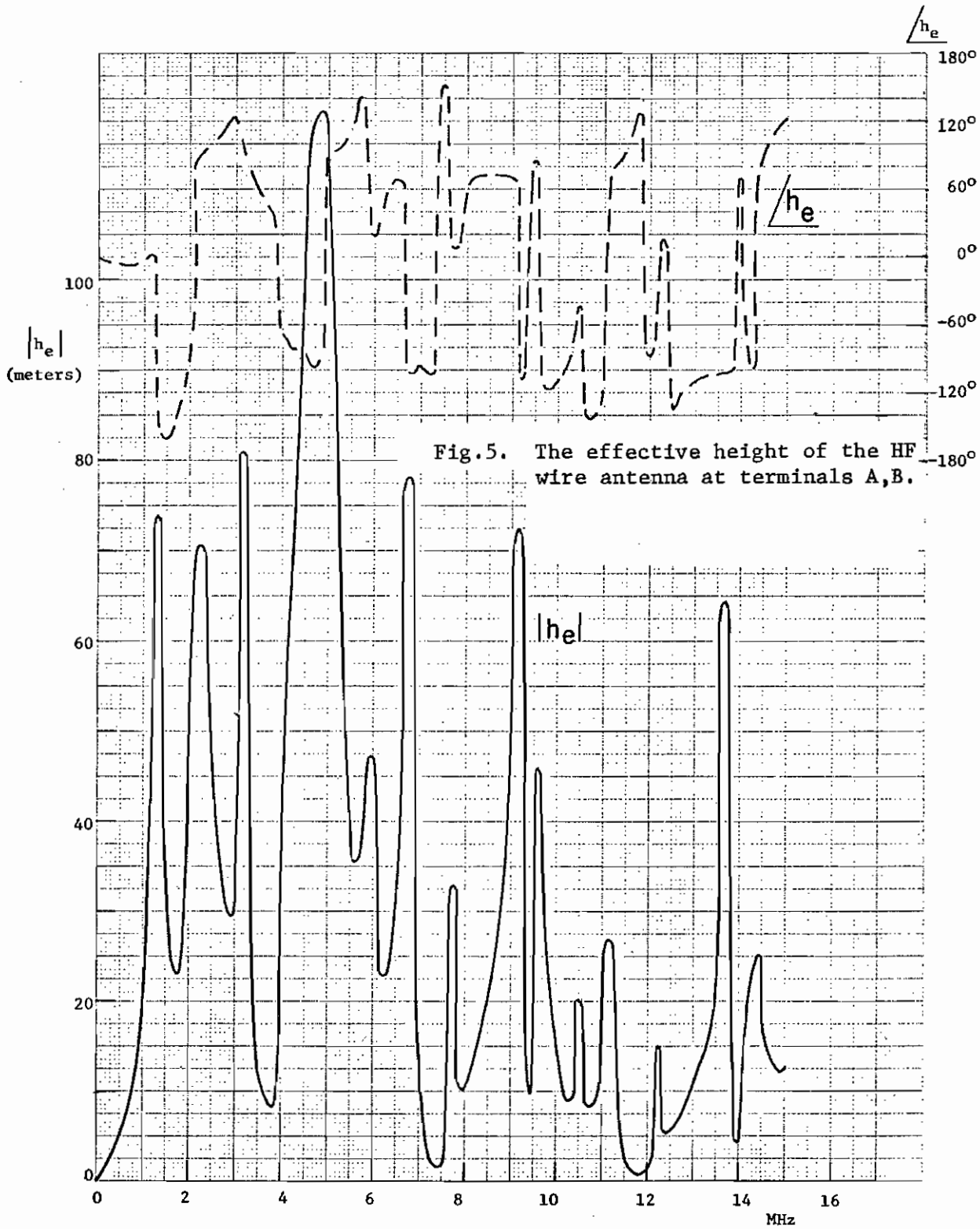

Fig.5. The effective height of the HF wire antenna at terminals A,B.

CHAPTER 14. S65-8262-2 VHF COMMUNICATION ANTENNA NO. 1 ON AABNCP

I. General Description

The VHF communication antenna is used for transmission and reception of vertically polarized signals in the frequency range 116 - 156 MHz (wavelengths ≈ 1.92 - 2.59 m). The antenna is externally mounted at the bottom center line of the fuselage at station 630. The location and a schematic drawing of the antenna are shown in Fig.1. As shown in Fig.2a, the antenna has a height of 44.8 cm , a width at the base of 29.8 cm and a maximum thickness of 3.6 cm.

II. Analysis

In Fig.2a, a schematic diagram of the internal structure of the antenna is shown. Basically, the antenna is a blade with an open-ended slot, the slot often being called a notch. The slot is fed at points D and F by a 50 Ω coaxial cable which goes to the coaxial connector at A,B located at the base of the antenna. In Fig.2b, the coaxial feed line is sketched together with two other coaxial cables which are introduced for impedance matching purposes. One of the two latter coaxial cables is short-circuited at one end and its other end is connected to the coaxial connector at A,B, whereas the other coaxial cable is open-circuited at one end and is connected to the feed points D,F at the other end. A circuit diagram of the three coaxial lines is presented in Fig.2c. The dielectric at the open end of the slot is of G 10 material which has a relative dielectric constant $\varepsilon_r = 5$.

Due to the internal structure and the feed-point arrangements as shown in Fig.2a, the antenna operates differently from the "ordinary" base-fed blade monopole antenna. However, the external antenna characteristics, i.e., the induced current and the antenna admittance of the VHF communication antenna can be derived from those of the base-fed blade antenna by the introduction of an ideal transformer in a way similar to the HF notch antenna on the B-1 (Chapter 10). The external characteristics of the antenna under consideration are presented in Fig.3a in the form of a combination of an ideal transformer with ratio n, an admittance Y_a and a current generator I_{ind}, the latter two quantities being respectively the antenna admittance and the induced short-circuit current of the base-fed blade monopole antenna. The induced current I_{ind} is given by (SSN 193)

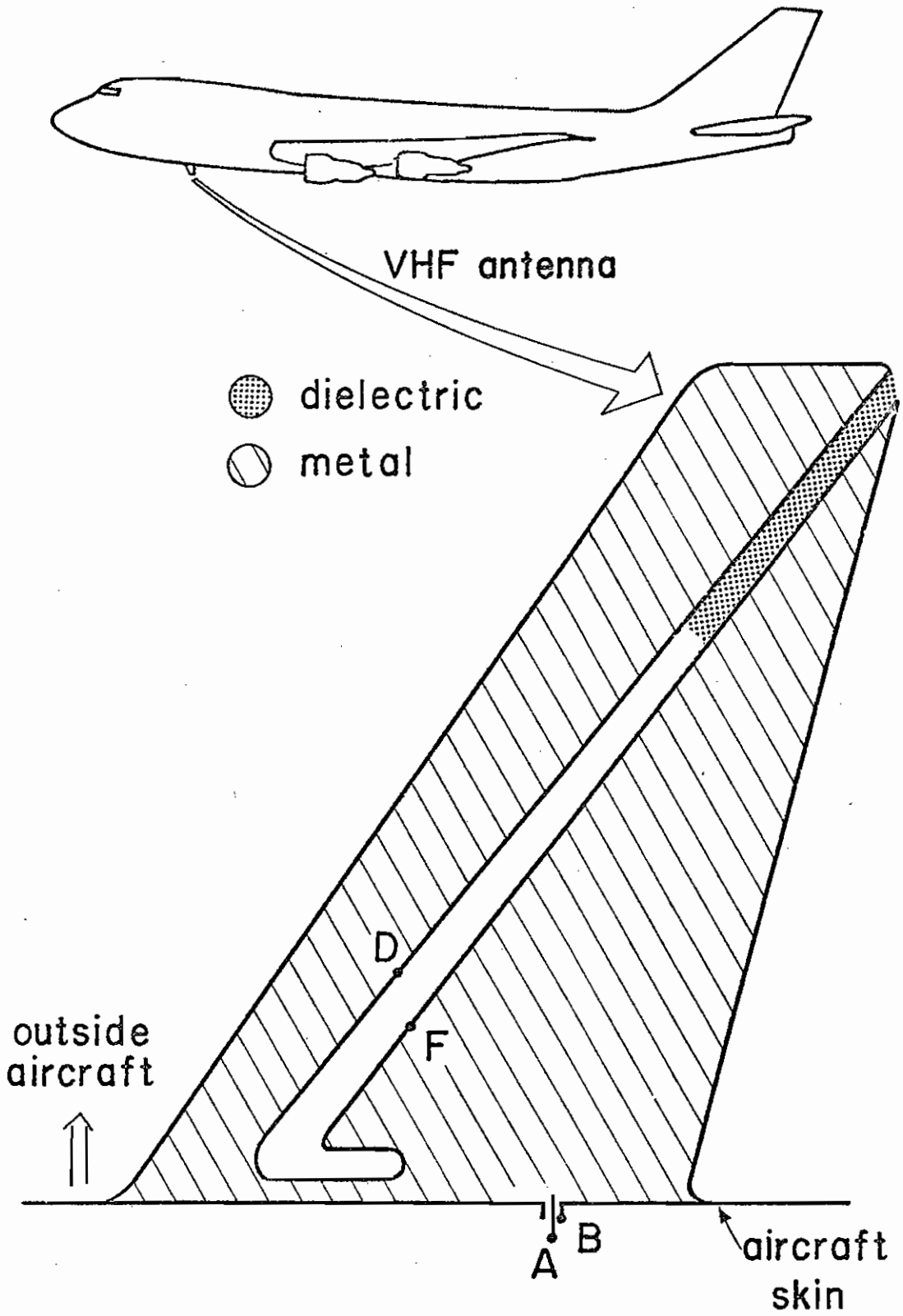

Fig.1. Location and schematic diagram of the VHF communication antenna.

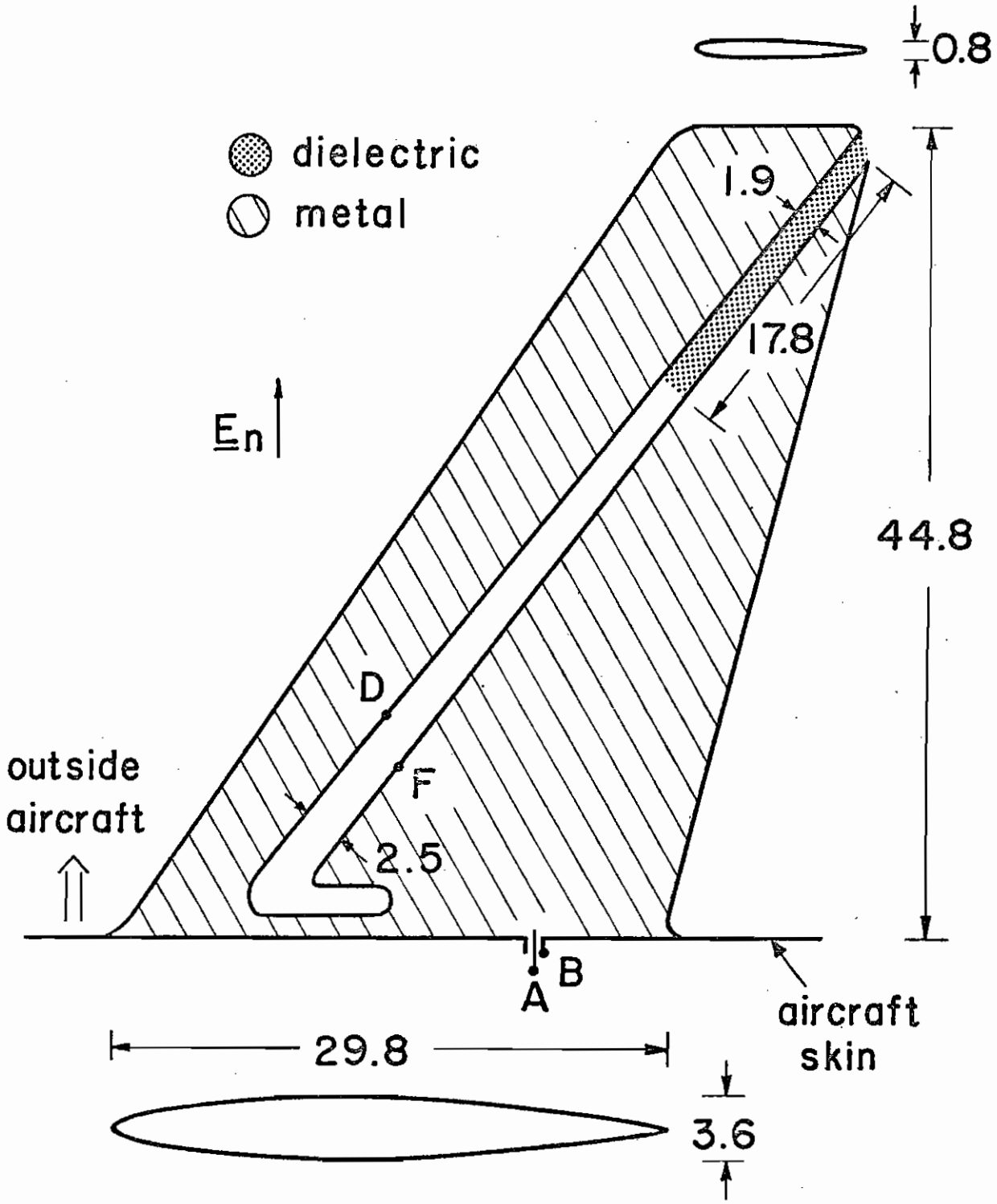

Fig.2. (a) The internal structure of the VHF communication antenna excluding the feeding and matching coaxial cable.

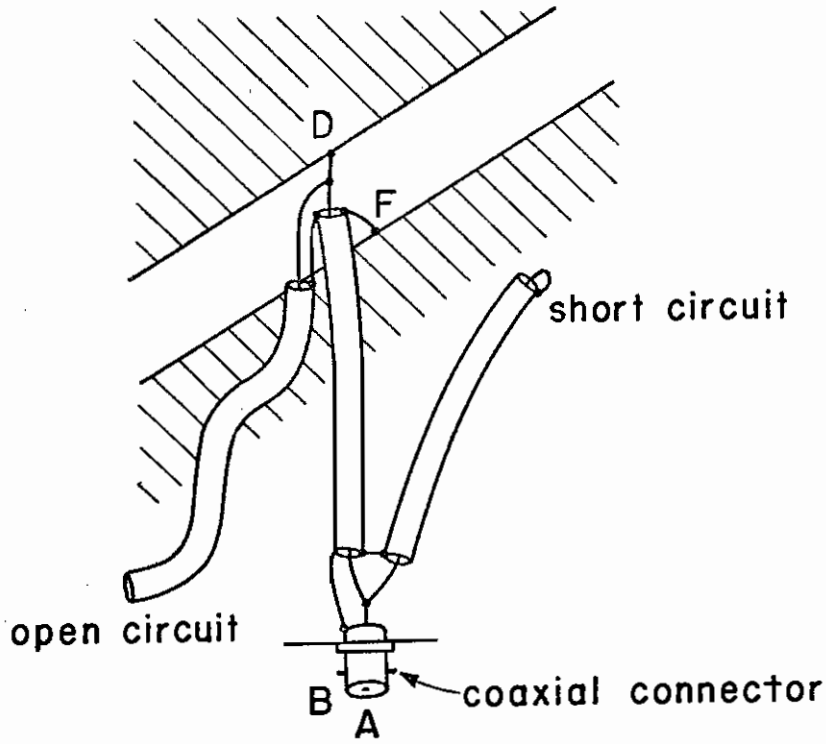

(b)

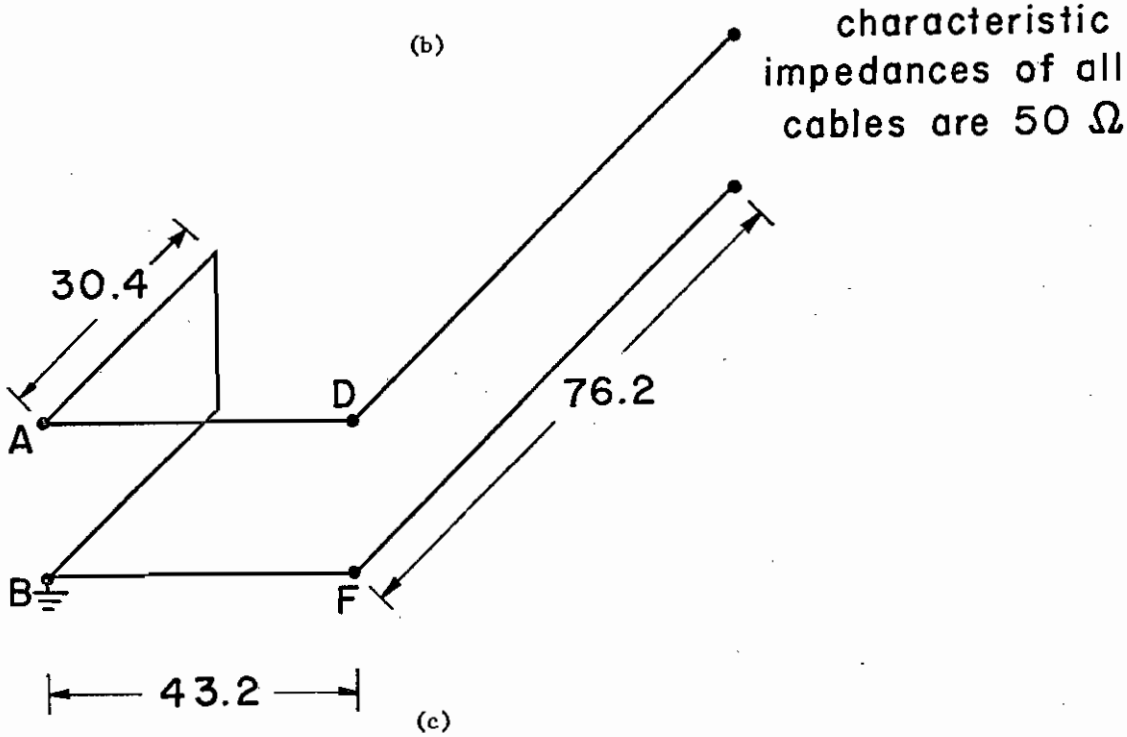

(c)

Fig.2. (b) The feeding coaxial cable and the impedance matching coaxial cables.
(c) Circuit diagram of the three coaxial cables.

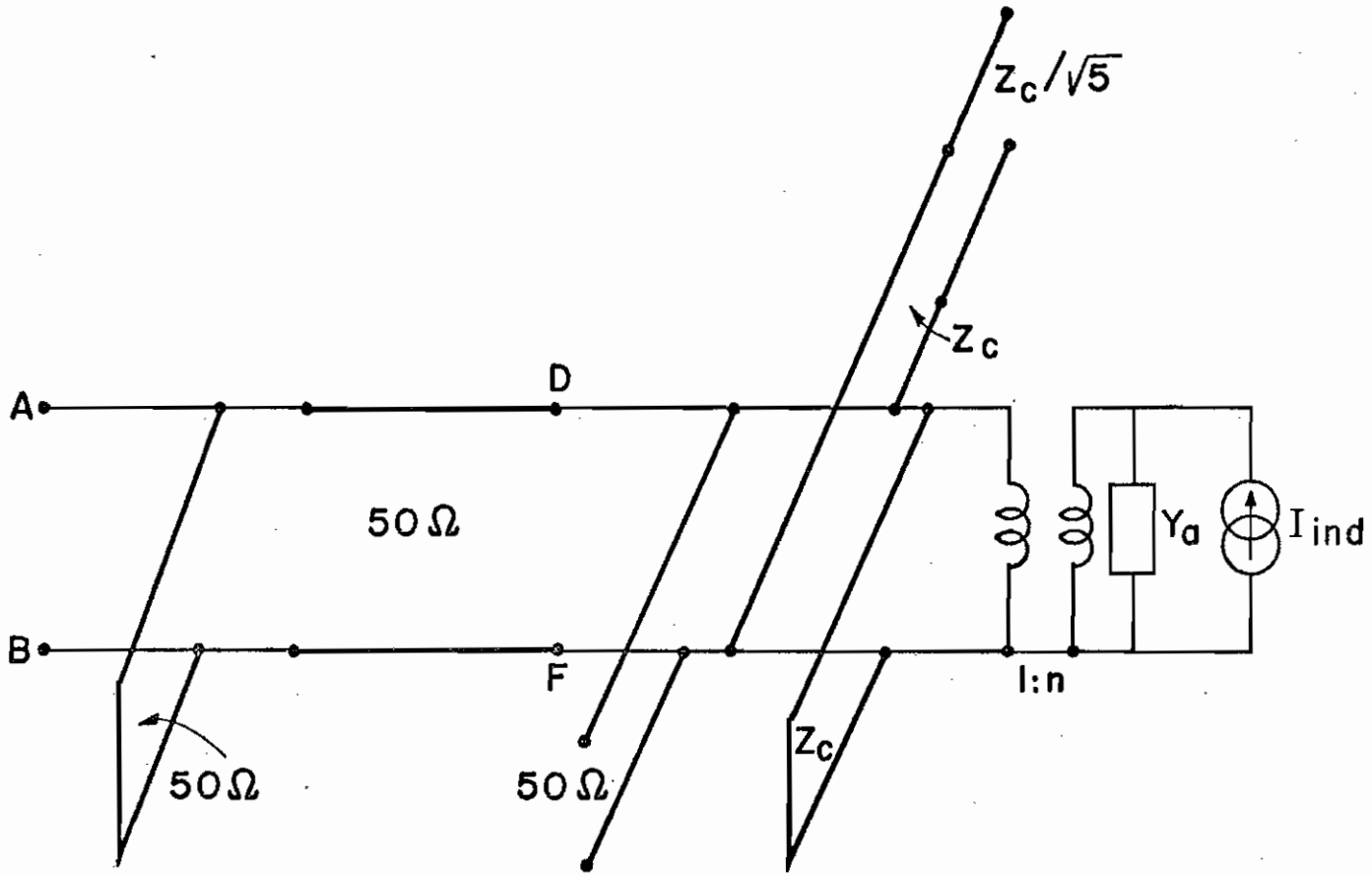

(a)

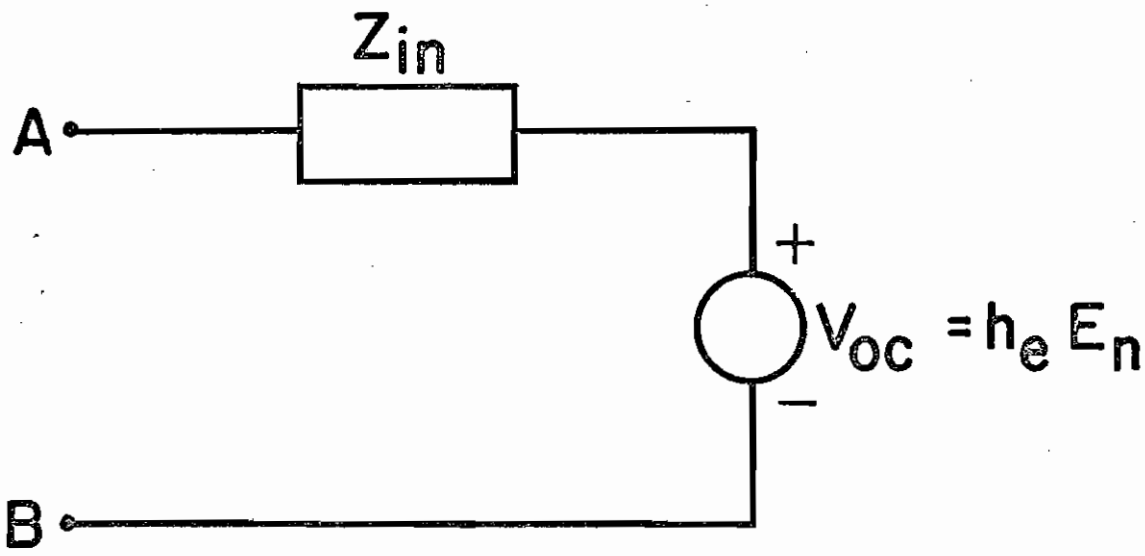

(b)

Fig.3. (a) The equivalent circuit of the VHF communication antenna.
(b) The Thevenin equivalent circuit at the terminals A,B.

$$I_{ind} = j\omega\varepsilon_o E_n [1-(b/a)^2][1-(c/a)^2]^{\frac{1}{2}} [F(\phi\backslash\alpha) - E(\phi\backslash\alpha)]^{-1} \qquad (1)$$

$$\phi = \sin^{-1} [1-(c/a)^2]^{\frac{1}{2}}$$

where

$$\alpha = \sin^{-1} [\{1-(b/a)^2\} \{1-(c/a)^2\}^{\frac{1}{2}}]$$

$F(\phi\backslash\alpha)$ and $E(\phi\backslash\alpha)$ are the incomplete elliptic functions of the first and the second kind, respectively. The quantities a, b, and c are the total height, the half width at the base and the half thickness at the base, respectively. Furthermore, E_n is the total electric field near the location of the antenna and is normal to the fuselage. In fact, E_n is related to the surface charge density σ on the aircraft skin near the antenna by

$$E_n = \sigma/\varepsilon_o.$$

Substituting the appropriate dimensions of the VHF antenna in (1), one gets

$$I_{ind} = j\omega\varepsilon_o E_n \times 0.398 \quad \text{Amperes.}$$

The transformer ratio n can be estimated by studying the current distribution on an electrically small ellipsoidal antenna (SSN 193). It is found that

$$n \simeq 0.4$$

The other components in the equivalent circuit of Fig.3a are readily identified. The two transmission lines with characteristic impedance Z_c are due to the slot: the short-circuited one being due to the portion below the terminals D,F, and the open-circuited one being due to the portion above D,F. The section of the transmission line having a characteristic impedance $Z_c/\sqrt{5}$ represents that portion of the slot containing the G 10 dielectric. The characteristic impedance of the slot is found to be $Z_c = 176\ \Omega$ (see IN 182). The three transmission lines with characteristic impedance of $50\ \Omega$ represent the coaxial cables drawn in Fig.2c.

The Thévenin equivalent circuit at terminals A,B as shown in Fig.3b can readily be obtained by applying circuit analysis techniques to the circuit in Fig.3a. The effective height h_e in Fig.3b is defined such that the open-circuit voltage V_{oc} is given by

$$V_{oc}(\omega) = h_e(\omega)\ E_n(\omega)$$

In Fig.4, the input impedance at terminals A,B is presented as a function of frequency. It is observed that in the in-band frequencies the antenna impedance varies within reasonable limits.

In Fig.5, the effective height is plotted versus frequency.

At low frequencies such that all physical dimensions of the antenna are small compared with the wavelength, a simplified equivalent circuit can readily be deduced. In this frequency range, the antenna admittance is almost entirely capacitive, whereas the short-circuited transmission lines can be represented by inductances and the open-circuited transmission lines can be represented by capacitances. Thus, the impedance at terminals D,F is due mainly to the short-circuited transmission line (see Fig.3a) which can be represented by an inductance being equal to the product of the distributed inductance and the length of the transmission line. Similarly, the two remaining transmission lines, i.e. the one connecting the terminals A,B to the terminals D,F and the short-circuited one at the terminals A,B are also represented by inductances. The low-frequency Thévenin equivalent circuit as shown in Fig.6 therefore has only an inductance L

$$L = 49.7 \text{ nH}$$

and a voltage generator $V_{oc} = h'_e\ E_n$ where the effective height h'_e is

$$h'_e = -7.02 \times 10^{-20}\ \omega^2 \quad \text{meters.}$$

The low-frequency input impedance and effective height are presented in Fig.7a and Fig.7b, respectively.

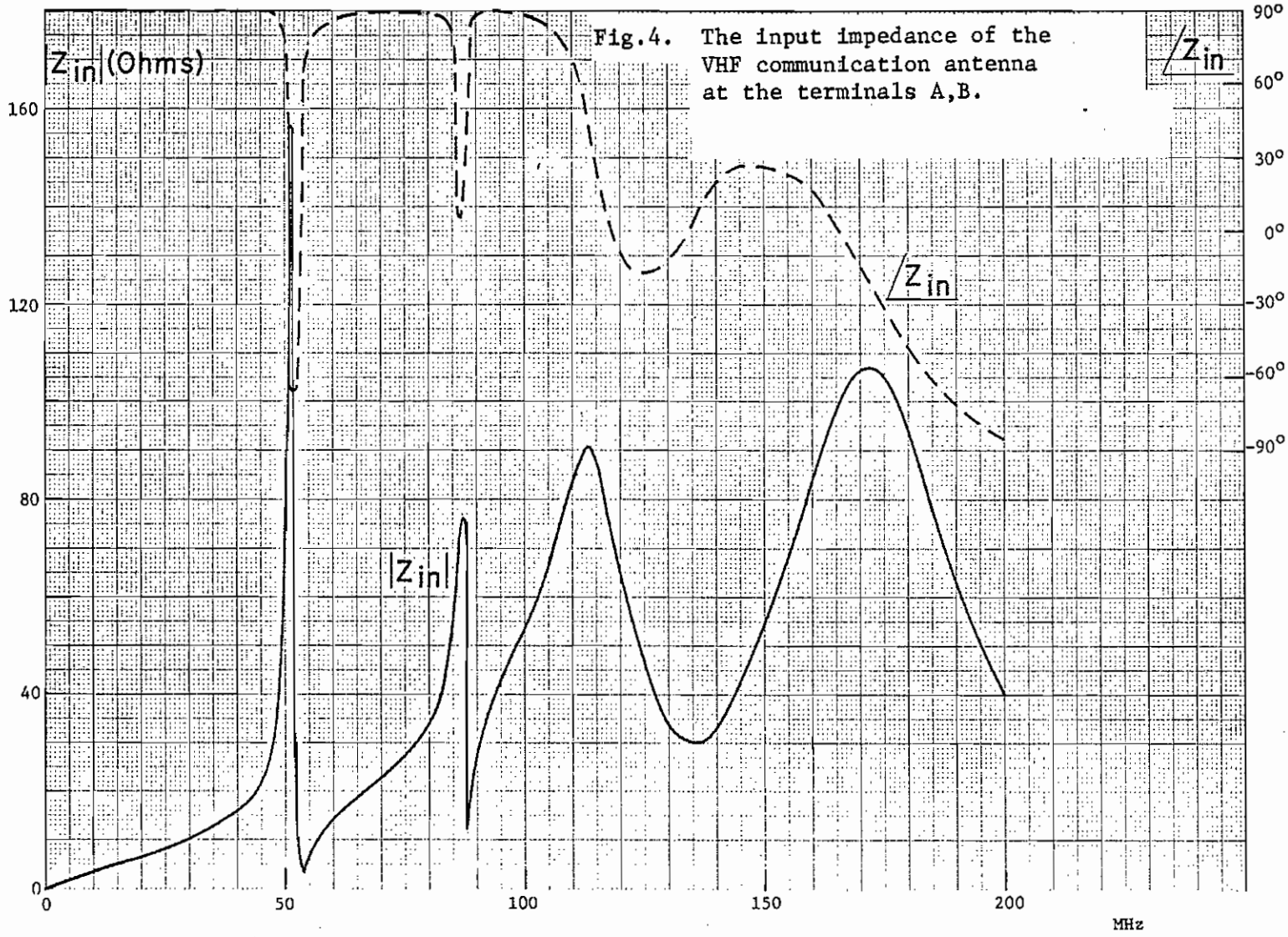

Fig.4. The input impedance of the VHF communication antenna at the terminals A,B.

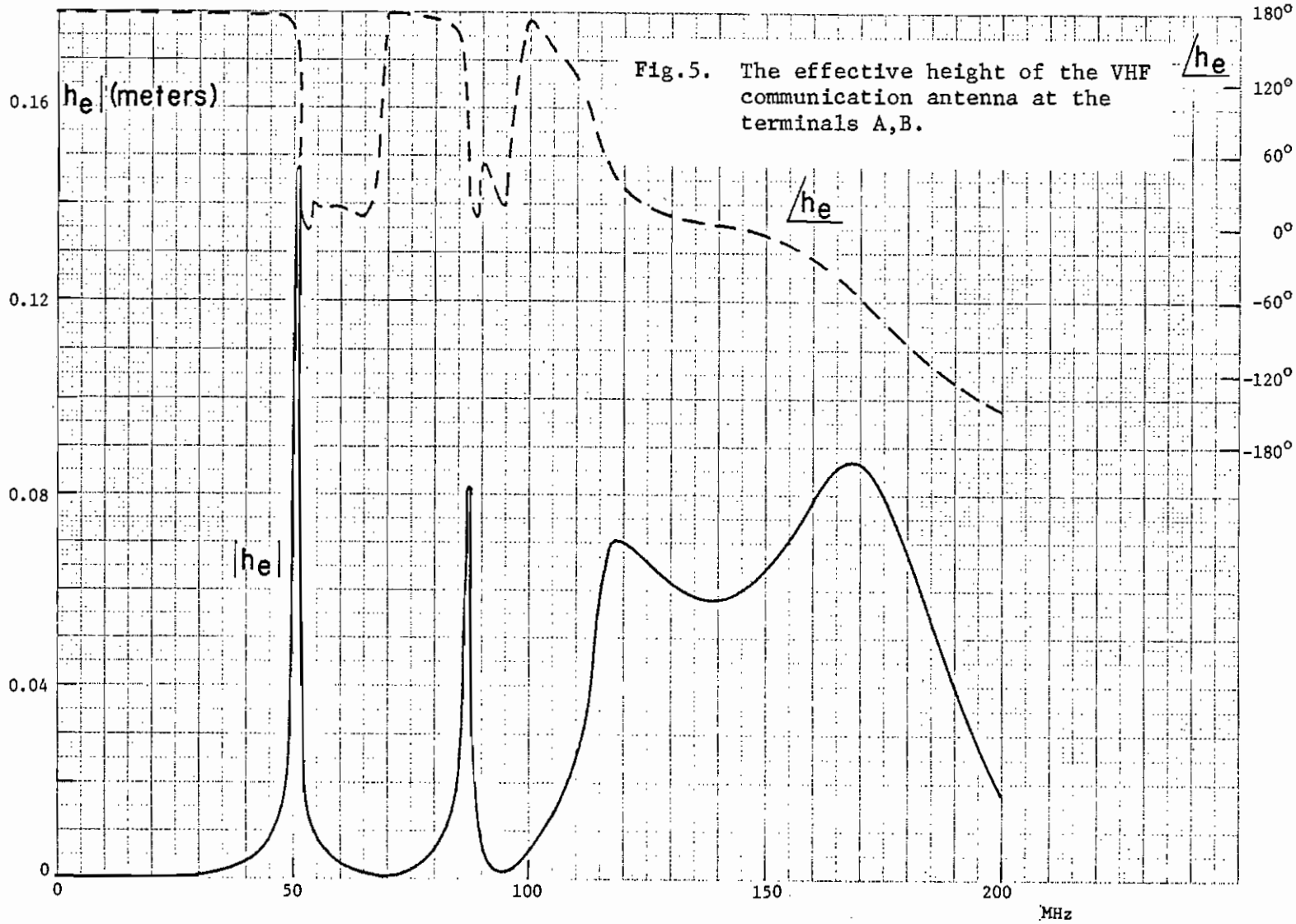

Fig.5. The effective height of the VHF communication antenna at the terminals A,B.

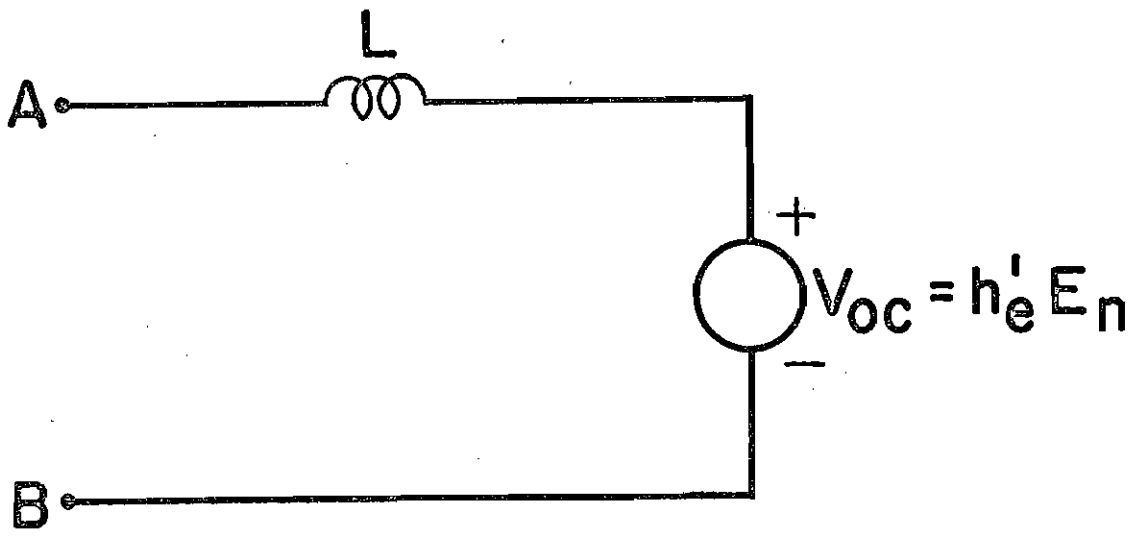

Fig.6. The low-frequency Thévenin equivalent circuit at the terminals A,B.

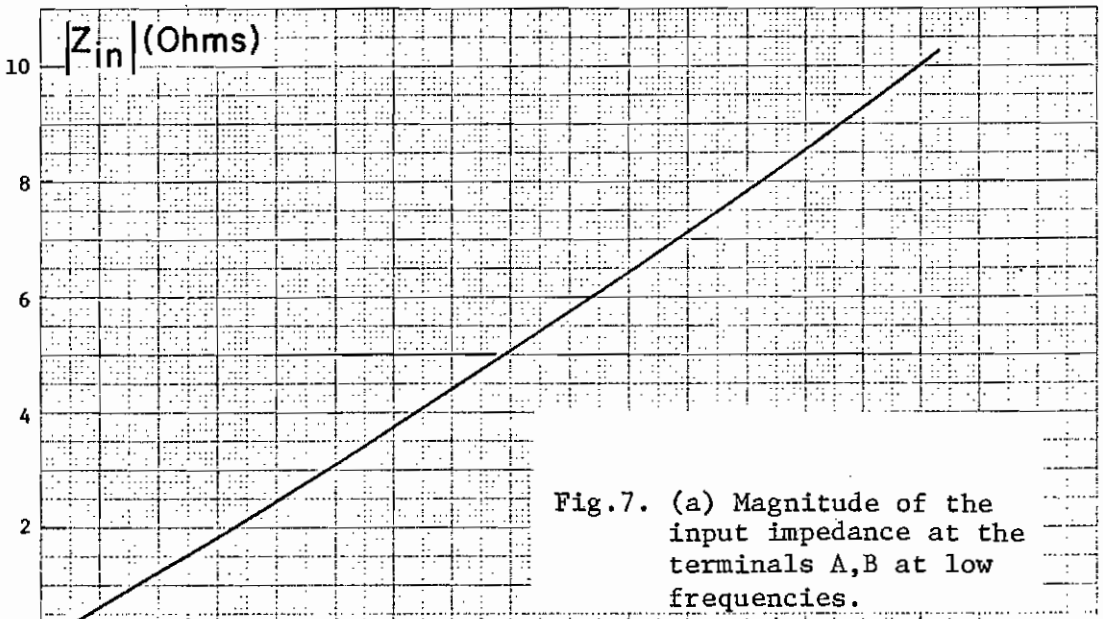

Fig.7. (a) Magnitude of the input impedance at the terminals A,B at low frequencies.

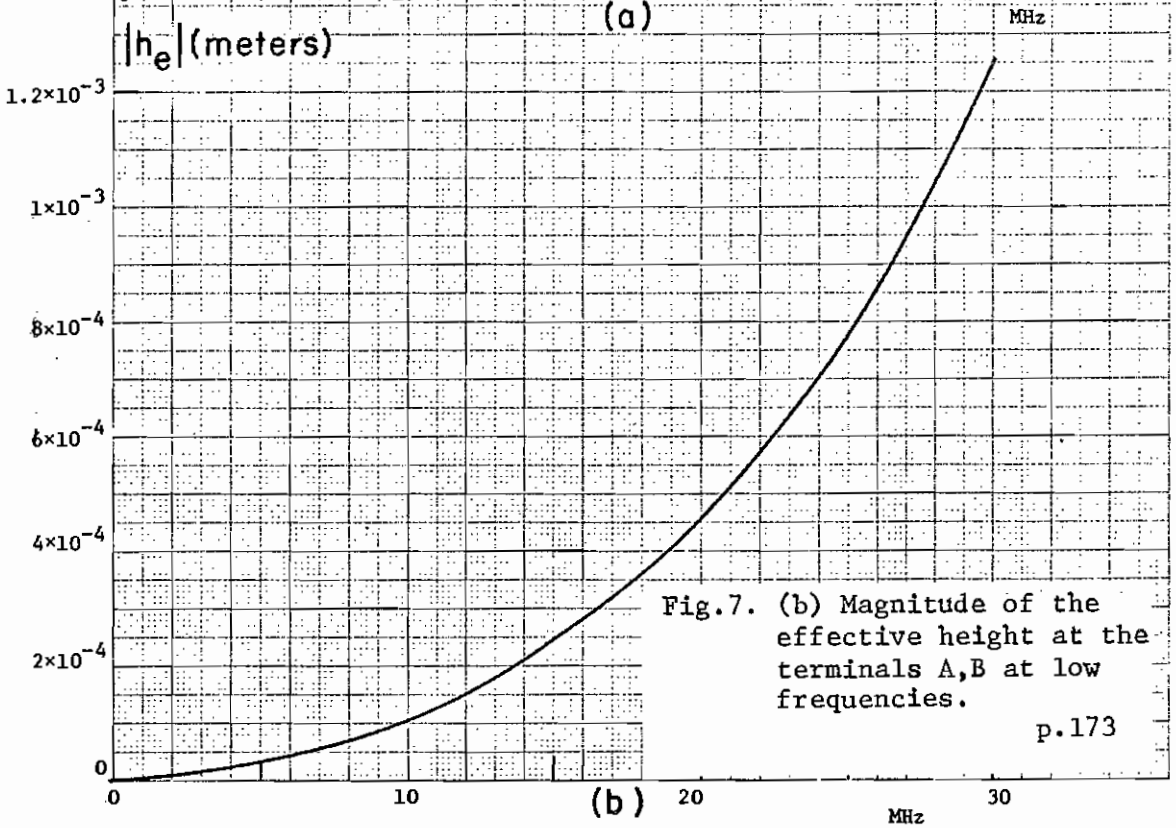

Fig.7. (b) Magnitude of the effective height at the terminals A,B at low frequencies.

p.173

CHAPTER 15. 60B00024 VOR ANTENNA ON AABNCP

I. General Description

The VOR (VHF Omni-Range) antenna is used to receive horizontally polarized signals in the frequency range 108-118 MHz (wavelengths ≈ 2.54-2.78 m). The antenna is mounted on the top of the vertical stabilizer inside a radome. The location and a schematic diagram of the antenna are shown in Fig. 1. The antenna itself is a rectangular loop (Fig. 1) and is connected to two input coaxial connectors via a hybrid circuit, a balun, and other lumped elements which are used for impedance matching (Fig. 2b).

II. Analysis

A top view and a cross-sectional view of the loop of the VOR antenna are depicted in Fig. 2a. The antenna is fed at the terminals D,F. The other two gaps on the antenna loop introduce capacitances to the antenna characteristics. To one of these two gaps a trimming capacitor is shunt-connected to provide tuning. The feeding points D,F are connected to a tuning circuit containing parallel inductances and capacitances, as shown in Fig. 2b. The tuning circuit is connected to a balun, which couples the balanced loop to the unbalanced circuit near the input terminals. The balun is a coaxial cable of about a quarter wavelength within the in-band frequencies wound on a ferrite core so as to limit the current flow on the outer conductor of the cable. The balun is connected to the hybrid circuit which splits the signal into two halves and delivers them to the two pairs of input terminals, A,B and A',B.

The two pairs of input terminals are connected to two identical instruments. Hence, at the terminals A,B and the terminals A',B, the electrical characteristics are the same. In the following, the electrical characteristics at only one pair of terminals, A,B, are evaluated.

The equivalent circuit of the antenna at the terminals A,B and A',B is presented in Fig. 3. The quantities Z_a and V_{ind} are respectively the antenna impedance of and the induced voltage in the loop antenna. The antenna admittance Y_a, being the inverse of the antenna impedance, is given by

$$Y_a = \frac{1}{Z_a} = \frac{1}{j\pi Z_o}\left[\frac{1}{a_o} + 2\sum_{n=1}^{\infty}\frac{1}{a_n}\right] \qquad (1)$$

where $Z_o = 377\Omega$ is the intrinsic impedance of free space. The complex

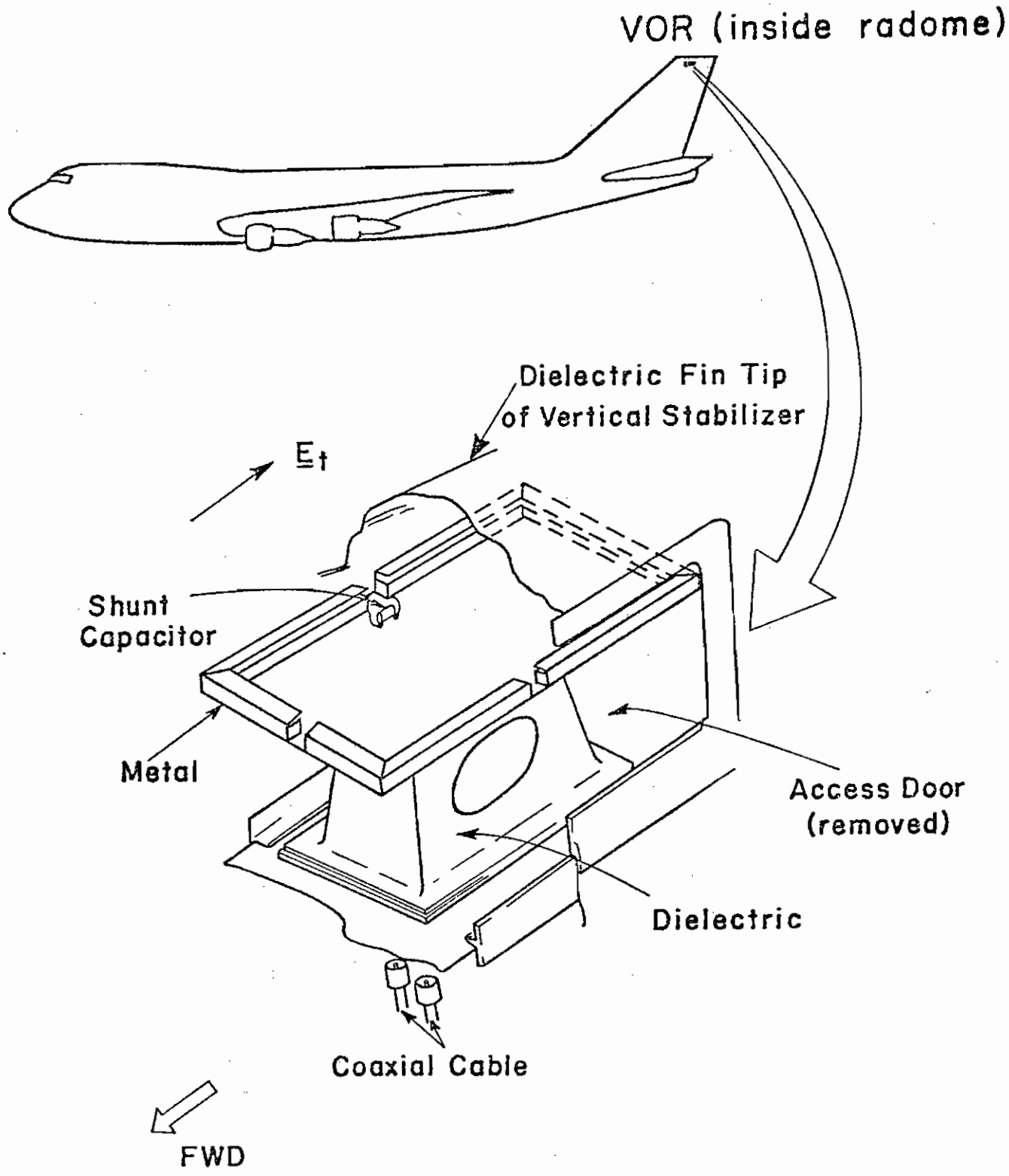

Fig. 1. The location and schematic diagram of the VOR antenna.

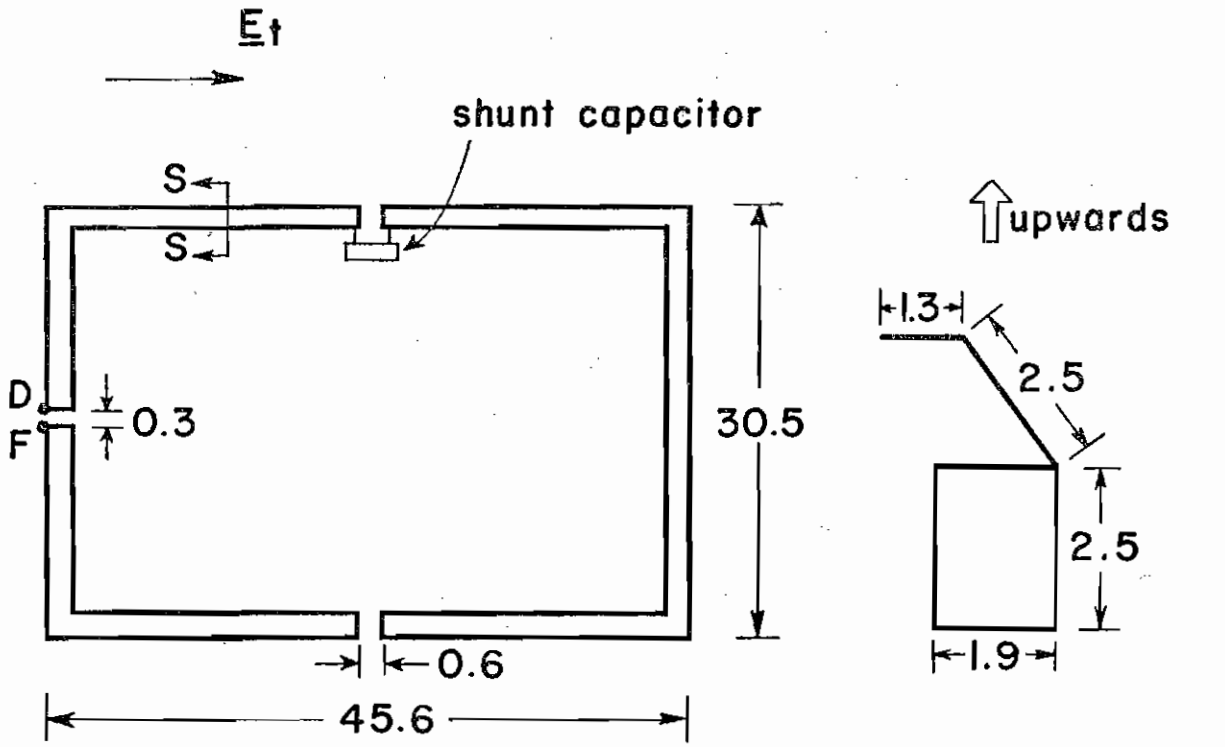

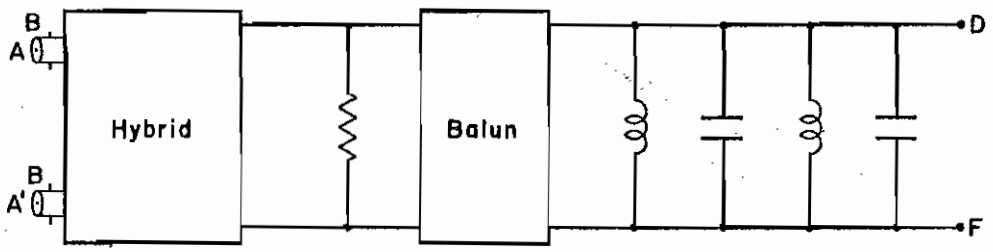

(b)

Fig.2. (a) The top view and a cross-sectional view of the VOR antenna.
(b) The circuit between the input coaxial connectors and the loop antenna.

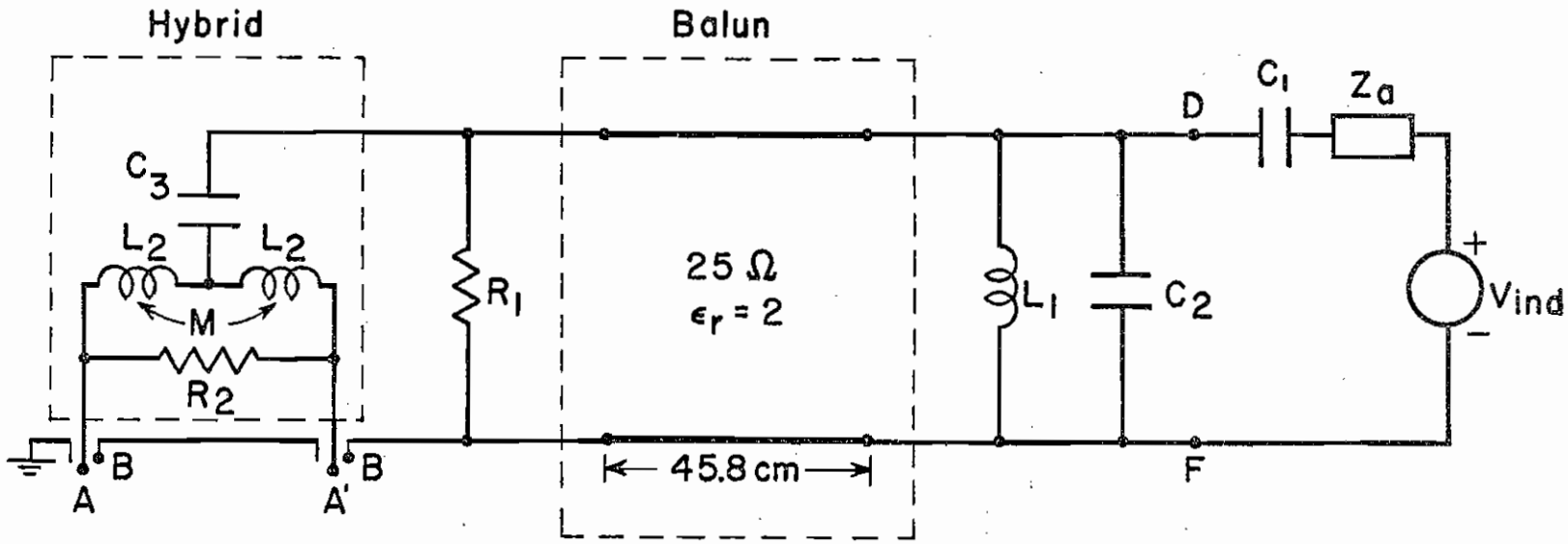

R_1 = 260 Ω
R_2 = 100 Ω
L_1 = 12.6 nH
L_2 = 64.7 nH
M ≃ 64.7 nH
C_1 = 24 pF
C_2 = 382 pF
C_3 = 245 pF

Fig. 3. The equivalent circuit of the VOR antenna.

quantities $1/a_n$ are available in the literature. For frequencies up to 150 MHz, the antenna admittance of the considered antenna can be accurately determined by including only the first two terms on the right-hand side of (1). Similarly, the induced voltage is given by

$$V_{ind} = \frac{E_t \pi kb}{(1/a_o)+(2/a_1)} \left[jkb \frac{1}{a_o} + \frac{2}{a_1} \right] \tag{2}$$

where b is the radius of an equivalent circular loop, i.e.,

$$\pi b^2 = A$$

and A is the area enclosed by the loop of the VOR antenna. In (2), the electric field E_t is in the plane of the loop. In fact, E_t is the total electric field equal to the vector sum of the incident and the scattered electric field.

In Fig. 3, the capacitance C_1 represents the combined capacitance of the two gaps on the long sides of the loop (Fig. 1) together with the shunt trimming capacitance. The capacitance C_2 accounts for the combined effect of the gap capacitance across D,F and the two lumped capacitors presented in Fig. 2b. The two inductors in Fig. 2b are combined into the inductance L_1 in Fig. 3. The elements of the balun and the hybrid circuit are also detailed in Fig. 3. The two inductors in the hybrid are closely coupled such that $M \simeq L_2$.

A simple circuit analysis can be carried out to obtain the Thévenin equivalent circuit in Fig. 4 at the terminals A,B. The effective height h_e is defined so that the open-circuit voltage V_{oc} is given by

$$V_{oc}(\omega) = h_e(\omega) E_t(\omega). \tag{3}$$

The input impedance Z_{in} is presented in Fig. 5, whereas the effective height h_e is presented in Fig. 6. The low frequency characteristics of these two quantities are presented in Fig. 7.

At low frequencies, the equivalent circuit can readily be simplified to

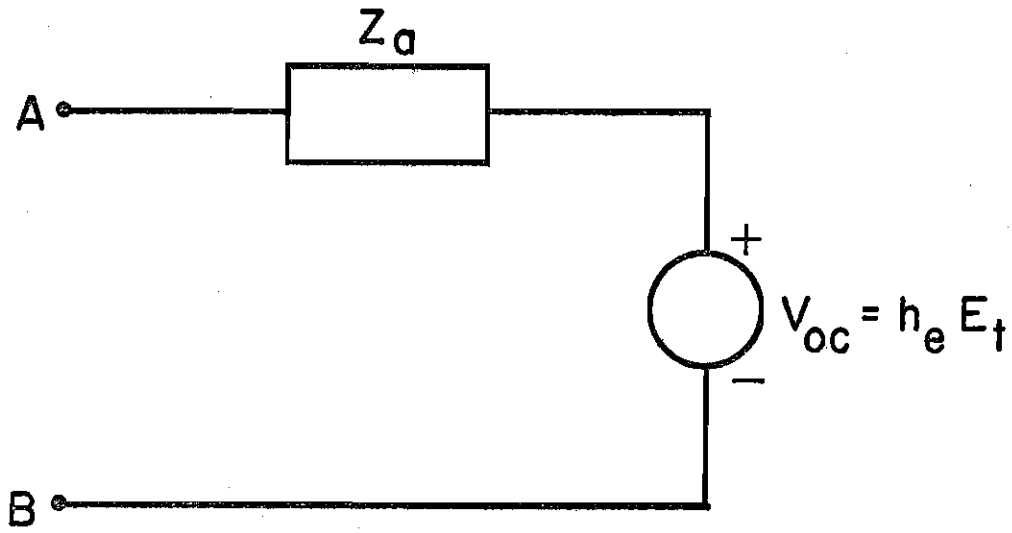

Fig. 4. The Thévenin equivalent circuit at the terminals A,B.

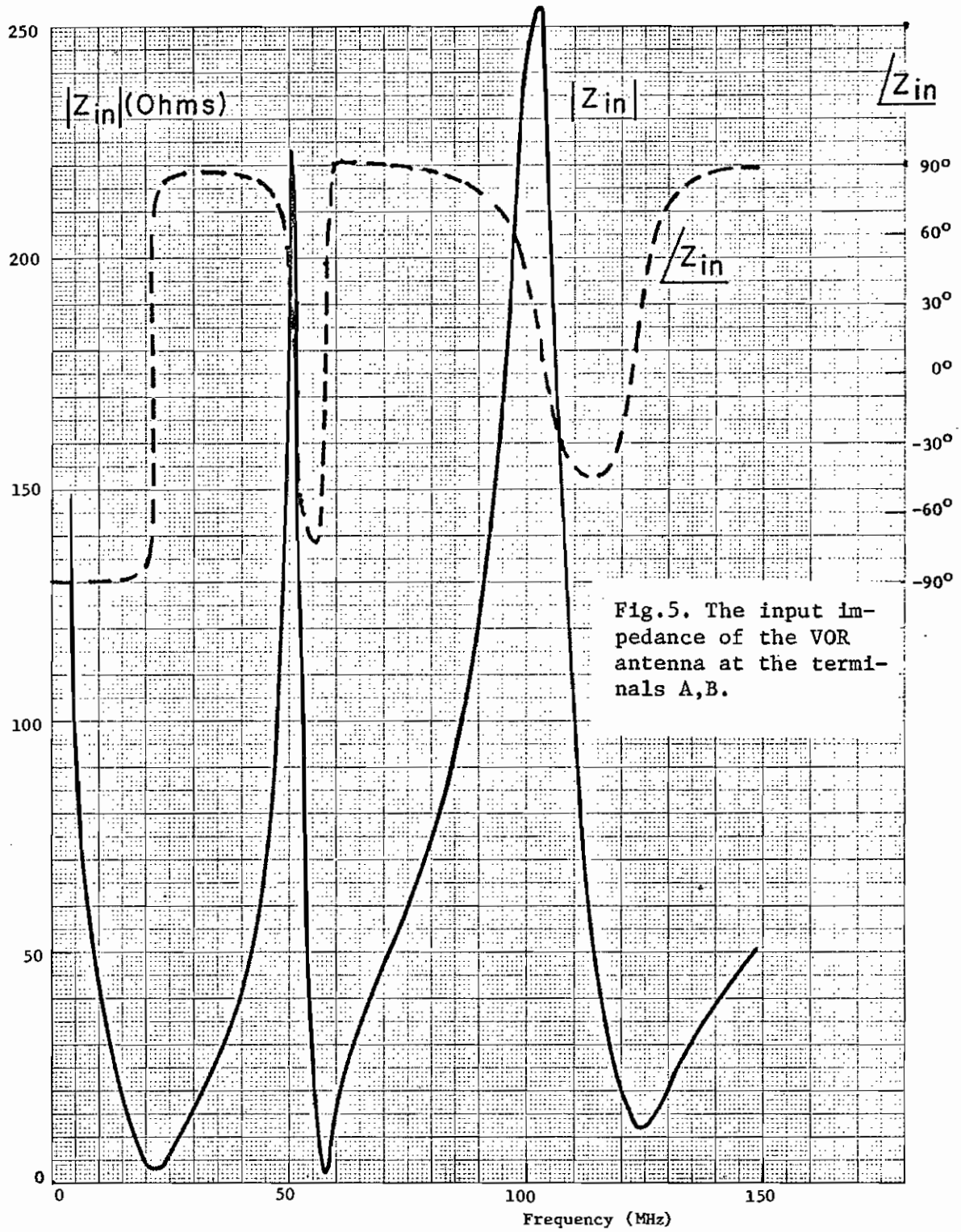

Fig.5. The input impedance of the VOR antenna at the terminals A,B.

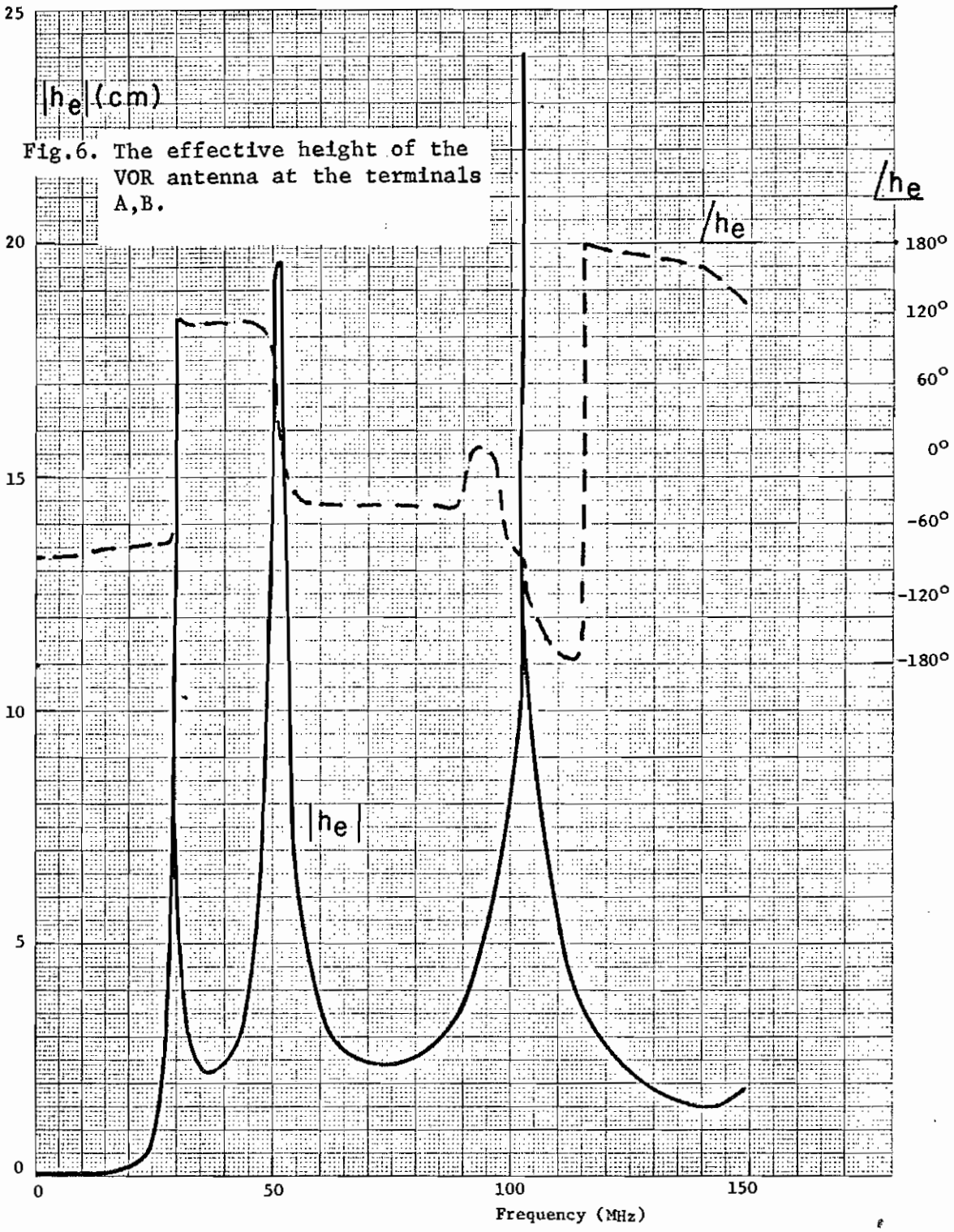

Fig.6. The effective height of the VOR antenna at the terminals A,B.

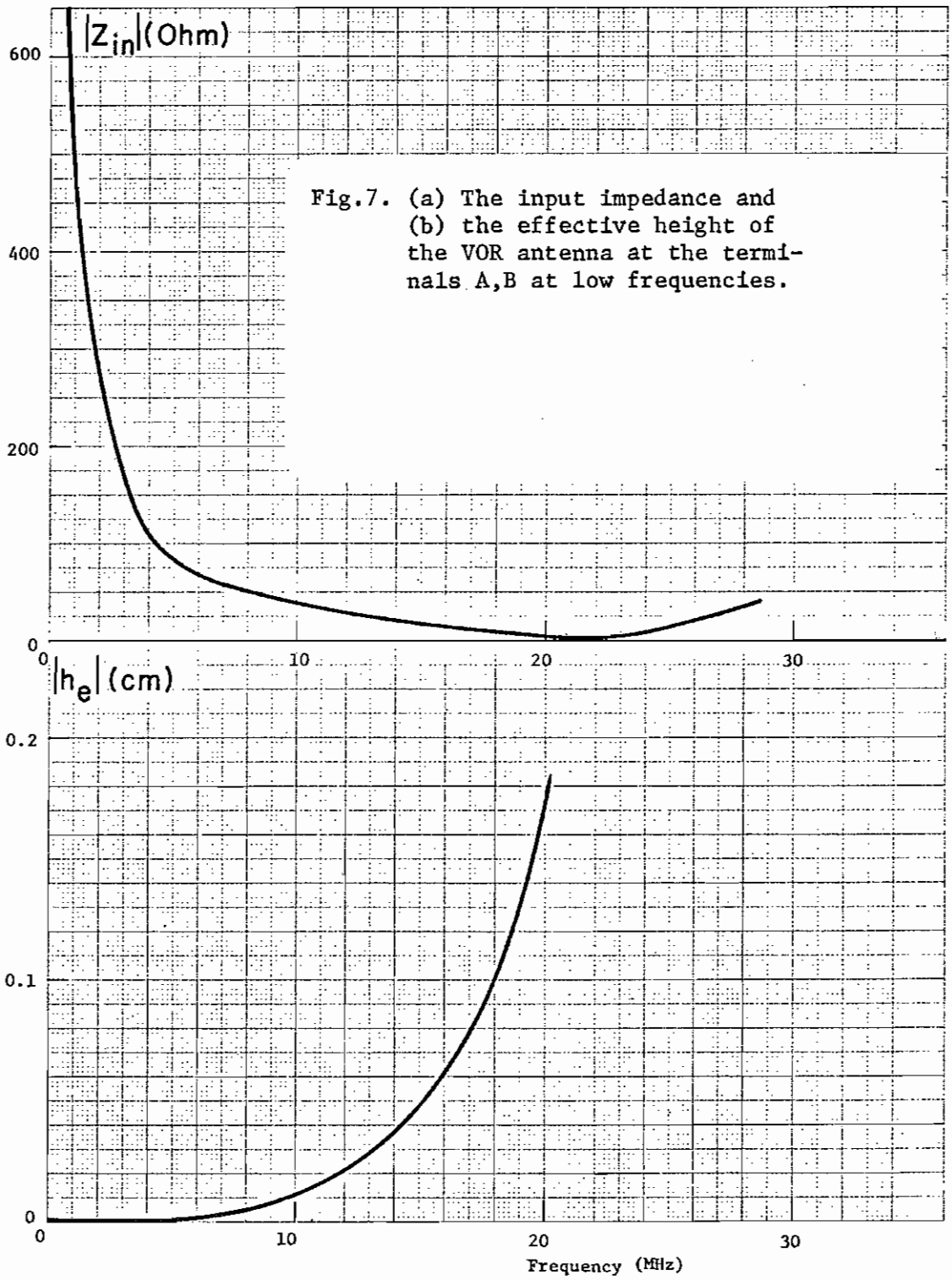

Fig.7. (a) The input impedance and (b) the effective height of the VOR antenna at the terminals A,B at low frequencies.

that of Fig. 8 where the low-frequency effective height h_e' is found to be

$$h_e' = jkA \tag{4}$$

and A is the area enclosed by the loop of the VOR antenna. The input impedance is mainly due to the capacitance C_3, i.e.,

$$Z_{in} = \frac{1}{j\omega C_3} \tag{5}$$

This low-frequency equivalent circuit is valid up to at most 5 MHz.

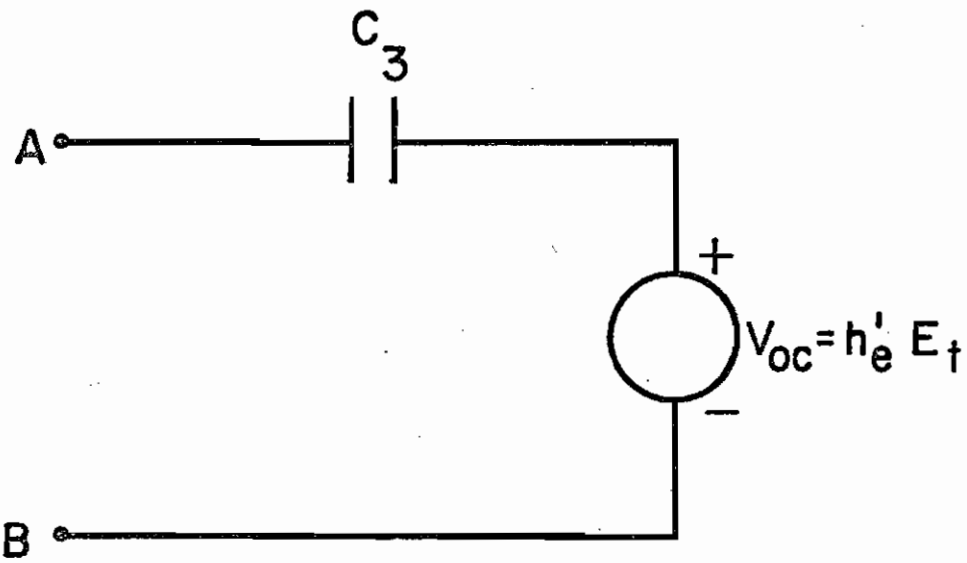

Fig. 8. The low frequency Thevenin equivalent circuit of the VOR antenna at the terminals A,B.

CHAPTER 16. 37R-2U VHF/UHF ANTENNA ON AABNCP

I. General Description

The Collins 37R-2U (military nomenclature AT-1108) blade antenna is used for communication purposes at two frequency ranges: 116-152 MHz (wavelengths ≈ 1.97 - 2.59 m) in the VHF range, and 225-400 MHz (wavelengths ≈ 0.75 - 1.33 m) in the UHF range. There are two such antennas on the AABNCP, and they are both externally mounted at the top of the fuselage at stations 830 and 1326. The locations of the two antennas are shown in Fig. 1a.

The radiating element of the antenna is a metal sheet which also serves as the "ground plane" of a printed-circuit board containing most coupling devices and impedance-matching networks on the other side of the board. The printed-circuit board is held in position by a foamed-in-place plastic enclosed inside a fiberglass shell. This arrangement is illustrated in the cut-away view of Fig. 1b. The printed-circuit board arrangement is depicted in Fig. 1c. The dotted area represents the radiating element on one side of the printed-circuit board, whereas the other circuit elements represented by the hatched area, the crossed area and the solid lines, are on the other side of the printed-circuit board. In Figs. 1c or 2a, the solid lines represent coaxial transmission lines; the hatched area together with the appropriate coaxial lines represents the VHF circuit elements used for signal coupling and impedance matching; the crossed area together with the appropriate coaxial lines represents the UHF circuit elements. The printed-circuit board is about 3.2 mm thick and is made of G-10 material which has a relative dielectric constant $\varepsilon_r = 5$. The pertinent dimensions of the printed-circuit board and a cross-sectional view are shown in Fig. 2a and Fig. 2b, respectively.

It is of interest to point out at this stage that the signals are capacitively coupled from the radiating element to the driving circuits through the rectangular plates and other microstrip line components shown in Fig. 2a.

II. Analysis of the VHF Section

The physical layout of the VHF section is depicted in Fig. 3a. The input coaxial connector at the terminals A,B is linked to the microstrip components via a coaxial transmission line whose outer conductor is in electrical contact with the "ground plane" of the microstrip circuit. A short-circuited coaxial

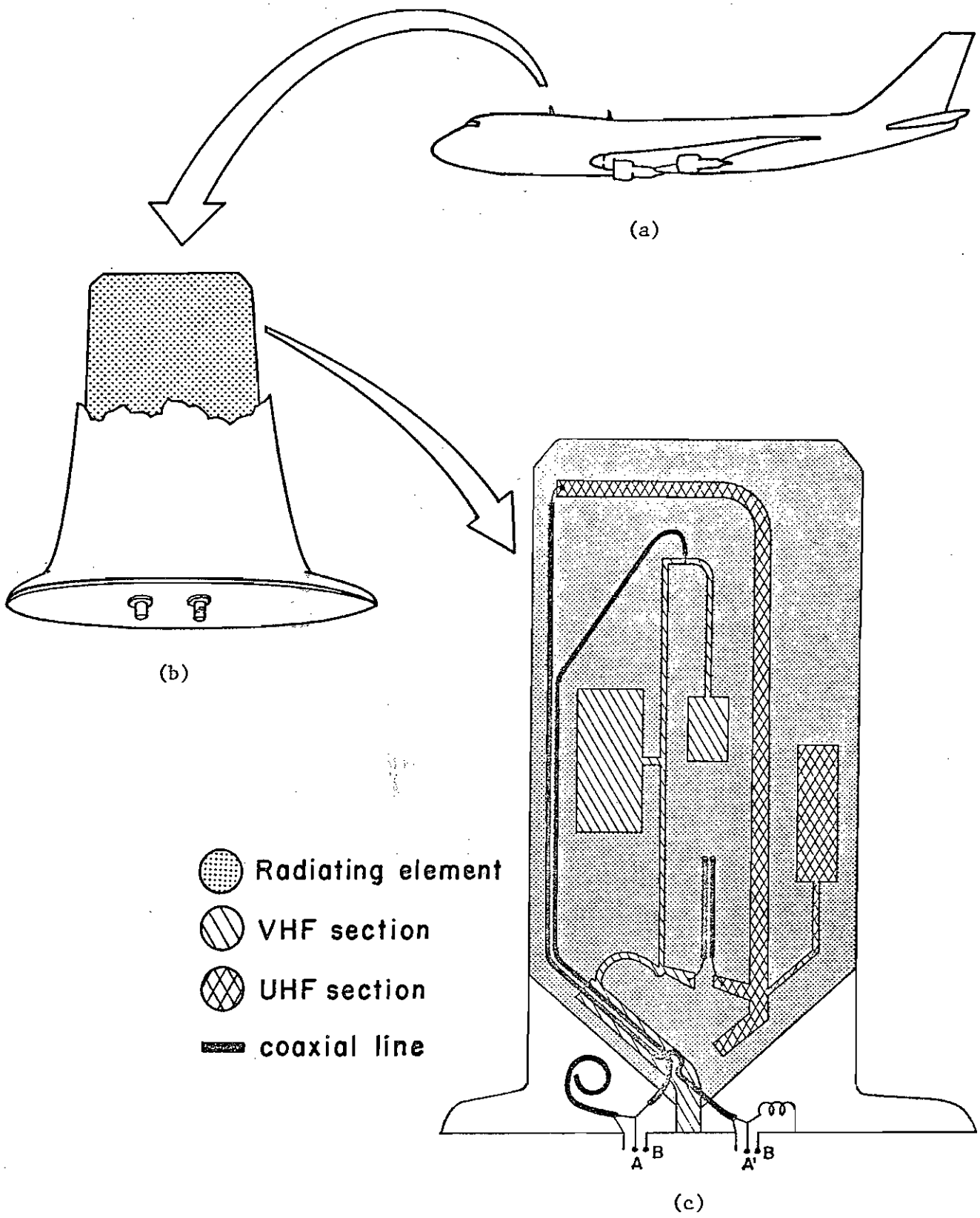

Fig.1 (a) The location, (b) a partial cut-away view and, (c) a schematic diagram of the VHF/UHF antenna.

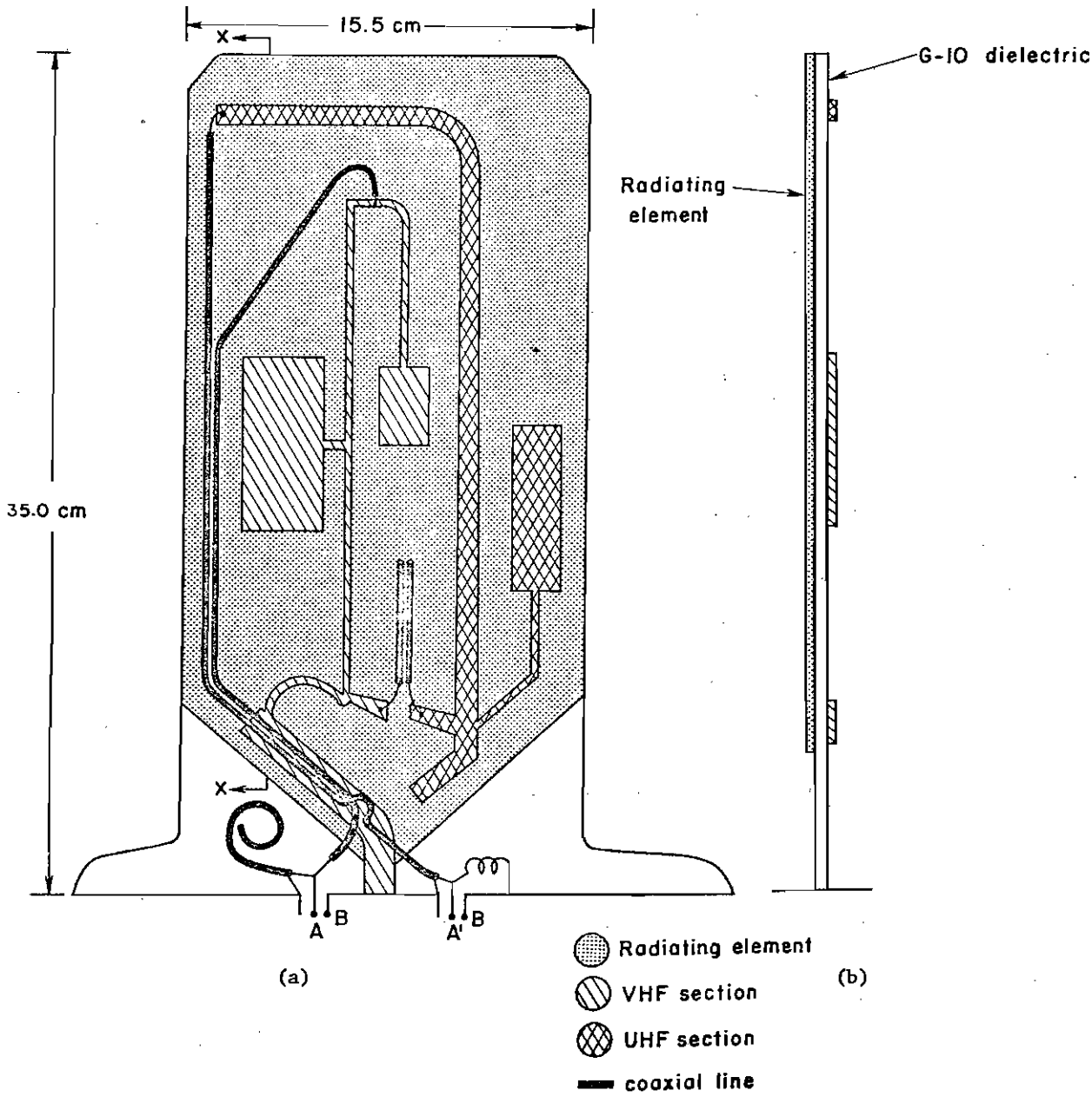

Fig.2 (a) A detailed sketch and (b) the cross-sectional view through X-X of the VHF/UHF antenna.

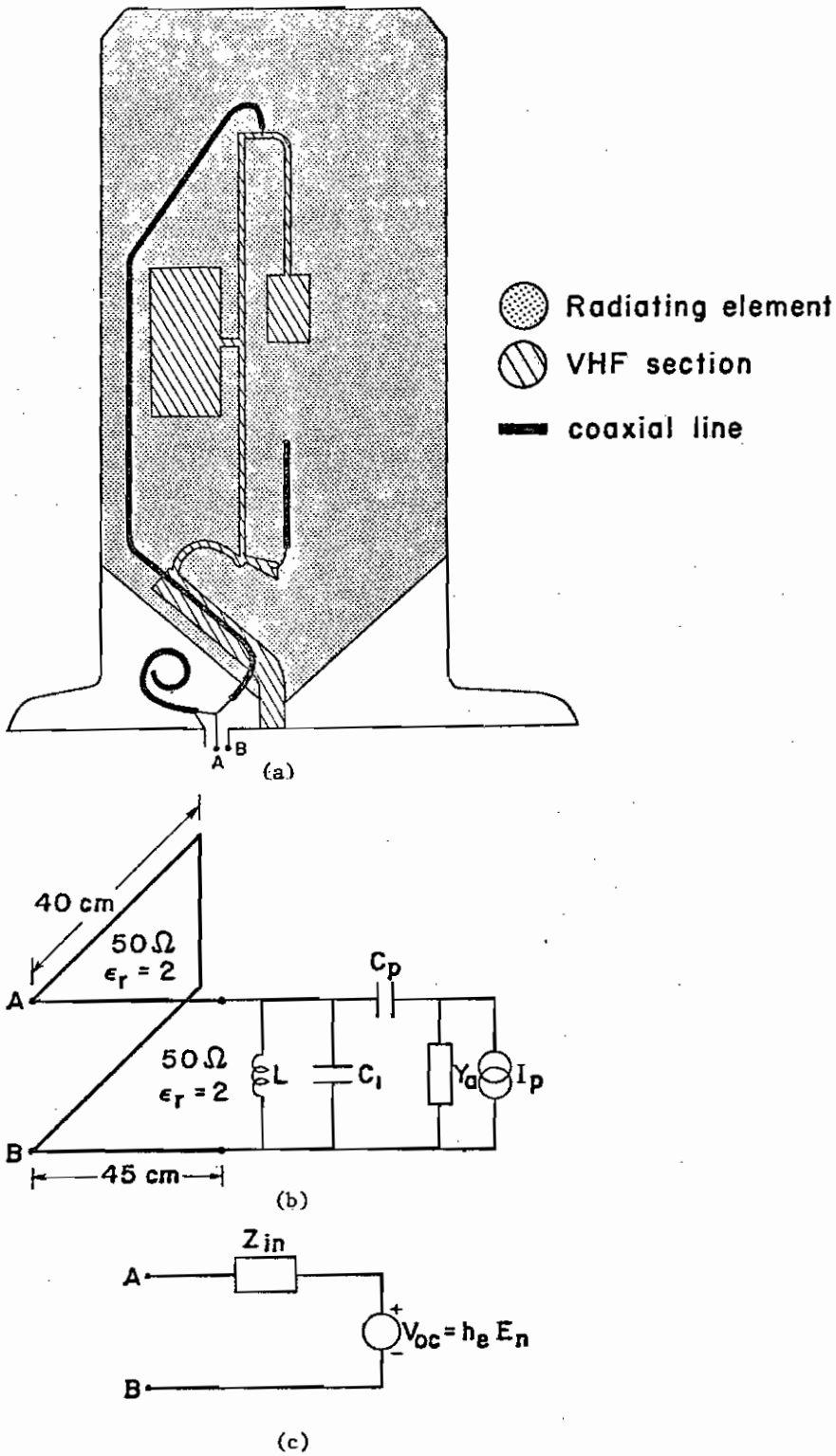

Fig.3 (a) The VHF section (b) the equivalent circuit and (c) the Thevenin equivalent circuit at the terminals A,B.

line is connected in shunt across the input terminals A,B. The microstrip circuit consists of two transmission lines connected to two capacitive plates which couple the induced signals on the radiating element (i.e., the "ground plane" of the printed-circuit board) to the input transmission line. One of the plates is also connected to a network of impedance matching elements consisting of a length of microstrip line and an open-circuited coaxial line.

The equivalent circuit of the VHF section is shown in Fig. 3b. The current source I_p represents the total current induced on the two plates through capacitive coupling to the induced current I_{ind} on the radiating element. The current source I_p is related to I_{ind} by

$$I_p = n_p I_{ind} \tag{1}$$

where the induced current I_{ind} is given by (see SSN 193)

$$I_{ind} = j\omega\varepsilon_o E_n \frac{\pi a b m_1}{\sqrt{1-m_1}[K(m_1)-E(m_1)]} \tag{2}$$

and

$$m_1 = 1 - (b/a)^2 \tag{3}$$

The quantities a and b are respectively the total height and the half width at the base of the radiating element. $K(m_1)$ and $E(m_1)$ are the complete elliptic integrals of the first and the second kind, respectively. Furthermore, E_n is the total electric field near the location of the antenna and it is normal to the fuselage. In fact, E_n is related to the surface charge density σ on the aircraft skin near the antenna by

$$E_n = \sigma/\varepsilon_o.$$

The constant n_p in (1) is the ratio of the charges induced on the two plates to the total charge induced on the entire radiating element. For the present configuration, a detailed evaluation shows that n_p is also approximately (within 10% accuracy) equal to the ratio of the total area of the two plates to the area of the radiating element. It is found that

$$n_p = 0.048 \tag{4}$$

Substitution of appropriate values into (1) gives

$$I_p = j\omega E_n \, 4.08\times10^{-14} \quad \text{Amperes}$$

The other elements in Fig. 3b can be readily identified. The antenna admittance Y_a is that of a base-fed blade monopole antenna. The capacitance C_p is the total capacitance due to the two plates. The capacitance C_1 accounts for part of the microstrip line and the open-circuited coaxial line. The inductance L represents the aggregated effect of the microstrip line. The transmission line with length 45 cm is the coaxial line connecting the microstrip line to the input terminals A,B, and the transmission line shunted across A,B is the short-circuited coaxial line near the input terminals.

The Thévenin equivalent circuit of the antenna at the terminals A,B is shown in Fig. 3c and it can be readily obtained by applying circuit analysis techniques to the circuit in Fig. 3b. The effective height h_e in Fig. 3c is defined, so that the open-circuit voltage V_{oc} at the terminals A,B is given by

$$V_{oc}(\omega) = h_e(\omega)E_n(\omega). \tag{5}$$

The input impedance Z_{in} and the effective height h_e are plotted versus frequency in Fig. 4 and Fig. 5, respectively. It is to be noted that the small values of the effective height (of the order of 2 mm) can be attributed to the capacitive coupling mechanism of the antenna feed.

At low frequencies, the equivalent circuit of Fig. 3b can be simplified to that of Fig. 6. The input impedance is inductive and

$$Z_{in} = j\omega L_1$$

$$= j\omega\times6.1\times10^{-8} \quad \text{Ohms.} \tag{6}$$

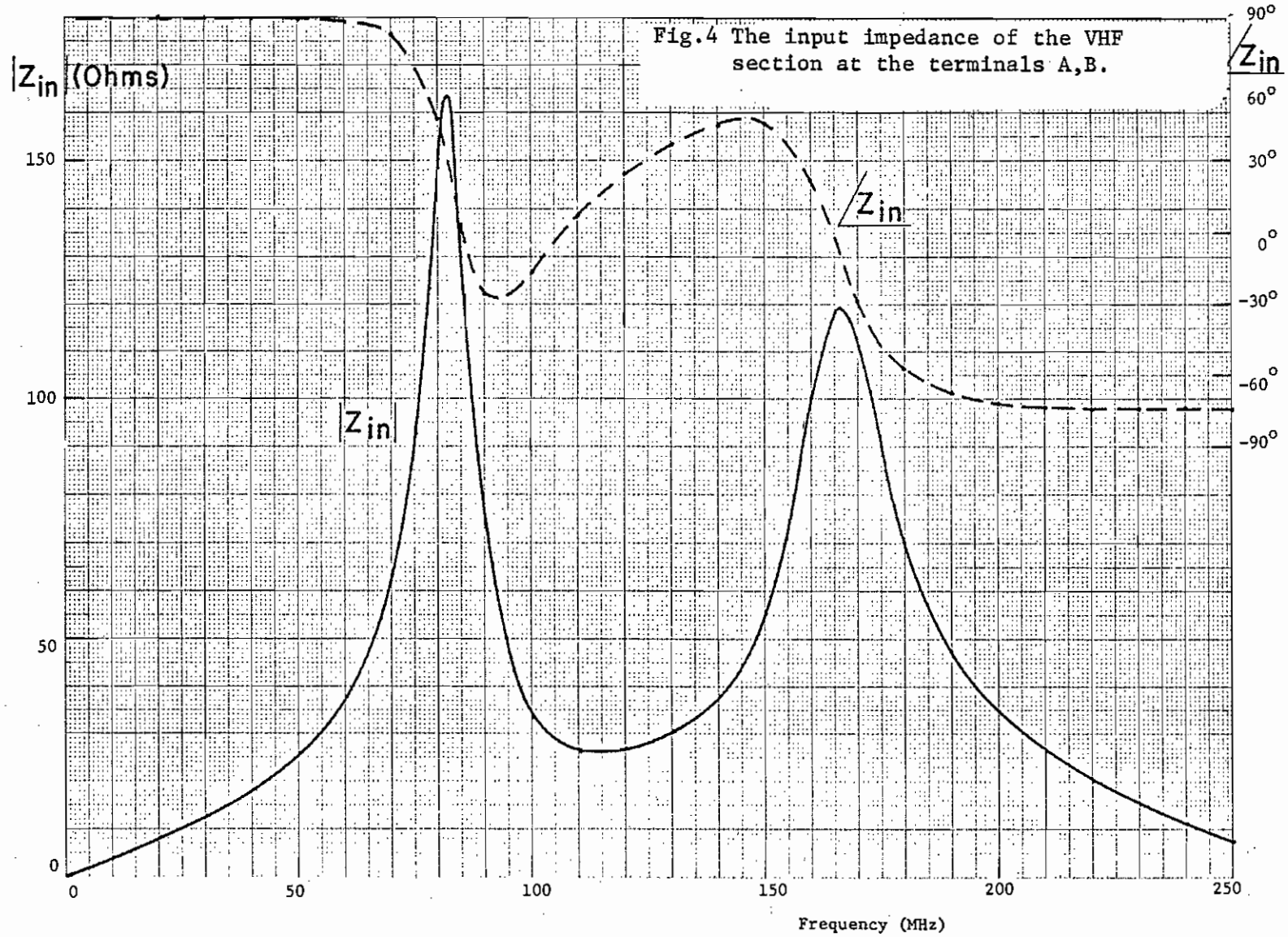

Fig.4 The input impedance of the VHF section at the terminals A,B.

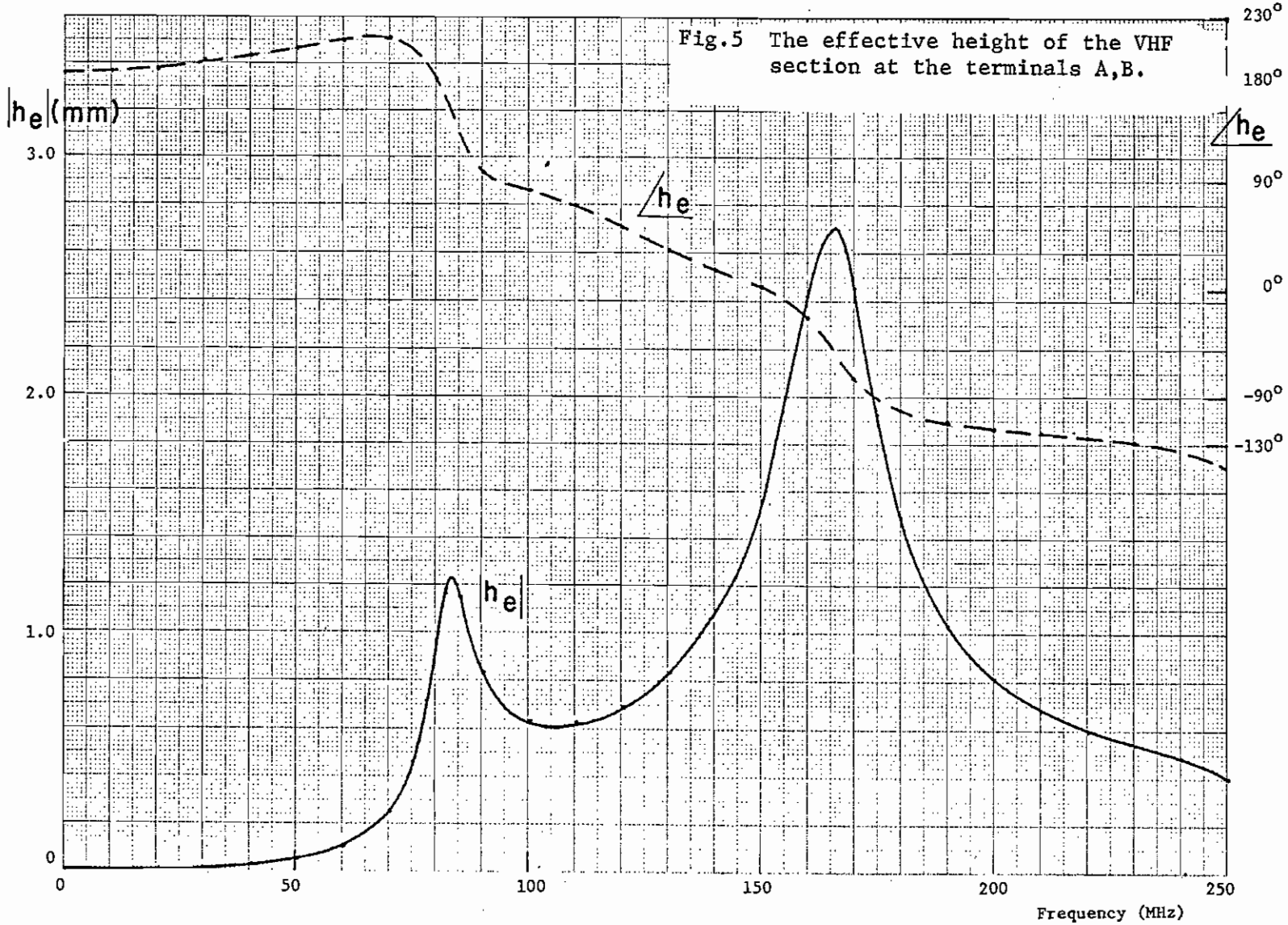

Fig.5 The effective height of the VHF section at the terminals A,B.

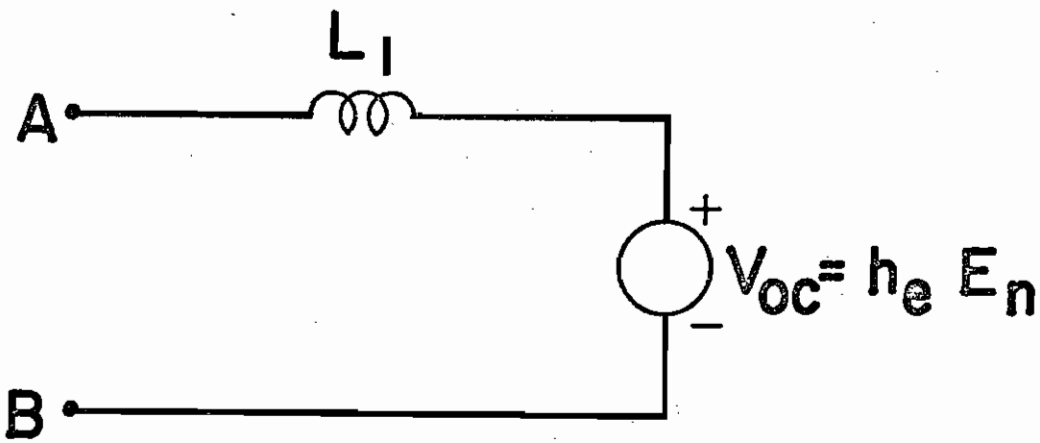

Fig.6 The low frequency equivalent circuit of the VHF section at the terminals A,B.

The effective height is given by

$$h_e = -3.5\times10^{-22}\ \omega^2 \qquad \text{Meters.} \tag{7}$$

In Fig. 7, the magnitudes of the input impedance and the effective height are presented for frequencies up to 40 MHz. In the same figures, the graphs based on the low-frequency formulas, (6) and (7), are also presented. It is observed that for the input impedance, the low-frequency model is valid up to about 15 MHz, whereas for the effective height it is good up to about 30 MHz.

III. Analysis of the UHF Section

The physical layout of the UHF section is depicted in Fig. 8a. The input coaxial connector at the terminals A',B is linked to the microstrip components via a coaxial transmission line whose outer conductor is connected to the "ground plane" of the printed-circuit board. An inductor is connected in shunt across the input terminals A',B. The microstrip circuit consists of a transmission line which is connected to a capacitive plate and an open-circuited coaxial line. In this case, because of the considerably larger width of the strip line, the signal is coupled to the input through both the strip line itself and the capacitive plate.

The equivalent circuit of the UHF section is shown in Fig. 8b. The current source I_s includes the contribution from both the strip, I_t, and the capacitive plate, I_p'. Both I_t and I_p' are proportional to the induced current, I_{ind}, on the radiating element in the same way as in the VHF section (equations (1) to (3)), i.e.,

$$I_t = n_t I_{ind} \tag{8}$$

$$I_p' = n_p' I_{ind} \tag{9}$$

and

$$I_s = I_t + I_p' = (n_t + n_p')I_{ind}. \tag{10}$$

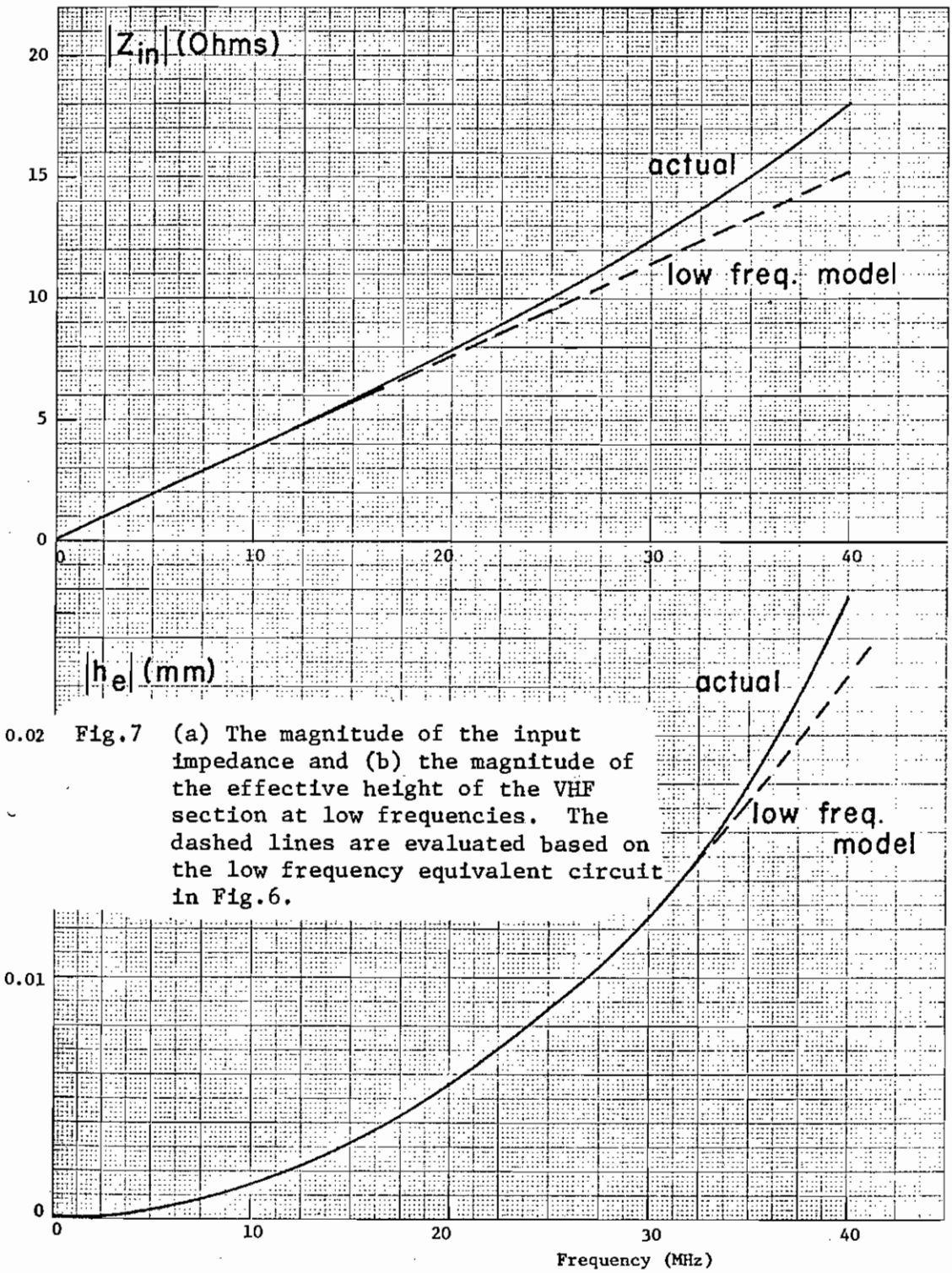

Fig.7 (a) The magnitude of the input impedance and (b) the magnitude of the effective height of the VHF section at low frequencies. The dashed lines are evaluated based on the low frequency equivalent circuit in Fig.6.

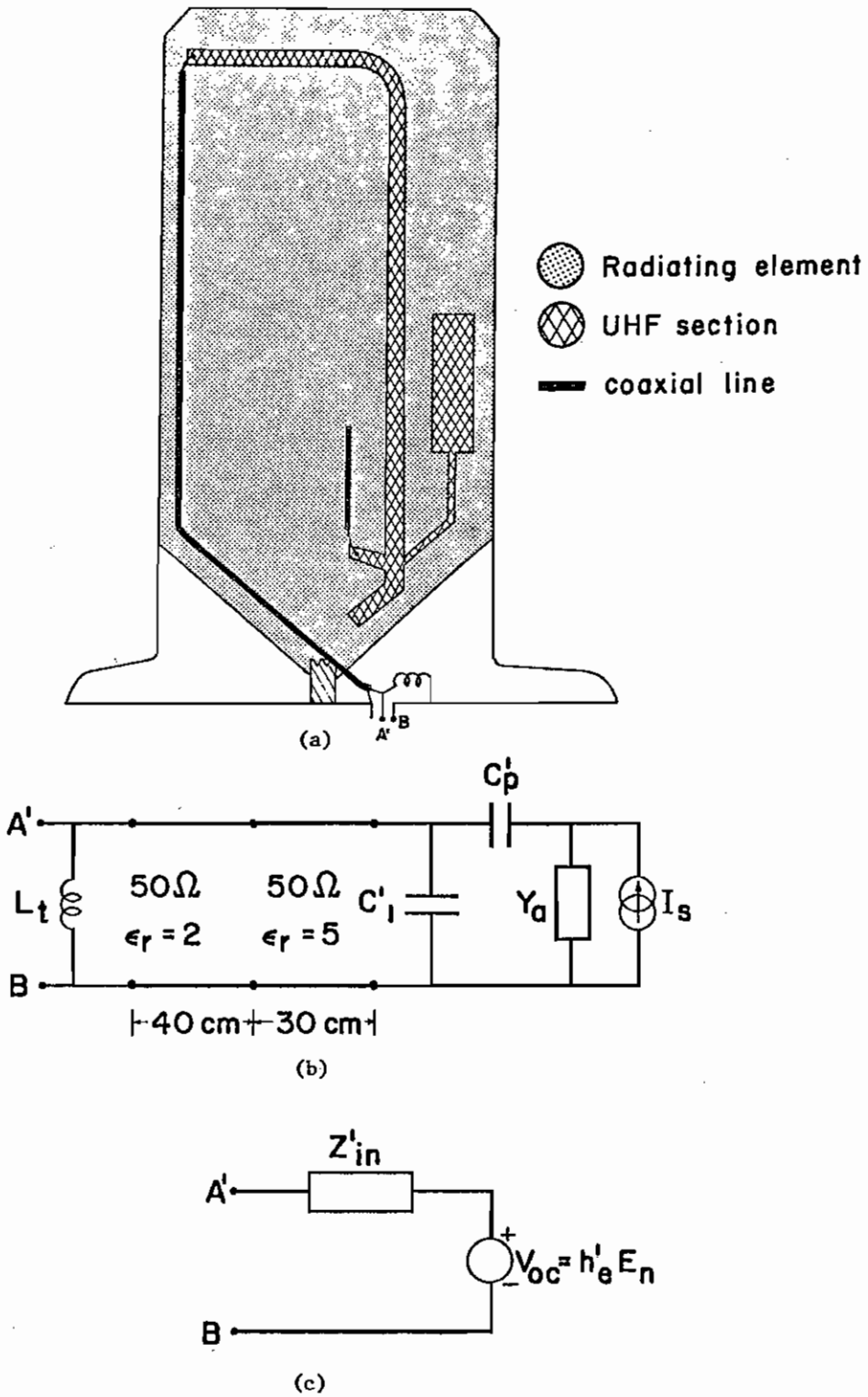

Fig.8 (a) The UHF section, (b) the equivalent circuit and (c) the Thevenin circuit at the terminals A',B.

The constants of proportionalities, i.e., n_t and n_p', are equal to the ratios of the charges induced on the strip and the plate, respectively, to the total charge induced on the whole radiating element. Again, it can be shown that these constants are approximately equal to the ratio of the strip area and the plate area, respectively, to the area of the radiating element. It is found that

$$n_t = 0.020 \tag{11}$$

and

$$n_p' = 0.020. \tag{12}$$

Substitution of appropriate values into (10) gives

$$I_s = j\omega E_n \times 3.52 \times 10^{-14}. \quad \text{Amperes}$$

The other components in Fig. 8b are now identified. The antenna admittance Y_a is that of the base-fed blade monopole antenna. The capacitance is the resultant capacitance due to the plate and the strip. The capacitance C_1' accounts for the part of the microstrip line and the open-circuited coaxial line. The transmission line with length 30 cm is the microstrip line, and the transmission line with length 40 cm is the coaxial line. The inductance L_t accounts for the shunt inductor across the input terminals A',B.

The Thévenin equivalent circuit of the UHF antenna at the terminals A',B is shown in Fig. 8c and it can be readily obtained by applying circuit analysis techniques to the circuit in Fig. 8b. Again, an effective height h_e' for the UHF section is defined, so that the open-circuit voltage V_{oc}' at the terminals A',B is given by

$$V_{oc}'(\omega) = h_e'(\omega) E_n(\omega). \tag{13}$$

The input impedance Z_{in}' and the effective height h_e' are plotted versus frequency in Fig. 9 and Fig. 10, respectively. The small values of the effective height can again be attributed to the capacitive coupling mechanism of the antenna feed.

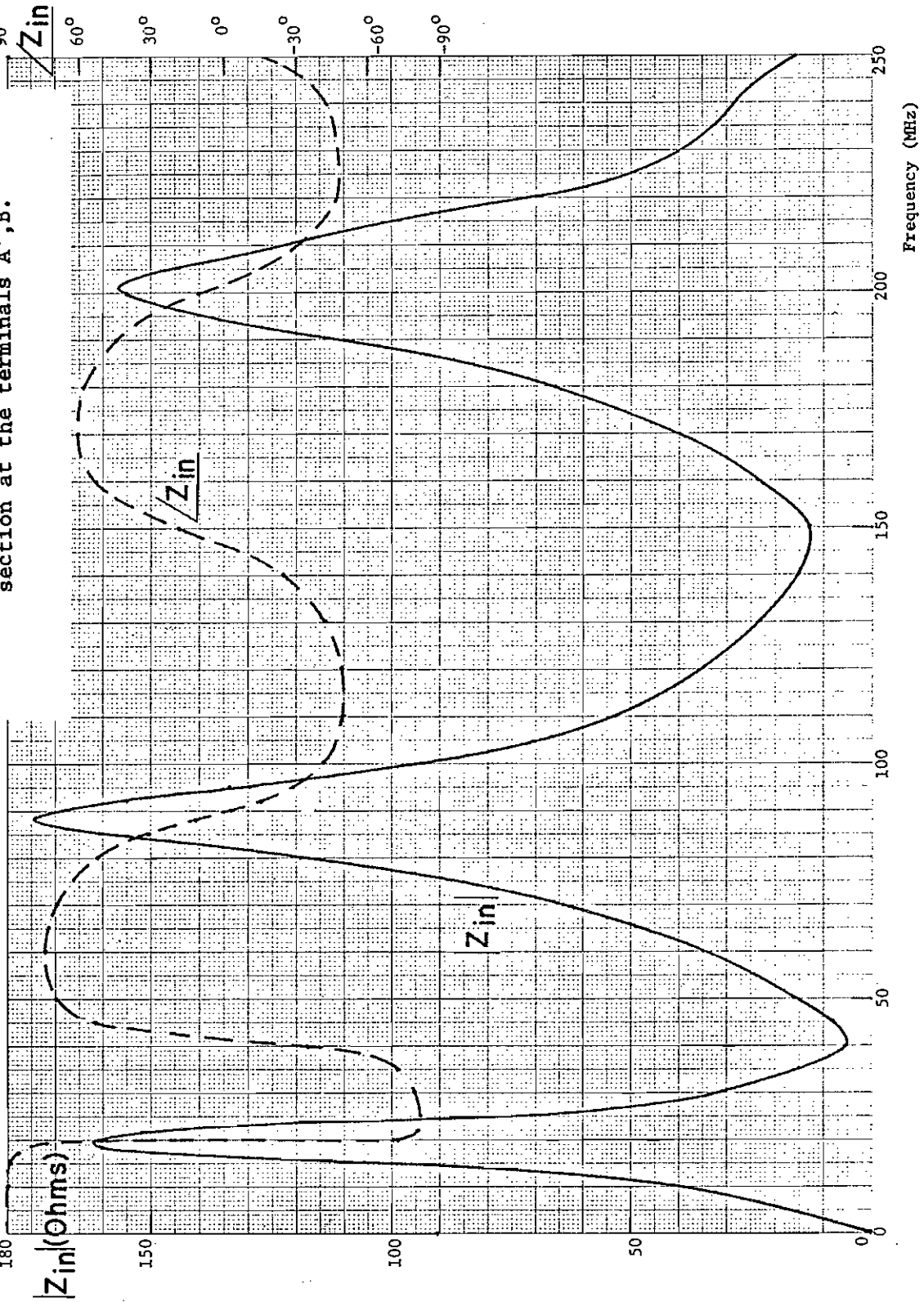

Fig.9 The input impedance of the UHF section at the terminals A',B.

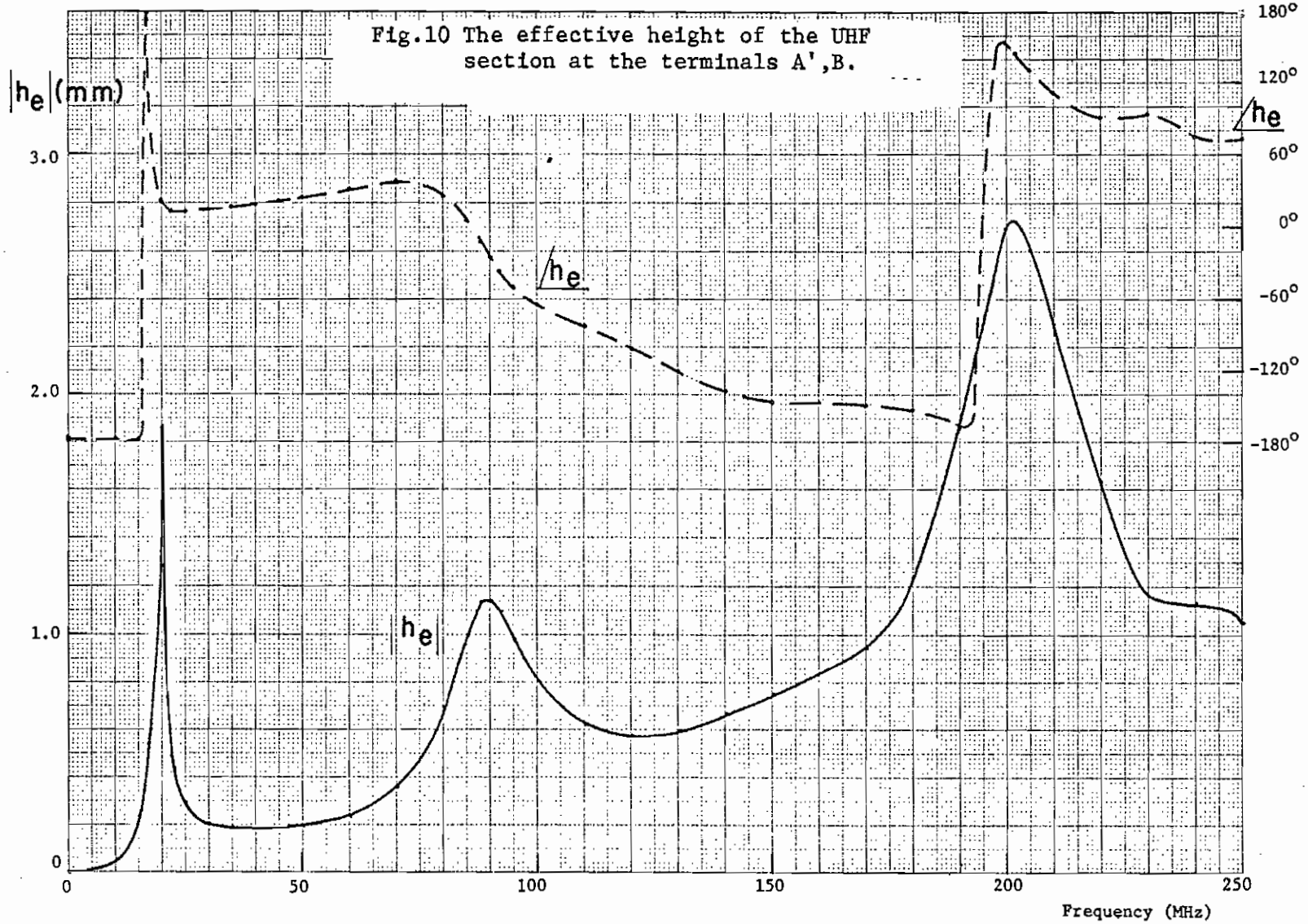
Fig.10 The effective height of the UHF section at the terminals A',B.
|he|(mm)
3.0
2.0
1.0
0
/he
|he|
180°
120°
/he
60°
0°
-60°
-120°
-180°
0
50
100
150
200
250
Frequency (MHz)

At low frequencies, the equivalent circuit of Fig.8b can be simplified to that of Fig. 11. The input impedance is due to the inductance L_t, and the effective height is given by

$$h_e = -6.10\times10^{-17}\ \omega^2 \qquad \text{Meters.} \tag{14}$$

In Fig. 12, the magnitudes of the input impedances and the effective height are presented for frequencies up to 15 MHz. In the same figures, the graphs based on the low-frequency model is also presented. The low-frequency model is valid up to frequencies noticeably below those of the corresponding quantities of the VHF section. This smaller range of validity for the low-frequency model is due to the two transmission lines which have a large combined electrical length, so that the model in Fig. 11 is valid only at fairly low frequencies.

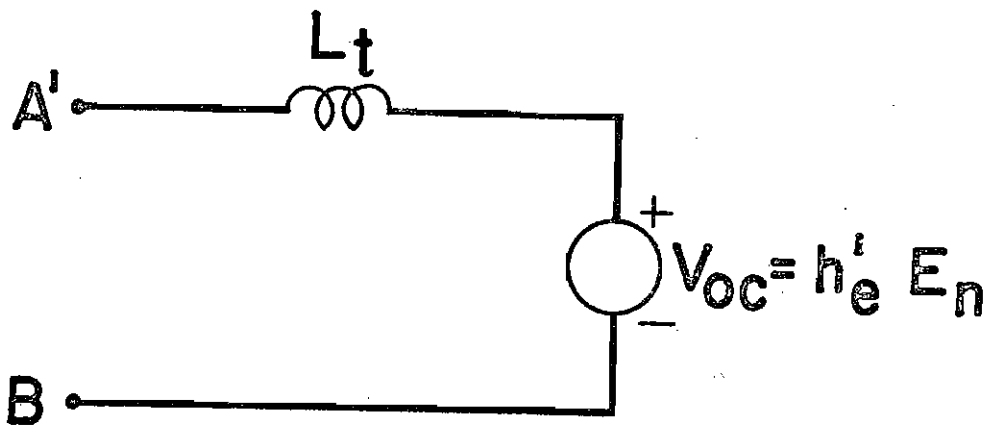

Fig.11 The low-frequency equivalent circuit of the UHF section at the terminals A',B.

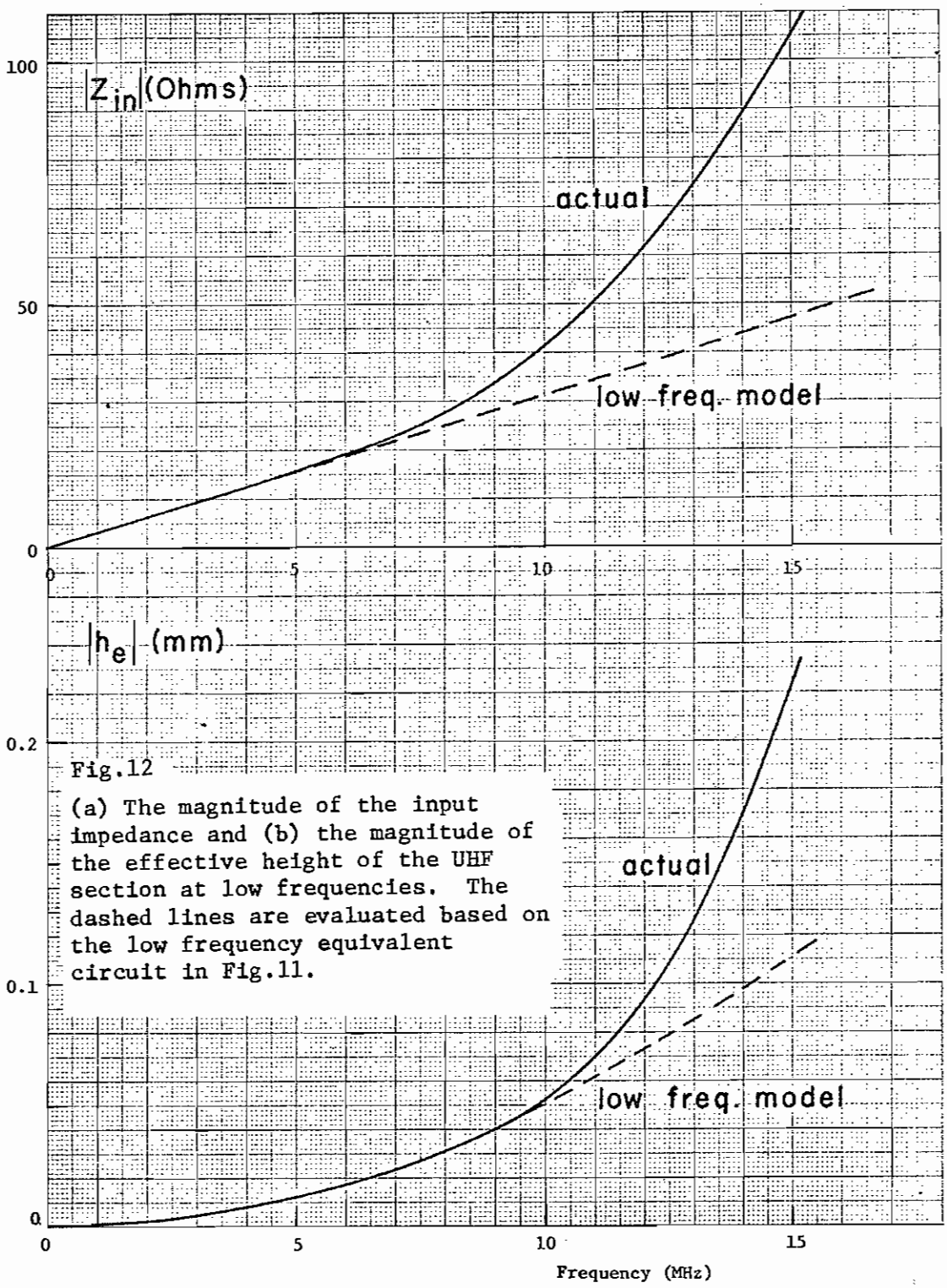

Fig.12

(a) The magnitude of the input impedance and (b) the magnitude of the effective height of the UHF section at low frequencies. The dashed lines are evaluated based on the low frequency equivalent circuit in Fig.11.

☆U.S. GOVERNMENT PRINTING OFFICE: 1975—A-0298/(42) 19